FINITE ELEMENT BASED SOLUTIONS OF THIN-SHELL PROBLEMS WITH A SMALL STRAIN

A thesis submitted to the University of Manchester
for the degree of Master of Philosophy
in the Faculty of Engineering and Physical Sciences

2013

Wassamon Phusakulkajorn
School of Mathematics

Contents

Abstract **11**

Declaration **12**

Copyright Statement **13**

Acknowledgements **14**

1 Introduction **15**

1.1 Motivations 15

1.2 Objective 18

1.3 Finite element method in practice 18

1.3.1 Discretisation 18

1.3.2 Consideration of approximation functions 19

1.3.3 Geometric approximation 20

1.3.4 Numerical integration 22

1.3.5 Assembly of element equations 24

1.3.6 The finite element solutions and post-processing 26

1.4 Outline 26

2 Literature review **28**

2.1 A C^1-finite element with a straight boundary domain 28

2.2 A C^1-finite element with a curved boundary domain 33

2.2.1 Isoparametric scheme 34

2.2.2 Subparametric scheme 36

2.3 Alternative methods of C^1 problems dealing with a straight boundary domain 38

2.4 Alternative methods of C^1 problems dealing with a curved boundary domain 40

3 Mechanics of a thin-elastic material 43

3.1 Introduction 43

3.2 Deformation 44

3.3 The governing equation of a thin-shell material with a small strain . . . 52

3.4 The linear theory 57

3.4.1 Linearisation of a beam governing equation 57

3.4.2 Linearisation of a shell governing equation 65

4 Finite element method for a beam 73

4.1 Introduction 73

4.2 Finite element method for a straight beam 75

4.2.1 The linearised governing equation 76

4.2.2 Finite element representations for C^0- and C^1-continuous solutions 79

4.2.3 Numerical comparisons between the Kirchhoff-Love linear and nonlinear governing equations 91

4.3 Finite element method for an elastic ring 94

4.3.1 The linearised governing equation 96

4.3.2 Numerical comparisons between the Kirchhoff-Love linear and nonlinear governing equations 99

4.4 Summary 102

5 Finite element method for a shell 104

5.1 Introduction 104

5.2 Finite element method for a flat plate 106

5.2.1 The linearised governing equation 106

5.2.2 A comparison between the Bell triangular and the Hermite rectangular elements: a Biharmonic equation as a case study 109

5.2.3 Numerical comparisons between the Kirchhoff-Love linear and nonlinear governing equations 123

5.3 Finite element method for a circular tube 127

5.3.1 The linearised governing equation . . . 127
5.3.2 Numerical comparisons between the Kirchhoff-Love linear and nonlinear governing equations . . . 131
5.4 Summary . . . 134

6 C^1-curved finite element 137
6.1 Introduction . . . 137
6.2 The C^1-curved finite element . . . 139
6.2.1 Approximation of a physical domain . . . 139
6.2.2 The mapping, F_{K_C}, associated the reference with the curved triangle . . . 142
6.2.3 Definition of the C^1-curved finite element compatible with the Bell triangles where the mapping is cubic . . . 143
6.2.4 Construction of the interpolation, $\Pi_K v$, of the function v defined over the curved element . . . 147
6.3 Numerical implementations of the curved finite element . . . 154
6.3.1 The Biharmonic equation . . . 155
6.3.2 Circular plate bending problem . . . 159
6.4 Summary . . . 163

7 Conclusion 165
7.1 Summary . . . 165
7.2 Outlook . . . 168

Bibliography 170

A Shape functions 179
A.1 Lagrange shape functions . . . 179
A.1.1 Interpolations in one dimension . . . 179
A.1.2 Interpolations in two dimensions . . . 181
A.2 Hermite shape functions . . . 183
A.2.1 Interpolations in one dimension . . . 183
A.2.2 Interpolations in two dimensions . . . 184

B Association matrix for the C^1-curved element **186**

Word count 49420

List of Tables

4.1 Specifications of boundary conditions at both ends with energy-norm error obtained from the solution associated with each case. 86
4.2 A tabular of weights and Gauss points used in the Gauss quadrature for an integral approximation when $r = 3$. 92

5.1 L^2-error obtained from solving the Biharmonic equation with various number of the Hermite rectangular elements. 121
5.2 L^2-error obtained from solving the Biharmonic equation with various number of the Bell triangular elements. 121

6.1 L^2-norm error of the solution obtained from the Biharmonic implementation using the Bell elements with various numbers of elements. 157
6.2 L^2-norm error of the solution obtained from the Biharmonic implementation using the C^1-curved elements with various numbers of elements. 157

List of Figures

1.1 The geometry of the reference triangle which has three nodes at vertices. 24

3.1 Geometry of an elastic material in the undeformed and deformed configurations. 44
3.2 A shell geometry. 49
3.3 Graphical geometries of beams with straight and curved shape. 57
3.4 Graphical geometries of shell with straight and curved shape. 66

4.1 The geometrical description of a straight beam with loads in normal direction. 76
4.2 (4.2a) The comparison between the finite element solution and the exact solution of the derivative degrees of freedom. (4.2b) Differences between the exact and the finite element solutions of the derivative degrees of freedom. These are computed under Case 1 with the boundary conditions that $u(1) = 1096.63$ and $\frac{du}{d\xi}(0) = 0$. 87
4.3 (4.3a) The comparison between the finite element solution and the exact solution of the derivative degrees of freedom. (4.3b) Differences between the exact and the finite element solutions of the derivative degrees of freedom. These are computed under Case 2 with the derivative degrees of freedom are specified at both ends. 88
4.4 (4.4a) The comparison between the finite element solution and the exact solution of the derivative degrees of freedom. (4.4b) Differences between the exact and the finite element solutions of the derivative degrees of freedom. These are computed under Case 2 with the derivative degrees of freedom are free at both ends. 89

4.5 Finite element discretisation of one-dimensional domains: a straight line beam. 92
4.6 Comparisons between the deformed positions obtained from nonlinear and linear equations of a straight line beam with a clamped support at the end points with the same constant loads $= 1.0e-8$ applied in normal direction. 94
4.7 Comparisons between displacements obtained from different implementations together with the analytic solution for a deformed straight line beam with different loads. 95
4.8 Comparisons between absolute error obtained from the difference between solutions of the mixed and Hermite formulations and the analytic solution for a deformed straight beam with different loads. 95
4.9 The geometrical description of an elastic ring with loads in normal direction. 96
4.10 Finite element discretisation of one-dimensional domains: a curved beam. 99
4.11 Displacements in x and y-direction between nonlinear and linear equations for a deformed curved beam after different loads have been applied from $f_{\hat{n}} = 0$ to $f_{\hat{n}} = 1 \times 10^{-5}$. 100
4.12 Comparisons between different implementations for a deformed curved beam with different loads. 101
4.13 Comparisons between absolute error obtained from the difference between two different implementations; Mixed and Hermite,and the analytic solution for a curved beam with different loads. 102

5.1 The geometry of the square plate with two clamped edges and two free edges. Forces applied to a body are uniform in normal direction. 106
5.2 Degrees of freedom configurations for expressing the displacement $\mathbf{u}$ over a triangle. 112
5.3 Degrees of freedom of two adjacent triangles. 112

5.4 (Top) The description of all parameters utilised within the definition of the Bell shape functions where L_j denotes the length of the side opposite to the vertex j. (Bottom) The Bell element with 18 degrees of freedom; the values u_j, first derivatives u_{xj}, u_{yj}, and all second derivatives $u_{xxj}, u_{xyj}, u_{yyj}$, at vertex $j; j = 1, 2, 3$. 114
5.5 The discretisation of the domain of interest with 4 elements in x_1-direction and 2 elements in x_2-direction. 117
5.6 Comparisons between solutions and errors obtained from finite element method based on Bell and Hermite elements and the exact solution. Figures are generated using the `trimesh` function in MatLab. 120
5.7 A comparison of the rate of convergence between the Bell triangular and the Hermite rectangular elements. 122
5.8 A log-plot comparison of the rate of convergence between the Bell triangular and the Hermite rectangular elements. 122
5.9 Displacements in cartesian coordinates for the clamped plate with the normal distributed loads=1×10^{-8}. 125
5.10 Differences between the displacement in z-direction obtained from the linear, the nonlinear, and the exact solutions with increasing loads from 0 to 1×10^{-7}. 126
5.11 The geometry of unit circular tube with a clamped support at both ends of the tube. Forces applied to a body are uniform in normal direction. . 128
5.12 Displacements in cartesian coordinates for the clamped circular tube with the normal distributed loads=1×10^{-6}. 133
5.13 Differences between the displacement in y-direction obtained from the linear and the Nonlinear governing equations for the circular tube with increasing loads from 0 to 1×10^{-5}. 134
5.14 Differences between the displacement in z-direction obtained from the linear and the Nonlinear governing equations for the circular tube with increasing loads from 0 to 1×10^{-5}. 135

6.1 A graphical description of the mappings associated between the reference coordinates $\hat{x}_\alpha$ and the physical coordinates $x_\alpha, \alpha = 1, 2$ where F_{K_I} is the mapping corresponding with the straight-sided triangle and F_{K_C} is the mapping corresponding with the curved triangle. 140
6.2 An exact curved boundary Γ and an approximated boundary Γ_h of one-curved side triangles K_C. 140
6.3 Adjacent triangles to a curved triangle K_C. 144
6.4 Description of the notations: $\mathbf{c}_1$ and $\mathbf{c}_2$ on the curved triangle K_C. . . . 145
6.5 The triple $(\hat{K}, \hat{P}, \hat{\Sigma})$ for a C^1-curved finite element compatible with the Bell triangle where the degree of polynomial approximating curved boundaries is cubic. 147
6.6 The description of the C^1-curved finite element compatible with the Bell element constituting of three vertices and three internal nodes where the set of dofs is $\{(D^\alpha v(\mathbf{a}_i), \alpha = 0, 1, 2), i = 1, 2, 3; v(\mathbf{e}_i), i = 1, 2, 3\}$. 148
6.7 The comparison of the convergence rate between the Bell triangular finite element and the C^1-curved triangular finite elements. 158
6.8 Linearised shell solutions of the circular plate problem obtained from the 29-element unstructured mesh with different loads. 161
6.9 The representation of the curved boundary by the Bell and the C^1-curved triangular finite elements having 29 elements in the mesh. . . . 162
6.10 The differences between the exact solution and the normal displacements obtained from the Bell and the C^1-curved elements with different loads. 163

A.1 The linear shape functions in one dimension which has two nodes in the element. 180
A.2 The quadratic shape functions in one dimension which has three nodes in the element. 181
A.3 The cubic Hermite basis functions. 184

B.1 Matrix $[A]_{36\times36}$. 197
B.2 Matrix $[A]_{36\times36}$ (cont.). 198

The University of Manchester

Wassamon Phusakulkajorn
Master of Philosophy
Finite element based solutions of thin-shell problems with a small strain
November 29, 2013

In this thesis, we consider the deformation of shell structures defined as thin three-dimensional elastic bodies. These can be modelled using a lower-dimensional theory but the governing partial differential equation of thin shells contains fourth-order derivatives which require C^1-continuity in their solutions. Consequently, both the unknown and its first derivatives have to be continuous.

Employing a finite element method in our study suggests that the C^1-finite element representation of the shell solution has to be employed. Therefore, appropriate interpolation functions defined on a typical finite element are studied on both straight and curvilinear boundary domains.

Our study of C^1-finite element representations shows that the Bell triangular finite element which is derived from the quintic polynomials is more appropriate than the bicubic Hermite rectangular element as it converges faster and provides higher accuracy on domains with straight boundaries. However, when the physical boundary is curved, a straight-line approximation is not exact and the performance of the Bell triangular element decreases in terms of both accuracy and convergence rate. To retain a convergence rate and accuracy of the solution of a C^1-problem on a curvilinear boundary domain, the C^1-curved triangular finite element is introduced. It is proved to show superiority in both convergence rate and accuracy when solving the C^1-problem on a curved boundary domain.

Furthermore, numerical comparisons between the solutions obtained from the linear and nonlinear governing equations with the linear constitutive law are also reported here. These comparisons confirm that the solutions obtained from the linearised governing equation agree with those of the nonlinear when a loading is small and they start to disagree when the loading becomes larger.

Declaration

No portion of the work referred to in the thesis has been submitted in support of an application for another degree or qualification of this or any other university or other institute of learning.

Copyright Statement

Acknowledgements

I would like to express my deep appreciations to Dr. Andrew Hazel, my supervisor, and Professor Matthias Heil, my co-supervisor, for their patience, help, comments and suggestions throughout the study.

Above all, I would like to express my gratitude to my family. The encouragement and many helpful suggestions from them were enable me get through the difficult times. For their unfailing love and support, this thesis is dedicated to them.

Chapter 1

Introduction

1.1 Motivations

In this thesis, we study the solution of problems in the thin-shell theory by the finite element method. An elastic body is defined to have the physical property that the material can return to its original shape after applied forces are removed. A shell is a three-dimensional elastic body whose thickness is small compared to the other two dimensions. Although the deformation of a shell arising in response to given loads can be accurately captured by directly solving the three-dimensional elastic equations, the shell theory provides a dimensional reduction of the problem.

When a shell is thin, it is reasonable to approximately define the geometry of the shell structure by only its middle surface of a cross section. Therefore, a system of differential equations defined on the middle surface that can effectively capture the displacement and stress of the thin-shell arising in response to applied forces will be the desired thin-shell model.

There are many assumptions that can be used with characteristics of a typical shell. However, when it comes to a thin-shell problem, a widely used assumption in dimensional reduction is the Kirchhoff-Love assumption [2]. The assumption states that a vector that is normal to the undeformed body has to be normal and unstretched after deformation. Both the transverse shear and normal stresses are neglected. The Kirchhoff-Love assumption has proved successful in practice and is widely employed in many engineering applications ([27], [83]).

Elasticity is the study of how solid objects deform and become internally stressed

due to a prescribed external force. The external force applied on a specified area is defined as stress which result in a deformation of a material. When a material changes as a consequence of stress, the strain tensor has to be considered to provide the relative amount of its deformation. The relationship between stress and strain is the so-called constitutive law which can be either linear or nonlinear. The linear relationship is called Hooke's law and the small strain is the most important assumption to make the relation linear.

In this thesis, the shell kinematics will be studied within the framework of thin-shell elasticity with the linear constitutive law. Its governing equation will be presented with more detailed descriptions in Chapter 3. Here, for a brief description of our thin-shell finite element implementations, the following form of the variational principle formulation is presented.

$$0 = \iint_{\Omega} F\left(\mathbf{u}, \frac{\partial \mathbf{u}}{\partial \xi_i}, \frac{\partial^2 \mathbf{u}}{\partial \xi_i \partial \xi_j}, \delta\mathbf{u}, \delta\frac{\partial \mathbf{u}}{\partial \xi_i}, \delta\frac{\partial^2 \mathbf{u}}{\partial \xi_i \partial \xi_j}\right) d\Omega, \tag{1.1}$$

where $\mathbf{u}$, $\frac{\partial \mathbf{u}}{\partial \xi_i}$, $\frac{\partial^2 \mathbf{u}}{\partial \xi_i \partial \xi_j}$, $i, j = 1, 2$, represent the unknown and its first- and second-order derivatives, respectively. Furthermore, $\delta(\cdot)$ denotes the variation of a function which represents an admissible change in the function at a fixed value of the independent variables [40].

From the equation (1.1), we can see that the first-order derivatives, $\frac{\partial \mathbf{u}}{\partial \xi_i}$, and the second-order derivatives of the unknown, $\frac{\partial^2 \mathbf{u}}{\partial \xi_i \partial \xi_j}$, appear in the governing equation of a thin shell. To ensure the integral is well defined, the unknown $\mathbf{u}$, its first, and second derivatives have to be square integrable over the domain. Hence, the unknown $\mathbf{u}$ belongs to a C^1-family [78].

In many applications of the continuum mechanics especially thin-shell elasticity, the finite element method has been commonly used for decades. The finite element method is a numerical technique for finding approximate solutions of partial differential equations (PDEs) as well as integral equations. The general idea of the finite element method is that a given domain is represented by a collection of simple domains called finite elements.

In each finite element, the solution of the PDE is approximated by a polynomial of a fixed degree. This polynomial is called a shape function or a basis function in the finite element method. Its construction employs ideas from the interpolation theory.

Most classical shape functions that have been employed are in the Lagrange- and Hermite-family polynomials.

Lagrange polynomials may be employed to approximate a solution that requires only C^0-continuity, whereas Hermite polynomials can be used to provide C^1-continuity in the approximate solution. Further details on Lagrange and Hermite polynomials can be found in [40], [60].

The choice of shape functions depends on the nature of the desired differential equation. Some equations require an inter-element continuity of only the unknown field, some require an inter-element continuity of both the unknowns and their derivatives. In this thesis, the finite element method will be studied with thin-shell problems whose governing equation contains the second-order derivatives of the displacement, as in (1.1). Therefore, the continuity conditions between the finite elements have to be imposed for both the displacements and their derivatives to ensure that the solution of the shell remains continuous. Hence, the Hermite-family polynomials have to be considered.

Regarding the shape of a finite element in two dimensions, either rectangular or triangular elements can be used to discretise a two-dimensional domain into pieces — called finite elements. In order to approximate functions defined on these finite elements, approximation or shape functions are derived so that they are associated to the shape of an element. Shape functions defined over typical elements have been studied by many researchers to satisfy the C^1-continuity in the solution of the C^1-problem. Examples of such an element in two-dimensional space can be found in [28], [41] for quadrilateral elements and in [38], [43], [54], [71] for a triangular elements.

In many engineering applications, the geometric boundary of a problem is not always straight. Also, many C^1-finite elements have straight sides for both rectangular and triangular elements. Representing a curved boundary domain with a series of straight-sided elements exhibits limitations in a convergence rate and accuracy in the finite element method. These were presented in the studies of [56], [50], [63], [65], where using straight-sided triangles to approximate a curved boundary domain was proved to illustrate poor accuracy and slow convergence.

Consequently, many researchers have developed and improved further finite elements in order to deal with the C^1-problems on a curved boundary. The main goal

of this development is to retain the rate of convergence and accuracy. Also, a curved boundary can be accurately approximated by an improved element.

1.2 Objective

The goal of this thesis is to understand and address problems about higher-order finite elements and boundary approximations for the thin-shell theory with the linear constitutive law. Emphasis will be placed on implementational aspects concerning topics like the performance of elements and the geometric representation of a circular domain. Also, we will consider problems related to computations of thin beams and shells in order to provide an understanding of a dimensional reduction. This is one of the motivations in a numerical simulation to represent the body with its intrinsically lower-dimensional space.

1.3 Finite element method in practice

In order to implement a problem, the finite element method works on each finite element to systematically construct the approximation functions of the solution of a problem. This will turn the desired PDE into an approximating system of equations. Then, this system are numerically solved using standard numerical techniques. More details on the finite element method can be found in [40], [60], [61], [78].

In the finite element method, there are steps involved as follows.

1.3.1 Discretisation

A discretisation is the first step in the finite element method. The given (complex) domain is represented by the finite element mesh. After this stage, the domain of interest is discretised by the typical elements and thus constitutes of many finite elements and nodes.

In the discretisation, the choice of element type, number of nodes and elements have to be analysed. The number of nodes and elements will play an essential role in minimising error of the solution. However, the greater number of both nodes and elements can be expensive in computational time.

1.3.2 Consideration of approximation functions

In the finite element method, the solution approach is based on a technique of representing by a finite set of basis functions. Therefore, we have to determine a set of functions to approximate quantities of interest that define over a particular finite element.

Before we determine approximation functions, the finite element model of the desired equation has to be considered. In solid mechanics, the finite element model of a problem can be developed either from the principle of virtual work or from the differential equations.

In this study, the finite element model of a thin-elastic problem will be developed from the principle of virtual displacement which will be derived in chapter 3. This model will be the governing equation that allows us to determine a functional space for both the solution and the approximation functions.

In order to obtain a finite element solution in this study, we exploit the Galerkin method which allows us to represent the solution with a finite set of global shape functions. Note that in the finite element method, it is often convenient to define local shape functions, ψ_j, on the reference element where the numerical integration is defined. Also, these local shape functions are parametrised by the local coordinates, s_i, of the reference element. Therefore, a finite element solution can be expressed as

$$u(x_k(s_i)) = \sum_{j=1}^{n} U_j \psi_j(s_i), i = 1, 2, \tag{1.2}$$

where U_j is discrete unknown coefficients determining the solution at node j in an element and n is the total number of shape functions defined on the reference element. Also, the d-order derivatives of the finite element solution on each element is represented by

$$\frac{\partial^d u}{\partial x_m^d}(x_k(s_i)) = \sum_{j=1}^{n} U_j \frac{\partial^d \psi_j}{\partial x_m^d}(x_k(s_i)). \tag{1.3}$$

From (1.2) and (1.3), we have that the variation for the finite element solution and its derivatives can be expressed as

$$\delta u(x_k(s_i)) = \sum_{j=1}^{n} \delta U_j \psi_j(s_i), \tag{1.4}$$

and,

$$\delta\left(\frac{\partial^d u}{\partial x_m^d}(x_k(s_i))\right) = \sum_{j=1}^{n} \delta U_j \frac{\partial^d \psi_j}{\partial x_m^d}(x_k(s_i)). \tag{1.5}$$

Note that, in order to determine the derivatives of the local shape functions ψ_j with respect to the global coordinates x_m, the Jacobian mapping will be employed to relate between the derivatives with respect to the global and local coordinates. This will be explained more in details in the next section.

After substituting the finite element solutions and its derivatives with their variations into the finite element model (the governing equation), the shape functions and the solution space can be determined. In the finite element method, a choice of shape functions plays an essential role in an implementation in order to obtain a high accuracy solution. The family of Lagrange and Hermite shape functions are the most two famous which we will consider in this study. More details on both Lagrange and Hermite shape functions can be found in Appendix A.

1.3.3 Geometric approximation

From the definition of shape functions, they are usually expressed over an interval of a numerical integration. Therefore, transformation of the geometry and the variables of the differential equation from the problem coordinates $\mathbf{x}$ have to be defined over the local coordinates $\mathbf{s}$ where the numerical integration is defined. Each element, Ω_e, of the finite element mesh, Ω, is transformed to the local-coordinated element, only for the purpose of numerically evaluating the integrals.

The transformation between the physical and local coordinates can be expressed as

$$x_k(s_i) = \sum_{j=1}^{n} X_{kj}\psi_j(s_i), i = 1, 2, \tag{1.6}$$

where X_{kj} are nodal positions of kth coordinate at element node j and $\psi_j(s_i)$ are shape functions associated with element node j approximating geometry. They are parametrised by the local coordinates s_i and defined over the reference element. Also, n is the number of nodes in the reference element.

Since the parametric shape functions are parametrised by local coordinates while unknowns and their derivatives are based on global ones, their evaluation in the global coordinates of the value, $u(\mathbf{x})$ and its derivatives, $\frac{\partial^d u}{\partial x_k^d}(\mathbf{x})$ are required. By applying

the chain rule, the first and second derivatives with respect to the global coordinates can now be evaluated as

$$\frac{\partial u}{\partial x_k} = \frac{\partial u}{\partial s_j}\frac{\partial s_j}{\partial x_k}, \tag{1.7}$$

$$\frac{\partial^2 u}{\partial x_h \partial x_k} = \frac{\partial^2 u}{\partial s_i \partial s_j}\frac{\partial s_i}{\partial x_h}\frac{\partial s_j}{\partial x_k} + \frac{\partial^2 s_j}{\partial x_h \partial x_k}\frac{\partial u}{\partial s_j}. \tag{1.8}$$

Note that the summation convention over the local coordinate $s_j, j = 1, 2$, is used.

In order to evaluate these derivatives with respect to the global coordinates, the Jacobian mapping is employed to transform from the local to the global coordinates. It is defined as a matrix of the first derivatives of (1.6) and can be expressed as

$$\mathcal{J}_{kj} = \frac{\partial x_k}{\partial s_j} = \sum_{l=1}^{n} X_{kl}\frac{\partial \psi_l}{\partial s_j}(\mathbf{s}). \tag{1.9}$$

By substituting the derivatives of the parametric approximation and the Jacobian mapping in (1.3) and (1.9) into (1.7) and (1.8), we have

$$\frac{\partial u}{\partial x_k} = \left(\sum_{l=1}^{n} U_l \frac{\partial \psi_l}{\partial s_j}(\mathbf{s})\right)\left[\mathcal{J}^{-1}\right]_{jk}, \tag{1.10}$$

and,

$$\frac{\partial^2 u}{\partial x_h \partial x_k} = \left(\sum_{l=1}^{n} U_l \frac{\partial^2 \psi_l}{\partial s_i \partial s_j}(\mathbf{s})\right)\left[\mathcal{J}^{-1}\right]_{ih}\left[\mathcal{J}^{-1}\right]_{jk} + \frac{\partial [\mathcal{J}^{-1}]_{jk}}{\partial x_h}\left(\sum_{l=1}^{n} U_l \frac{\partial \psi_l}{\partial s_j}(\mathbf{s})\right). \tag{1.11}$$

Since we expressed all quantities by the local coordinates s and the shape functions are considered on the local-coordinated element, this turns the approximations to an element level.

Also, the integration over the element have to be transformed in order to perform in the local coordinates as

$$\iint_{\Omega_e} (...) d\mathbf{x} = \int_{-1}^{1}\int_{-1}^{1} (...)\hat{\mathcal{J}} d\mathbf{s}, \tag{1.12}$$

where

$$\hat{\mathcal{J}} = \det(\mathcal{J}_{kj}) \tag{1.13}$$

is the determinant of the Jacobian mapping between the global coordinates and the local coordinates.

In general, these geometric shape functions do not have to be the same as parametric shape functions. In the finite element method, the degree of geometric shape

functions can be defined to be lower or higher than the degree of polynomials for parametric shape functions. The idea of using a lower degree in geometric shape functions is known as the subparametric scheme while using the higher is the so-called superparametric scheme.

Regarding the subparametric scheme, the linear shape function is widely used to minimise some difficulties in an implementation. As we can see from (1.8), the second-order derivatives of the unknown u with respect to the global coordinates involve also the second-order derivatives of the mapping from local to global coordinates. Therefore, the C^1-geometric shape functions is required to approximate geometry in order to assure the existence of the second-order derivatives. Using the linear shape function can thus eliminate the effect of the second-order derivatives term out of the evaluation of the unknown's derivatives. However, the linear geometric approximation can be less accurate when we deal with complex domains as we will illustrate in Chapter 6.

Contrary to the subparametric and superparametric scheme, the isoparametric scheme is the idea in which the same degree of polynomial is utilised in both geometric and parametric shape functions. One big advantage of this scheme is that more accuracy of the geometry approximation is obtained when a non-polygon domain is concerned.

1.3.4 Numerical integration

In the finite element method, partial differential equations are usually transformed to a weak formulation which is an integral form and can be obtained by moving all terms to one side of the equation, introducing a weight-residual function, and then integrating through the domain (see [40], [78]). Exact evaluation of the integral is not always possible because of the complexity of the equation. Therefore, a numerical integration is taken into account when a finite element implementation is performed.

Several formula are presented and designed to exactly integrate complete polynomials of a given degree. The accuracy of an approximation depends on a choice of integration schemes, i.e. number of Gauss points and weights. Therefore, the degree of precision and the number of Gauss points and weights must be determined so that the function under an integral can be accurately approximated. The formula of various

degree of precision for integration schemes defined over a rectangle and a triangle can be found in [21], [40], [53].

Gaussian quadrature in 1D

The 1D-Gaussian quadrature has been specified as

$$\int_{-1}^{1} f(\xi)d\xi \approx \sum_{i=0}^{r-1} f(\xi_i)w_i \tag{1.14}$$

where r is the number of integral points, w_i are the weight factors, $\xi_i \in [-1, 1]$ are the integral points. The r-point Gaussian quadrature formula exactly integrates all polynomials of degree $2r - 1$ or lower [40].

To approximate an integral in a two-dimensional space using a Gaussian quadrature, one-dimensional quadrature schemes are set up in each direction. Consider the function $f(\xi_1, \xi_2)$ which depends on the two variables ξ_1 and ξ_2 defined to contain in the surface of interest, Ω.

Gaussian quadrature in 2D for a rectangular element

An integration on a square element usually relies on tensor products of the one-dimensional formula illustrated in (1.14). It normally expresses on $[-1, 1] \times [-1, 1]$ square element. Thus, two-dimensional integral on an arbitrary rectangular element yields the approximation as follows

$$\begin{aligned}\int_{-1}^{1}\int_{-1}^{1} f(\xi_1, \xi_2)d\xi_2 d\xi_1 &\approx \int_{-1}^{1}\sum_{i=1}^{I} w_i f(\xi_1, \xi_2^{(i)})d\xi_1 \\ &\approx \sum_{i=1}^{I}\sum_{j=1}^{J} w_i w_j f(\xi_1^{(i)}, \xi_2^{(j)}),\end{aligned} \tag{1.15}$$

where a quadrature scheme with I Gauss points and weights is firstly employed in the ξ_2 direction ($\xi_2^{(i)}$ and w_i, respectively) followed by a scheme with J Gauss points and weights for the ξ_1 direction ($\xi_1^{(j)}$ and w_j, respectively).

Gaussian quadrature in 2D for a triangular element

In two-dimensional integrals on triangles, the quadrature scheme will express the formula in terms of triangular coordinates as

$$\iint_{\Omega} f(\xi_1, \xi_2)d\xi_1 d\xi_2 \approx A_e \sum_{i=1}^{I} w_i f(\lambda_1^i, \lambda_2^i, \lambda_3^i), \tag{1.16}$$

where w_i is the weight associated with the point i and A_e denotes the area of the triangle. Furthermore, $(\lambda_1^i, \lambda_2^i, \lambda_3^i)$ are the area coordinates or barycentric coordinates of the point i in the triangle described as follows.

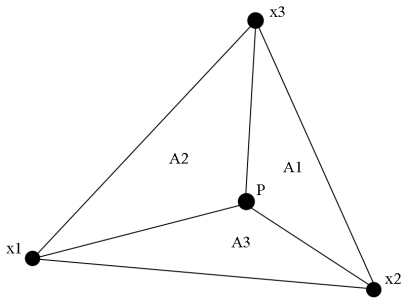

Figure 1.1: The geometry of the reference triangle which has three nodes at vertices.

The barycentric coordinates of the point $\mathbf{p}$ in the triangle illustrated in Fig. 1.1 are simply defined to be ratios of triangle areas as,

$$\lambda_1 = \frac{A_1}{A}, \quad \lambda_2 = \frac{A_2}{A}, \quad \lambda_3 = \frac{A_3}{A}, \tag{1.17}$$

where the area A is the area of total triangle, and the areas $A_j, j = 1, 2, 3$ are sub-areas. These ratios of areas form dimensionless coordinates in the plane defined by points $\mathbf{x}_1, \mathbf{x}_2, \mathbf{x}_3$ which are vertices of the triangle illustrated in Fig. 1.1.

A barycentric combination of three points takes the form: $\mathbf{p} = \lambda_1\mathbf{x}_1 + \lambda_2\mathbf{x}_2 + \lambda_3\mathbf{x}_3$ where $\lambda_1 + \lambda_2 + \lambda_3 = 1$. Thus, the three vertices of the triangle have barycentric coordinates as

$$\mathbf{x}_1 \equiv (1, 0, 0), \quad \mathbf{x}_2 \equiv (0, 1, 0), \quad \mathbf{x}_3 \equiv (0, 0, 1). \tag{1.18}$$

1.3.5 Assembly of element equations

Since an implementation works on each element in the finite element method, equations are systematically constructed at this stage to approximate the solution of a PDE. The problem is reduced to a finite set of nonlinear residuals by choosing a finite number of weight, or test, functions in the weak form. This system of equations can be solved using an iterative method. In this study, the Newton method will be our selected numerical technique:

$$U_j^{m+1} = U_j^m + \Delta U_j, \quad j = 1, ..., N, \tag{1.19}$$

$$\sum J_{ij}\Delta U_j = -r_i \quad \text{for } i = 1, ..., N, \tag{1.20}$$

where U_j^m are the values of the unknown at node j in the mth iteration, J_{ij} denotes the global Jacobian of derivatives and r_i is the global residuals vector. Also, N denotes the number of unknowns in the finite element mesh.

In general, the set of deviations $\Delta U_j; j = 1, ..., N$ at each iteration m is used to improve the new approximation to the solution of the system from the initial guess U_j^0. The approximate solution at the $(m+1)^{th}$ iteration can be computed by (1.19). In the iteration method, the residuals r_i are evaluated using the solution from the previous iteration. The iteration is continued until the convergence criteria is satisfied. For additional details, see [40].

Each element will provide a contribution to the residuals for which the test function is non-zero over the element. The residuals $r_i^{e_k}$ of the element e_k corresponding to the ith test function can be obtained by using Gaussian quadrature discussed in section 1.3.4. Furthermore, the Jacobian matrix $J_{ij}^{e_k}$ evaluated in element e_k corresponding to the ith test function can be obtained as follow

$$J_{ij}^{e_k} = \frac{\partial r_i^{e_k}}{\partial U_j} \quad \text{for } i, j = 1, ..., n. \tag{1.21}$$

The residuals, $r_i^{e_k}$, and the Jacobian matrix, $J_{ij}^{e_k}$, obtained from the weak formulation, which is an integral form of a given PDE, are in element-level. Therefore, the residuals and the Jacobian matrices in each element have to be assembled to obtain the global system of algebraic equations. For instance, the Jacobian matrix and the residuals for K 2-node elements in one dimension can be connected in series as the following forms:

$$\mathbf{J} = \begin{pmatrix} J_{11}^{e_1} & J_{12}^{e_1} & & & & & \\ J_{21}^{e_1} & J_{22}^{e_1} + J_{11}^{e_2} & J_{12}^{e_2} & & & & \\ & J_{21}^{e_2} & J_{22}^{e_2} + J_{11}^{e_3} & J_{12}^{e_3} & & & \\ & & J_{21}^{e_3} & J_{22}^{e_3} + J_{11}^{e_4} & & & \\ & & & & \ddots & & \\ & & & & & & J_{22}^{e_K} \end{pmatrix}, \tag{1.22}$$

$$\mathbf{r} = \begin{pmatrix} r_1^{e_1} \\ r_2^{e_1} + r_1^{e_2} \\ r_2^{e_2} + r_1^{e_3} \\ \vdots \\ r_2^{e_{K-1}} + r_1^{e_K} \\ r_2^{e_K} \end{pmatrix}. \tag{1.23}$$

For further details on the assembly scheme, see [40], [78].

1.3.6 The finite element solutions and post-processing

Now, at this stage, the residual and the Jacobian matrices develop a system of equations as follow

$$\sum J_{ij} \Delta U_j = -r_i \qquad \text{for } i = 1, ..., N, \tag{1.24}$$

where J_{ij} denotes the global Jacobian of derivatives and r_i is the global residual which can be obtained from (1.22) and (1.23), respectively. Also, N denotes the number of nodes in the finite element mesh.

This system of equations will be solved iteratively. With a linear problem, this is a special case for which Newton's method converges in one step. The solutions to this system are the set of deviation $\Delta U_j; j = 1, ..., N$ where U_j is the nodal values in a finite-element mesh. We have that some of these values of U_j can be determined from the boundary conditions and other constraints which have to be imposed before an implementation. Hence, only some values of U_j are unknowns and have to be specified an initial guess.

After we obtained the nodal values, U_j, in the mesh, the finite element solution and its derivatives throughout the domain can be computed by using equations (1.2) and (1.3).

1.4 Outline

This thesis is organised into seven chapters. Followed by this chapter, literature review is detailed in chapter 2. In chapter 3, the elasticity mechanics will be elaborated where the concepts and notations will be provided. Also, we will describe the shell

kinematics and present the basic shell mathematical model within the framework of the linear constitutive law. From the general frame work in chapter 3 where the governing equations with the linear theory of beams and shells are presented in a general geometry, chapters 4 and 5 will consider a thin beam and a thin shell, respectively, in the straight and the curved geometries. Furthermore, the finite element implementations and comparison results between the linear and nonlinear governing equations will be illustrated in chapter 4 for a beam and chapter 5 for a shell.

Besides the topic of the consistency between the linear and nonlinear governing equations with a small strain performed in chapters 4 and 5, a finite element implementation of a C^1-problem on a curvilinear boundary is considered in chapter 6. Finally, we conclude the thesis by chapter 7. Directions for future work are also presented there.

Chapter 2

Literature review

2.1 A C^1-finite element with a straight boundary domain

In this section, we present a perspective review of C^1-finite elements with a straight boundary domain regarding the constructions of the continuously differentiable interpolation functions where the functions themselves and their first derivatives are continuous between elements. Firstly, we will present an intuitive idea to construct C^1-interpolation functions in one dimension. This will follow by ideas in constructing those defined in two dimensions for both rectangular and triangular elements.

Regarding a one-dimensional domain, the construction of C^1-continuous interpolation functions is very straightforward. Since an unknown is parametrised by only one-dimensional coordinate, the C^1-continuity can be imposed by constraining both the unknown and the first derivative at the boundary between elements, which is a single point in each case. The cubic Hermite element is a well-known element that is constructed with this idea. This element consists of two degrees of freedom of both the unknown and its first derivative at nodes. Hence, there are in total 4 degrees of freedom defined on an element. This element has been used successfully in problems of bending of beams [60].

However, ensuring the continuity of both unknown and its derivatives (or normal slope) along element edges is difficult to achieve in a two-dimensional space. One reason for this is that both the unknown and its normal slope have to be uniquely

defined along the boundary of such an element. When a node-based element is concerned, three nodal parameters of unknown value and its first derivatives have to be prescribed at corner nodes in order to enforce the C^1-continuity.

The well-known Zienkiewicz triangle, introduced by Bazeley et al. [33] in 1966, is an example of the C^1-element that employed the intuitive idea of specifying three degrees of freedom of both unknown and its first derivatives at nodes. This element has in total 9 degrees of freedom where each vertex contains the unknowns and two rotational slopes.

Unfortunately, the Zienkiewicz triangle came with one big disadvantage. When general meshes were concerned, the numerical results showed that the obtained solutions from the finite element method using the Zienkiewicz triangle did not converge to the exact solution as the mesh was refined. Typically, this is a situation when an element does not pass a patch test. Note that, we say that the element passes the patch test if the finite element solutions converge to the exact solution for any patch of elements. In constructing an arbitrary patch, it is important to use an irregular geometry since some elements pass the patch test in certain special configurations but not others.

In 1965, the study of B.M. Irons [12] justified the failure of [33] by showing that these simple elements were firstly based on low order polynomials for the displacement field and, secondly, they were non-conforming. Non-conforming in this context means that the mixed second-order derivative is not always the same in neighbouring elements and, specifically, it has different values at shared vertices. These may cause convergence problems and unreliable finite approximations. A reader may refer to chapter 5 for more details.

Regarding the study of B.M. Irons, many researchers like P.G. Bergan [66] in 1980 and B. Specht [14] in 1988 tried to overcome the failure of the patch test by proposing a new set of polynomials. However, only B. Specht successfully constructed the element that passed the patch test. His element was proposed by using a new set of quartic polynomial to define the shape functions. However, the moderate accuracy of solutions could be obtained from this element.

To deal with different values of the mixed derivatives at shared vertices, Bogner

et al. [28] in 1966 proposed a bicubic quadrilateral element which included the mix-derivative as one of the nodal parameters at nodes. This element, called the Bogner-Fox-Schmidt element, had 16 degrees of freedom comprising of the unknown, the first derivatives and the mixed second derivative at corner nodes.

The Bogner-Fox-Schmidt element has been widely used with success. Prescribing an additional mix-derivative degree of freedom at the corner nodes in the element removed the problem of incompatibility of continuous functions at nodes. However, it has two main disadvantages. The first is that only structured mesh can be applied with this element. The second is that the normal slopes do not match continuously along boundaries when elements meet with different angles.

To circumvent the restriction of structured mesh in the Bogner-Fox-Schmidt, triangular elements have been taken into account. The reason for this is that rectangular elements are somewhat limited in their boundary shape applicability, whereas triangular elements can be used to represent almost any shape of boundary.

One way to deal with the second disadvantage is to constrain the mid-side node degree of freedom. This can be done by either using a macro-element or using higher order derivatives degrees of freedom. In what follows, we expand on these two approaches and people who developed them.

There are two kinds of element that can be used to construct a macro-element: quadrilateral and triangle. The quadrilateral macro-element was first introduced in 1968 by B. Fraeijs de Veubeke and G. Sander [10]. Two key triangular macro-elements were constructed by R. W. Clough and J. L. Tocher in 1966 [71] and M.J.D. Powell and M.A. Sabin in 1977 [54].

In the construction of the quadrilateral macro-element, B. Fraeijs de Veubeke and G. Sander employed cubic polynomials as shape functions. These shape functions were defined over each four triangular regions delimited by the edges of the quadrilateral and its diagonals. The way they defined degrees of freedom at nodes was similar to that of the Bogner-Fox-Schmidt element. The results showed that it satisfied continuity of unknowns and slopes at the interfaces and also showed good convergence characteristics.

The triangular element developed by R. W. Clough and J. L. Tocher was constructed by using cubic polynomials. It had in total 9 degrees of freedom consisting of

both unknown and its derivatives at each vertex. Note that this element was defined similarly to that of Zienkiewicz but the shape functions were defined over the sub-triangles. The element produced excellent results and was named the HCT element, after Hsieh, Clough and Tocher. Also, it provided nice C^1-continuity of the solutions.

It is worth noting that in the early stage of the C^1-element construction, the third-order (or cubic) polynomials gained popularity as shape functions for providing a C^1-continuity over the finite elements. Both complete and non-complete cubic polynomials were employed in the C^1-element constructions. In two dimensions a complete nth degree polynomial is given by

$$P_n(x, y) = \sum_{k=0}^{n} \alpha_{i,j} x^i y^j, \quad i + j \leq k, \tag{2.1}$$

where i and j are permuted accordingly, and $\alpha_{i,j}$ are coefficients. The number of terms in the nth degree complete polynomial is equal to $(n + 1)(n + 2)/2$. However, there were some attempts to construct interpolation functions with lower order polynomials such as quadratic polynomials [46], [54].

In 1971, L. Morley introduced what is now known as the Morley triangle [46] which had the lowest possible number of degrees of freedom to provide C^1-continuity. The shape functions were defined by using the quadratic polynomials with 6 degrees of freedom in total. Unfortunately, the Morley triangle came with a disadvantage. It did not converge for certain meshes and for general second order elliptic problems as illustrated in [73].

In 1977, M.J.D. Powell and M.A. Sabin [54] introduced the PSH (Powell-Sabin-Heindl) macro-element. Its shape functions were the piecewise quadratic defined over subtriangles. There are variations of the PSH macro-element classified by the number of subelements where 6 subelements are the minimal case. In general, the PSH element comes with 9 degrees of freedom corresponding to function values and the first derivatives at each vertex but an additional value of the mid-normal derivative can be introduced. The results showed that the PSH macro-elements were applicable to arbitrary shaped meshes.

A common advantage of aforementioned macro-elements is that they can greatly reduce the total number of degrees of freedom defined on an element and the computation time. However, these elements did not show reliable convergence behaviour for

some problems like gradient elasticity, see [63].

According to all discussions above, the degree of polynomials employed as a shape function were lower than or equal to cubic. This resulted in an inadequacy of terms in polynomial that employed to constrain the C^1-continuity along element boundaries. Also, lower rate of convergence can be seen. Therefore, using higher number degrees of freedom is another way to ensure the C^1-continuity along the boundary element and also to enhance the rate of convergence.

In 1966, R.W. Clough and C.A. Felippa [15] proposed an element with quadratic slope variation with 12 degrees of freedom defined over a triangle. The accuracy of the solutions by using this element were much improved compared to that of elements with lower number degrees of freedom discussed before.

In 1968, J. H. Argyris et al. [38] introduced a 21-dof triangular element. The element was constructed by using the complete fifth-order polynomial interpolations including all second derivatives at vertices and constraining normal derivatives at mid-side nodes. This element resulted in excellent accuracy and higher rate of convergence which was quintic. However, having normal derivatives at mid-side nodes as a degree of freedom made the element more difficult to impose boundary conditions.

Later on in 1969, K. Bell [43] introduced a reduced version of the Argyris element. It had 18 degrees of freedom with shape functions defined by a complete quartic and some terms from a quintic polynomials. The Bell element was constructed in order to neglect the normal derivatives at mid-side nodes in order to make the element more practical to implement. Eliminating the mid-side nodes degrees of freedom can effect only small loss of accuracy and a slightly drop of the convergence rate to be quartic. These features of the Bell element made it very attractive to use. More details can be seen later in Chapter 5.

There are still many more finite elements with different degrees of freedom and different sets of polynomials that provide C^1-continuity (see [4], [5], [11], [17], [29], [30], [44], [62]). However, the Argyris and the Bell triangles seem to be two well-known C^1-triangular elements that are widely used in many applications. One reason for their popularity is that very good accuracy and high rate of convergence are demonstrated from using the quartic and quintic shape functions.

In overall, we have that including higher order derivatives degrees of freedom can

make a finite element impractical. Even though a quartic or quintic element provides better accuracy and higher rate of convergence, the difficulties from imposing boundary conditions and physical interpretation make an element less attractive. Therefore, simple elements which have the unknown and its slopes derivative only as degrees of freedom at nodes are still of interest to many researchers.

2.2 A C^1-finite element with a curved boundary domain

It is worth noting that certain C^1-finite elements mentioned previously successfully satisfied the requirements of high accuracy and good convergence. Examples can be seen in [38], [43], [54], [71]. These elements were proved to obtain excellent results for a problem with straight boundary domains.

However, there are many engineering applications dealing with problems on a curved boundary domain. Such problems have been solved by many researchers with a common idea of approximating the curved edge with a series of straight-edged elements. Even though the straight-element approximation of the curved edge gives a fairly good accuracy, it is well known and is shown by many authors that such an approximation limit a convergence rate. Numerical evidences for this were given in some literature ([31], [56], [57], [65]).

In order to obtain the same accuracy and the same rate of convergence, several ways have been tried and proposed. In [16], [52], [57], [58], [59], special purpose elements were developed in order to be applicable with the second-order problems and in [7], [18], [56], [47] for the fourth-order problems.

Unfortunately, the methods derived for the second-order problems are not suitable for the fourth-order problems. The requirement of C^1-continuity makes the construction of a curved finite element in the fourth-order problem more difficult than one of the second order. When the fourth-order problem is implemented on a curved boundary, the use of C^1-curved finite elements is required .

In principle, there are two approaches to improve the accuracy of boundary approximation in the C^1-curved finite element: isoparametric and subparametric schemes.

2.2.1 Isoparametric scheme

An isoparametric scheme is the idea to represent parametric and geometric spaces by the same set of interpolation functions. Using higher degree of polynomial functions, rather than linear, to approximate the geometry is the crucial idea that improves accuracy in this scheme.

In 1973, R. Scott [70] presented an idea of the isoparametric method. In his study, a 2D finite element was studied with the mapping approximating the boundary was of any arbitrary order. However, it seemed rather impossible to extend this procedure to 3D elements.

In 1986, M. Lenoir [55] generalised the isoparametric idea developed by R. Scott to an arbitrary n-dimensional domain where the optimal error estimates for the finite element solutions of second-order elliptic problems were obtained.

Unfortunately, none of the elements constructed by Scott [70] and Lenoir [55] could be developed any further to represent an arbitrarily curved edge.

Recently, a study by P. Fischer [65] suggested big disadvantages of the linear geometric aprroximation in C^1-elements: poor geometric approximation and the restriction in the convergence behavior. In this study, numerical comparisons between various C^1-triangular elements with different degrees of interpolation functions illustrated the convergence restriction. With the linear geometry approximation to a curved boundary, it can also be seen that no visible difference in the convergence rates among elements. This result did not conform with the expectation that a higher polynomial order of element would show a better result.

In order to improve the isoparametric C^1-finite elements, the construction of meshes play an important role. Since the C^1-continuity is required in the fourth-order problem, meshes that represented the geometry need to be smooth. Therefore, the construction of isoparametric C^1-smooth mesh have to be developed. There are two key researchers that are noteworthy in this direction: P. Fischer et al. [64] and J. Petera and J. Pittman [41].

In the study of Petera and Pittman in 1994 [41], the mesh was constructed relating to the bilinear reference geometry. The algorithm was described by the minimisation of the quadratic expression with respect to the generalised coordinates.

In 2009, P. Fischer et al. [64] proposed another mesh construction by minimising

the values of the second-order derivatives of a generalised nodal position. The idea concerning these second-order derivatives comes from their observation that the variation of tangent vectors are of highest value along the points where non-smooth initial mesh with differently oriented elements meet.

Note that both studies of Petera and Pittman [41] and Fischer [64] applied their mesh constructions on the quadrilateral Bogner-Fox-Schmidt element.

The disadvantage of the mesh construction algorithm presented by P. Fischer [64] is the requirement of geometric boundary conditions for the minimisation problem. This makes the algorithm of Petera and Pittman [41] easier to implement than the one in Fischer's [64]. On the other hand, the advantage of the Fischer algorithm [64] for the mesh construction is that it gives higher quality meshes. This opposes to the result obtained from Petera and Pittman which, relatively, has a poor quality of mesh. Also, the Fischer method results in more accurate solutions than those of Petera and Pittman as illustrated in [64].

The performance and applicability of a numerical method of these isoparametric elements is also presented in the study given by A. Zervos et al. [8]. Nevertheless, it is noteworthy that only the isoparametric quadrilateral Boxner-Fox-Schmidt element is considered in most of isoparametric literature.

Due to the good ability of isoparametric meshes in a curved boundary approximation, P. Fischer [63] extended the isoparametric idea further from a quadrilateral element to a triangular element. In the Appendix of his thesis, Fischer tried to construct the C^1-continuous isoparametric finite elements by using the optimisation algorithm presented by himself [64] to smooth the mesh and applying it to the triangular Bell element. This was the first time that isoparametric triangular elements with unstructured meshes were used to solve a fourth-order problem.

In his construction of the isoparametric triangular Bell elements, he employed the "Lagrange parameters"to construct the shape of triangles by introducing some conditions to an angle at nodes. The mesh optimization proposed in [64] was applied to smooth the domain geometry. The finite element implementations of the triangular Bell element showed that nice C^1-continuous solutions with good accuracy were obtained. These nice results were obtained when boundaries of the domain were convex.

However, when a more complex geometry, a plate with a hole at the centre, was discretised, small discontinuities of the solutions occurred within the mesh construction at the semicircular boundary of the hole. This was resulted from using the "Lagrange parameters"to construct the shape of the triangles. Unfortunately, an optimally conditioned system of equations cannot be obtained and it can be satisfied up to only a small numerical error. Therefore, this leads to an error in the solution.

Besides the difficulties in the mesh construction, the use of isoparametric triangular elements introduces second-order derivatives for the interpolation of the geometry which increases the complexity of the boundary interpolation. The construction of an isoparametric C^1-continuous function is not so easy and hence only little work has been done in the field of isoparametric C^1-finite elements.

2.2.2 Subparametric scheme

In the classical subparametric element, the domain of interest is represented by a linear approximation. Using such a linear mapping between the reference and physical geometry has the advantage of minimising the complexity of the boundary interpolation as the mapping is affine. However, it still does not solve the problem of poor boundary approximation of the curved boundary. In order to provide an accurate approximation of the curved boundary, one curve-sided element can be used.

The curved finite element constructions were initially developed for dealing with the second-order problems (in the work of Olson and Lindberg [52], and Zlamal [57]). Later on, these constructions were extended further to be applicable to the fourth-order problem (in the work of Zenisek [7], Qing and Li [34], Mansfield [44], Chernuka [56], and Bernadou [48]).

In 1969, Olson and Lindberg [52] developed annular and circular sector finite elements in the second-order problem that permitted the exact representation of circular boundaries. But, this element could not be developed any further to represent an arbitrarily curved edge.

In 1973, Zlamal [57] presented the transformation from the reference triangle to the physical triangle, for the second-order problem, that could approximate a curved boundary. This transformation was defined by including the nonlinear mapping only for the side of the reference triangle associated with the curved boundary and keeping

the transformation of the other two sides to be linear. It was employed only along the curved part of the boundary.

The disadvantage of Zlamal's element was that the transformation was restricted to the second-order problem. However, it was still suitable for solving boundary value problems with an arbitrary boundary. The numerical results given in the study of Zlamal showed a remarkable improvement in accuracy. Therefore, these curved elements were very promising as we can get the same order of accuracy as when the original boundary is a polygon. The proof of the approximation theorem and error bounds for a model problem concerning the order of accuracy can be found in [58], [59].

Overall, the work of M. Zlamal ([57], [58], [59]) was an achievement in the construction of a curved finite element for the second order problems.

In 1972, M. W. Chernuka et al. [56] worked on a similar element for the fourth-order problem. In order to consider circular and elliptical plate bending problems with curved boundaries, they modified each triangle to include one curved and two straight edges. In their study, the polynomial space was defined over the original triangle with no modification in the shape functions.

A disadvantage of this element was that the areas of integration changed and were extended over the additional curved area. This additional area of integration from the extended curve made the method even more difficult when complicated integrands were involved. This made the method unpopular and impractical, even though the results obtained from this method gave excellent accuracy and good convergence rate.

The method used by Chernuka et al. was similar but independently developed from Zlamal's. The next four methods introduced here are variations of Zlamal's method in [57], [58], and [59] but for the fourth-order problems.

In 1978, Mansfield [44] presented a method which reduced the effect of the extension of the area integration referred to. His method was a combination of Zlamal's idea of separating the coordinate transformation and the definition of the C^1-finite elements on the standard triangle. Later on, this method was modified and generalised to C^m-elements by Zenisek [7].

A common disadvantage of both Mansfield and Zenisek's methods was that they provide the solution on the approximate but not the real domain. Hence, the approximate solution they provided was not satisfy the boundary conditions of the real

domain.

In 1993, M. Bernadou [48] constructed another curved finite elements compatible with the Argyris triangle and the Bell triangle. He employed a similar idea to that of M.W. Chernuka et al. [56] and Zlamal [57] where a triangle was modified to have one curved side. Each curved finite element was constructed in correspondence with a reference element which makes this method very straightforward to work in numerical integration. On the other hand, working on the reference element was more complicated than the corresponding straight finite elements. The shape functions used more degrees of freedom to define the curved element in order to be compatible with the Argyris or the Bell triangle.

The detailed description of how to implement such curved C^1-elements and some numerical results can be found in [49], [50], [51].

In 1996, G. Qing and L. Li [34] extended M. Bernadou's work further to modify and construct more efficient and accurate curved C^1-finite elements which satisfy given boundary conditions on the approximate boundary.

The curved finite elements constructed in both [34] and [48] were quite powerful in approximating the fourth-order problems on curved boundary domains and, in both, the associate curved elements retained the convergence rate with good accuracy. Nevertheless, the implementation of the curved C^1-finite element is more expensive than using just straight finite elements as will show later on in chapter 6 and can alternatively be found in [34], [49]. This, in my opinion, might be what limits the use of these elements and motivates some developments from different approaches.

2.3 Alternative methods of C^1 problems dealing with a straight boundary domain

Due to the complexity of C^1-finite element constructions, many alternative approaches have been introduced to implement problems which require the derivatives continuity. These approaches are developed in order to obtain interpolation functions without requirements of the C^1-continuity. Meshless (or meshfree) methods, penalty parameters, Lagrange multipliers are examples of alternative methods when dealing with the implementation of the fourth order problem on the straight boundary domain.

Meshless or meshfree methods is defined to directly use the geometry of the simulated domain for calculations as oppose to the traditional finite element method that relied on a grid or a mesh. The discretisation for this method is usually based on a set of nodes.

The construction of the shape functions in the meshless method is flexible with a help of the weight functions. The constructed shape functions consist of only nodal displacements degrees of freedom where their continuity is primarily governed by the continuity of the weight function. Therefore, the accuracy of the method can be easily optimised by the choice of the weight functions and thus the numerical approach is greatly simplified.

Examples in this regime are as follows. The Meshless Local Petrov-Galerkin Method (MLPG), was introduced by Z. Tang et al. [85] for higher-order problems. In another study by H. Askes and E. C. Aifantis [36], linear gradient elasticity was modelled with the Element Free Galerkin Method (EFG). P. Krysl et al. [68] applied the Element-Free Galerkin (EFG) method to thin (Kirchhoff) plates.

In the penalty method, a penalty parameter is introduced to form a series of unconstrained problems by adding this parameter to the constrained function. The selection of the penalty parameter is arbitrary and depends on the smoothness of the original problem. Since the penalty method is of C^0-continuity, it is much simpler than C^1 finite element methods. Examples of this method applied to the fourth order problems can be found in the studies of S. C. Brenner and L. Y. Sang [73] and I. Babuska and M. Zlamal [37].

Regarding the Lagrange multiplier method, it is usually used to enforce the essential boundary conditions in other approaches like the meshless method for instance. Examples can be found in the studies by P. Krysl and T. Belytschko [68] and Shu et al. [42].

All of the studies mentioned in [36], [37], [42], [68], [85], provide good quality approximate solutions. Also, these methods can reduce complexity of using higher order derivatives degrees of freedom required in C^1-element so that numerical treatment such as boundary conditions can be simplified.

However, these alternatives come along with different numerical problems. One of their disadvantages is that a high number of degrees of freedom has to be used for the

additional approximation fields. This is the consequence of their shape functions are, by definitions, of higher continuity and carry only nodal value. Therefore, many nodal values have to be defined on an element to be ensure the C^1-continuity.

Even though these methods can reduce complexity of using higher order derivatives degrees of freedom required in C^1-element, they involve another drawback in some problems like the thin shell. The difficulties of undesired physical results are encountered when using C^0-elements for example shear and membrane locking.

Shear and membrane locking are physical phenomena that describe a stiffening effect in finite element method. An inadequate representation of certain deformations results in making the elements behave too stiff. Hence, the implementation often illustrates poor performance and can lead to wrong results.

2.4 Alternative methods of C^1 problems dealing with a curved boundary domain

Regarding a C^1-finite element with a curved boundary domain, many efforts have been undertaken to improve a boundary approximation and to overcome the limitation of convergence rate. We note that a finite element mesh, which is an approximation of the geometry, can in many situations create errors in numerical results. To overcome this geometric error, isogeometric analysis and Subdivision surfaces are two alternative approaches that have been employed by many authors.

The isogeometric framework has been introduced by T.J.R. Hughes, et al. in 2005 [79]. Owing to an important role in engineering designs of Computer Aided Design (CAD) to approximate the complex geometry, Hughes and his colleagues adopted the functions that employed in the CADs geometric description to use for the analysis. These functions typically are B-splines or nonuniform rational B-splines (NURBS) functions. Therefore, in the isogeometric analysis (IGA) presented by Hughes et al., those basis functions that represent the geometry become a basis for the solution space of variational formulations of the problem as well.

Subdivision surfaces are another research scheme that has been employed to produce smooth curves and surfaces for many years. The idea of the method is that each finer mesh is obtained from a coarse mesh by using a recursively subdivision scheme.

Many schemes have been proposed and employed which, in turn, lead to limit surfaces with different smoothness characteristics. The most often employed schemes are from C. Loop [19] and E. Catmull [24] since they are closely related to splines and generate C^2-continuous surfaces over arbitrary meshes. However, the subdivision surfaces was recently emerged with finite element analysis by F. Cirak et al. [26]. Their work is based on the framework of the Kirchhoff-Love theory of thin shells with Loop's subdivision scheme. The interpolation functions are described locally by quartic box splines.

Even though these methods arise as an alternative of the finite element method, they have some drawbacks. Non-locality is one disadvantage of the subdivision surfaces. In this scheme, the interpolation of displacement field over one element depends not only on the nodal values of the element nodes but also depends on those from the nodes of neighbouring elements. This was described in the work of F. Cirak et al. [26]. Unlike the curved C^1-elements, the elements constructed from both the isogeometric and subdivision schemes have just the nodal value prescribed at nodes. This makes the methods more difficult to handle when dealing with boundary conditions of clamped edge problems as derivatives are involved.

On the other hand, these methods also provide advantages over the curved C^1-finite elements. Both the isogeometric analysis and subdivision surfaces decrease a number of degrees of freedom used in the finite element implementation. Only the unknown values are carried at nodes. As a consequence, this reduces the coding and computational time which is relatively costly in the curved C^1-implementation. Also, no nodal rotations are used in the interpolation of these alternative methods as opposed to the C^1-elements that have many degrees of freedom including first and higher order derivatives and are difficult to implement. Moreover, numerical tests demonstrate the high accuracy and optimal rate of convergence for both schemes. Evidence can be found in the numerical study in [26], [79].

Regarding their simplicity of carrying only the unknown value at nodes, many engineering applications employ these alternative approaches. Examples are in problems of linear and nonlinear static and dynamic analysis of thin-wall structures, fluid mechanics, fluid structure interaction and others (see [22], [23], [67], [75], [77], [82], [27]). Moreover, some works have been extended from the idea of initial work to obtain more

accurate results and to generalise an idea. Recently, in the isogeometric analysis, Y. Bazilevs et.al. [83] altered a basis function to be T-spline function in order to generalise the method from using NURBS. In T-spline isogeometric analysis which defined similarly as NURBS, reducing the number of superfluous control points in NURBS is the generalise idea to allow local refinements in the mesh. The accuracy of results obtained from the isogeometric T-spline is good in all cases in their study.

Chapter 3

Mechanics of a thin-elastic material with a small strain

3.1 Introduction

An elastic material is defined to have a physical property that the material can return to its original shape after applied forces (stress) are removed. A shell is defined as a thin three-dimensional elastic body where the thickness, h, is smaller compared to the other two dimensions. Many analyses of thin shells neglect the effect of the transverse shear and follow the theory of Kirchhoff-Love. This theory states that a normal vector of the undeformed mid-surface remains normal to the deformed mid-surface throughout the deformation and it deforms inextensionally.

Employing the Kirchhoff-Love assumption in a shell theory intends to reduce the dimension of a shell from the three-dimensional to the two-dimensional theory. Therefore, the shell governing equation which is derived from the principle of virtual displacement can be reduced to two-dimensional space. This is a result of allowing the integration in the coordinate perpendicular to the mid-surface to be carried out analytically. Therefore, all quantities can be expressed only on the two Lagrangian coordinates of the mid-surface.

Since the elastic material under consideration is a thin shell, the structure can experience large deflections and rotations, although strains and stresses may remain small. In such thin bodies, an assumption for small strains is employed to simplify

excessive deflections. This has been done by employing the linear (or Hookean) constitutive equation to represent the stress components as a linear function of all strain components.

In section 3.2, we will firstly introduce shell kinematics, where quantities in the undeformed and deformed configurations will be defined. Next, the concept of stress and the linear (or Hookean) constitutive law will be discussed in section 3.3. Also, the dimensional reduction of the governing equations will be derived afterwards in this section by applying the Kirchhoff-Love assumption and using only the mid-surface coordinates. Finally, section 3.4 closes this chapter with the linearisation of the governing equations with a small strain for a beam and a shell as you will see in section 3.4.1 and 3.4.2, respectively.

3.2 Deformation

In this section, the general theory for the deformation of an elastic material will be presented first. This will begin by introducing an elastic material which is parametrised by three-dimensional coordinate lines $\xi_j; j = 1, 2, 3$. The kinematics of a shell with the Kirchhoff-Love assumption will be discussed afterwards so that all shell's quantities is rather expressed by two-dimensional coordinates on the midplane.

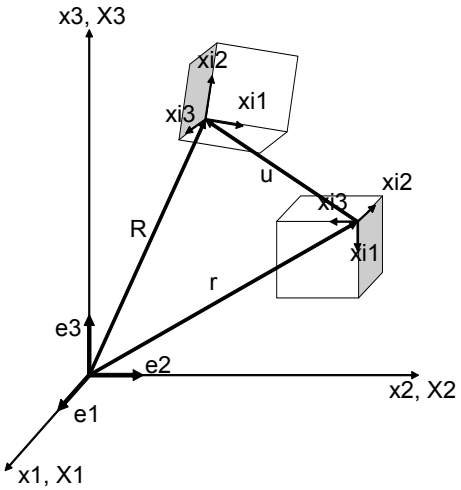

Figure 3.1: Geometry of an elastic material in the undeformed and deformed configurations.

Let $\mathbf{r} = \mathbf{r}(\xi_j) = x_k(\xi_j)\mathbf{e}_k$, and $\mathbf{R} = \mathbf{R}(\xi_j) = X_k(\xi_j)\mathbf{e}_k$, denote the position vectors of any point in the undeformed and deformed configurations of an elastic material,

respectively, and $\mathbf{e}_k$ are usual bases of Cartesian coordinates as depicted in Fig. 3.1. These positions are parametrised by the coordinate ξ_j. Therefore, the corresponding base vectors in the undeformed and deformed configurations can be defined as

$$\begin{aligned} \mathbf{g}_j &= \mathbf{r}_{,j} = x_{k,j}\mathbf{e}_k, \\ \mathbf{G}_j &= \mathbf{R}_{,j} = X_{k,j}\mathbf{e}_k, \end{aligned} \tag{3.1}$$

respectively. Note that the comma preceding the subscript j signifies partial differentiation with respect to the coordinate ξ_j.

Throughout this study, the convention of summation over indices is used. A Latin index represents any of the numbers $1, 2, 3$ $(1, 2)$ to the number of material's dimension and a Greek index represents the numbers $1, 2$ (1) to the number of material's dimension minus one. Also, the lowercase and the uppercase letters will be use for all quantities associated with the undeformed and deformed configurations, respectively.

The base vectors in (3.1) are tangential to the associated coordinate line ξ_j. Therefore, they are called tangent base vectors and also known as the covariant base vectors. However, there is another set of base vectors which is normal to the coordinate surfaces. Let us define the normal base vectors $\mathbf{g}^j$ and $\mathbf{G}^j$ such that

$$\mathbf{g}^i \cdot \mathbf{g}_j = \mathbf{G}^i \cdot \mathbf{G}_j = \delta^i_j, \tag{3.2}$$

where $\mathbf{g}^j$ and $\mathbf{G}^j$ denote normal base vectors to coordinate surface ξ_j of the undeformed and deformed configurations, respectively. These normal base vectors are also known as the contravariant base vectors. Also, δ^i_j denotes the Kronecker delta illustrating unity when indices $i = j$.

In general, these tangent and normal base vectors are not unit vectors. It can be seen from (3.2) that the contravariant base vectors $\mathbf{g}^j$ are perpendicular to the two covariant base vector $\mathbf{g}_i, i \neq j$. Furthermore, the tangent base vector $\mathbf{g}_i$ can be written as a linear combination of the contravriant base vectors $\mathbf{g}^j$ as

$$\mathbf{g}_i = g_{ij}\mathbf{g}^j, \tag{3.3}$$

and vice versa

$$\mathbf{g}^i = g^{ij}\mathbf{g}_j, \tag{3.4}$$

where the g_{ij} and g^{ij} are second order tensors.

The derivatives of a tangent base vector in accordance with (3.1) is

$$\begin{aligned}\mathbf{g}_{i,j} &\equiv \frac{\partial \mathbf{g}_i}{\partial \xi_j} \\ &= \frac{\partial^2 \mathbf{r}}{\partial \xi_i \partial \xi_j} \\ &= \frac{\partial^2 x_k}{\partial \xi_i \partial \xi_j}\mathbf{e}_k,\end{aligned} \tag{3.5}$$

where x_k is a k-th component of a position vector $\mathbf{r}$ in the direction of the vector $\mathbf{e}_k$. Since the derivatives are assumed to be continuous, we have

$$\mathbf{g}_{i,j} = \mathbf{g}_{j,i}.$$

Furthermore, the vectors $\mathbf{g}_{i,j}$ can be expressed as a linear combination of the base vectors $\mathbf{g}_k$ or $\mathbf{g}^k$ as

$$\mathbf{g}_{i,j} = \Gamma_{ijk}\mathbf{g}^k = \Gamma^k_{ij}\mathbf{g}_k, \tag{3.6}$$

where the coefficients are defined by

$$\Gamma_{ijk} = \mathbf{g}_k \cdot \mathbf{g}_{i,j}, \quad \Gamma^k_{ij} = \mathbf{g}^k \cdot \mathbf{g}_{i,j}. \tag{3.7}$$

The coefficients Γ_{ijk} and Γ^k_{ij} are known as the Christoffel symbols of the first and second kind, respectively [35]. Note that the symbol is symmetric in two lower indices, that is

$$\begin{aligned}\Gamma^k_{ij} &= \mathbf{g}^k \cdot \mathbf{g}_{i,j} \\ &= \mathbf{g}^k \cdot \mathbf{g}_{j,i} \\ &= \Gamma^k_{ji}.\end{aligned} \tag{3.8}$$

Similarly, $\Gamma_{ijk} = \Gamma_{jik}$.

An infinitesimal line element ds in the undeformed configuration is given by

$$ds = \mathbf{r}_{,j}d\xi_j = \mathbf{g}_j d\xi_j, \tag{3.9}$$

and the square of its length is

$$\begin{aligned}(ds)^2 &= d\mathbf{r} \cdot d\mathbf{r} \\ &= \mathbf{g}_i d\xi_i \cdot \mathbf{g}_j d\xi_j \\ &= \mathbf{g}_i \cdot \mathbf{g}_j d\xi_i d\xi_j \\ &= g_{ij} d\xi_i d\xi_j.\end{aligned} \tag{3.10}$$

Similarly, the infinitesimal line element dS and the square of its length in the deformed configuration are defined as

$$\begin{aligned} dS &= \mathbf{R}_{,j} d\xi_j = \mathbf{G}_j d\xi_j, \\ (dS)^2 &= \mathbf{G}_i d\xi_i \cdot \mathbf{G}_j d\xi_j \\ &= \mathbf{G}_i \cdot \mathbf{G}_j d\xi_i d\xi_j \\ &= G_{ij} d\xi_i d\xi_j. \end{aligned} \tag{3.11}$$

We have that the coefficients $g_{ij} = \mathbf{g}_i \cdot \mathbf{g}_j$ and $G_{ij} = \mathbf{G}_i \cdot \mathbf{G}_j$ are components of the undeformed and deformed metric tensors, respectively. These components are fundamental in differential geometry as they provide the measure of length along the ξ_j coordinate line when $i \neq j$. Also, a component where $i \neq j$ determines the angle between ξ_i and ξ_j line elements in a coordinate system.

Furthermore, an infinitesimal area element da_i which is perpendicular to the coordinates line ξ_i in the undeformed and deformed configurations are given by

$$\begin{aligned} da_i &= |\mathbf{r}_{,j} \times \mathbf{r}_{,k}| d\xi_j d\xi_k, \quad (i \neq j \neq k), \\ &= |\mathbf{g}_j \times \mathbf{g}_k| d\xi_j d\xi_k, \quad (i \neq j \neq k), \\ &= \sqrt{g}\sqrt{g_{(ii)}} d\xi_j d\xi_k, \quad (i \neq j \neq k), \end{aligned} \tag{3.12}$$

$$\begin{aligned} dA_i &= |\mathbf{R}_{,j} \times \mathbf{R}_{,k}| d\xi_j d\xi_k, \quad (i \neq j \neq k), \\ &= |\mathbf{G}_j \times \mathbf{G}_k| d\xi_j d\xi_k \quad (i \neq j \neq k), \\ &= \sqrt{G}\sqrt{G_{(ii)}} d\xi_j d\xi_k, \quad (i \neq j \neq k), \end{aligned} \tag{3.13}$$

where $g = \det(g_{ij})$ and $G = \det(G_{ij})$. Hence, infinitesimal area elements in the mid-plane surface $\xi_3 = const$ in the undeformed and deformed configurations are given by

$$\begin{aligned} da_3 &= |\mathbf{g}_1 \times \mathbf{g}_2| d\xi_1 d\xi_2, \\ &= \sqrt{g}\sqrt{g_{(33)}} d\xi_1 d\xi_2, \\ &= \sqrt{g} d\xi_1 d\xi_2, \end{aligned} \tag{3.14}$$

$$\begin{aligned} dA_3 &= |\mathbf{G}_1 \times \mathbf{G}_2| d\xi_1 d\xi_2, \\ &= \sqrt{G}\sqrt{G_{(33)}} d\xi_1 d\xi_2, \\ &= \sqrt{G} d\xi_1 d\xi_2, \end{aligned} \tag{3.15}$$

respectively.

An infinitesimal volume element dv in the undeformed and deformed configurations are defined by

$$\begin{aligned} dv &= \mathbf{r}_{,1} \cdot (\mathbf{r}_{,2} \times \mathbf{r}_{,3}) d\xi_1 d\xi_2 d\xi_3 \\ &= \mathbf{g}_1 \cdot (\mathbf{g}_2 \times \mathbf{g}_3) d\xi_1 d\xi_2 d\xi_3 \\ &= \sqrt{g} d\xi_1 d\xi_2 d\xi_3, \end{aligned} \tag{3.16}$$

$$\begin{aligned} dV &= \mathbf{R}_{,1} \cdot (\mathbf{R}_{,2} \times \mathbf{R}_{,3}) d\xi_1 d\xi_2 d\xi_3 \\ &= \mathbf{G}_1 \cdot (\mathbf{G}_2 \times \mathbf{G}_3) d\xi_1 d\xi_2 d\xi_3 \\ &= \sqrt{G} d\xi_1 d\xi_2 d\xi_3. \end{aligned} \tag{3.17}$$

The deformation of a body is determined by the displacement field $\mathbf{u}$ which can be determined from the difference between the referenced position $\mathbf{r}(\xi_i)$ and a new position $\mathbf{R}(\xi_i)$ as

$$\mathbf{u}(\xi_i) = \mathbf{R}(\xi_i) - \mathbf{r}(\xi_i). \tag{3.18}$$

To determine a component of a displacement field, either the Cartesian or the tangential base vectors can be considered as its basis. In our study, we determine a component of a displacement field as a linear combination of the base vectors. Thus, a displacement vector $\mathbf{u}$ can be written as

$$\mathbf{u} = \mathbf{u}(\xi_i) = u_k(\xi_i)\mathbf{g}^k = u^k(\xi_i)\mathbf{g}_k, \tag{3.19}$$

where u_k and u^k is a k-th component of the displacement $\mathbf{u}$ in the direction of the base vector $\mathbf{g}^k$ and $\mathbf{g}_k$, respectively.

Since the deformation of a body is manifested by the extension of coordinate lines and the distortion of angles between coordinate lines, the measurement of those geometrical quantities can provide some information of how the body deforms. In the initial system, extensions and distortions are determined by the metric tensor g_{ij} while those of the deformed system are considered by the metric tensor G_{ij}. Therefore, a strain tensor which is the measurement of the deformation can be mathematically defined as

$$\epsilon_{ij} = \frac{1}{2}(G_{ij} - g_{ij}). \tag{3.20}$$

This is the so-called Green-Lagrange strain tensor which considers from the difference between the undeformed and deformed metric tensors g_{ij} and G_{ij}.

To develop a mathematical description of a deformation of a three-dimensional shell, we consider a shell geometry illustrated in Fig. 3.2. From the thinness feature of a shell, its geometry is allowed to specify by the two-dimensional reference surface and its thickness. We can choose the coordinate $\xi_3 = 0$ to be the shell's mid-surface and the reference surface. Therefore, we have that two coordinates ξ_1 and ξ_2 are located on the reference surface where the third coordinate ξ_3 is normal to the reference surface. The upper and lower surfaces of the shell have the coordinates $\xi_3 = h/2$ and $\xi_3 = -h/2$, respectively, where h is the thickness of the shell.

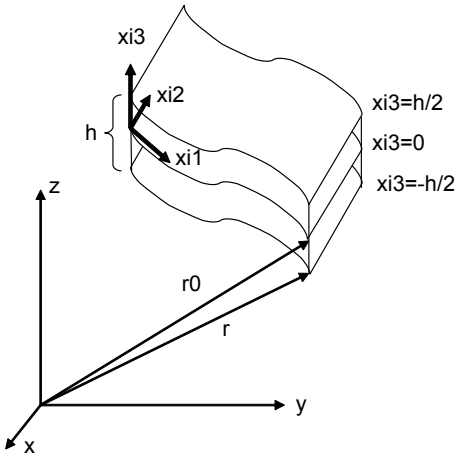

Figure 3.2: A shell geometry.

Let $\mathbf{r}^0(\xi_\alpha)$, and $\mathbf{R}^0(\xi_\alpha)$, denote the position vectors of any point on the mid-surface of the undeformed and deformed configurations, respectively, which are parametrised by the mid-surface coordinates $\xi_\alpha, \alpha = 1, 2,$. From the Kirchhoff-Love theory, the position of the undeformed and deformed configurations of any point on the body can be written in terms of those positions on the midplane coordinates and its thickness as

$$\mathbf{r}(\xi_j) = \mathbf{r}^0(\xi_\alpha) + \xi_3 \hat{\mathbf{n}}(\xi_\alpha), \tag{3.21}$$

and

$$\mathbf{R}(\xi_j) = \mathbf{R}^0(\xi_\alpha) + \xi_3 \hat{\mathbf{N}}(\xi_\alpha), \tag{3.22}$$

where $\hat{\mathbf{n}}$ and $\hat{\mathbf{N}}$ denote the unit normals to the midplane surface of undeformed and deformed configurations, respectively, and can be computed as

$$\begin{aligned} \hat{\mathbf{n}} &= \frac{\mathbf{g}_1 \times \mathbf{g}_2}{|\mathbf{g}_1 \times \mathbf{g}_2|}, \\ \hat{\mathbf{N}} &= \frac{\mathbf{G}_1 \times \mathbf{G}_2}{\mathbf{G}_1 \times \mathbf{G}_2}. \end{aligned} \tag{3.23}$$

The Kirchhoff-Love shell assumption is very useful to represent the displacement throughout the elastic body by a quantity on the midplane surface. Therefore, the thin body of consideration will employ the differential geometry on the reference midplane surface to represent the entire body's deformation.

Before we will represent quantities in the shell by using the Kirchhoff-Love shell assumption, let us consider quantities on the midplane $\xi_3 = 0$. We have that all quantities of the undeformed, deformed and displacement of a material point on the shell's midplane can be expressed by

$$\begin{aligned} \mathbf{r}(\xi_j) &= \mathbf{r}^0(\xi_\alpha), \\ \mathbf{R}(\xi_j) &= \mathbf{R}^0(\xi_\alpha), \\ \mathbf{u}(\xi_j) &= \mathbf{u}^0(\xi_\alpha). \end{aligned} \tag{3.24}$$

Also, the corresponding base vectors to the coordinate lines ξ_α on the midplane are given by

$$\begin{aligned} \mathbf{r}_{,\beta}(\xi_j) &= \mathbf{r}^0_{,\beta}(\xi_\alpha) \equiv \mathbf{t}_\beta, \\ \mathbf{R}_{,\beta}(\xi_j) &= \mathbf{R}^0_{,\beta}(\xi_\alpha) \equiv \mathbf{T}_\beta, \end{aligned} \tag{3.25}$$

for the undeformed and deformed coordinate line β on a mid-surface, respectively.

By (3.21) and (3.22), the corresponding tangent base vectors at an arbitrary material point in a shell are

$$\begin{aligned} \mathbf{g}_\alpha = \mathbf{r}_{,\alpha} &= \mathbf{r}^0_{,\alpha} + \xi_3 \hat{\mathbf{n}}_{,\alpha}, \\ &= \mathbf{r}^0_{,\alpha} + \xi_3 \mathbf{t}_{3,\alpha}, \\ &= \mathbf{t}_\alpha + \xi_3 \mathbf{t}_{3,\alpha}, \end{aligned} \tag{3.26}$$

$$\begin{aligned} \mathbf{G}_\alpha = \mathbf{R}_{,\alpha} &= \mathbf{R}^0_{,\alpha} + \xi_3 \hat{\mathbf{N}}_{,\alpha}, \\ &= \mathbf{R}^0_{,\alpha} + \xi_3 \mathbf{T}_{3,\alpha}, \\ &= \mathbf{T}_\alpha + \xi_3 \mathbf{T}_{3,\alpha}, \end{aligned} \tag{3.27}$$

for the undeformed and deformed configurations, respectively.

The derivative of the base vector $\mathbf{t}_3$ with respect to the midplane coordinate ξ_α can be considered by decomposing into the midplane base vector as

$$\mathbf{t}_{3,\alpha} = -b_{\alpha\beta}\mathbf{t}^\beta = -b^\beta_\alpha \mathbf{t}_\beta, \tag{3.28}$$

where

$$b_{\alpha\beta} = b_{\beta\alpha} = -\mathbf{t}_\beta \cdot \mathbf{t}_{3,\alpha}, \tag{3.29}$$

and

$$b_{\alpha}^{\beta} = b_{\alpha\gamma}t^{\gamma\beta} = -\mathbf{t}^{\beta} \cdot \mathbf{t}_{3,\alpha}, \tag{3.30}$$

are the covariant and mixed variance curvature tensors of the undeformed midplane, respectively. In the deformed configuration, the derivative of the base vector $\mathbf{T}_{3,\alpha}$ can be considered similarly as

$$\mathbf{T}_{3,\alpha} = -B_{\alpha\beta}\mathbf{T}^{\beta} = -B_{\alpha}^{\beta}\mathbf{T}_{\beta}, \tag{3.31}$$

where

$$B_{\alpha\beta} = B_{\beta\alpha} = -\mathbf{T}_{\beta} \cdot \mathbf{T}_{3,\alpha}, \tag{3.32}$$

and

$$B_{\alpha}^{\beta} = B_{\alpha\gamma}T^{\gamma\beta} = -\mathbf{T}^{\beta} \cdot \mathbf{T}_{3,\alpha}, \tag{3.33}$$

are the covariant and mixed variance curvature tensors of the deformed midplane, respectively. With (3.28) and (3.31), the off-midplane base vectors $\mathbf{g}_{\alpha}$ in (3.26) and $\mathbf{G}_{\alpha}$ in (3.27) can be written as

$$\mathbf{g}_{\alpha} = \mathbf{t}_{\alpha} - \xi_3 b_{\alpha\beta}\mathbf{t}^{\beta} = \mathbf{t}_{\alpha} - \xi_3 b_{\alpha}^{\beta}\mathbf{t}_{\beta}, \tag{3.34}$$

$$\mathbf{G}_{\alpha} = \mathbf{T}_{\alpha} - \xi_3 B_{\alpha\beta}\mathbf{T}^{\beta} = \mathbf{T}_{\alpha} - \xi_3 B_{\alpha}^{\beta}\mathbf{T}_{\beta}, \tag{3.35}$$

respectively.

Next, we consider the components of the off-midplane metric tensor g_{ij} and G_{ij} of the undeformed and deformed configurations. We have that

$$\begin{aligned} g_{\alpha\beta} &= t_{\alpha\beta} - 2\xi_3 t_{\alpha\beta} + (\xi_3)^2 b_{\alpha\gamma}b_{\beta}^{\gamma}, \\ g_{\alpha 3} &= 0 \quad \text{and} \quad g_{33} = 1. \end{aligned} \tag{3.36}$$

The last line obtains from the fact that the base vector $\mathbf{g}_3$ is normal to the mid-surface's base vectors and it is a unit vector. Also, the components of the off-midplane metric tensor G_{ij} in the deformed configuration is given by

$$\begin{aligned} G_{\alpha\beta} &= T_{\alpha\beta} - 2\xi_3 T_{\alpha\beta} + (\xi_3)^2 B_{\alpha\gamma}B_{\beta}^{\gamma}, \\ G_{\alpha 3} &= 0 \quad \text{and} \quad G_{33} = 1. \end{aligned} \tag{3.37}$$

According to the Kirchhoff-Love assumption, the deformation of the midplane fully determines the deformation of the entire shell. Hence, the strain tensor ϵ_{ij} can be

expressed in terms of the change of the midplane metric and curvature tensors during the deformation as in (3.38). This can be worked out by a straightforward algebra from (3.20), (3.36), and (3.37).

$$\epsilon_{\alpha\beta} = \gamma_{\alpha\beta} + \xi_3\kappa_{\alpha\beta} + (\xi_3)^2\bar{\kappa}_{\alpha\beta}, \tag{3.38}$$

where

$$\gamma_{\alpha\beta} = \frac{1}{2}\left(T_{\alpha\beta} - t_{\alpha\beta}\right), \tag{3.39}$$

is the midplane strain tensor and

$$\kappa_{\alpha\beta} = -(B_{\alpha\beta} - b_{\alpha\beta}), \tag{3.40}$$

is the bending tensor and the last tensor $\bar{\kappa}_{\alpha\beta}$ is given by

$$\bar{\kappa}_{\alpha\beta} = \frac{1}{2}(B^{\gamma}_{\alpha}B_{\beta\gamma} - b^{\gamma}_{\alpha}b_{\beta\gamma}). \tag{3.41}$$

3.3 The governing equation of a thin-shell material with a small strain

In this section, we will formulate the governing equation of a thin shell from the principle of virtual displacements based on the assumption of a small strain. The concept of virtual displacement is based upon the principle variations of work and energy which states that, at the equilibrium, the strain energy changed due to a small virtual displacement (internal forces) is equal to the work done by the (external) forces in moving through the virtual displacement (see [1], [35]). Therefore, to derive the governing equation of a thin shell, the equilibrium equation of the internal and external forces has to be considered.

Previously in section 3.2, we introduced the concept of strain to describe the deformation of a point in a body. Before we will derive the governing equation of a thin shell, let us now introduce the concept of stress which can be described as the distribution of forces interacting on a body. The stress vector σ^i is defined as follow

$$\sigma^i = \lim_{\Delta S \to 0} \frac{\Delta F}{\Delta S_i}, \tag{3.42}$$

where ΔF is a force acting on the elemental area ΔS_i which is normal to the coordinate line ξ_i. Furthermore, the stress vector σ^i can be decomposed into components σ^{ij} in

the direction of a unit vector of the ξ_j coordinate line. These components σ^{ij} are called the physical components of the stress vector.

In general, the stress vector σ^i can be decomposed into either the base vectors of the undeformed or the deformed configurations. For instance, a component σ^{ij} in the direction of a defomed based vector $\hat{\mathbf{G}}_j$ can be expressed by

$$\begin{aligned} \sigma^i &= \sigma^{ij}\hat{\mathbf{G}}_j \\ &= \sigma^{ij}\frac{\mathbf{G}_j}{\sqrt{G_{(jj)}}}, \end{aligned} \tag{3.43}$$

where both $\hat{\mathbf{G}}_1, \hat{\mathbf{G}}_2$ are tangent to the surface and $\hat{\mathbf{G}}_3$ is normal.

Likewise, the force ΔF can be associated with either the deformed or the undeformed area element. However, in a small-strain regime, the undeformed area element is our choice to formulate the principle of virtual displacements as there is no significantly different between the undeformed and the deformed configurations.

Now, let us consider the governing equation of a thin shell. Since the principle of virtual work is employed, the work done by both the internal and external forces has to be considered. Therefore, we will determine the virtual work done by the internal and external forces separately.

Firstly, we consider the virtual work done by the internal force. For a steady deformation, the force acting on the undeformed area element which is normal to the coordinate line ξ_i is given by

$$\mathbf{F}^i = \sigma^i da_{(i)}. \tag{3.44}$$

After decomposing the stress vector by using (3.43) and using the definition of area element (3.12), we have

$$\begin{aligned} \mathbf{F}^i &= \sigma^{ij}\hat{\mathbf{G}}_j da_{(i)}, \\ &= \sigma^{ij}\frac{\mathbf{G}_j}{\sqrt{G_{(jj)}}}\sqrt{g}\sqrt{g_{(ii)}}d\xi_k d\xi_l, (i \neq k \neq l) \\ &\approx \sigma^{ij}\mathbf{G}_j\sqrt{g}d\xi_k d\xi_l, (i \neq k \neq l), \end{aligned} \tag{3.45}$$

where σ^{ij} denotes the 2^{nd} Piola-Kirchhoff stress tensor. Note that the last line can be obtained as there is no significantly different between the undeformed and deformed area. This is a consequence of the small strain assumption.

For the infinitesimal volume dv, the variation of the strain energy $d\delta\Pi_{internal}$ during a virtual displacement $\delta\mathbf{u}$ is done by internal forces $\mathbf{F}^i$ and body forces $\mathbf{b}$, and is given

by

$$\begin{aligned} d\delta\Pi_{internal} &= d(\mathbf{F}^i \cdot \delta\mathbf{u}) + \rho\mathbf{b}dv \cdot \delta\mathbf{u}, \\ &= \mathbf{F}^i \cdot d(\delta\mathbf{u}) + d\mathbf{F}^i \cdot \delta\mathbf{u} + \rho\mathbf{b}dv \cdot \delta\mathbf{u}, \\ &= \mathbf{F}^i \cdot (\delta\mathbf{u})_{,i} d\xi_i + \mathbf{F}^i_{,i} d\xi_i \cdot \delta\mathbf{u} + \rho\mathbf{b}dv \cdot \delta\mathbf{u}, \\ &= \mathbf{F}^i \cdot (\delta\mathbf{u})_{,i} d\xi_i, \end{aligned} \tag{3.46}$$

where ρ denotes the material density. Note that the second and the third terms in the third line cancel out at equilibrium.

Expressing $\mathbf{F}^i$ with (3.45) in (3.46) and integrating through the equation, we have that the virtual work expended by stresses per volume is

$$\delta\Pi_{\text{internal}} = \int_\Omega \sigma^{ij}\mathbf{G}_j \cdot (\delta\mathbf{u})_{,i}\sqrt{g}d\xi_1 d\xi_2 d\xi_3. \tag{3.47}$$

Considering the following with the fact that the undeformed base vector $\mathbf{g}_i$ are independent of the displacement gives

$$\begin{aligned} \delta\mathbf{u} &= \delta\mathbf{R} - \delta\mathbf{r}, \\ (\delta\mathbf{u})_{,i} &= (\delta\mathbf{R})_{,i} - (\delta\mathbf{r})_{,i}, \\ &= \delta\mathbf{G}_i. \end{aligned} \tag{3.48}$$

Therefore, the virtual work done by internal forces (3.47) can be rewritten as

$$\begin{aligned} \delta\Pi_{\text{internal}} &= \int_\Omega \sigma^{ij}\mathbf{G}_j \cdot \delta\mathbf{G}_i\sqrt{g}d\xi_1 d\xi_2 d\xi_3 \\ &= \int_\Omega \frac{1}{2}\left(\sigma^{ij}\mathbf{G}_j \cdot \delta\mathbf{G}_i + \sigma^{ji}\mathbf{G}_i \cdot \delta\mathbf{G}_j\right)\sqrt{g}d\xi_1 d\xi_2 d\xi_3 \\ &= \int_\Omega \sigma^{ij}\delta\epsilon_{ij}\sqrt{g}d\xi_1 d\xi_2 d\xi_3. \end{aligned} \tag{3.49}$$

where $\delta\epsilon_{ij}$ denotes the variation of Green's strain tensor. Note that the second line comes from the symmetry property of the stress tensor.

Since the elastic material under consideration is a thin shell, the strain remains small even the material undergoes large displacement. Therefore, the linear (or Hookean) constitutive equation is utilised to represent the relationship between stress and strain. This linear (or Hookean) constitutive law states that every stress component is a linear function of all strain components and can be calculated by using the Taylor expansion as follow

$$\sigma^{ij} = \sigma_0^{ij} + E^{ijkl}\epsilon_{kl} + O(\epsilon^2), \tag{3.50}$$

where σ^{ij} is the ij-th component of a stress tensor, σ_0^{ij} is a pre-stress tensor, and ϵ_{kl} denotes the kl-th component of a strain tensor. Furthermore, E^{ijkl} is the plane stress stiffness fourth-order tensor and is given by

$$E^{ijkl} = \frac{E}{2(1+\nu)}\left(g^{ik}g^{jl} + g^{il}g^{jk} + \frac{2\nu}{1-\nu}g^{ij}g^{kl}\right), \tag{3.51}$$

with the Poisson's ratio ν [81].

In a thin-shell regime, the Kirchhoff-Love assumption is exploited. Therefore, the stress σ^{3i} on the shell surface $\xi_3 = \pm\frac{h}{2}$ are approximately zero throughout the body. This is the consequence of the assumption that shear stresses are neglect and normal vector to the surface is unstretched, i.e. no normal stress. Also, we assume that the initial state is stress free so that a pre-stress tensor σ_0^{ij} vanishes. These allow the constitutive equation (3.50) to be expressed by plane stresses as

$$\sigma^{\alpha\beta} = E^{\alpha\beta\delta\gamma}\epsilon_{\delta\gamma}. \tag{3.52}$$

With the assumption of a small strain on a thin shell, the Hookean constitutive equation is employed together with the fact from the Kirchhoff-Love assumption that the strain ϵ_{3j} on the shell's surface are zero. Hence, the variational work done by internal forces (3.49) becomes,

$$\delta\Pi_{\text{internal}} = \int_\Omega (E^{\alpha\beta\delta\gamma}\epsilon_{\alpha\beta})\delta\epsilon_{\delta\gamma}\sqrt{g}d\xi_1 d\xi_2 d\xi_3. \tag{3.53}$$

It can be seen that the assumption of Kirchhoff-Love allows all quantities to express with the midplane coordinates. Therefore, the integration in the coordinate perpendicular to the mid-surface, i.e. ξ_3, to be carried out analytically. Also, all quantities can be expressed only on the two Lagrangian coordinates, ξ_1, and ξ_2, of the mid-surface. Hence, (3.53) becomes

$$\begin{aligned}\delta\Pi_{\text{internal}} &= \int_{\partial\Omega}\left\{\int_{-h/2}^{h/2}\left(E^{\alpha\beta\delta\gamma}\epsilon_{\alpha\beta}\delta\epsilon_{\delta\gamma}\right)\sqrt{g}d\xi_3\right\}d\xi_1 d\xi_2 \\ &= \delta\int_{\partial\Omega}\left\{\frac{1}{2}\int_{-h/2}^{h/2}E^{\alpha\beta\delta\gamma}\epsilon_{\alpha\beta}\epsilon_{\delta\gamma}\sqrt{g/a}d\xi_3\right\}\sqrt{a}d\xi_1 d\xi_2,\end{aligned} \tag{3.54}$$

where a denotes the determinant of the undeformed metric tensor t_{ij} defined on the midplane. Note that the plane stress stiffness $E^{\alpha\beta\delta\gamma}$ is given by (3.51). It is a function of the undeformed metric tensor $g^{\alpha\beta}$ which describes off-midplane points in a shell.

Also, the strain tensor $\epsilon_{\alpha\beta}$ under the integration is off-midplane. Hence, expressing the strain tensor $\epsilon_{\alpha\beta}$ and the undeformed metric tensor $g^{\alpha\beta}$ by their corresponding mid-plane fields as in (3.36) and (3.38) allows the integration with respect to the coordinate line ξ_3 can be carried out analytically. Therefore, we have that

$$\frac{1}{2}\int_{-h/2}^{h/2} E^{\alpha\beta\delta\gamma}\epsilon_{\alpha\beta}\epsilon_{\delta\gamma}\sqrt{g/a}d\xi_3 = \frac{1}{2}h\tilde{E}^{\alpha\beta\delta\gamma}\left(\gamma_{\alpha\beta}\gamma_{\delta\gamma} + \frac{1}{12}h^2\kappa_{\alpha\beta}\kappa_{\delta\gamma}\right), \tag{3.55}$$

where the plane stress stiffness tensor on the midplane is given by

$$\tilde{E}^{\alpha\beta\delta\gamma} = E^{\alpha\beta\delta\gamma}|_{\xi_3=0} = \frac{E}{2(1+\nu)}\left(t^{\alpha\delta}t^{\beta\gamma} + t^{\alpha\gamma}t^{\beta\delta} + \frac{2\nu}{1-\nu}t^{\alpha\beta}t^{\delta\gamma}\right). \tag{3.56}$$

Substituting the equation (3.55) back into (3.54) gives

$$\begin{aligned}
&\delta\int_{\partial\Omega}\left\{\frac{1}{2}\int_{-h/2}^{h/2} E^{\alpha\beta\delta\gamma}\epsilon_{\alpha\beta}\epsilon_{\delta\gamma}\sqrt{g/a}d\xi_3\right\}\sqrt{a}d\xi_1 d\xi_2 \\
&= \delta\int_{\partial\Omega}\left\{\frac{1}{2}h\tilde{E}^{\alpha\beta\delta\gamma}\left(\gamma_{\alpha\beta}\gamma_{\delta\gamma} + \frac{1}{12}h^2\kappa_{\alpha\beta}\kappa_{\delta\gamma}\right)\right\}\sqrt{a}d\xi_1 d\xi_2 \\
&= \int_{\partial\Omega} h\tilde{E}^{\alpha\beta\delta\gamma}\left(\gamma_{\alpha\beta}\delta\gamma_{\delta\gamma} + \frac{1}{12}h^2\kappa_{\alpha\beta}\delta\kappa_{\delta\gamma}\right)\sqrt{a}d\xi_1 d\xi_2.
\end{aligned} \tag{3.57}$$

Therefore, (3.53) becomes

$$\delta\Pi_{internal} = \int_{\partial\Omega} h\tilde{E}^{\alpha\beta\delta\gamma}\left(\gamma_{\alpha\beta}\delta\gamma_{\delta\gamma} + \frac{1}{12}h^2\kappa_{\alpha\beta}\delta\kappa_{\delta\gamma}\right)\sqrt{a}d\xi_1 d\xi_2. \tag{3.58}$$

Next, let us consider the virtual work done by an external force $\hat{\mathbf{f}}$ during a virtual displacement. Normally, this external force acts on the deformed surface $\xi_3 = \pm h/2$ whose area element is described as in (3.15). If the body forces are neglect, the virtual work done by external forces is given by

$$\begin{aligned}
\delta\Pi_{\text{external}} &= \iint\left(\hat{\mathbf{f}}\cdot\delta\mathbf{u}\right)\sqrt{A}d\xi_1 d\xi_2, \\
&= \iint\left(\hat{\mathbf{f}}\cdot\delta\mathbf{R}\right)\sqrt{A}d\xi_1 d\xi_2.
\end{aligned} \tag{3.59}$$

In the small-strain regime, an area element between the undeformed and deformed configurations are indistinguishable. Hence, the external force is preferable to express on the area element of the undeformed midplane which is related with that of the deformed midplane as

$$\mathbf{f}\sqrt{A} = \hat{\mathbf{f}}\sqrt{a}, \tag{3.60}$$

where $\mathbf{f}$ denotes the external force expressed on the area element of the undeformed midplane. Therefore, we can express the external work on the mid-plane surface as

$$\delta\Pi_{\text{external}} = \iint\sqrt{\frac{A}{a}}\left(\mathbf{f}\cdot\delta\mathbf{R}\right)\sqrt{a}d\xi_1 d\xi_2. \tag{3.61}$$

From the principle of virtual work which states that the work done by internal forces have to be equal to the work done by external forces at equilibrium, therefore,

$$\Pi_{internal} - \Pi_{external} = 0.$$

Combining (3.58) and (3.61) gives the equation that governs the deformation of a thin shell as follow

$$\iint \left\{ \tilde{E}^{\alpha\beta\delta\gamma} \left(\gamma_{\alpha\beta}\delta\gamma_{\alpha\beta} + \frac{1}{12}h^2\kappa_{\alpha\beta}\delta\kappa_{\alpha\beta} \right) - \frac{1}{h}\sqrt{\frac{A}{a}} \left(\mathbf{f} \cdot \delta\mathbf{R} \right) \right\} \sqrt{a} d\xi_1 d\xi_2 = 0. \quad (3.62)$$

3.4 The linear theory

In this section, we will derive a linearisation of the governing equation (3.62) with a small strain in two-dimensional and three-dimensional spaces. The linearisation of a beam governing equation which is in two dimensions will be considered first and that of shell which is in higher dimensions will be determined afterwards.

3.4.1 Linearisation of a beam governing equation

A beam is a two-dimensional elastic material which has a very small thickness as illustrated in Fig. 3.3. Two kinds of elastic beam are considered in our study of the linearisation: straight and curved beams. Fig. 3.3a illustrates a straight beam where the curvature tensor is zero, unlike a curved beam shown in Fig. 3.3b where the curvature tensor is nonzero.

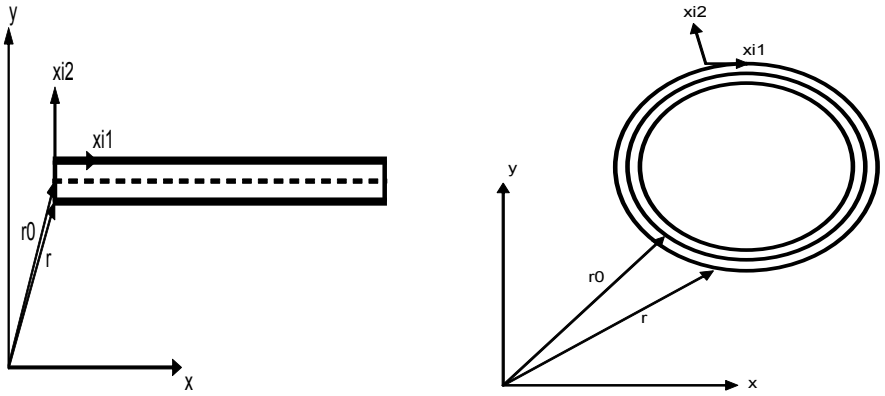

(a) straight beam (b) curved beam

Figure 3.3: Graphical geometries of beams with straight and curved shape.

The deformation of both straight and curved beams can be constructed from a one-dimensional midplane coordinate by employing the Kirchhoff-Love assumption.

The derivation of their governing equations can be obtained similarly as described in (3.62) but the integration has to be taken over a line element rather than an area element.

In this section, we firstly consider a static beam in a general geometry. The governing equation (3.62) is modified to have just one intrinsic coordinate, say ξ, as expressed in (3.63). This equation is a nonlinear governing equation for a thin shell that undergoes large displacements where all quantities is nonlinear and can be obtained as expressed in section 3.2.

$$\int_0^L \left(\gamma\delta\gamma + \frac{1}{12}h^2\kappa\delta\kappa - \frac{1}{h}\sqrt{\frac{A}{a}}\mathbf{f}\cdot\delta\mathbf{R} \right) \sqrt{a}d\xi = 0. \tag{3.63}$$

After a linearisation of the governing equation for a general beam is obtained, some specifications will be introduced to obtain the linear version of the governing equation for a straight and a curved beam. However, these linear versions will be considered later on in chapter 4 with a finite element implementation.

To obtain a linear version of (3.63) for a beam in a general shape, all terms under the integral have to be linearised with the assumption of a small displacement. Since a loading applied to the beam is small under the small-displacement regime, a small loading and a small displacement field can be represented respectively by, for some $\epsilon << 1$,

$$\mathbf{f} = \epsilon\tilde{\mathbf{f}}, \text{ and, } \mathbf{u} = \epsilon\tilde{\mathbf{u}}, \tag{3.64}$$

where $\tilde{(\cdot)}$ represents a quantity whose magnitude is large. With this assumption, the nonlinear terms are neglected as we will illustrate next. This is the result of the magnitude in nonlinear terms are of order ϵ^2 which is very small so that those terms should not have any contribution to the equations.

Since a loading $\mathbf{f}$ is applied to the undeformed beam in the normal direction, all terms in the governing equation are preferable to be considered in tangential and normal components. At each point in a beam, tangential and unit normal vectors are defined as

$$\mathbf{t} = \frac{\partial\mathbf{r}}{\partial\xi}, \text{ and, } \hat{\mathbf{n}} = \frac{1}{|\mathbf{e_z}\times\mathbf{t}|}(\mathbf{e_z}\times\mathbf{t}), \tag{3.65}$$

respectively. Note that, throughout this study, the normal vector is outward to the surface. Since tangential and unit normal vectors depend on an undeformed position

$\mathbf{r}$, they are different at points. The tangential and normal vector are perpendicular to each other. However, the tangential vectors are not unit in this consideration.

Now, let us consider the vector $\mathbf{r} = \mathbf{r}(\xi)$ which is a position vector of the undeformed configuration. Since it is preferable to consider all terms in tangential and normal coordinates, a displacement $\mathbf{u}$ which is the unknown field in our beam problems can be decomposed as follow

$$\epsilon\tilde{\mathbf{u}} = \mathbf{u} = (u^1\mathbf{t} + u^2\hat{\mathbf{n}}) \tag{3.66}$$

where u^1 and u^2 are displacements in tangential and normal directions, respectively.

For the deformed configuration, a position vector is defined as

$$\mathbf{R} = \mathbf{r} + \epsilon\tilde{\mathbf{u}}, \tag{3.67}$$

and, its first-order and second-order derivatives are, respectively,

$$\frac{\partial\mathbf{R}}{\partial\xi} = \frac{\partial\mathbf{r}}{\partial\xi} + \frac{\partial\epsilon\tilde{\mathbf{u}}}{\partial\xi} = \mathbf{t} + \epsilon\frac{\partial\tilde{\mathbf{u}}}{\partial\xi}, \tag{3.68}$$

and,

$$\frac{\partial^2\mathbf{R}}{\partial\xi^2} = \frac{\partial^2\mathbf{r}}{\partial\xi^2} + \frac{\partial^2\epsilon\tilde{\mathbf{u}}}{\partial\xi^2} = \frac{\partial\mathbf{t}}{\partial\xi} + \epsilon\frac{\partial^2\tilde{\mathbf{u}}}{\partial\xi^2}. \tag{3.69}$$

Next, we will use the assumptions (3.64) to linearise all terms in the governing equation (3.63). In order to obtain the linear version of the strain and bending tensors, the associated metric tensor and the curvature tensor have to be linearised. We have that the linearisation of the metric tensor in an undeformed configuration can be considered as

$$a = \frac{\partial\mathbf{r}}{\partial\xi}\cdot\frac{\partial\mathbf{r}}{\partial\xi} = \mathbf{t}\cdot\mathbf{t}, \tag{3.70}$$

and, that of a deformed configuration is

$$\begin{aligned} A &= \frac{\partial\mathbf{R}}{\partial\xi}\cdot\frac{\partial\mathbf{R}}{\partial\xi} \\ &= \frac{\partial\mathbf{r}}{\partial\xi}\cdot\frac{\partial\mathbf{r}}{\partial\xi} + 2\frac{\partial\mathbf{r}}{\partial\xi}\cdot\frac{\partial\epsilon\tilde{\mathbf{u}}}{\partial\xi} + O(\epsilon^2) \\ &\approx a + 2\mathbf{t}\cdot\frac{\partial\mathbf{u}}{\partial\xi}. \end{aligned} \tag{3.71}$$

The curvature of the beam's centreline before and after the deformation can be represented by

$$b = \hat{\mathbf{n}}\cdot\frac{\partial^2\mathbf{r}}{\partial\xi^2}$$

and

$$B = \hat{\mathbf{N}} \cdot \frac{\partial^2 \mathbf{R}}{\partial \xi^2},$$

respectively.

Note that the first-order and the second-order derivatives of a displacement in (3.68), (3.69), and (3.71) still have components in Cartesian coordinates. To determine their components in tangential and normal directions, we have

$$\begin{aligned}
\frac{\partial \mathbf{u}}{\partial \xi} &= u^\alpha \frac{\partial \mathbf{t}_\alpha}{\partial \xi} + \frac{\partial u^\alpha}{\partial \xi}\mathbf{t}_\alpha \\
&= \frac{\partial u^\alpha}{\partial \xi}\mathbf{t}_\alpha + u^\alpha \left[\left(\frac{\partial \mathbf{t}_\alpha}{\partial \xi} \cdot \mathbf{t}_\beta \right) \mathbf{t}_\beta \right], \\
&= \left[\frac{\partial u^\alpha}{\partial \xi} + u^\beta \left(\frac{\partial \mathbf{t}_\beta}{\partial \xi} \cdot \mathbf{t}_\alpha \right) \right] \mathbf{t}_\alpha, \\
&= M_\alpha \mathbf{t}_\alpha,
\end{aligned} \tag{3.72}$$

and, the first-order derivative of the displacement $\mathbf{u}$ can be obtained as

$$\begin{aligned}
\frac{\partial^2 \mathbf{u}}{\partial \xi^2} &= M_\alpha \frac{\partial \mathbf{t}_\alpha}{\partial \xi} + \frac{\partial M_\alpha}{\partial \xi}\mathbf{t}_\alpha \\
&= M_\alpha \left(\frac{\partial \mathbf{t}_\alpha}{\partial \xi} \cdot \mathbf{t}_\beta \right) \mathbf{t}_\beta + \frac{\partial M_\alpha}{\partial \xi}\mathbf{t}_\alpha \\
&= M_\alpha \left(\frac{\partial \mathbf{t}_\alpha}{\partial \xi} \cdot \mathbf{t}_\beta \right) \mathbf{t}_\beta + \left[\frac{\partial^2 u^\alpha}{\partial \xi^2} + \frac{\partial u^\beta}{\partial \xi} \left(\frac{\partial \mathbf{t}_\beta}{\partial \xi} \cdot \mathbf{t}_\alpha \right) + u^\beta \frac{\partial}{\partial \xi} \left(\frac{\partial \mathbf{t}_\beta}{\partial \xi} \cdot \mathbf{t}_\alpha \right) \right] \mathbf{t}_\alpha \\
&= \left[M_\beta \left(\frac{\partial \mathbf{t}_\beta}{\partial \xi} \cdot \mathbf{t}_\alpha \right) + \frac{\partial^2 u^\alpha}{\partial \xi^2} + \frac{\partial u^\beta}{\partial \xi} \left(\frac{\partial \mathbf{t}_\beta}{\partial \xi} \cdot \mathbf{t}_\alpha \right) + u^\beta \frac{\partial}{\partial \xi} \left(\frac{\partial \mathbf{t}_\beta}{\partial \xi} \cdot \mathbf{t}_\alpha \right) \right] \mathbf{t}_\alpha \\
&= P_\alpha \mathbf{t}_\alpha,
\end{aligned} \tag{3.73}$$

where $\mathbf{t}_1, \mathbf{t}_2$, are based vectors in tangential and normal directions, respectively. In the study of a beam, we set $\mathbf{t}_1 \equiv \mathbf{t}$ denotes tangential vector to the undeformed midplane and $\mathbf{t}_2 \equiv \hat{\mathbf{n}}$ denotes the unit normal to the undeformed midplane.

After the linearisation of the metric tensor in both the undeformed and deformed configurations together with the derivatives in tangential and normal components are obtained, the Green strain tensor can be approximated by (see (3.20))

$$\begin{aligned}
\gamma &= \frac{1}{2}(A - a) \\
&\approx \mathbf{t} \cdot \frac{\partial \mathbf{u}}{\partial \xi} \\
&= \left[u^1 \left(\frac{\partial \mathbf{t}}{\partial \xi} \cdot \mathbf{t} \right) + \frac{\partial u^1}{\partial \xi} + u^2 \left(\frac{\partial \hat{\mathbf{n}}}{\partial \xi} \cdot \mathbf{t} \right) \right] \mathbf{t} \cdot \mathbf{t} \\
&= a(\xi) \left[u^1 \left(\frac{\partial \mathbf{t}}{\partial \xi} \cdot \mathbf{t} \right) + \frac{\partial u^1}{\partial \xi} + u^2 \left(\frac{\partial \hat{\mathbf{n}}}{\partial \xi} \cdot \mathbf{t} \right) \right],
\end{aligned} \tag{3.74}$$

and its variation is

$$\begin{aligned}\delta\gamma &= \frac{\partial\gamma}{\partial u^\alpha}\delta(u^\alpha) + \frac{\partial\gamma}{\partial\left(\frac{\partial u^\alpha}{\partial\xi}\right)}\delta\left(\frac{\partial u^\alpha}{\partial\xi}\right) \\ &= \left[a(\xi)\left(\frac{\partial\mathbf{t}}{\partial\xi}\cdot\mathbf{t}\right)\right]\delta(u^1) + \left[a(\xi)\right]\delta\left(\frac{\partial u^1}{\partial\xi}\right) + \left[a(\xi)\left(\frac{\partial\hat{\mathbf{n}}}{\partial\xi}\cdot\mathbf{t}\right)\right]\delta(u^2).\end{aligned} \tag{3.75}$$

For the beam curvature in the undeformed configuration b, we have

$$b = \hat{\mathbf{n}}\cdot\frac{\partial^2\mathbf{r}}{\partial\xi^2} = \hat{\mathbf{n}}\cdot\frac{\partial\mathbf{t}}{\partial\xi}, \tag{3.76}$$

where $\hat{\mathbf{n}} = \frac{1}{|\mathbf{e_z}\times\mathbf{t}|}(\mathbf{e_z}\times\mathbf{t})$ is the unit vector and normal to the undeformed midplane. Then (3.76) becomes,

$$b = \frac{1}{|\mathbf{e_z}\times\mathbf{t}|}(\mathbf{e_z}\times\mathbf{t})\cdot\frac{\partial\mathbf{t}}{\partial\xi}. \tag{3.77}$$

Before we will consider the linearised bending tensor in the deformed configurations, the unit normal vectors $\hat{\mathbf{N}}$ has to be linearised. Now, let us consider the deformed normal vector which can be obtained as

$$\begin{aligned}\mathbf{N} &= \mathbf{e_z}\times\frac{\partial\mathbf{R}}{\partial\xi}, \\ &= \mathbf{e_z}\times\left(\mathbf{t} + \epsilon\frac{\partial\tilde{\mathbf{u}}}{\partial\xi}\right), \\ &= (\mathbf{e_z}\times\mathbf{t}) + \left(\mathbf{e_z}\times\epsilon\frac{\partial\tilde{\mathbf{u}}}{\partial\xi}\right).\end{aligned} \tag{3.78}$$

Considering in tangential and normal directions gives

$$\begin{aligned}\mathbf{N} &= \begin{pmatrix} 0 \\ a(\xi)\end{pmatrix} + \epsilon\begin{pmatrix} -M_2 \\ M_1\end{pmatrix}, \\ &= \begin{pmatrix} -\epsilon M_2 \\ a(\xi)+\epsilon M_1\end{pmatrix},\end{aligned} \tag{3.79}$$

where a is an arc-length along the material line ξ defined as the determinant of (3.70) and it is parametrised by ξ. Also, the modulus of the normal vector $\mathbf{N}$ can be computed as follow

$$|\mathbf{N}| = |\,(\mathbf{e_z}\times\mathbf{t}) + \left(\mathbf{e_z}\times\epsilon\frac{\partial\tilde{\mathbf{u}}}{\partial\xi}\right)| \;\; = \sqrt{a^2(\xi) + 2\epsilon a(\xi)M_1 + O(\epsilon^2)}. \tag{3.80}$$

where M_1 and M_2 are displacement gradients in tangential and normal directions defined in (3.72).

Thus, the linearised unit normal vector $\hat{\mathbf{N}}$ is considered as

$$\begin{aligned}\hat{\mathbf{N}} &= \frac{1}{\sqrt{a^2(\xi)+2\epsilon a(\xi)M_1+O(\epsilon^2)}}\begin{pmatrix}-\epsilon M_2\\ a(\xi)+\epsilon M_1\end{pmatrix}\\ &\approx \frac{1}{a}\begin{pmatrix}0\\ a(\xi)\end{pmatrix}+\epsilon\left[\frac{1}{a}\begin{pmatrix}-M_2\\ M_1\end{pmatrix}-\frac{a}{a^3}M_1\begin{pmatrix}0\\ a(\xi)\end{pmatrix}\right]+O(\epsilon^2)\\ &\approx \hat{\mathbf{n}}+\epsilon\left[\frac{1}{a}\begin{pmatrix}-M_2\\ M_1\end{pmatrix}-\frac{1}{a^2}M_1\begin{pmatrix}0\\ a(\xi)\end{pmatrix}\right],\end{aligned} \tag{3.81}$$

where the modulus of a normal vector in the last line can be obtained by employing Taylor expansion about $\epsilon = 0$. Thus, the linear version of the deformed curvature B can be obtained as follows

$$\begin{aligned}B &= \hat{\mathbf{N}}\cdot\frac{\partial^2\mathbf{R}}{\partial\xi^2}\\ &= \hat{\mathbf{N}}\cdot\left(\frac{\partial\mathbf{t}}{\partial\xi}+\epsilon\frac{\partial^2\tilde{\mathbf{u}}}{\partial\xi^2}\right)\\ &= \hat{\mathbf{N}}\cdot\frac{\partial\mathbf{t}}{\partial\xi}+\epsilon\hat{\mathbf{N}}\cdot\frac{\partial^2\tilde{\mathbf{u}}}{\partial\xi^2}\\ &\approx \hat{\mathbf{n}}\cdot\frac{\partial^2\mathbf{r}}{\partial\xi^2}+\epsilon\left[\frac{1}{a}\begin{pmatrix}-M_2\\ M_1\end{pmatrix}-\frac{1}{a^2}M_1\begin{pmatrix}0\\ a(\xi)\end{pmatrix}\right]\cdot\begin{pmatrix}\frac{\partial\mathbf{t}}{\partial\xi}\cdot\mathbf{t}\\ \frac{\partial\mathbf{t}}{\partial\xi}\cdot\hat{\mathbf{n}}\end{pmatrix}+\epsilon\hat{\mathbf{n}}\cdot N_\alpha\mathbf{t}_\alpha+O(\epsilon^2)\\ &\approx b+\left[\frac{1}{a}\begin{pmatrix}-M_2\\ M_1\end{pmatrix}-\frac{1}{a^2}M_1\begin{pmatrix}0\\ a(\xi)\end{pmatrix}\right]\cdot\begin{pmatrix}\frac{\partial\mathbf{t}}{\partial\xi}\cdot\mathbf{t}\\ \frac{\partial\mathbf{t}}{\partial\xi}\cdot\hat{\mathbf{n}}\end{pmatrix}+P_2.\end{aligned} \tag{3.82}$$

After substituting M_1, M_2 and P_2 defined in (3.72) and (3.73), the linearised bending

tensor κ becomes

$$
\begin{aligned}
\kappa &= b - B \\
&= -\left[\frac{1}{a}\begin{pmatrix} -M_2 \\ M_1 \end{pmatrix} - \frac{1}{a^2}M_1\begin{pmatrix} 0 \\ a(\xi) \end{pmatrix}\right]\cdot\begin{pmatrix} \frac{\partial \mathbf{t}}{\partial \xi}\cdot\mathbf{t} \\ \frac{\partial \mathbf{t}}{\partial \xi}\cdot\hat{\mathbf{n}} \end{pmatrix} - P_2 \\
&= \frac{M_2}{a}\left(\frac{\partial \mathbf{t}}{\partial \xi}.\mathbf{t}\right) - P_2 \\
&= -\left[\left(\frac{\partial}{\partial \xi}\left(\frac{\partial \mathbf{t}}{\partial \xi}\cdot\hat{\mathbf{n}}\right) + \left(\frac{\partial \mathbf{t}}{\partial \xi}.\mathbf{t}\right)\left(\frac{\partial \mathbf{t}}{\partial \xi}\cdot\hat{\mathbf{n}}\right) + \left(\frac{\partial \hat{\mathbf{n}}}{\partial \xi}\cdot\hat{\mathbf{n}}\right)\left(\frac{\partial \mathbf{t}}{\partial \xi}\cdot\hat{\mathbf{n}}\right)\right)u^1\right. \\
&+ \frac{\partial^2 u^2}{\partial \xi^2} + 2\left(\frac{\partial \mathbf{t}}{\partial \xi}\cdot\hat{\mathbf{n}}\right)\frac{\partial u^1}{\partial \xi} + 2\left(\frac{\partial \hat{\mathbf{n}}}{\partial \xi}\cdot\hat{\mathbf{n}}\right)\frac{\partial u^2}{\partial \xi} \\
&\left.+ \left(\frac{\partial}{\partial \xi}\left(\frac{\partial \hat{\mathbf{n}}}{\partial \xi}\cdot\hat{\mathbf{n}}\right) + \left(\frac{\partial \mathbf{t}}{\partial \xi}\cdot\hat{\mathbf{n}}\right)\left(\frac{\partial \hat{\mathbf{n}}}{\partial \xi}\cdot\mathbf{t}\right) + \left(\frac{\partial \hat{\mathbf{n}}}{\partial \xi}\cdot\hat{\mathbf{n}}\right)^2\right)u^2\right] \\
&+ \left[\frac{1}{a}\left(\frac{\partial \mathbf{t}}{\partial \xi}\cdot\mathbf{t}\right)\left(\frac{\partial \mathbf{t}}{\partial \xi}\cdot\hat{\mathbf{n}}\right)\right]u^1 + \left[\frac{1}{a}\left(\frac{\partial \mathbf{t}}{\partial \xi}\cdot\mathbf{t}\right)\right]\frac{\partial u^2}{\partial \xi} + \left[\frac{1}{a^2}\left(\frac{\partial \mathbf{t}}{\partial \xi}\cdot\mathbf{t}\right)^2\right]u^2 \\
&= \left[-\frac{\partial}{\partial \xi}\left(\frac{\partial \mathbf{t}}{\partial \xi}\cdot\hat{\mathbf{n}}\right) - \left(\frac{\partial \mathbf{t}}{\partial \xi}.\mathbf{t}\right)\left(\frac{\partial \mathbf{t}}{\partial \xi}\cdot\hat{\mathbf{n}}\right) - \left(\frac{\partial \hat{\mathbf{n}}}{\partial \xi}\cdot\hat{\mathbf{n}}\right)\left(\frac{\partial \mathbf{t}}{\partial \xi}\cdot\hat{\mathbf{n}}\right)\right. \\
&\left.+\frac{1}{a}\left(\frac{\partial \mathbf{t}}{\partial \xi}\cdot\mathbf{t}\right)\left(\frac{\partial \mathbf{t}}{\partial \xi}\cdot\hat{\mathbf{n}}\right)\right]u^1 - 2\left(\frac{\partial \mathbf{t}}{\partial \xi}\cdot\hat{\mathbf{n}}\right)\frac{\partial u^1}{\partial \xi} \\
&+ \left[-\frac{\partial}{\partial \xi}\left(\frac{\partial \hat{\mathbf{n}}}{\partial \xi}\cdot\hat{\mathbf{n}}\right) - \left(\frac{\partial \mathbf{t}}{\partial \xi}\cdot\hat{\mathbf{n}}\right)\left(\frac{\partial \hat{\mathbf{n}}}{\partial \xi}\cdot\mathbf{t}\right) - \left(\frac{\partial \hat{\mathbf{n}}}{\partial \xi}\cdot\hat{\mathbf{n}}\right)^2 + \frac{1}{a^2}\left(\frac{\partial \mathbf{t}}{\partial \xi}\cdot\mathbf{t}\right)^2\right]u^2 \\
&+ \left[-2\left(\frac{\partial \hat{\mathbf{n}}}{\partial \xi}\cdot\hat{\mathbf{n}}\right) + \frac{1}{a}\left(\frac{\partial \mathbf{t}}{\partial \xi}\cdot\mathbf{t}\right)\right]\frac{\partial u^2}{\partial \xi} - \frac{\partial^2 u^2}{\partial \xi^2}.
\end{aligned}
\tag{3.83}
$$

Thus, the variations of the linearised bending tensor is as follows

$$
\begin{aligned}
\delta\kappa &= \frac{\partial \kappa}{\partial u^\alpha}\delta u^\alpha + \frac{\partial \kappa}{\partial\left(\frac{\partial u^\alpha}{\partial \xi}\right)}\delta\left(\frac{\partial u^\alpha}{\partial \xi}\right) + \frac{\partial \kappa}{\partial\left(\frac{\partial^2 u^\alpha}{\partial \xi^2}\right)}\delta\left(\frac{\partial^2 u^\alpha}{\partial \xi^2}\right) \\
&= \left[-\frac{\partial}{\partial \xi}\left(\frac{\partial \mathbf{t}}{\partial \xi}\cdot\hat{\mathbf{n}}\right) - \left(\frac{\partial \mathbf{t}}{\partial \xi}.\mathbf{t}\right)\left(\frac{\partial \mathbf{t}}{\partial \xi}\cdot\hat{\mathbf{n}}\right) - \left(\frac{\partial \hat{\mathbf{n}}}{\partial \xi}\cdot\hat{\mathbf{n}}\right)\left(\frac{\partial \mathbf{t}}{\partial \xi}\cdot\hat{\mathbf{n}}\right)\right. \\
&\left.+\frac{1}{a}\left(\frac{\partial \mathbf{t}}{\partial \xi}\cdot\mathbf{t}\right)\left(\frac{\partial \mathbf{t}}{\partial \xi}\cdot\hat{\mathbf{n}}\right)\right]\delta u^1 - 2\left(\frac{\partial \mathbf{t}}{\partial \xi}\cdot\hat{\mathbf{n}}\right)\delta\left(\frac{\partial u^1}{\partial \xi}\right) \\
&+ \left[-\frac{\partial}{\partial \xi}\left(\frac{\partial \hat{\mathbf{n}}}{\partial \xi}\cdot\hat{\mathbf{n}}\right) - \left(\frac{\partial \mathbf{t}}{\partial \xi}\cdot\hat{\mathbf{n}}\right)\left(\frac{\partial \hat{\mathbf{n}}}{\partial \xi}\cdot\mathbf{t}\right) - \left(\frac{\partial \hat{\mathbf{n}}}{\partial \xi}\cdot\hat{\mathbf{n}}\right)^2 + \frac{1}{a^2}\left(\frac{\partial \mathbf{t}}{\partial \xi}\cdot\mathbf{t}\right)^2\right]\delta u^2 \\
&+ \left[-2\left(\frac{\partial \hat{\mathbf{n}}}{\partial \xi}\cdot\hat{\mathbf{n}}\right) + \frac{1}{a}\left(\frac{\partial \mathbf{t}}{\partial \xi}\cdot\mathbf{t}\right)\right]\delta\left(\frac{\partial u^2}{\partial \xi}\right) - \delta\left(\frac{\partial^2 u^2}{\partial \xi^2}\right).
\end{aligned}
\tag{3.84}
$$

Finally, we will consider the governing equation (3.63) in terms of variation of the displacement vector $\mathbf{u}$ and its derivatives in tangential and normal components. Also, the linear version of the governing equation will be obtained by substituting all

linearised terms into (3.63). In order to do this, let us consider each term under the integral separately. Regarding the first term, we have

$$\begin{aligned}\gamma\delta\gamma &= \left\{a(\xi)\left[u^1\left(\frac{\partial \mathbf{t}}{\partial \xi}\cdot\mathbf{t}\right)+\frac{\partial u^1}{\partial \xi}+u^2\left(\frac{\partial \hat{\mathbf{n}}}{\partial \xi}\cdot\mathbf{t}\right)\right]\right\}\delta\gamma \\ &= \left\{\left(a^2(\xi)\left[u^1\left(\frac{\partial \mathbf{t}}{\partial \xi}\cdot\mathbf{t}\right)+\frac{\partial u^1}{\partial \xi}+u^2\left(\frac{\partial \hat{\mathbf{n}}}{\partial \xi}\cdot\mathbf{t}\right)\right]\right)\left(\frac{\partial \mathbf{t}}{\partial \xi}\cdot\mathbf{t}\right)\right\}\delta u^1 \\ &+ \left\{a^2(\xi)\left[u^1\left(\frac{\partial \mathbf{t}}{\partial \xi}\cdot\mathbf{t}\right)+\frac{\partial u^1}{\partial \xi}+u^2\left(\frac{\partial \hat{\mathbf{n}}}{\partial \xi}\cdot\mathbf{t}\right)\right]\right\}\delta\left(\frac{\partial u^1}{\partial \xi}\right) \\ &+ \left\{\left(a^2(\xi)\left[u^1\left(\frac{\partial \mathbf{t}}{\partial \xi}\cdot\mathbf{t}\right)+\frac{\partial u^1}{\partial \xi}+u^2\left(\frac{\partial \hat{\mathbf{n}}}{\partial \xi}\cdot\mathbf{t}\right)\right]\right)\left(\frac{\partial \hat{\mathbf{n}}}{\partial \xi}\cdot\mathbf{t}\right)\right\}\delta u^2.\end{aligned} \tag{3.85}$$

Next, the second term can be obtained as

$$\begin{aligned}&\frac{1}{12}h^2\kappa\delta\kappa \\ &= \frac{1}{12}h^2\kappa\left[-\frac{\partial}{\partial \xi}\left(\frac{\partial \mathbf{t}}{\partial \xi}\cdot\hat{\mathbf{n}}\right)-\left(\frac{\partial \mathbf{t}}{\partial \xi}\cdot\mathbf{t}\right)\left(\frac{\partial \mathbf{t}}{\partial \xi}\cdot\hat{\mathbf{n}}\right)-\left(\frac{\partial \hat{\mathbf{n}}}{\partial \xi}\cdot\hat{\mathbf{n}}\right)\left(\frac{\partial \mathbf{t}}{\partial \xi}\cdot\hat{\mathbf{n}}\right)\right. \\ &\left.+\frac{1}{a}\left(\frac{\partial \mathbf{t}}{\partial \xi}\cdot\mathbf{t}\right)\left(\frac{\partial \mathbf{t}}{\partial \xi}\cdot\hat{\mathbf{n}}\right)\right]\delta u^1-\frac{1}{6}h^2\kappa\left(\frac{\partial \mathbf{t}}{\partial \xi}\cdot\hat{\mathbf{n}}\right)\delta\left(\frac{\partial u^1}{\partial \xi}\right) \\ &+\frac{1}{12}h^2\kappa\left[-\frac{\partial}{\partial \xi}\left(\frac{\partial \hat{\mathbf{n}}}{\partial \xi}\cdot\hat{\mathbf{n}}\right)-\left(\frac{\partial \mathbf{t}}{\partial \xi}\cdot\hat{\mathbf{n}}\right)\left(\frac{\partial \hat{\mathbf{n}}}{\partial \xi}\cdot\mathbf{t}\right)-\left(\frac{\partial \hat{\mathbf{n}}}{\partial \xi}\cdot\hat{\mathbf{n}}\right)^2+\frac{1}{a^2}\left(\frac{\partial \mathbf{t}}{\partial \xi}\cdot\mathbf{t}\right)^2\right]\delta u^2 \\ &-\frac{1}{12}h^2\kappa\left[-2\left(\frac{\partial \hat{\mathbf{n}}}{\partial \xi}\cdot\hat{\mathbf{n}}\right)+\frac{1}{a}\left(\frac{\partial \mathbf{t}}{\partial \xi}\cdot\mathbf{t}\right)\right]\delta\left(\frac{\partial u^2}{\partial \xi}\right) \\ &-\frac{1}{12}h^2\kappa\delta\left(\frac{\partial^2 u^2}{\partial \xi^2}\right),\end{aligned} \tag{3.86}$$

and, the last term gives

$$\frac{1}{h}\sqrt{\frac{A}{a}}\epsilon\tilde{\mathbf{f}}\cdot\delta\mathbf{R}=\frac{1}{h}\sqrt{\frac{A}{a}}\epsilon\tilde{\mathbf{f}}\cdot\delta\mathbf{u}. \tag{3.87}$$

Since $A=a+\epsilon\gamma$, we have that $\sqrt{\frac{A}{a}}=\sqrt{1+\epsilon\frac{\gamma}{a}}$. Applying the binomial expansion gives $\sqrt{1+\frac{\epsilon\gamma}{a}}\approx 1$. Next, the Taylor expansion about $\epsilon=0$ gives

$$\begin{aligned}\frac{1}{h}\sqrt{\frac{A}{a}}\epsilon\tilde{\mathbf{f}}\cdot\delta\mathbf{u} &\approx \frac{1}{h}\sqrt{1+\frac{\gamma}{a}}\epsilon\tilde{\mathbf{f}}.\,\delta\mathbf{u} \\ &\approx \frac{1}{h}\mathbf{f}\cdot\delta\mathbf{u}.\end{aligned} \tag{3.88}$$

After substitute equations (3.85), (3.86), and (3.87) back into (3.63), separating the displacement in each direction will give us two governing equations for the tangential and normal displacements. Thus, the linearised governing equation (3.63) in tangential

direction can be expressed as

$$
\begin{aligned}
0 = \int_0^L \Bigg\{ \Bigg[& -\frac{1}{h} f^1 + a^2 \left(\frac{\partial \mathbf{t}}{\partial \xi} \cdot \mathbf{t} \right) \left(u^1 \left(\frac{\partial \mathbf{t}}{\partial \xi} \cdot \mathbf{t} \right) + \frac{\partial u^1}{\partial \xi} + u^2 \left(\frac{\partial \hat{\mathbf{n}}}{\partial \xi} \cdot \mathbf{t} \right) \right) \\
& + \frac{1}{12} h^2 \kappa \left(-\frac{\partial}{\partial \xi} \left(\frac{\partial \mathbf{t}}{\partial \xi} \cdot \hat{\mathbf{n}} \right) - \left(\frac{\partial \mathbf{t}}{\partial \xi} \cdot \mathbf{t} \right) \left(\frac{\partial \mathbf{t}}{\partial \xi} \cdot \hat{\mathbf{n}} \right) - \left(\frac{\partial \hat{\mathbf{n}}}{\partial \xi} \cdot \hat{\mathbf{n}} \right) \left(\frac{\partial \mathbf{t}}{\partial \xi} \cdot \hat{\mathbf{n}} \right) \right. \\
& \left. + \frac{1}{a} \left(\frac{\partial \mathbf{t}}{\partial \xi} \cdot \mathbf{t} \right) \left(\frac{\partial \mathbf{t}}{\partial \xi} \cdot \hat{\mathbf{n}} \right) \right) \Bigg] \delta(u^1) \\
& + \left[a^2 \left(\frac{\partial \mathbf{t}}{\partial \xi} \cdot \mathbf{t} \right) u^1 + a^2 \frac{\partial u^1}{\partial \xi} + a^2 u^2 \left(\frac{\partial \hat{\mathbf{n}}}{\partial \xi} \cdot \mathbf{t} \right) \right. \\
& \left. - \frac{1}{6} h^2 \kappa \left(\frac{\partial \mathbf{t}}{\partial \xi} \cdot \hat{\mathbf{n}} \right) \right] \delta \left(\frac{\partial u^1}{\partial \xi} \right) \Bigg\} \sqrt{a} d\xi,
\end{aligned}
\tag{3.89}
$$

and the linearised governing equation in normal direction is given by

$$
\begin{aligned}
0 = \int_0^L \Bigg\{ \Bigg[& -\frac{1}{h} f^2 + a^2 \left(\frac{\partial \hat{\mathbf{n}}}{\partial \xi} \cdot \mathbf{t} \right) \left(u^1 \left(\frac{\partial \mathbf{t}}{\partial \xi} \cdot \mathbf{t} \right) + \frac{\partial u^1}{\partial \xi} + u^2 \left(\frac{\partial \hat{\mathbf{n}}}{\partial \xi} \cdot \mathbf{t} \right) \right) \\
& + \frac{1}{12} h^2 \kappa \left(-\frac{\partial}{\partial \xi} \left(\frac{\partial \hat{\mathbf{n}}}{\partial \xi} \cdot \hat{\mathbf{n}} \right) - \left(\frac{\partial \mathbf{t}}{\partial \xi} \cdot \hat{\mathbf{n}} \right) \left(\frac{\partial \hat{\mathbf{n}}}{\partial \xi} \cdot \mathbf{t} \right) - \left(\frac{\partial \hat{\mathbf{n}}}{\partial \xi} \cdot \hat{\mathbf{n}} \right)^2 + \frac{1}{a^2} \left(\frac{\partial \mathbf{t}}{\partial \xi} \cdot \mathbf{t} \right)^2 \right) \Bigg] \delta u^2 \\
& - \frac{1}{12} h^2 \kappa \left[-2 \left(\frac{\partial \hat{\mathbf{n}}}{\partial \xi} \cdot \hat{\mathbf{n}} \right) + \frac{1}{a} \left(\frac{\partial \mathbf{t}}{\partial \xi} \cdot \mathbf{t} \right) \right] \delta \left(\frac{\partial u^2}{\partial \xi} \right) \\
& - \frac{1}{12} h^2 \kappa \delta \left(\frac{\partial^2 u^2}{\partial \xi^2} \right) \Bigg\} \sqrt{a} d\xi.
\end{aligned}
\tag{3.90}
$$

From the governing equations of a beam, both the nonlinear equation (3.63) and the linear one (3.89), (3.90), will be implemented and compared in chapter 4. Also, the equation in the specific form of the straight and the curved geometry will be presented.

3.4.2 Linearisation of a shell governing equation

In the previous section, it can be seen that a beam which is a two-dimensional body can be modelled by an equation defined on a one-dimensional domain. In this section, the idea of linear theory will be generalised to a shell which is a three-dimensional elastic material with a very small thickness as illustrated in Fig. 3.4.

There are two kinds of elastic shell that will be considered in our study of the linearisation: straight and curved shells as shown in Fig. 3.4a and Fig. 3.4b, respectively. However, the linearisation of the governing equation for a straight and a curved shell will be considered afterwards in chapter 5 with a finite element implementation.

In this section, we consider the linearisation of the governing equation of a static shell in general shape. We will show how an elastic shell can be modelled by equations

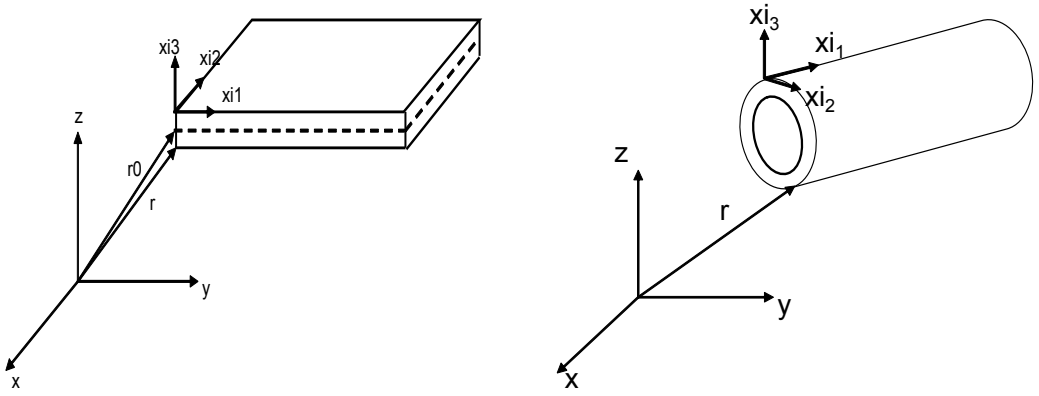

(a) straight shell (b) curved shell

Figure 3.4: Graphical geometries of shell with straight and curved shape.

defined on a two-dimensional domain. Similar to the beam problem considered in section 3.4.1, a small displacement will be assumed in order to eliminate certain terms of lesser order of magnitude with respect to the thickness of the shell. This is to obtain a new equation which may be viewed as a simplification of the governing equation of a three-dimensional elasticity.

Since a shell is a three-dimensional elastic body, the governing equation of a static shell with zero pre-stress can be obtained from (3.62) as

$$\iint_{\Omega} \left\{ \tilde{E}^{\alpha\beta\gamma\delta} \left(\gamma_{\alpha\beta}\delta\gamma_{\gamma\delta} + \frac{1}{12}h^2\kappa_{\alpha\beta}\delta\kappa_{\gamma\delta} \right) - \frac{1}{h}\sqrt{\frac{A}{a}}\mathbf{f}\cdot\delta\mathbf{R} \right\} \sqrt{a}d\xi_1 d\xi_2 = 0, \tag{3.91}$$

where $\tilde{E}^{\alpha\beta\gamma\delta}$ represents the plane stress stiffness tensor defined on the mid-surface and can be computed by

$$\tilde{E}^{\alpha\beta\gamma\delta} = \frac{E}{2(1+\nu)} \left(t^{\alpha\gamma}t^{\beta\delta} + t^{\alpha\delta}t^{\beta\gamma} + \frac{2\nu}{1-\nu}t^{\alpha\beta}t^{\gamma\delta} \right), \tag{3.92}$$

where ν denotes the Poisson's ratio [35]. This equation is a governing equation for a nonlinear theory where all quantities are nonlinear and can be obtained as expressed in section 3.2.

In order to obtain a linearised version of the governing equation of the shell deformation, all terms in the equation (3.91) have to be linearised. Similar to a beam, a small displacement is assumed. Therefore, we have that $\forall\epsilon << 1$,

$$\mathbf{f} = \epsilon\tilde{\mathbf{f}}, \quad \mathbf{u} = \epsilon\tilde{\mathbf{u}}. \tag{3.93}$$

The equation (3.93) will play an essential role in considering the linearisation of the governing equation (3.91).

In order to obtain the strain tensor, the linear version of undeformed and deformed metric tensor have to be determined. The undeformed covariant metric tensor of the mid-surface is then expressed as

$$a_{\alpha\beta} = \mathbf{t}_\alpha \cdot \mathbf{t}_\beta. \tag{3.94}$$

and, the linear version of the deformed metric tensor can be considered as follows

$$\begin{aligned} A_{\alpha\beta} &= \mathbf{T}_\alpha \cdot \mathbf{T}_\beta \\ &= \frac{\partial \mathbf{R}}{\partial \xi_\alpha} \cdot \frac{\partial \mathbf{R}}{\partial \xi_\beta} \\ &= \frac{\partial}{\partial \xi_\alpha}(\mathbf{r} + \epsilon\tilde{\mathbf{u}}) \cdot \frac{\partial}{\partial \xi_\beta}(\mathbf{r} + \epsilon\tilde{\mathbf{u}}) \\ &= a_{\alpha\beta} + \epsilon \frac{\partial \mathbf{r}}{\partial \xi_\alpha} \cdot \frac{\partial \tilde{\mathbf{u}}}{\partial \xi_\beta} + \epsilon \frac{\partial \mathbf{r}}{\partial \xi_\beta} \cdot \frac{\partial \tilde{\mathbf{u}}}{\partial \xi_\alpha} + O(\epsilon^2) \\ &\approx a_{\alpha\beta} + (\mathbf{u}_{,\alpha} \cdot \mathbf{t}_\beta + \mathbf{u}_{,\beta} \cdot \mathbf{t}_\alpha), \end{aligned} \tag{3.95}$$

where $\mathbf{u}$ is a displacement vector. The determinants of the covariant metric tensor in undeformed and deformed shell are a and A, respectively and can be calculated by the determinant of the associated metric tensors.

Note that, in general, the undeformed and deformed metric tensor for a shell body is a three dimensional matrix. Since the Kirchhoff-Love assumption has been used, the normal to the surface remains normal after the deformation. Hence, $\mathbf{t}_{3\alpha} = \mathbf{t}_{\alpha 3} = \mathbf{t}_3 \cdot \mathbf{t}_\alpha = 0$. Also, the normal vector is unstretched and unit, i.e. $\mathbf{t}_{33} = 1$,.

As mentioned in section 3.4.1, it is preferable to consider a deformation of the shell in the tangential and normal directions. Therefore, a displacement $\mathbf{u}$ on the midplane which is parametrised by the two-dimensional coordinates can be decomposed into two tangential and normal components as

$$\mathbf{u} = u^j \mathbf{t}_j. \tag{3.96}$$

where the covariant base vectors $\mathbf{t}_1, \mathbf{t}_2$ are tangent in direction of coordinate lines ξ_1, ξ_2, respectively, and $\hat{\mathbf{t}}_3$ is a unit normal vector to the undeformed mid-surface. Coefficients $u^j, j = 1, 2, 3$ are associated components of a displacement $\mathbf{u}$ in two tangential and one normal directions.

In the governing equation of a shell deformation, not just the displacement field but its first and second derivatives are concerned. Thus, we will consider all derivatives in

the tangential and normal coordinate system. Now, let us consider the first derivatives of $\mathbf{u}$ in tangential and normal directions with respect to coordinate lines $\xi_\alpha, \alpha = 1, 2$. Decomposing in the tangential and normal components gives

$$\begin{aligned}
\frac{\partial \mathbf{u}}{\partial \xi_\alpha} &= \frac{\partial u^j}{\partial \xi_\alpha}\mathbf{t}_j + u^j \frac{\partial \mathbf{t}_j}{\partial \xi_\alpha} \\
&= \frac{\partial u^j}{\partial \xi_\alpha}\mathbf{t}_j + u^j \left[\left(\frac{\partial \mathbf{t}_j}{\partial \xi_\alpha}\cdot \mathbf{t}_i\right)\mathbf{t}_i\right] \\
&= \left[\frac{\partial u^j}{\partial \xi_\alpha} + u^i\left(\frac{\partial \mathbf{t}_i}{\partial \xi_\alpha}\cdot \mathbf{t}_j\right)\right]\mathbf{t}_j \\
&= \left(u^j_{,\alpha} + u^i\Gamma^j_{i\alpha}\right)\mathbf{t}_j \\
&= u^j|_\alpha \mathbf{t}_j
\end{aligned} \tag{3.97}$$

where $\Gamma^j_{i\alpha} = \left(\frac{\partial \mathbf{t}_i}{\partial \xi_\alpha}\cdot \mathbf{t}_j\right)$ denotes Christoffel symbol of the second kind and the quantity $u^j|_\alpha = (u^j_{,\alpha} + u^i\Gamma^j_{i\alpha})$ is the j-component of α-derivative of a displacement $\mathbf{u}$.

Next, the second derivative of the displacement $\mathbf{u}$ in tangential and normal directions can be obtained as

$$\begin{aligned}
\frac{\partial^2 \mathbf{u}}{\partial \xi_\alpha^2} &= u^j|_\alpha \frac{\partial \mathbf{t}_j}{\partial \xi_\alpha} + \frac{\partial u^j|_\alpha}{\partial \xi_\alpha}\mathbf{t}_j \\
&= u^j|_\alpha \Gamma^i_{j\alpha}\mathbf{t}_i + \left(u^j_{,\alpha\alpha} + u^k\frac{\partial \Gamma^j_{k\alpha}}{\partial \xi_\alpha} + \frac{\partial u^k}{\partial \xi_\alpha}\Gamma^j_{k\alpha}\right)\mathbf{t}_j \\
&= \left(u^i|_\alpha \Gamma^j_{i\alpha} + u^j_{,\alpha\alpha} + u^k\frac{\partial \Gamma^j_{k\alpha}}{\partial \xi_\alpha} + \frac{\partial u^k}{\partial \xi_\alpha}\Gamma^j_{k\alpha}\right)\mathbf{t}_j,
\end{aligned} \tag{3.98}$$

and the mixed derivative is

$$\begin{aligned}
\frac{\partial^2 \mathbf{u}}{\partial \xi_\alpha \partial \xi_\beta} &= u^j|_\alpha \frac{\partial \mathbf{t}_j}{\partial \xi_\beta} + \frac{\partial u^j|_\alpha}{\partial \xi_\beta}\mathbf{t}_j \\
&= u^j|_\alpha \Gamma^i_{j\beta}\mathbf{t}_i + \left(u^j_{,\alpha\beta} + u^k\frac{\partial \Gamma^j_{k\alpha}}{\partial \xi_\beta} + \frac{\partial u^k}{\partial \xi_\beta}\Gamma^j_{k\alpha}\right)\mathbf{t}_j \\
&= \left(u^i|_\alpha \Gamma^j_{i\beta} + u^j_{,\alpha\beta} + u^k\frac{\partial \Gamma^j_{k\alpha}}{\partial \xi_\beta} + \frac{\partial u^k}{\partial \xi_\beta}\Gamma^j_{k\alpha}\right)\mathbf{t}_j.
\end{aligned} \tag{3.99}$$

After we consider the derivatives of the displacement in the tangential and normal components and the linear version of the undeformed and deformed metric tensors are obtained, the linearised strain tensor is expressed as follows

$$\begin{aligned}
\gamma_{\alpha\beta} = \frac{1}{2}\left(A_{\alpha\beta} - a_{\alpha\beta}\right) \approx \frac{1}{2}\left(\mathbf{u}_{,\alpha}\cdot \mathbf{t}_\beta + \mathbf{u}_{,\beta}\cdot \mathbf{t}_\alpha\right) &= \frac{1}{2}\left(u^j|_\alpha \mathbf{t}_j\cdot \mathbf{t}_\beta + u^j|_\beta \mathbf{t}_j\cdot \mathbf{t}_\alpha\right) \\
&= \frac{1}{2}\left(u^\beta|_\alpha + u^\alpha|_\beta\right),
\end{aligned} \tag{3.100}$$

and the linear version of its variation is

$$\begin{aligned}\delta\gamma_{\alpha\beta} &= \frac{\partial\gamma_{\alpha\beta}}{\partial u^i}\left(\delta u^i\right) + \frac{\partial\gamma_{\alpha\beta}}{\partial u^i_{,\beta}}\left(\delta u^i_{,\beta}\right) \\ &= \frac{1}{2}\left(\delta u^\alpha_{,\beta} + \delta u^\beta_{,\alpha} + \left(\Gamma^\alpha_{i\beta} + \Gamma^\beta_{i\alpha}\right)\delta u^i\right).\end{aligned} \tag{3.101}$$

Before we will consider for the linearised bending tensor, the unit normal vectors $\hat{\mathbf{t}}_3$ and $\hat{\mathbf{T}}_3$ for the undeformed and deformed configurations have to be linearised. Now, consider first the unit normal to the middle surface of the undeformed configuration which is defined by

$$\hat{\mathbf{n}} = \hat{\mathbf{t}}_3 = \frac{\mathbf{t}_1 \times \mathbf{t}_2}{|\mathbf{t}_1 \times \mathbf{t}_2|}. \tag{3.102}$$

with the associated curvature tensor is specified as follow

$$b_{\alpha\beta} = \hat{\mathbf{n}} \cdot \mathbf{r}_{,\alpha\beta}. \tag{3.103}$$

Next, the linear version of the unit normal vector $\hat{\mathbf{T}}_3$ for a deformed configuration has to be determined. Consider,

$$\begin{aligned}\mathbf{T}_3 &= \mathbf{T}_1 \times \mathbf{T}_2 \\ &= \left(\mathbf{t}_1 + \epsilon\frac{\partial\tilde{\mathbf{u}}}{\partial\xi_1}\right) \times \left(\mathbf{t}_2 + \epsilon\frac{\partial\tilde{\mathbf{u}}}{\partial\xi_2}\right) \\ &= (\mathbf{t}_1 \times \mathbf{t}_2) + \left(\mathbf{t}_1 \times \epsilon\frac{\partial\tilde{\mathbf{u}}}{\partial\xi_2}\right) + \left(\epsilon\frac{\partial\tilde{\mathbf{u}}}{\partial\xi_1} \times \mathbf{t}_2\right) + O(\epsilon^2) \\ &\approx \mathbf{t_3} + \epsilon\left[\left(\mathbf{t}_1 \times \frac{\partial\tilde{\mathbf{u}}}{\partial\xi_2}\right) + \left(\frac{\partial\tilde{\mathbf{u}}}{\partial\xi_1} \times \mathbf{t}_2\right)\right].\end{aligned} \tag{3.104}$$

where the modulus equals to

$$|\mathbf{T}_3| \approx \sqrt{a^2 + 2\epsilon\left(\mathbf{t}_3 \cdot \mathbf{L}\right)} + O(\epsilon^2),$$

and $\mathbf{L} = \left(\mathbf{t}_1 \times \frac{\partial\tilde{\mathbf{u}}}{\partial\xi_2}\right) + \left(\frac{\partial\tilde{\mathbf{u}}}{\partial\xi_1} \times \mathbf{t}_2\right)$.

Now, to make the normal vector to be unit, we have to divide the normal vector $\mathbf{T}_3$ by its magnitude. With the help of Taylor's expansion, the unit normal $\hat{\mathbf{T}}_3$ can be described as

$$\hat{\mathbf{T}}_{\mathbf{3}} \approx \hat{\mathbf{t}}_3 + \epsilon\left[\frac{1}{a}\mathbf{L} - \frac{\mathbf{t}_3 \cdot \mathbf{L}}{a^2}\mathbf{t_3}\right]. \tag{3.105}$$

Thus a curvature tensor for a deformed shell is calculated by

$$\begin{aligned}B_{\alpha\beta} &= \hat{\mathbf{T}}_3 \cdot \frac{\partial^2\mathbf{R}}{\partial\xi_\alpha\partial\xi_\beta} \\ &= \hat{\mathbf{T}}_3 \cdot \frac{\partial}{\partial\xi_\beta}\left(\mathbf{t}_\alpha + \epsilon\frac{\partial\tilde{\mathbf{u}}}{\partial\xi_\alpha}\right) \\ &= \hat{\mathbf{T}}_3 \cdot \frac{\partial\mathbf{t}_\alpha}{\partial\xi_\beta} + \epsilon\hat{\mathbf{T}}_3 \cdot \frac{\partial\tilde{\mathbf{u}}^2}{\partial\xi_\alpha\xi_\beta}.\end{aligned} \tag{3.106}$$

Since tangential and normal components of a curvature tensor has to be consider, the second derivatives of the displacement field and also the derivatives of tangential base vector have to be decomposed in the tangential and normal directions. Therefore, substituting the equation (3.99) into (3.106) gives

$$B_{\alpha\beta} = \hat{\mathbf{T}}_3 \cdot \Gamma^j_{\alpha\beta}\mathbf{t}_j + \epsilon\hat{\mathbf{T}}_3 \cdot \left(u^i|_\alpha \Gamma^j_{i\beta} + u^j_{,\alpha\beta} + u^k \frac{\partial \Gamma^j_{k\alpha}}{\partial \xi_\beta} + \frac{\partial u^k}{\partial \xi_\beta}\Gamma^j_{k\alpha} \right) \mathbf{t}_j. \tag{3.107}$$

After substituting (3.105) into (3.107), we have

$$\begin{aligned} B_{\alpha\beta} &= \hat{\mathbf{t}}_3 \cdot \boldsymbol{\Gamma}_{\alpha\beta} + \epsilon \left[\frac{1}{a}\mathbf{L} - \frac{\hat{\mathbf{t}}_3 \cdot \mathbf{L}}{a^2}\hat{\mathbf{t}}_\mathbf{3} \right] \cdot \boldsymbol{\Gamma}_{\alpha\beta} \\ &\quad + \epsilon\hat{\mathbf{t}}_3 \cdot \left(u^i|_\alpha \Gamma^j_{i\beta} + u^j_{,\alpha\beta} + u^k \frac{\partial \Gamma^j_{k\alpha}}{\partial \xi_\beta} + \frac{\partial u^k}{\partial \xi_\beta}\Gamma^j_{k\alpha} \right) \mathbf{t}_j + O(\epsilon^2) \\ &\approx b_{\alpha\beta} + \left[\frac{1}{a} L_j \Gamma^j_{\alpha\beta} - \frac{L_3}{a^2}\Gamma^3_{\alpha\beta} \right] + \left(u^i|_\alpha \Gamma^3_{i\beta} + u^3_{,\alpha\beta} + u^k \frac{\partial \Gamma^3_{k\alpha}}{\partial \xi_\beta} + \frac{\partial u^k}{\partial \xi_\beta}\Gamma^3_{k\alpha} \right). \end{aligned} \tag{3.108}$$

Hence, the linearised bending tensor can be obtained as

$$\begin{aligned} \kappa_{\alpha\beta} &= b_{\alpha\beta} - B_{\alpha\beta} \\ &\approx -\left[\frac{1}{a} L_j \Gamma^j_{\alpha\beta} - \frac{L_3}{a^2}\Gamma^3_{\alpha\beta} \right] - \left(u^i|_\alpha \Gamma^3_{i\beta} + u^3_{,\alpha\beta} + u^k \frac{\partial \Gamma^3_{k\alpha}}{\partial \xi_\beta} + \frac{\partial u^k}{\partial \xi_\beta}\Gamma^3_{k\alpha} \right) \end{aligned} \tag{3.109}$$

where L_j is defined as in (3.104) but decomposes in tangential and normal directions which can be described as

$$\mathbf{L} = \begin{pmatrix} a_{12}u^3|_2 - a_{22}u^3|_1 \\ -a_{11}u^3|_2 + a_{21}u^3|_1 \\ a_{11}u^2|_2 - a_{12}u^1|_2 + a_{22}u^1|_1 - a_{21}u^2|_1 \end{pmatrix}. \tag{3.110}$$

Finally, we substitute all linearised terms of the strain tensor, $\gamma_{\alpha\beta}$, in (3.100) and the bending tensor, $\kappa_{\alpha\beta}$, in (3.109) and their variations back into the following shell governing equation

$$0 = \iint_\Omega \tilde{E}^{\alpha\beta\gamma\delta} \left\{ \gamma_{\alpha\beta}\delta\gamma_{\gamma\delta} + \frac{1}{12}h^2\kappa_{\alpha\beta}\delta\kappa_{\gamma\delta} \right\} - \frac{1}{h}\mathbf{f} \cdot \delta\mathbf{u}\sqrt{a}d\xi_1 d\xi_2. \tag{3.111}$$

Writing into a variational equation for each displacement direction, displacements in two tangential and one normal direction are obtained. Note that the third term of forcing function can be linearised with the help of Taylor's and Binomial expansion as described in section 3.4.1.

Therefore, the linearised equation for a displacement $\mathbf{u}$ in tangential direction in the coordinate ξ_1 is

$$\begin{aligned}
0 = \iint & -\frac{1}{h} f^1 \delta u^1 + \tilde{E}^{\alpha\beta\gamma\delta} \left\{ \left[\frac{1}{2} \gamma_{\alpha\beta} (\Gamma^{\delta}_{1\gamma} + \Gamma^{\gamma}_{1\delta}) + \frac{1}{12} h^2 \kappa_{\alpha\beta} (-\Gamma^{k}_{1\delta} \Gamma^{3}_{k\gamma}) \right.\right. \\
& + \frac{1}{12} h^2 \kappa_{\alpha\beta} \left(-\frac{1}{a} \Gamma^{1}_{\delta\gamma} \left(a_{12} \Gamma^{3}_{12} - a_{22} \Gamma^{3}_{11} \right) - \frac{1}{a} \Gamma^{2}_{\delta\gamma} \left(-a_{11} \Gamma^{3}_{12} + a_{21} \Gamma^{3}_{11} \right) \right. \\
& \left.\left. + \left(\frac{1}{a^2} - \frac{1}{a} \right) \Gamma^{3}_{\delta\gamma} \left(a_{11} \Gamma^{2}_{12} - a_{12} \Gamma^{1}_{12} + a_{22} \Gamma^{1}_{11} - a_{21} \Gamma^{2}_{11} \right) \right) \right] \delta u^1 \\
& + \left[\gamma_{\alpha\beta} - \frac{1}{12} h^2 \kappa_{\alpha\beta} \Gamma^{3}_{1\delta} \right] \delta u^{1}_{,\gamma} \\
& - \left[\frac{1}{12} h^2 \kappa_{\alpha\beta} \Gamma^{3}_{1\gamma} \right] \delta u^{1}_{,\delta} + \frac{1}{12} h^2 \kappa_{\alpha\beta} \left[\left(\frac{1}{a^2} - \frac{1}{a} \right) \Gamma^{3}_{\delta\gamma} a_{22} \right] \delta u^{1}_{,1} \\
& - \frac{1}{12} h^2 \kappa_{\alpha\beta} \left[\left(\frac{1}{a^2} - \frac{1}{a} \right) \Gamma^{3}_{\delta\gamma} a_{12} \right] \delta u^{1}_{,2} \Bigg\} \sqrt{a} d\xi_1 d\xi_2.
\end{aligned} \tag{3.112}$$

Also, the linearised equation for a displacement $\mathbf{u}$ in tangential direction in the coordinate ξ_2 is

$$\begin{aligned}
0 = \iint & -\frac{1}{h} f^2 \delta u^2 + \tilde{E}^{\alpha\beta\gamma\delta} \left\{ \left[\frac{1}{2} \gamma_{\alpha\beta} (\Gamma^{\delta}_{2\gamma} + \Gamma^{\gamma}_{2\delta}) + \frac{1}{12} h^2 \kappa_{\alpha\beta} (-\Gamma^{k}_{2\delta} \Gamma^{3}_{k\gamma}) \right.\right. \\
& + \frac{1}{12} h^2 \kappa_{\alpha\beta} \left(-\frac{1}{a} \Gamma^{1}_{\delta\gamma} \left(a_{12} \Gamma^{3}_{22} - a_{22} \Gamma^{3}_{21} \right) - \frac{1}{a} \Gamma^{2}_{\delta\gamma} \left(-a_{11} \Gamma^{3}_{22} + a_{21} \Gamma^{3}_{21} \right) \right. \\
& \left.\left. + \left(\frac{1}{a^2} - \frac{1}{a} \right) \Gamma^{3}_{\delta\gamma} \left(a_{11} \Gamma^{2}_{22} - a_{12} \Gamma^{1}_{22} + a_{22} \Gamma^{1}_{21} - a_{21} \Gamma^{2}_{21} \right) \right) \right] \delta u^2 \\
& + \left[\gamma_{\alpha\beta} - \frac{1}{12} h^2 \kappa_{\alpha\beta} \Gamma^{3}_{2\delta} \right] \delta u^{2}_{,\gamma} \\
& - \left[\frac{1}{12} h^2 \kappa_{\alpha\beta} \Gamma^{3}_{2\gamma} \right] \delta u^{2}_{,\delta} + \frac{1}{12} h^2 \kappa_{\alpha\beta} \left[\left(\frac{1}{a^2} - \frac{1}{a} \right) \Gamma^{3}_{\delta\gamma} a_{11} \right] \delta u^{2}_{,2} \\
& - \frac{1}{12} h^2 \kappa_{\alpha\beta} \left[\left(\frac{1}{a^2} - \frac{1}{a} \right) \Gamma^{3}_{\delta\gamma} a_{21} \right] \delta u^{2}_{,1} \Bigg\} \sqrt{a} d\xi_1 d\xi_2.
\end{aligned} \tag{3.113}$$

And, the linearised equation for a displacement $\mathbf{u}$ in normal direction to the undeformed surface is

$$
\begin{aligned}
0 = \iint & -\frac{1}{h} f^3 \delta u^3 + \tilde{E}^{\alpha\beta\gamma\delta} \left\{ \left[\frac{1}{2} \gamma_{\alpha\beta} (\Gamma^{\delta}_{3\gamma} + \Gamma^{\gamma}_{3\delta}) + \frac{1}{12} h^2 \kappa_{\alpha\beta} (-\Gamma^{k}_{3\delta} \Gamma^{3}_{k\gamma}) \right.\right. \\
& + \frac{1}{12} h^2 \kappa_{\alpha\beta} \left(-\frac{1}{a} \Gamma^{1}_{\delta\gamma} \left(a_{12} \Gamma^{3}_{32} - a_{22} \Gamma^{3}_{31} \right) - \frac{1}{a} \Gamma^{2}_{\delta\gamma} \left(-a_{11} \Gamma^{3}_{32} + a_{21} \Gamma^{3}_{31} \right) \right. \\
& \left.\left. + \left(\frac{1}{a^2} - \frac{1}{a} \right) \Gamma^{3}_{\delta\gamma} \left(a_{11} \Gamma^{2}_{32} - a_{12} \Gamma^{1}_{32} + a_{22} \Gamma^{1}_{31} - a_{21} \Gamma^{2}_{31} \right) \right) \right] \delta u^3 \\
& - \left[\frac{1}{12} h^2 \kappa_{\alpha\beta} \Gamma^{3}_{3\delta} \right] \delta u^{3}_{,\gamma} - \left[\frac{1}{12} h^2 \kappa_{\alpha\beta} \Gamma^{3}_{3\gamma} \right] \delta u^{3}_{,\delta} \\
& - \frac{1}{12} h^2 \kappa_{\alpha\beta} \delta u^{3}_{,\delta\gamma} + \frac{1}{12} h^2 \kappa_{\alpha\beta} \left[\left(\Gamma^{2}_{\delta\gamma} a_{11} - \Gamma^{1}_{\delta\gamma} a_{12} \right) \frac{1}{a} \right] \delta u^{3}_{,2} \\
& \left. + \frac{1}{12} h^2 \kappa_{\alpha\beta} \left[\left(\Gamma^{1}_{\delta\gamma} a_{22} - \Gamma^{2}_{\delta\gamma} a_{21} \right) \frac{1}{a} \right] \delta u^{3}_{,1} \right\} \sqrt{a} d\xi_1 d\xi_2 .
\end{aligned}
\tag{3.114}
$$

Similar to a beam, the shell governing equation for both the nonlinear (3.91) and the linear (3.112), (3.113), and (3.114), will be implemented and compared in chapter 5 with a finite element method. The equation in the specific form of the straight and the curved geometry will be also presented.

Chapter 4

Finite element method for beam governing equations

4.1 Introduction

This chapter will be concerned with the finite element implementations of a beam problem in order to show that its linearised governing equations with the linear constitutive law can describe a beam's behaviour within a small deformation. The Kirchhoff-Love assumption plays an important role to derive its dimension-reduced governing equations as we already discussed in chapter 3. The general form of the linearised governing equation for a beam is as follow (see chapter 3 for details)

$$\int_0^L \left(\gamma \delta\gamma + \frac{1}{12} h^2 \kappa \delta\kappa - \frac{1}{h} \mathbf{f} \cdot \delta\mathbf{u} \right) \sqrt{a} d\xi = 0. \tag{4.1}$$

Note that the intrinsic coordinate ξ is used to parametrise all beam's quantities. All strain tensor γ, bending tensor κ, and their variation, $\delta\gamma, \delta\kappa$ are linearised and expressed as (3.74), (3.83), (3.75), (3.84), respectively. Also, $\delta\mathbf{u}$ and $\mathbf{f}$ denotes, respectively, a virtual displacement and an external force expressed on the area element of the undeformed midplane.

In the equation (4.1), a linearisation of the governing equation is for a beam in a general geometry. In this chapter, the governing equation will be specific to a straight and a curved beam. Section 4.2 will start a beam implementation with the straight beam problem whose domain of interest has a zero curvature while section 4.3 will illustrate the curved beam problem whose domain of interest has a non-zero curvature.

To perform a finite element implementation of the straight beam in section 4.2, its deformation's governing equation will be decomposed into two governing equations for the tangential and normal directions. In section 4.2.1, we will illustrate that the order of differential equations that govern displacements in tangential and normal directions are different. Therefore, different order of continuity is required in their weak formulations. Furthermore, we will see that the tangential governing equation is of second order and contains the first-order derivative of the tangential displacement in the weak formulation. Unlike the tangential displacement, the normal governing equation is of fourth order and contains the second-order derivative of the normal displacement in its weak form. Therefore, the continuity of both the displacement and its derivative is required in the implementation of the normal displacement while only the continuity of the displacement is required in the tangential displacement.

Next, in section 4.2.2, there will be three subsections describing the finite element representations of both tangential and normal displacements. Two interpolations will be considered in this study: Lagrange and Hermite family functions. In a Lagrange-type interpolation function, the solution for a field variable being approximated can retain C^0-continuity while the Hermite interpolation provides C^1-continuity in the solution.

In the first two subsections of section 4.2.2, both theoretical and numerical investigations will be performed to determine the appropriate finite element representations for the tangential displacement. Examination of the terms in its weak form will indicate that either the Lagrange or the Hermite functions can be used to approximate the tangential displacement as only C^0-continuity is required in the weak form.

In order to consider the appropriate interpolation function for the solution of the second-order PDE, the number of conditions needed to be specified at boundaries for each interpolation will have to be determined from its weak formulation associated with each interpolation. Since there is a derivative defined as a degree of freedom in the Hermite interpolation, its consistency with the natural boundary condition is concerned. Therefore, various specifications at boundaries for the Hermite interpolation will be numerically illustrated in order to check the consistency and to consider for the appropriateness.

Section 4.2.2 ends with the finite element representation for the normal displacements where the appropriate interpolation for the fourth-order differential equation is determined.

After the finite element formulation that capable of modelling the Biharmonic-type (the fourth-order PDE) and Poisson-type (the second-order PDE) equations are selected, numerical comparisons between the linear and nonlinear governing equations will be described in section 4.2.3 for a straight beam. This is to show that with a small deformation the linearised governing equation can describe behaviours for a zero-curvature beam.

Since the straight beam has a zero curvature, its governing equation cannot be a representative for a thin-beam behaviour in general. Therefore, implementations for the deformations of the curved beam by the finite element method have to be considered. Their specific form of the linearised governing equations will be derived in section 4.3.1. It will be seen that the weak formulations for the tangential and normal directions required the same C^0- and C^1-continuity, respectively, as in the straight beam. Therefore, the same formulation that capable of modelling the displacements in tangential and normal directions in the straight beam will be required establishing practical means of approximation for a curved beam in the finite element method. Numerical results will be shown in section 4.3.2 in order to conclude the comparison between the linear and nonlinear governing equations in a general non-zero curvature of a beam within a small-strain regime.

4.2 Finite element method for a straight beam

In this chapter, we will start a beam problem with a straight beam. Let consider a straight beam under consideration extends from $x = 0$ to $x = 1$ with y-direction initially at $y = 0$ as shown in Fig. 4.1. The beam is subjected to constant forces which act in the normal direction to it. Also, the beam is clamped at both ends which means that $\mathbf{u}(0) = \mathbf{0} = \mathbf{u}(1)$ and $\mathbf{u}'(0) = \mathbf{0} = \mathbf{u}'(1)$ are applied into the problem.

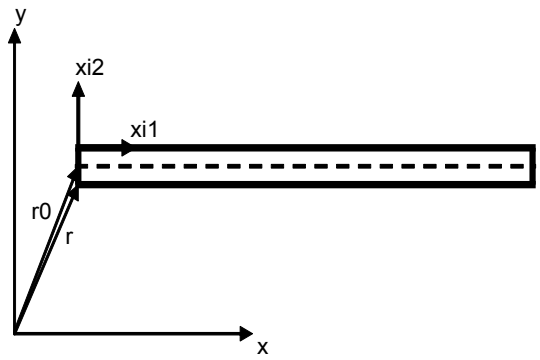

Figure 4.1: The geometrical description of a straight beam with loads in normal direction.

4.2.1 The linearised governing equation

Now, the specific form of the linearised governing equation for a straight beam will be derived. All formula and definitions were expressed in section 3.4.1 where u^1 and u^2 denote a displacement in tangential and normal directions, respectively.

At the initial position of the straight beam, we have $\mathbf{r} = \begin{pmatrix} \xi \\ 0 \end{pmatrix}$ where ξ is the intrinsic coordinate lies between $[0, 1]$. The metric tensor in the undeformed configuration can be expressed as

$$a = \frac{\partial \mathbf{r}}{\partial \xi} \cdot \frac{\partial \mathbf{r}}{\partial \xi} = \begin{pmatrix} 1 \\ 0 \end{pmatrix} \cdot \begin{pmatrix} 1 \\ 0 \end{pmatrix} = 1, \tag{4.2}$$

and, that of the deformed configuration can be obtained from (3.71) as,

$$A \approx 1 + 2\frac{\partial u^1}{\partial \xi}. \tag{4.3}$$

The beam curvature tensors in the undeformed and deformed configurations are expressed as

$$\begin{aligned} b &= 0, \\ B &\approx \frac{\partial^2 u^2}{\partial \xi^2}. \end{aligned} \tag{4.4}$$

Hence, the linear version of the strain and bending tensors and their associated variations for the straight beam can be computed as (3.74), (3.75), (3.83), and (3.84) in

Chapter 3 as

$$\begin{aligned}\gamma &\approx \frac{\partial u^1}{\partial \xi},\\ \delta\gamma &\approx \delta\left(\frac{\partial u^1}{\partial \xi}\right),\\ \kappa &\approx \frac{\partial^2 u^2}{\partial \xi^2},\\ \delta\kappa &\approx \delta\left(\frac{\partial^2 u^2}{\partial \xi^2}\right).\end{aligned} \tag{4.5}$$

Now, the linearised governing equation for a straight line beam will be considered in terms of variation of the displacement vector $\mathbf{u}$ and its derivatives in tangential and normal components. Substituting all linearised terms into (4.1), the governing equation for a straight line beam is

$$\begin{aligned}0 &= \int_0^L \left\{-\frac{1}{h}f^1\delta(u^1) + \left(\frac{\partial u^1}{\partial \xi}\right)\delta\left(\frac{\partial u^1}{\partial \xi}\right) + \left[-\frac{1}{h}f^2\right]\delta(u^2) + \frac{1}{12}h^2\frac{\partial^2 u^2}{\partial \xi^2}\delta\left(\frac{\partial^2 u^2}{\partial \xi^2}\right)\right\}d\xi,\\ &= \int_0^L \left\{-\frac{1}{h}f^1\delta(u^1) + \frac{\partial u^1}{\partial \xi}\delta\left(\frac{\partial u^1}{\partial \xi}\right) + \left[-\frac{1}{h}f^2\right]\delta(u^2) - \frac{1}{12}h^2\frac{\partial^3 u^2}{\partial \xi^3}\delta\left(\frac{\partial u^2}{\partial \xi}\right)\right\}d\xi\\ &+ \frac{1}{12}h^2\frac{\partial^2 u^2}{\partial \xi^2}\delta\left(\frac{\partial u^2}{\partial \xi}\right)\Big|_0^L,\\ &= \int_0^L \left\{\left[-\frac{1}{h}f^1 - \frac{\partial^2 u^1}{\partial \xi^2}\right]\delta(u^1) + \left[-\frac{1}{h}f^2 + \frac{1}{12}h^2\frac{\partial^4 u^2}{\partial \xi^4}\right]\delta(u^2)\right\}d\xi\\ &+ \frac{\partial u^1}{\partial \xi}\delta(u^1)\Big|_0^L + \frac{1}{12}h^2\frac{\partial^2 u^2}{\partial \xi^2}\delta\left(\frac{\partial u^2}{\partial \xi}\right)\Big|_0^L - \frac{1}{12}h^2\frac{\partial^3 u^2}{\partial \xi^3}\delta(u^2)\Big|_0^L,\end{aligned} \tag{4.6}$$

where, the second and the third equations obtained from integrations by parts.

Comparing (4.6) with (3.89) and (3.90) which are the governing equations in the tangential and normal displacements for a beam in general shape, respectively, we can see that there are some terms missing which make (4.6) a lot more simpler. This is a consequence of having a zero curvature in the straight undeformed domain as shown in (4.4).

Next, we would like to show that our obtained linearised governing equations for a straight beam is correspond to the Euler-Bernoulli equation. Note that our beam of consideration is static. From (4.6), the PDEs for a displacement $\mathbf{u}$ of a straight line beam is given by

$$\frac{1}{12}h^2\frac{\partial^4 u^2}{\partial \xi^4} - \frac{1}{h}f^2 = 0, \tag{4.7}$$

for the normal displacement, and

$$\frac{\partial^2 u^1}{\partial \xi^2} + \frac{1}{h} f^1 = 0, \tag{4.8}$$

for the tangential displacement.

Since (4.7) and (4.8) are obtained by non-dimensionalising all length on some length scale $\mathcal{L}$, by scaling the applied force on the beam's effective Young's modulus $E_{eff} = \frac{E}{1-\nu^2}$ so that the dimensional and non-dimensional variables are related by

$$\Lambda^2 = \frac{\mathcal{L}^2 \rho}{\mathcal{T}^2 E_{eff}}, \tag{4.9}$$

$$h = \mathcal{L} h^\star, \tag{4.10}$$

where $\mathcal{T}$ denotes some timescale $\mathcal{T}$ for non-dimensionalising time. Note that we use $\Lambda = 1$ as the default value in all solid mechanics equations and asterisks are used to label those dimensional quantities.

Hence, the dimensional form of (4.7) becomes

$$\begin{aligned} \frac{1}{12} h^2 \frac{\partial^4 u^2}{\partial \xi^4} &= \frac{1}{h} f^2 \\ \frac{1 h^2}{12 \Lambda^2} \frac{\partial^4 u^2}{\partial \xi^4} &= \frac{1}{h \Lambda^2} f^2 \\ \frac{1 h^{\star 2} \mathcal{T}^2 E}{12 \rho (1-\nu^2)} \frac{\partial^4 u^2}{\partial \xi^4} &= \frac{\mathcal{T}^2 E}{\rho \mathcal{L}^3 h^\star (1-\nu^2)} f^2 \\ \frac{1 h^{\star 2} E}{12 (1-\nu^2)} \frac{\partial^4 u^2}{\partial \xi^4} &= \frac{E}{\mathcal{L}^3 h^\star (1-\nu^2)} f^2, \end{aligned} \tag{4.11}$$

and that of (4.8) becomes,

$$\begin{aligned} \frac{\partial^2 u^1}{\partial \xi^2} &= -\frac{1}{h} f^1 \\ \frac{1}{\Lambda^2} \frac{\partial^2 u^1}{\partial \xi^2} &= -\frac{1}{\Lambda^2 h} f^1 \\ \frac{E}{(1-\nu^2)} \frac{\partial^2 u^1}{\partial \xi^2} &= -\frac{E}{\mathcal{L} h^\star (1-\nu^2)} f^1, \end{aligned} \tag{4.12}$$

which correspond to the Euler-Bernoulli equation for a static beam.

Therefore, the partial differential equation that governs the displacement in tangential direction is of second order as shown in (4.8). Also, the partial differential equation that governs the displacement in normal direction is of fourth order as shown in (4.7).

4.2.2 Finite element representations for C^0- and C^1-continuous solutions

To implement the tangential and normal displacements by the finite element method, the formulation should be capable of modelling the coupled equations between the second and the fourth order. From (4.7) and (4.8), we have that the transverse (normal) deflection of a straight beam in the linear elasticity theory is governed by a fourth-order differential equation and a tangential displacement is governed by a second-order differential equation.

It can be seen from (4.6) that the weak formulation of the normal displacement's governing equation contains the second-order derivative. In order to make the integral exists, the second-order derivative has to be square-integrable. Also, from the differentiability of the first-order derivative, the existence of the second-order derivative requires the first-order derivative to be continuous. Hence, by Sobolev's theorem [78], the normal displacement are C^1. This means that both the normal displacement itself and its first-order derivative are required to be continuous between elements.

To approximate the normal displacement, a C^1-continuous interpolation function has to be considered in order to ensure the continuity of the derivative in the finite element method. Since the Hermite element provides the continuity between elements for both the unknown and its first derivative, it is sufficient to represent the normal displacement with Hermite-family functions as we will describe more in details later in this section.

However, an interpolation function approximating the solution of the tangential displacements does not require a continuity for its derivative. As seen in (4.6), the first-order derivative is the highest order under the integral which requires only the displacement in the tangential direction, u_1, itself to be continuous. When Lagrange polynomials are employed as shape functions, the resulting approximation is continuous between elements. Therefore, the tangential displacement can be approximated by either Hermite-type or Lagrange-type interpolation functions.

To identify an appropriate set of shape functions to approximate the solution of the second-order differential equation, theoretical and numerical investigations will be illustrated later on in the next two subsections. This is to establish practical means of

approximation for beam and shell problems in finite element method in the linearised governing equations.

Finite element representation of the second-order partial differential equation

Now, let us determine the suitable shape function for the second-order partial differential equation which is the governing equation for the tangential displacement expressed as follow

$$\frac{d^2u}{d\xi^2} + \frac{1}{h}f = 0. \tag{4.13}$$

In order to do this, we will begin by considering the weak formulation of (4.13) which is expressed as

$$0 = \int_0^1 \left\{ \left(\frac{d^2u}{d\xi^2} + \frac{1}{h}f \right) \delta(u) \right\} d\xi. \tag{4.14}$$

After integrating the weak formulation in (4.14) by parts, the following equation is obtained with the boundary term appearing as follow

$$0 = \int_0^1 \left\{ \left(-\frac{1}{h}f \right) \delta(u) + \left(\frac{du}{d\xi} \right) \delta \left(\frac{du}{d\xi} \right) \right\} d\xi - \left[\frac{du}{d\xi} \delta(u) \right]_0^1. \tag{4.15}$$

Without loss of generality, we assume that the domain of interest is discretised into $N-1$ pieces with N nodes in the mesh (two nodes per element). To illustrate the appropriate shape function for an unknown variable u of the second-order equation, two families of shape function: Lagrange and Hermite families, are considered.

In this case for 2-node elements, the linear shape function will be considered for the Lagrange family while the cubic shape function will be considered for the Hermite family. Therefore, we have that the solution $u(\xi)$, its derivative $\frac{du}{d\xi}$, and their variations can be represented by a set of shape functions which associated with the kth node in the mesh as

$$\begin{aligned} u(\xi) &= \sum_{k=1}^{N} U_k \psi_k(\xi), \quad & \delta u(\xi) &= \sum_{k=1}^{N} \delta U_k \psi_k(\xi), \\ \frac{du}{d\xi}(\xi) &= \sum_{k=1}^{N} U_k \frac{d\psi_k}{d\xi}(\xi), \quad & \delta \left(\frac{du}{d\xi}(\xi) \right) &= \sum_{k=1}^{N} \delta U_k \frac{d\psi_k}{d\xi}(\xi), \end{aligned} \tag{4.16}$$

for the linear Lagrange shape function and

$$\begin{aligned} u(\xi) &= \sum_{k=1}^{N}\sum_{l=1}^{2} U_{kl}\psi_{kl}(\xi), \quad \delta u(\xi) = \sum_{k=1}^{N}\sum_{l=1}^{2} \delta U_{kl}\psi_{kl}(\xi), \\ \frac{du}{d\xi}(\xi) &= \sum_{k=1}^{N}\sum_{l=1}^{2} U_{kl}\frac{d\psi_{kl}}{d\xi}(\xi), \quad \delta\left(\frac{du}{d\xi}(\xi)\right) = \sum_{k=1}^{N}\sum_{l=1}^{2} \delta U_{kl}\frac{d\psi_{kl}}{d\xi}(\xi), \end{aligned} \tag{4.17}$$

for the cubic Hermite shape function. Note that U_k denotes the nodal value associated at node kth for the Lagrange interpolations and U_{kl} denotes the nodal value associated at node k with l position type for the Hermite interpolations. The reader may refer to Appendix A for their definitions and properties.

Next, the implemented equation for the second-order equation using the linear Lagrange and the cubic Hermite interpolation will be considered. After substituting the approximations of the variations back into (4.15), we have

$$\begin{aligned} 0 &= \int_0^1 \left(\frac{du}{d\xi}\sum_{k=1}^{N}\delta U_k\frac{d\psi_k}{d\xi}(\xi) - \frac{1}{h}f(\xi)\sum_{k=1}^{N}\delta U_k\psi_k(\xi)\right)d\xi - \left[\frac{du}{d\xi}\sum_{k=1}^{N}\delta U_k\psi_k(\xi)\right]_0^1, \\ &= \sum_{k=1}^{N}\delta U_k\left(\int_0^1\left(\frac{du}{d\xi}\frac{d\psi_k}{d\xi} - \frac{1}{h}f(\xi)\psi_k(\xi)\right)d\xi - \left[\frac{du}{d\xi}\psi_k(\xi)\right]_0^1\right), \end{aligned} \tag{4.18}$$

for the linear Lagrange shape function, and

$$\begin{aligned} 0 &= \int_0^1 \left(\frac{du}{d\xi}\sum_{k=1}^{N}\sum_{l=1}^{2}\delta U_{kl}\frac{d\psi_{kl}}{d\xi}(\xi) - \frac{1}{h}f(\xi)\sum_{k=1}^{N}\sum_{l=1}^{2}\delta U_{kl}\psi_{kl}(\xi)\right)d\xi \\ &\quad - \left[\frac{du}{d\xi}\sum_{k=1}^{N}\sum_{l=1}^{2}\delta U_{kl}\psi_{kl}(\xi)\right]_0^1, \\ &= \sum_{k=1}^{N}\sum_{l=1}^{2}\delta U_{kl}\left(\int_0^1\left(\frac{du}{d\xi}\frac{d\psi_{kl}}{d\xi} - \frac{1}{h}f(\xi)\psi_{kl}(\xi)\right)d\xi - \left[\frac{du}{d\xi}\psi_{kl}(\xi)\right]_0^1\right), \end{aligned} \tag{4.19}$$

for the cubic Hermite shape function. These equations must be zero for any values δU_k and δU_{kl}, i.e.,

$$\begin{aligned} 0 &= \sum_{k=1}^{N}\delta U_k r_k(U_1, U_2, ..., U_N), \\ 0 &= \sum_{k=1}^{N}\sum_{l=1}^{2}\delta U_{kl} r_{kl}(U_{11}, U_{12}, ..., U_{N1}, U_{N2}). \end{aligned} \tag{4.20}$$

Therefore, for any nonzero value of the coefficients $\delta U_k; k = 1, ..., N$, and $\delta U_{kl}; k = 1, ..., N; l = 1, 2$, we have that

$$0 = r_k(U_1, U_2, ..., U_N) = \int_0^1\left(\frac{du}{d\xi}\frac{d\psi_k}{d\xi} - \frac{1}{h}f(\xi)\psi_k(\xi)\right)d\xi - \left[\frac{du}{d\xi}\psi_k(\xi)\right]_0^1, \tag{4.21}$$

and,

$$0 = r_{kl}(U_{11}, U_{12}, ..., U_{N1}, U_{N2}) = \int_0^1 \left(\frac{du}{d\xi}\frac{d\psi_{kl}}{d\xi} - \frac{1}{h} f(\xi)\psi_{kl}(\xi) \right) d\xi - \left[\frac{du}{d\xi}\psi_{kl}(\xi) \right]_0^1, \tag{4.22}$$

for the linear Lagrange and the cubic Hermite shape functions, respectively. Note that, in the present case, the global coordinate is considered in order to specify conditions at the boundaries 0 and 1 for the Poisson equation.

After substituting the approximation of the solution (4.16) into (4.21) and (4.17) into (4.22), we have

$$0 = r_k(U_1, U_2, ..., U_N) = \int_0^1 \left(\sum_{l=1}^{N} U_l \frac{d\psi_l}{d\xi}\frac{d\psi_k}{d\xi} - \frac{1}{h} f(\xi)\psi_k(\xi) \right) d\xi - \left[\frac{du}{d\xi}\psi_k(\xi) \right]_0^1, \tag{4.23}$$

for the Lagrange shape function, and

$$\begin{aligned} 0 &= r_{kl}(U_{11}, U_{12}, ..., U_{N1}, U_{N2}) \\ &= \int_0^1 \left(\sum_{m=1}^{N}\sum_{n=1}^{2} U_{mn} \frac{d\psi_{mn}}{d\xi}\frac{d\psi_{kl}}{d\xi} - \frac{1}{h} f(\xi)\psi_{kl}(\xi) \right) d\xi - \left[\frac{du}{d\xi}\psi_{kl}(\xi) \right]_0^1, \end{aligned} \tag{4.24}$$

for the Hermite shape function, respectively.

From (4.23), the discrete form of the equation becomes

$$\begin{aligned} 0 = r_k = \int_0^1 \left(U_1 \frac{d\psi_1}{d\xi}\frac{d\psi_k}{d\xi} + U_N \frac{d\psi_N}{d\xi}\frac{d\psi_k}{d\xi} + \sum_{l=2}^{N-1} U_l \frac{d\psi_l}{d\xi}\frac{d\psi_k}{d\xi} - \frac{1}{h} f(\xi)\psi_k(\xi) \right) d\xi \\ - \left[\frac{du}{d\xi}\psi_k(\xi) \right]_0^1. \end{aligned} \tag{4.25}$$

On the other hand, employing the cubic Hermite function as an approximation function in (4.24) gives

$$\begin{aligned} 0 = r_{kl} = \int_0^1 \Bigg(U_{11} \frac{d\psi_{11}}{d\xi}\frac{d\psi_{kl}}{d\xi} + U_{12} \frac{d\psi_{12}}{d\xi}\frac{d\psi_{kl}}{d\xi} + U_{N1} \frac{d\psi_{N1}}{d\xi}\frac{d\psi_{kl}}{d\xi} + U_{N2} \frac{d\psi_{N2}}{d\xi}\frac{d\psi_{kl}}{d\xi} \\ + \sum_{m=2}^{N-1}\sum_{n=1}^{2} U_{mn} \frac{d\psi_{mn}}{d\xi}\frac{d\psi_{kl}}{d\xi} - \frac{1}{h} f(\xi)\psi_{kl}(\xi) \Bigg) d\xi - \left[\frac{du}{d\xi}\psi_{kl}(\xi) \right]_0^1. \end{aligned} \tag{4.26}$$

These equations (4.25) and (4.26) are the implemented equations in the finite element method for the Poisson equation using the Lagrange and the Hermite interpolation, respectively. It can be seen from those two equations that there exists the condition for $\frac{du}{d\xi}$ appeared in the boundary terms $\left[\frac{du}{d\xi}\psi_k(\xi) \right]_0^1$ and $\left[\frac{du}{d\xi}\psi_{kl}(\xi) \right]_0^1$ in the

implemented equations which need to be taken care. This boundary condition is the so-called natural boundary condition.

Note that Neumann boundary conditions or other boundary conditions prescribing derivatives are usually called natural boundary conditions because they follow directly from the weak formulation and are not explicitly imposed. It can be seen later on that the natural boundary conditions impose no constraints on a continuity of functions but rather alter the implemented equation. On the other hand, the essential boundary conditions must be imposed explicitly in the problem's formulation. In the clamped beam problem, the essential boundary conditions are $u = 0$ at both boundaries.

Examination of the terms in (4.25) indicates that two conditions at the boundaries have to be considered for the Lagrange functions, U_1, U_N, while four boundary conditions, $U_{11}, U_{12}, U_{N1}, U_{N2}$ are needed for the Hermite functions as shown in (4.26). Therefore, specifications on the boundary conditions will play an essential role on the consistency between the finite element solution and the natural boundary condition.

To elaborate the effect of boundary specifications for each interpolation, two main cases are considered − relaxing the unknown degree of freedom at one end and pinning the unknown degree of freedom at both ends. In the first case, we will relax the unknown degree of freedom at one end, says at $\xi = 0$, i.e., we prescribe the value of $u(1) = \alpha$. Hence, $U_N = \alpha$ for the Lagrange interpolation and $U_{N1} = \alpha$ for the Hermite interpolation. Now, (4.25) and (4.26) become, for $k = 1, ..., N-1$ and $l = 1, 2$,

$$\begin{aligned} 0 = r_k = \int_0^1 \left(U_1 \frac{d\psi_1}{d\xi}\frac{d\psi_k}{d\xi} + \alpha \frac{d\psi_N}{d\xi}\frac{d\psi_k}{d\xi} + \sum_{l=2}^{N-1} U_l \frac{d\psi_l}{d\xi}\frac{d\psi_k}{d\xi} - \frac{1}{h} f(\xi)\psi_k(\xi) \right) d\xi \\ + \frac{du}{d\xi}(0)\psi_k(0), \end{aligned} \tag{4.27}$$

and,

$$\begin{aligned} 0 = r_{kl} = \int_0^1 \Bigg(U_{11}\frac{d\psi_{11}}{d\xi}\frac{d\psi_{kl}}{d\xi} + U_{12}\frac{d\psi_{12}}{d\xi}\frac{d\psi_{kl}}{d\xi} + \alpha \frac{d\psi_{N1}}{d\xi}\frac{d\psi_{kl}}{d\xi} + U_{N2}\frac{d\psi_{N2}}{d\xi}\frac{d\psi_{kl}}{d\xi} \\ + \sum_{m=2}^{N-1}\sum_{n=1}^{2} U_{mn}\frac{d\psi_{mn}}{d\xi}\frac{d\psi_{kl}}{d\xi} - \frac{1}{h} f(\xi)\psi_{kl}(\xi) \Bigg) d\xi + \frac{du}{d\xi}(0)\psi_{kl}(0), \end{aligned} \tag{4.28}$$

respectively.

Now, let us consider the consistency between the natural boundary condition $\frac{du}{d\xi}$ at $\xi = 0$ and the nodal value U_{12} which is associated with the unknown derivative at $\xi = 0$. For the Lagrange interpolation function, if another given boundary condition

$\frac{du}{d\xi}$ at $\xi = 0$ is zero, there is no contribution of the natural boundary condition into the implemented equation. But if we have non-zero derivative, $\frac{du}{d\xi}(0) \neq 0$, the natural boundary condition $\frac{du}{d\xi}(0)$ must be included in the implemented equation as in (4.27). However, we don't have to worry about the consistency with the natural boundary condition in this case since there is no derivative degree of freedom defined in the Lagrange shape functions.

For the Hermite interpolation function, we can similarly perform as described in the Lagrange interpolation function. However, since there is the derivative degree of freedom defined in the Hermite interpolation function, the consistency between the natural boundary condition $\frac{du}{d\xi}(0)$ and the nodal value U_{12} has to be concerned. In this case, knowing the values $u(1)$ and $\frac{du}{d\xi}(0)$ still gives another two additional values, U_{11}, U_{N2}, to be taken care. Numerical results for the specification of these two degrees of freedom will be illustrated in the next subsection.

Regarding the second case of the boundary specifications, we will pin the unknown degree of freedom at both ends of the boundary. In this case, the unknown u have been imposed to some values, say $u(0) = \alpha, u(1) = \beta$. Hence, $U_1 = \alpha, U_N = \beta$ for the Lagrange interpolation and $U_{11} = \alpha, U_{N1} = \beta$ for the Hermite interpolation. Now, the implemented equation for the Poisson problem using the Lagrange interpolations becomes, for $k = 2, ..., N-1$,

$$0 = r_k = \int_0^1 \left(\alpha \frac{d\psi_1}{d\xi}\frac{d\psi_k}{d\xi} + \beta \frac{d\psi_N}{d\xi}\frac{d\psi_k}{d\xi} + \sum_{l=2}^{N-1} U_l \frac{d\psi_l}{d\xi}\frac{d\psi_k}{d\xi} - \frac{1}{h} f(\xi)\psi_k(\xi) \right) d\xi. \tag{4.29}$$

Similarly, the implemented equation for the Poisson problem using the Hermite interpolations, (4.26), becomes, for r_{12}, r_{N2}, and $r_{kl}; k = 2, ..., N-1, l = 1, 2$,

$$\begin{aligned} 0 = r_{kl} = \int_0^1 \Bigg(& \alpha \frac{d\psi_{11}}{d\xi}\frac{d\psi_{kl}}{d\xi} + U_{12}\frac{d\psi_{12}}{d\xi}\frac{d\psi_{kl}}{d\xi} + \beta \frac{d\psi_{N1}}{d\xi}\frac{d\psi_{kl}}{d\xi} + U_{N2}\frac{d\psi_{N2}}{d\xi}\frac{d\psi_{kl}}{d\xi} \\ & + \sum_{m=2}^{N-1}\sum_{n=1}^{2} U_{mn}\frac{d\psi_{mn}}{d\xi}\frac{d\psi_{kl}}{d\xi} - \frac{1}{h} f(\xi)\psi_{kl}(\xi) \Bigg) d\xi. \end{aligned} \tag{4.30}$$

However, there are still two additional values U_{12} and U_{N2} that have to be specified at the boundaries for the Hermite interpolation. These are values associated with the derivative degree of freedom which will be determined as part of the solution. Since there is no natural boundary conditions in this case, using the Hermite interpolation functions to approximate the unknown for the Poisson equation is not problematic as we will numerically show in the next section.

Numerical implementations of solving the Poisson equation with the Hermite interpolation

In this section, we will solve the Poisson equation by using the Hermite interpolation. The objective is to check the consistency between the finite element solution obtained from the Hermite interpolation and the specified natural boundary conditions. The numerical results from different cases of boundary specifications as discussed in the previous section will be illustrated.

Let consider the following Poisson equation

$$\frac{d^2u}{d\xi^2} + \frac{1}{h}f(\xi) = 0, \quad \xi \in [0,1], \tag{4.31}$$

where $h = 1$ and $f(\xi) = -(4\xi^2+2)e^{(\xi^2+6)}$ with the following boundary conditions. For the boundary condition specifications in case 1 explained in (4.27) and (4.28), we have

$$u(1) = 1096.63, \quad \frac{du}{d\xi}(0) = 0, \tag{4.32}$$

and those in case 2 explained in (4.29) and (4.30) are

$$u(0) = 403.4288, \quad u(1) = 1096.63. \tag{4.33}$$

The exact solution for (4.31) with boundary conditions in both cases is

$$u(\xi) = e^{(\xi^2+6)}. \tag{4.34}$$

Therefore, its first derivative is

$$u'(\xi) = 2\xi e^{(\xi^2+6)}. \tag{4.35}$$

As mention previously, using the Hermite interpolation functions to approximate the solution of the second-order differential equation will introduce additional derivative degrees of freedom at boundaries. In order to implement the Poisson equation (4.31) using the Hermite interpolation in the finite element method, the implemented equations (4.28) and (4.30) will be considered for case 1 and case 2, respectively. Note that the finite element implementations for all cases in this section are done using 100 elements in the mesh.

Firstly, we consider the first case where the unknown degree of freedom is pinned at one boundary and free at the other end. In this Poisson problem, the boundary

conditions are $u(1) = 1096.63$ and $\frac{du}{d\xi}(0) = 0$. Now, we still have another two additional degrees of freedom to specify. If we constrain the unknown degree of freedom at the boundary $\xi = 0$, this situation will refer to case 2 which will be discussed later on. But if we specify a value to the derivative degree of freedom at $\xi = 1$, the equation system will be over-constrained. Therefore, we will let the unknown $u(0)$ and the derivative $\frac{du}{d\xi}(1)$ degrees of freedom be free.

case	$u(x=0)$	$u(x=1)$	$u'(x=0)$	$u'(x=1)$	Energy-norm error
1	free	pinned	pinned	free	7.66697×10^{-7}
2	pinned	pinned	pinned	pinned	1.03397×10^{-7}
2	pinned	pinned	free	free	7.66622×10^{-7}

Table 4.1: Specifications of boundary conditions at both ends with energy-norm error obtained from the solution associated with each case.

Fig. 4.2 illustrates that the finite element solution for the derivative degree of freedom at $\xi = 0$ is consistent with the natural boundary condition, $\frac{du}{d\xi}(0) = 0$. Moreover, the obtained finite element solution and the exact solution for the derivative degrees of freedom are consistent along the mesh with very small differences. As can be seen in Table 4.1, the obtained error for this case is in order of 10^{-7}. Note that error computes in Table 4.1 obtained from the energy norm which can be expressed as

$$\|u_{exact} - u_{FE}\|_m = \left(\int \sum_{i=0}^{m} \left| \frac{d^i u_{exact}}{dx^i} - \frac{d^i u_{FE}}{dx^i} \right|^2 dx \right)^{1/2}, \tag{4.36}$$

where $2m$ is the order of the differential equation being solved.

In order to illustrate the derivative specifications for case 2 using the Hermite interpolation, two cases of derivatives degree of freedom at boundaries will be determined. The first case is that the derivative degrees of freedom are pinned and specified to the exact solution at both ends while the second case is to relax the boundary conditions by letting the derivative degrees of freedom to be free at both ends.

The goal in case 2 is to show that the specification of the two additional values U_{12} and U_{N2} for the derivative degree of freedom at the boundaries does not matter since there is no contribution from the natural boundary condition to the implemented equation as shown in (4.30). Validations can be found in Table 4.1. Comparisons between the finite element solution and the exact solution of the derivative degrees

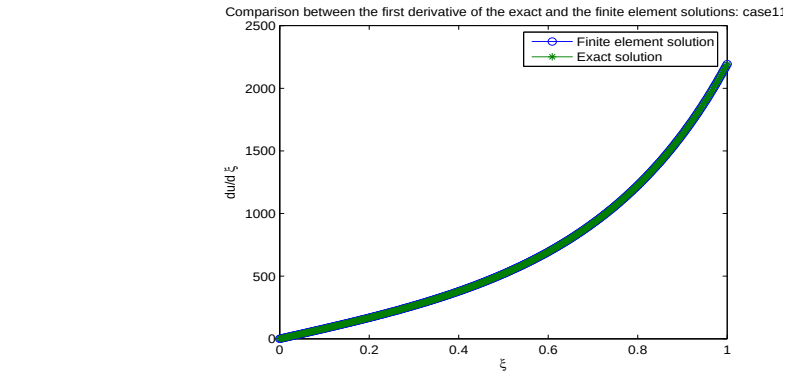

(a)

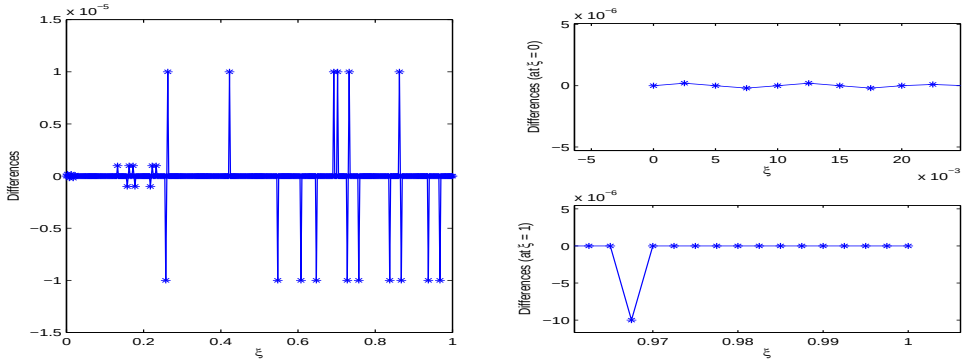

(b)

Figure 4.2: (4.2a) The comparison between the finite element solution and the exact solution of the derivative degrees of freedom. (4.2b) Differences between the exact and the finite element solutions of the derivative degrees of freedom. These are computed under Case 1 with the boundary conditions that $u(1) = 1096.63$ and $\frac{du}{d\xi}(0) = 0$.

of freedom for both cases show the consistency with very small differences as seen in Figs. 4.3 and 4.4.

Regarding error between subcases of case 2, Table 4.1 illustrates that there is little distinction between different cases of the derivative specifications. These confirm that there is no contribution from the natural boundary condition.

Hence, employing the Hermite interpolation to approximate the solution of the second-order equation with the Dirichlet boundary conditions can be a promising way to do in the finite element method as no further information requires in order to specify the derivative degree of freedom. However, ones have to be aware that the implemented equation in the finite element method for the Neumann boundary value problem can be altered to satisfy the consistency with the natural boundary conditions.

Unlike the Hermite function, the implemented equation for the Lagrange interpolation can be kept very simple as there is no unnecessary degree of freedom included.

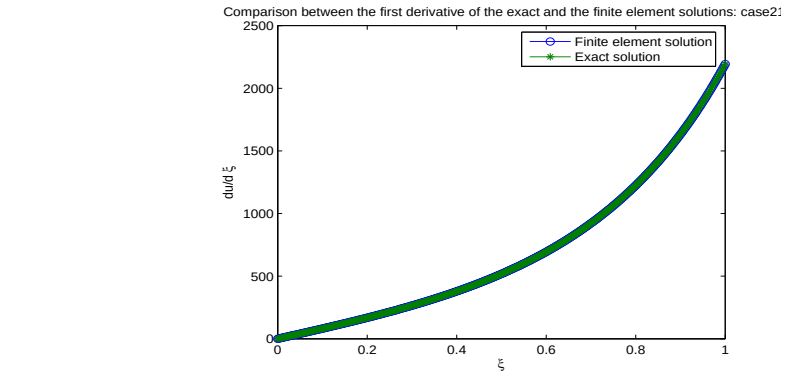

(a)

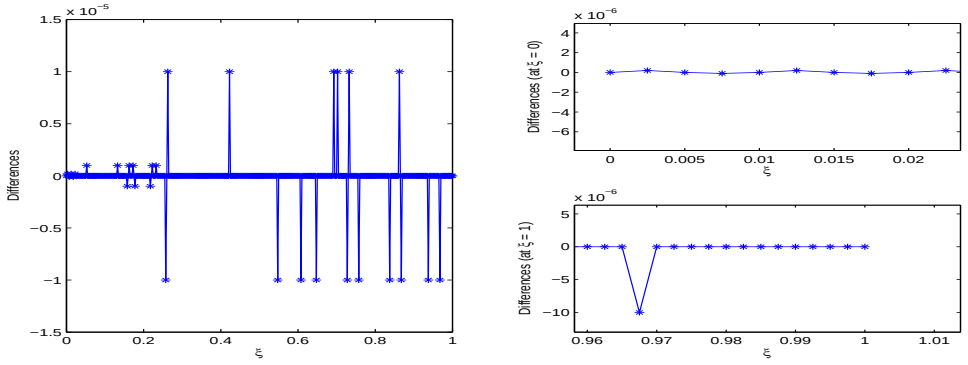

(b)

Figure 4.3: (4.3a) The comparison between the finite element solution and the exact solution of the derivative degrees of freedom. (4.3b) Differences between the exact and the finite element solutions of the derivative degrees of freedom. These are computed under Case 2 with the derivative degrees of freedom are specified at both ends.

Consequently, there is no concern about the consistency between the natural boundary conditions and the derivative degrees of freedom. Therefore, it is better to employ the Lagrange interpolation to approximate the solution of the second-order differential equation.

Finite element representation of the fourth-order partial differential equation

In an area of continuum mechanics, especially in linear elastic theory, not only the Poisson-type equation but the Biharmonic-type equation might be concerned as it is the governing equation for the normal displacement. The normal governing equation which is the Biharmonic-type equation can be described as follow (see 4.7)

$$\frac{1}{12}h^2\frac{d^4u}{d\xi^4} - \frac{1}{h}f(\xi) = 0, \tag{4.37}$$

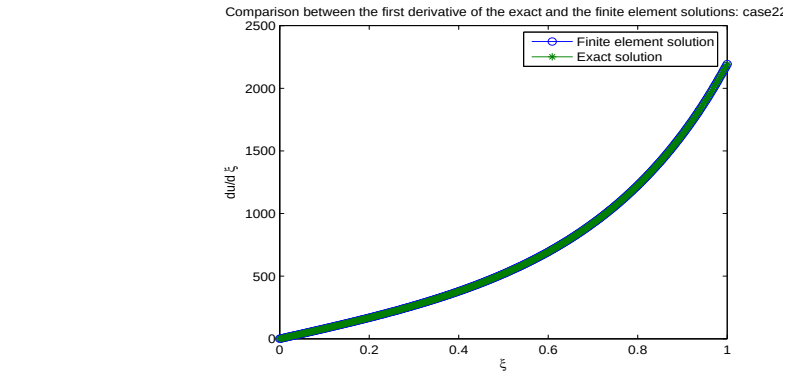

(a)

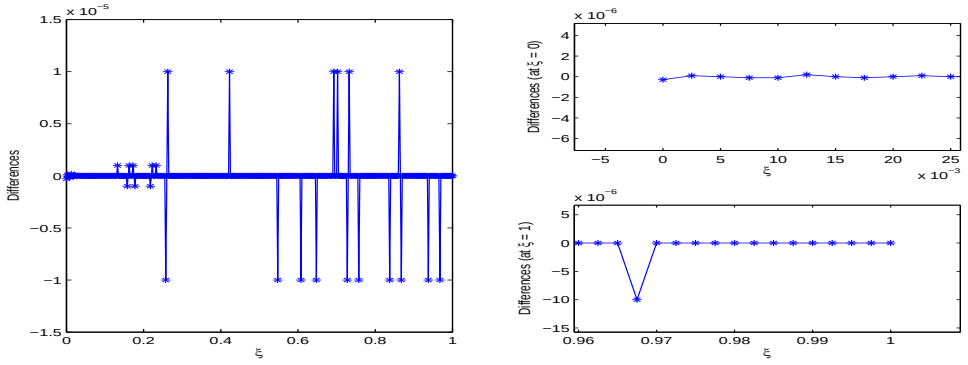

(b)

Figure 4.4: (4.4a) The comparison between the finite element solution and the exact solution of the derivative degrees of freedom. (4.4b) Differences between the exact and the finite element solutions of the derivative degrees of freedom. These are computed under Case 2 with the derivative degrees of freedom are free at both ends.

where its weak formulation after integration by parts twice is

$$0 = \int_0^1 \left\{ \left(-\frac{1}{h} f \right) \delta(u) + \frac{1}{12} h^2 \frac{d^2u}{d\xi^2} \delta \left(\frac{d^2u}{d\xi^2} \right) \right\} d\xi + \frac{d^3u}{d\xi^3} \delta u \Big|_0^1 - \frac{d^2u}{d\xi^2} \delta \left(\frac{du}{d\xi} \right) \Big|_0^1. \quad (4.38)$$

Similar to the second-order equation, the boundary terms appearing in (4.38) have to be determined from boundary conditions. In order to consider approximate functions for the solution of (4.37), we will simplify the implemented equation by applying homogeneous boundary conditions for the unknown and its derivatives at both ends. Therefore, $\delta u = 0, \delta \left(\frac{du}{d\xi} \right) = 0$ at the boundaries and we can employ (4.38) to develop the implemented equation for the Biharmonic equation with no boundary terms.

Substituting the approximation of the variations of the unknown u and its derivatives (4.17) back into (4.38), we have

$$\begin{aligned} 0 &= \int_0^1 \left(\frac{1}{12} h^2 \frac{d^2u}{d\xi^2} \sum_{k=1}^{N} \sum_{l=1}^{2} \delta U_{kl} \frac{d^2\psi_{kl}}{d\xi^2} - \frac{1}{h} f(\xi) \sum_{k=1}^{N} \sum_{l=1}^{2} \delta U_{kl} \psi_{kl}(\xi) \right) d\xi \\ &= \sum_{k=1}^{N} \sum_{l=1}^{2} \delta U_{kl} \left[\int_0^1 \left(\frac{1}{12} h^2 \frac{d^2u}{d\xi^2} \frac{d^2\psi_{kl}}{d\xi^2} - \frac{1}{h} f(\xi) \psi_{kl}(\xi) \right) d\xi \right. \\ &= \sum_{k=1}^{N} \sum_{l=1}^{2} \delta U_{kl} r_{kl}(U_{11}, U_{12}, ..., U_{N1}, U_{N2}). \end{aligned} \tag{4.39}$$

Therefore, for any value of the coefficients $\delta U_{kl}; k = 1, ..., N; l = 1, 2$, we have that

$$0 = r_{kl}(U_{11}, U_{12}, ..., U_{N1}, U_{N2}) = \int_0^1 \left(\frac{1}{12} h^2 \frac{d^2u}{d\xi^2} \frac{d^2\psi_{kl}}{d\xi^2} - \frac{1}{h} f(\xi) \psi_{kl}(\xi) \right) d\xi. \tag{4.40}$$

After substituting the approximation of the solution into (4.40), the implemented equation for the Biharmonic-type equation is obtained as

$$\begin{aligned} 0 &= r_{kl}(U_{11}, U_{12}, ..., U_{N1}, U_{N2}) \\ &= \int_0^1 \left(\frac{1}{12} h^2 \frac{d^2u}{d\xi^2} \frac{d^2\psi_{kl}}{d\xi^2} - \frac{1}{h} f(\xi) \psi_{kl}(\xi) \right) d\xi, \\ &= \int_0^1 \left(\frac{1}{12} h^2 \sum_{m=1}^{N} \sum_{n=1}^{2} U_{mn} \frac{d^2\psi_{mn}}{d\xi^2} \frac{d^2\psi_{kl}}{d\xi^2} - \frac{1}{h} f(\xi) \psi_{kl}(\xi) \right) d\xi. \end{aligned} \tag{4.41}$$

It can be seen from (4.41) that global basis functions approximating the solution have to be continuous with nonzero derivatives up to order two. Also, in order to make the integral exists, the value and its derivative have to be continuous and constrained at nodes. This results in having two unknowns per nodes which gives a total of four conditions in an element that have to be specified. Therefore, the appropriate polynomial used to interpolate an unknown variable u in this type of equation has to be cubic. Moreover, the interpolation function that used in an approximation of u have to be continuous for both values and its derivative between elements.

Since the Hermite family of shape functions is associated with u and $\frac{du}{d\xi}$, the continuity of both unknowns required in (4.41) can be assured. Moreover, a cubic Hermite element will have four degree of freedoms per element, two at each node for u and $\frac{du}{d\xi}$, which allows us to specify conditions for the implementation of the fourth-order problem.

Recall that the cubic Lagrange interpolation functions are derived from interpolating a function but not its derivatives. Even though a cubic Lagrange element have

four unknowns of the dependent variable, there is no derivative degree of freedom to ensure the C^1-continuity. Since the slope of the dependent variable is also required by the weak form to be continuous between nodes, the cubic Lagrange interpolation of u is not suitable in the finite element approximation of $\frac{du}{d\xi}$.

In conclusion, to implement a finite element method, it has been found that the Lagrange interpolation is preferable to approximate the solution in the case of the second-order equation as we illustrated theoretically in the first subsection and numerically in the second subsection of section 4.2.2. Moreover, the third subsection of section 4.2.2 elaborated that the Hermite interpolation should be employed to approximate the solution of the fourth-order equation. Therefore, our finite element implementations in this thesis will employ this mix-formulation to obtain the solutions of linearised beam and shell problems which govern by the coupled equations between the second and the fourth order differential equation.

4.2.3 Numerical comparisons between the Kirchhoff-Love linear and nonlinear governing equations

In this section, implementations of the linearised governing equation for the straight beam will be discussed and compared with the nonlinear equations that associate with the problem.

Regarding the linear-theory implementations, there are two formulations to be compared. The first one is the Hermite formulation which employed the Hermite interpolation functions as a shape function for both tangential and normal displacements. The other formulation is the mixed formulation which employs the Lagrange interpolation for a tangential displacement and the Hermite interpolation for a normal displacement. This is to illustrate that the Lagrange shape function shall be employed to approximate the tangential displacement which governs by the second-order partial differential equation. Therefore, numerical comparisons will be made between the solutions obtained from the two formulation schemes as well as the solutions of the linear and the nonlinear equations.

In order to perform a finite element implementation, the domain of interest will be first discretised. Since we are going to consider the straight beam in this section, the

given one-dimensional domain is divided into a set of line elements being of length h_e as illustrated in Fig. 4.5.

In this problem, the choice of number of nodes and elements is chosen to have 100 elements with 201 nodes in the mesh. This is a result from using 3-node elements which employ a quadratic Lagrange shape function to approximate the tangential displacement.

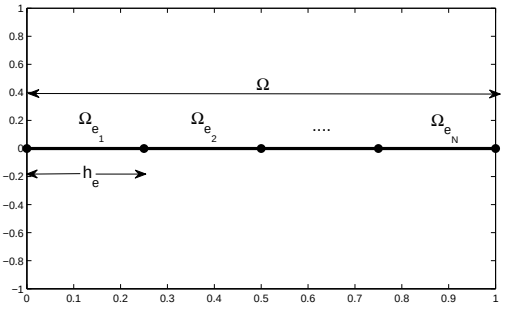

Figure 4.5: Finite element discretisation of one-dimensional domains: a straight line beam.

In order to perform the Gaussian integration, the degree of precision and the number of Gauss points and weights must be determined so that the function under an integral can be accurately approximated. Since the cubic polynomial is the highest order of the considered interpolation functions, it can be seen from the governing equation (4.6) that the highest order of function in the beam element under the integral between the second- and the fourth-order equations is quartic. Therefore, the 3-point rule is specified and defined as in Table 4.2. Note that the r number of weights w_i and the integral points ξ_i can be accurately approximated a polynomial of degree $2r - 1$ [40].

Points i	ξ_i	Weights w_i
0	-0.7745966692	0.8888888889
1	0	0.5555555555
2	0.7745966692	0.8888888889

Table 4.2: A tabular of weights and Gauss points used in the Gauss quadrature for an integral approximation when $r = 3$.

Next, we will consider boundary conditions that will be specified in tangential and normal displacements for the beam with a clamped support. As the beam is

clamped at both ends, the displacement in tangential direction has to be specified so that $u^1(\xi = 0) = 0$ and $u^1(\xi = 1) = 0$. To determine boundary conditions for the normal displacement, there are two degrees of freedom to be concerned at nodes; the displacement value and its derivative. Since the beam is clamped, we have that both value and its derivative have to be set to zero at both boundaries 0 and 1, i.e., $u^2(\xi = 0) = 0, u^{2'}(\xi = 0) = 0$ and $u^2(\xi = 1) = 0, u^{2'}(\xi = 1) = 0$.

After we have specified boundary conditions, the linear governing equation (4.6) is solved numerically using a finite-element method in `Oomph-lib` [53] while the nonlinear governing equation can be formulated from (3.63). Note that there is no initial stress and constant external forces are uniformly distributed in normal direction to a beam. Within a small-deformation regime, the load applied in the normal direction to both linear and nonlinear equations is small and the same. It equals to $1.0e-8$.

The finite element solutions obtained from the linear and nonlinear equations is indistinguishable as can be seen in Fig. 4.6a and Fig. 4.6b. The error obtained by the maximum norm between the linear and nonlinear equations for $f = 1 \times 10^{-8}$ is in the order of 10^{-7} which is so small that it is effectively zero. In these figures, deformed positions are compared and they can be computed as

$$\mathbf{R}(\xi) = \mathbf{r}(\xi) + \mathbf{u}(\xi). \tag{4.42}$$

Since we consider the positions in the Cartesian coordinate system, the tangential and normal displacement, u_1 and u_2, have to be considered in the same coordinate system. The transformation of the tangential and normal displacements to the Cartesian coordinate system can be done by

$$\begin{aligned} u_x &= u^1 t_1 + u^2 \hat{n}_1, \\ u_y &= u^1 t_2 + u^2 \hat{n}_2, \end{aligned} \tag{4.43}$$

where $t_i, \hat{n}_i;, i = 1, 2$, denote components of the tangent, $\mathbf{t}$, and the unit normal, $\hat{\mathbf{n}}$, vectors, respectively. After substituting (4.43) back into (4.42), deformed positions in the Cartesian coordinate system are obtained.

Next, we will investigate how the magnitude of a loading term will effect on the solution of the linear and nonlinear equations. To appreciate this, the external forces that applied to the beam in the normal direction are varied and increased from 0 by $1.0e-8$ for 21 steps.

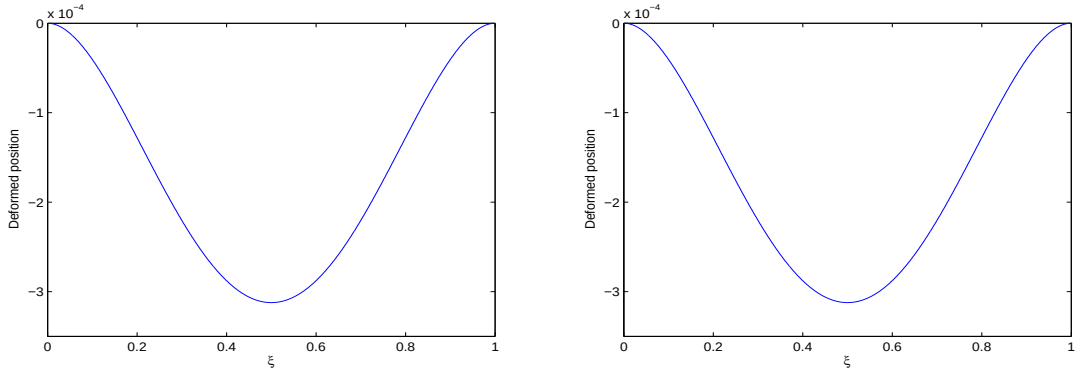

(a) Deformed positions obtained from Nonlinear eqn (b) Deformed positions obtained from Linear eqn

Figure 4.6: Comparisons between the deformed positions obtained from nonlinear and linear equations of a straight line beam with a clamped support at the end points with the same constant loads $= 1.0e - 8$ applied in normal direction.

Figure 4.7 depicts the finite element solutions of displacements obtained from the linear and nonlinear beam equations compared with the analytic solution. It can be seen that solutions obtained from both the Hermite and the mixed formulation of the linearised beam give better accuracy than the nonlinear solutions as they are consistent with the analytic solutions. Furthermore, when a loading is small, the solutions obtained from linear and nonlinear equations agree. They start to disagree when loading becomes larger. For the straight beam, the maximum displacement which the linear and nonlinear equations still agree with 0.01% relative error is 3.12% of the thickness.

Regarding the comparison between the mixed and the Hermite formulations, it can be seen from Fig. 4.8 that the error between them is effectively zero. This has proved that there is no contribution from the natural boundary condition into the implemented equation for the Hermite formulation when boundary conditions for the value are pinned at both ends. Therefore, the Hermite formulation can be employed for the clamped support problem.

4.3 Finite element method for an elastic ring

In the previous section, we consider the straight beam whose undeformed configuration has a zero curvature. Even though the solutions obtained from the linear and nonlinear

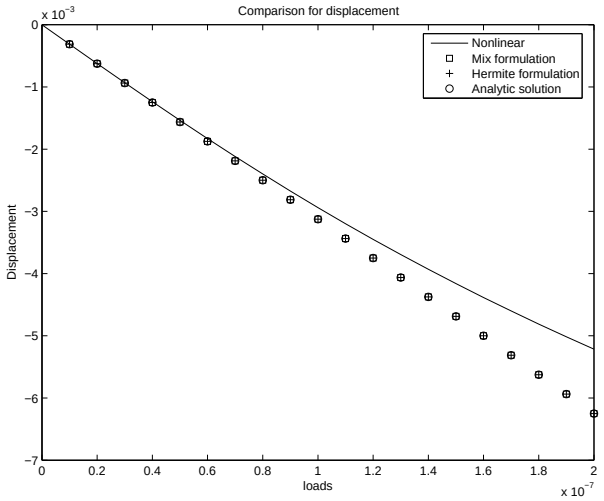

Figure 4.7: Comparisons between displacements obtained from different implementations together with the analytic solution for a deformed straight line beam with different loads.

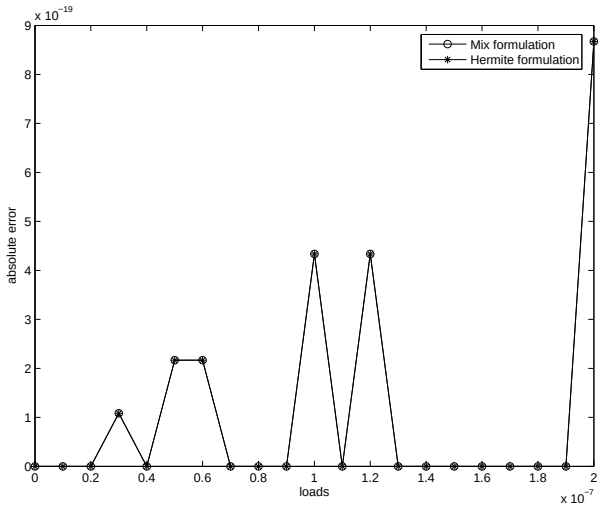

Figure 4.8: Comparisons between absolute error obtained from the difference between solutions of the mixed and Hermite formulations and the analytic solution for a deformed straight beam with different loads.

governing equations for the straight beam agree when a force is small, it still can not be concluded that the thin-beam behaviour can be described by the linear governing equation within a small-deformation regime. This is a consequence of some missing terms from the governing equations of a general shape expressed in (3.89) and (3.90) when comes to the straight beam. Hence, we will consider the beam whose domain of interest has a non-zero curvature in this section in order to investigate the consistency between the linear and nonlinear solutions.

4.3.1 The linearised governing equation

In this section, an elastic ring is considered. It is a curved beam whose initial geometry is a unit circle. To implement the deformation of an elastic ring in this study, the symmetric assumption is applied since the quarter of a unit circle is considered as illustrated in Fig. 4.9. Therefore, intrinsic coordinate ξ (which can be thought as an angle) extends from 0 to $\frac{\pi}{2}$. The elastic ring is subjected to the constant loads which is normally distributed.

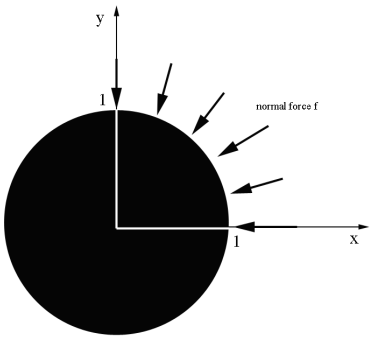

Figure 4.9: The geometrical description of an elastic ring with loads in normal direction.

The initial positions of an elastic ring are $\mathbf{r} = \begin{pmatrix} \cos(\xi) \\ \sin(\xi) \end{pmatrix}$, $\xi \in [0, \pi/2]$. The linear version of the metric tensors in the undeformed and deformed configurations are, respectively,

$$a = \frac{\partial \mathbf{r}}{\partial \xi} \cdot \frac{\partial \mathbf{r}}{\partial \xi} = \begin{pmatrix} -\sin(\xi) \\ \cos(\xi) \end{pmatrix} \cdot \begin{pmatrix} -\sin(\xi) \\ \cos(\xi) \end{pmatrix} = 1, \tag{4.44}$$

and, from (3.71),

$$A = 1 + 2\mathbf{t} \cdot \frac{\partial \mathbf{u}}{\partial \xi}. \tag{4.45}$$

The linear version of the beam curvature tensor in the undeformed and deformed configurations are

$$\begin{aligned} b &= \hat{\mathbf{n}} \cdot \frac{\partial^2 \mathbf{r}}{\partial \xi^2}, \\ B &= b + \left(2\frac{\partial u^1}{\partial \xi} + u^2 - \frac{\partial^2 u^2}{\partial \xi^2} \right). \end{aligned} \tag{4.46}$$

Therefore, the linearised strain and bending tensors and their variations can be computed from (3.74), (3.75), (3.83), and (3.84) as

$$\begin{aligned}
\gamma &= a\left(\frac{\partial u^1}{\partial \xi} + u^2\right), \\
\delta\gamma &= a\delta\left(\frac{\partial u^1}{\partial \xi}\right) + a\delta\left(u^2\right), \\
\kappa &= 2\frac{\partial u^1}{\partial \xi} + u^2 - \frac{\partial^2 u^2}{\partial \xi^2}, \\
\delta\kappa &= 2\delta\left(\frac{\partial u^1}{\partial \xi}\right) + \delta u^2 - \delta\left(\frac{\partial^2 u^2}{\partial \xi^2}\right)
\end{aligned} \tag{4.47}$$

Thus, the linearised governing equation for an elastic ring displacement in tangential direction is,

$$\begin{aligned}
0 &= \int_0^L \left\{ \left[-\frac{1}{h} f^1\right] \delta u^1 + \left[a^2 \frac{\partial u^1}{\partial \xi} + a^2 u^2 \right.\right. \\
&+ \left.\left. \frac{1}{6} h^2 \left(2\frac{\partial u^1}{\partial \xi} + u^2 - \frac{\partial^2 u^2}{\partial \xi^2}\right)\right] \delta\left(\frac{\partial u^1}{\partial \xi}\right) \right\} \sqrt{a} d\xi \\
&= \int_0^L \left\{ -\frac{1}{h} f^1 - a^2 \frac{\partial^2 u^1}{\partial \xi^2} - a^2 \frac{\partial u^2}{\partial \xi} - \frac{1}{3} h^2 \frac{\partial^2 u^1}{\partial \xi^2} \right. \\
&- \left. \frac{1}{6} h^2 \frac{\partial u^2}{\partial \xi} + \frac{1}{6} h^2 \frac{\partial^3 u^2}{\partial \xi^3} \right\} \delta u^1 \sqrt{a} d\xi \\
&+ \left[a^2 \frac{\partial u^1}{\partial \xi} + a^2 u^2 + \frac{1}{6} h^2 \left(2\frac{\partial u^1}{\partial \xi} + u^2 - \frac{\partial^2 u^2}{\partial \xi^2}\right)\right] \delta(u^1)\Big|_0^L,
\end{aligned} \tag{4.48}$$

where the last equation is obtained from the integration by parts. Since the clamped boundaries are applied at both ends, the boundary term appeared in the last line vanishes.

Now, we will consider the partial differential equation obtained from the tangential governing equation (4.48). We have that the PDE for a displacement in tangential direction u^1 of an elastic ring is given by

$$\begin{aligned}
\frac{a}{h} f^1 = &- \left(1 + \frac{1}{3}\left(\frac{h}{a}\right)^2\right) \frac{\partial^2 u^1}{\partial \xi^2} \\
&- \left(1 + \frac{1}{6}\left(\frac{h}{a}\right)^2\right) \frac{\partial u^2}{\partial \xi} + \frac{1}{6}\left(\frac{h}{a}\right)^2 \frac{\partial^3 u^2}{\partial \xi^3}.
\end{aligned} \tag{4.49}$$

Also, the linearised governing equation for an elastic ring displacement in normal

direction is expressed as

$$
\begin{aligned}
0 = & \int_0^L \left\{ \left[-\frac{1}{h} f^2 + a^2 \frac{\partial u_1}{\partial \xi} + a^2 u^2 + \frac{1}{6} h^2 \frac{\partial u^1}{\partial \xi} + \frac{1}{12} h^2 u^2 \right.\right. \\
& \left. - \frac{1}{12} h^2 \frac{\partial^2 u^2}{\partial \xi^2} \right] \delta u^2 + \left[-\frac{1}{6} h^2 \frac{\partial u^1}{\partial \xi} - \frac{1}{12} h^2 u^2 + \frac{1}{12} h^2 \frac{\partial^2 u^2}{\partial \xi^2} \right] \delta \left(\frac{\partial^2 u^2}{\partial \xi^2} \right) \left. \right\} \sqrt{a} d\xi \\
= & \int_0^L \left\{ -\frac{1}{h} f^2 + a^2 \frac{\partial u^1}{\partial \xi} + a^2 u^2 + \frac{1}{6} h^2 \frac{\partial u^1}{\partial \xi} + \frac{1}{12} h^2 u^2 \right. \\
& \left. - \frac{1}{12} h^2 \frac{\partial^2 u^2}{\partial \xi^2} - \frac{1}{6} h^2 \frac{\partial^3 u^1}{\partial \xi^3} - \frac{1}{12} h^2 \frac{\partial^2 u^2}{\partial \xi^2} + \frac{1}{12} h^2 \frac{\partial^4 u^2}{\partial \xi^4} \right\} \delta u^2 \sqrt{a} d\xi \\
& + \left[-\frac{1}{6} h^2 \frac{\partial u^1}{\partial \xi} - \frac{1}{12} h^2 u^2 + \frac{1}{12} h^2 \frac{\partial^2 u^2}{\partial \xi^2} \right] \delta \left(\frac{\partial u^2}{\partial \xi} \right) \Big|_0^L \\
& - \left[-\frac{1}{6} h^2 \frac{\partial^2 u^1}{\partial \xi^2} - \frac{1}{12} h^2 \frac{\partial u^2}{\partial \xi} + \frac{1}{12} h^2 \frac{\partial^3 u^2}{\partial \xi^3} \right] \delta (u^2) \Big|_0^L,
\end{aligned}
\tag{4.50}
$$

where, the last equation obtained from the integration by parts twice. Since the clamped boundaries are applied at both ends, all boundary terms appeared in the last line vanish. Similarly, the PDE for a displacement in normal direction u^2 of an elastic ring can be obtained as

$$
\begin{aligned}
\frac{a}{h} f^2 = & \left(1 + \frac{1}{6} \left(\frac{h}{a} \right)^2 \right) \frac{\partial u^1}{\partial \xi} - \frac{1}{6} \left(\frac{h}{a} \right)^2 \frac{\partial^3 u^1}{\partial \xi^3} \\
& + \left(1 + \frac{1}{12} \left(\frac{h}{a} \right)^2 \right) u^2 - \frac{1}{6} \left(\frac{h}{a} \right)^2 \frac{\partial^2 u^2}{\partial \xi^2} + \frac{1}{12} \left(\frac{h}{a} \right)^2 \frac{\partial^4 u^2}{\partial \xi^4}.
\end{aligned}
\tag{4.51}
$$

Note that the partial differential equations that govern displacements in both tangential and normal directions for the curved beam are more complicated than those of the straight beam. We can notice that the equations (4.48) and (4.50) are coupled between displacements in both directions. This is unlike the straight case that each governing equation is for the displacement in each direction. Therefore, the displacement in both directions has to be solved simultaneously for the curved beam.

Although the highest order of derivative in the normal governing equation shown in (4.7) and (4.51) is the same (quartic), the highest order derivative of the tangential governing equation in the curved beam case is of order 3 (see (4.49)) while that of the straight beam is of order 2 (see (4.8)). The higher order derivative in the tangential equation of the curved case is a result of having a non-zero curvature in the undeformed configuration.

Regarding the weak formulation for the curved beam, it can be seen from (4.48) and (4.50) that the finite element representations for displacements in both directions

are the same as in the straight case. Since the weak formulation of the normal governing equation (4.50) for the curved beam contains the variation of the second-order derivative of the normal displacement, the Hermite interpolation is employed to ensure the C^1-continuity. Also, (4.48) suggests that only C^0-continuity is required in order to make the integral exists as the integral contains only the variation of the first derivative of the tangential displacement. Therefore, the Lagrange interpolation function is employed to approximate the tangential displacement for the curved beam. Similar to the straight beam, the mixed formulation will be employed to implement the governing equations of the curved beam.

4.3.2 Numerical comparisons between the Kirchhoff-Love linear and nonlinear governing equations

Similar to section 4.2.3 for a straight beam, implementations of the linearised curved beam equations will be discussed and compared with the nonlinear equations that associate with the problem. Also, the Hermite and the mixed formulations of linear equations will be illustrated in order to validate the conclusion on the appropriate interpolation for a tangential displacement.

Firstly, the domain of interest will be discretised. Since we are going to consider a curved beam in this section, the given one-dimensional domains are divided into a set of line elements being of length h_e as illustrated in Fig. 4.10. In the implementations of the curved beam problem, the choice of number of nodes and elements and the numerical integration are chosen to be the same as in the straight beam case.

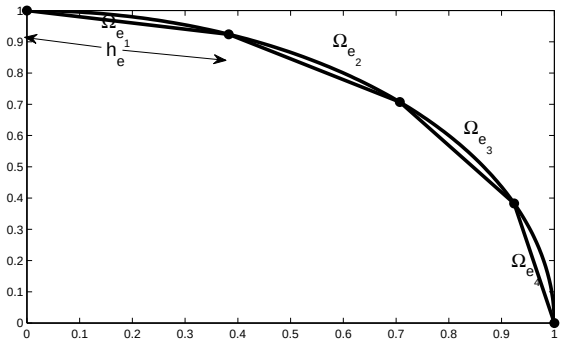

Figure 4.10: Finite element discretisation of one-dimensional domains: a curved beam.

Next, comparisons between nonlinear and linear governing equations for an elastic

ring are illustrated. Since only a quarter circular domain is implemented, both boundaries are assumed for a symmetry. Therefore, a displacement in normal direction is set to be free but its slope of the beam is pinned to be zero. A displacement in tangential direction is adjusted in such a way that both the positions are fixed (and so is the slope of the beam, in Hermite formulation) at end points so that a beam satisfies symmetric conditions at both ends.

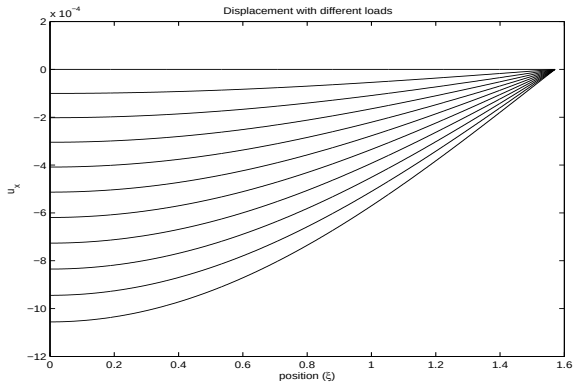

(a) Displacements in x-direction obtained from Nonlinear eqn

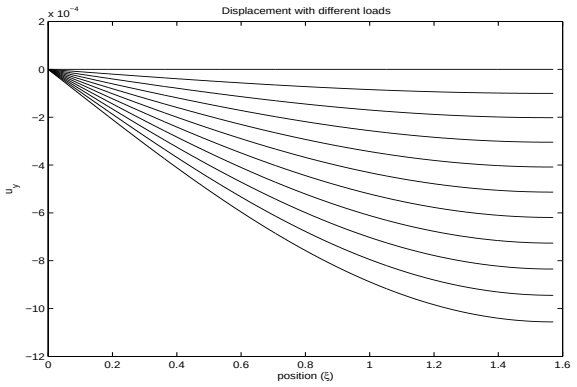

(b) Displacements in y-direction obtained from Nonlinear eqn

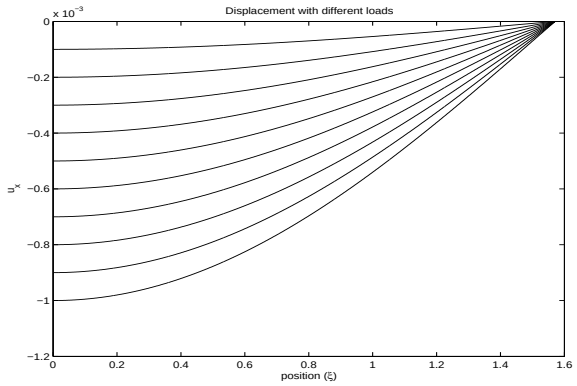

(c) Displacements in x-direction obtained from Linear eqn

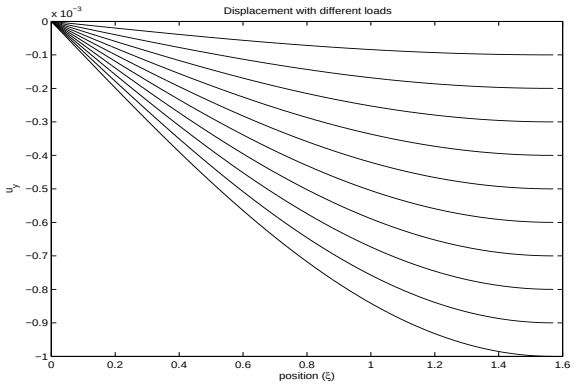

(d) Displacements in y-direction obtained from Linear eqn

Figure 4.11: Displacements in x and y-direction between nonlinear and linear equations for a deformed curved beam after different loads have been applied from $f_{\hat{n}} = 0$ to $f_{\hat{n}} = 1 \times 10^{-5}$.

Fig. 4.11 depicts displacement in x- and y-directions of an elastic ring with normally distributed loads from $f_{\hat{n}} = 0$ to $f_{\hat{n}} = 1 \times 10^{-5}$. It can be seen that the displacement in x- and y-directions are symmetric which introduces that the beam deforms axisymmetrically. Note that the transformation of the tangential and normal displacement to the Cartesian coordinate system can be done by (4.43).

Furthermore, Fig. 4.12 illustrates that a displacement obtained from the linear

governing equations increases when a load increases and it varies linearly with a load. Also, when a load increases, the results obtained from the linear and the nonlinear governing equations start to disagree. They agree only when applied loads are small. These results agree with those of the straight beam. For the elastic ring, the maximum displacement which the linear and nonlinear equations still agree is 1% of the thickness.

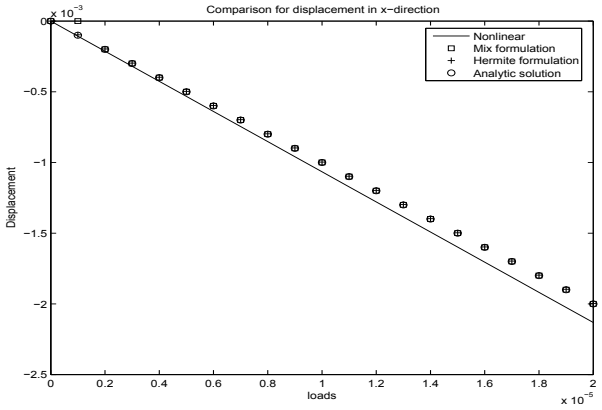

Figure 4.12: Comparisons between different implementations for a deformed curved beam with different loads.

In Fig. 4.12, the results between the two formulations of linear, nonlinear beams and the analytic solutions for an elastic ring displacement are also compared. We have that both formulations of linearised beam give better solutions than the nonlinear solutions as they are consistent with the analytic solution.

To compare a difference between the results obtained from the Hermite and the mixed formulations of linear equations, we will investigate from the absolute error between them and the analytic solution. Fig. 4.13 illustrates that the difference between the linear solutions obtained from the mixed and the Hermite are quite small which is consistent with the straight beam's result when the value degree of freedom is pinned at both ends.

Note that the analytic solution for an elastic ring can be obtained from the following expression

$$u_{exact} = -(R - r) = \frac{f_{\hat{n}}}{E_{eff}} \frac{1}{h}, \tag{4.52}$$

where R and r denote the deformed and undeformed radius of an elastic ring [3]. Equation (4.52) gives the relation between the radius of the deformed beam and the applied force in normal direction.

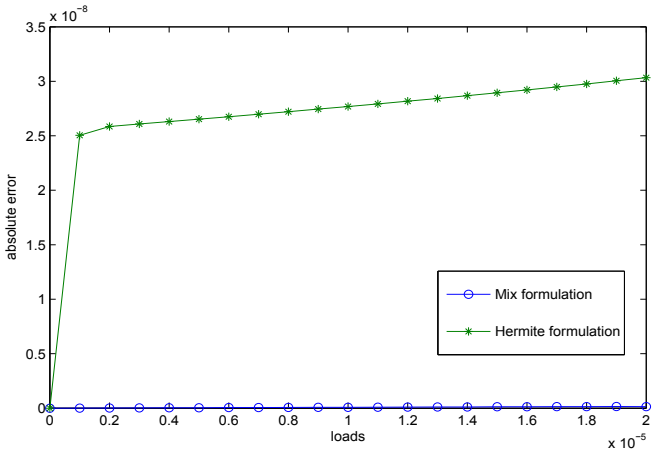

Figure 4.13: Comparisons between absolute error obtained from the difference between two different implementations; Mixed and Hermite,and the analytic solution for a curved beam with different loads.

4.4 Summary

In this chapter, finite element implementations of the classical beam theories in both linear and nonlinear governing equations with the linear constitutive law have been illustrated and compared. There are two kinds of beam geometry considered; a straight and a curved beam.

From section 4.2 and section 4.3, it can be seen that numerical comparisons between the linear and nonlinear governing equations corresponded for both cases of the straight and the curved beam. The linear and nonlinear solutions agree when a loading is small and start to disagree when a loading is large. This suggests that within a small-strain regime, the linear governing equation can be used to describe behaviours of a thin-beam when a displacement is small. Furthermore, an applied load should be in the range that gives displacements not greater than, approximately, 1-3% of the thickness.

Regarding the comparison between the linear solutions obtained from the mixed and the Hermite configurations, Figs. 4.8 and 4.13 showed that there were no significantly different between them. This is because there is no contribution from the natural boundary conditions as the clamped support problems are considered.

However, it is reasonable to continue using the mixed formulation scheme in the implementations of the linear beam problems and the rest of this study. The underlying reason is that using Hermite functions for the second-order differential equation gives

extra conditions for the derivative at boundaries that have to be concerned about the consistency with the natural boundary conditions. Also, the implemented equation for the finite element method has to be altered so that the consistency can be satisfied as illustrated in section 4.2.2. Therefore, Hermite polynomials are not of the correct order for the interpolation of a C^0-continuous solution.

Also, the theoretical investigation in section 4.2.2 suggested that Lagrange interpolation is suitable for an representation of the second-order differential equation. This is because there is no derivative degree of freedom defined in the Lagrange shape functions which have to be concerned with the natural boundary conditions. Therefore, the consistency between them is no longer an issue in this case.

Chapter 5

Finite element method for shell governing equations

5.1 Introduction

In this chapter, we will consider a thin shell which is defined as a thin three-dimensional elastic body. Similar to a thin beam, many analyses of thin shells also neglect the effect of transverse shear and follow the theory of Kirchhoff-Love. In Chapter 3, we considered the linearisation of the governing equation of a static shell in a general geometry where, in this chapter, we will consider the specific examples of a straight and a curved shell in sections 5.2 and 5.3, respectively. Also, the finite element implementations will be presented with their solutions.

Similar to a thin beam, the main objective for the finite element implementations of a straight and a curved shell in this chapter is that, with a small deformation, the linearised governing equations can be employed to describe deformations of a thin-elastic body. This is to generalise the method to a thin-shell theory in order to illustrate its capability in higher dimension.

It will be seen in section 5.2.1 that the governing equations for the displacements in tangential directions needs C^0-continuity and that of normal direction requires C^1-continuity. These orders of continuity are the same as those of the straight beam for the associated directions. Hence, Lagrange shape functions are taken into account for the tangential displacements and the Hermite family is needed to approximate the normal displacement as suggested in section 4.2.

Regarding the Hermite shape functions in two-dimensional spaces, either rectangular or triangular elements can be used to define functions assuring the C^1-continuity. In a rectangular element, the most well-known shape functions are the bicubic Hermite functions. There are many well-known shape functions defined over a triangular element to assure C^1-continuity. Some of the elements like the Argyris [38] and the Bell [43] are constructed with higher degree of polynomials in order to obtain C^1-continuity and, also, achieve higher rate of convergence. However, they come with a drawback of greater computational time. Hence, the Hsieh-Clough-Tocher (HCT) [71], the Powell-Sabin-Hsieh (PSH) [54] elements, and the one presented by C.A. Felippa [15] are introduced in order to decrease the computational time by using lower degree of polynomials. Unfortunately, their rates of convergence decrease compared to those of the Argyris and Bell elements.

In section 5.2.2 of this chapter, the numerical comparison between two families of C^1-conforming finite elements defined over a rectangle and a triangle will be determined. The bi-cubic Hermite functions will be our choice of shape functions for a rectangular elements and the Bell shape functions will be employed for a triangular element.

To appreciate the performance of the Hermite and the Bell elements, section 5.2.2 will illustrate numerical results from solving the two-dimensional Biharmonic equation with the finite element method. Note that we use the Biharmonic equation as it requires the same C^1-continuity in the approximation as in the governing equation of the normal displacement.

After the appropriate interpolations for the normal displacement in the shell problem are selected, the governing equations with the linear constitutive law of a flat plate will be implemented in section 5.2.3. This is to compare between the solutions obtained from the linear and nonlinear governing equations of a thin shell. The solutions obtained from those two equations will be checked for the consistency in order to validate the range of the linearised equation within a small-deformation regime for a zero-curvature case.

Similar to implementations of thin beams, the governing equations of a zero-curvature geometry cannot be a representative for a shell behaviour in general. The governing equations of a circular tube, whose undeformed geometry has a non-zero

curvature, will be derived in section 5.3.1. In order to conclude the comparison between the governing equation with the linear and nonlinear governing equations for a thin-elastic body, implementations for the curved shell deformations by the finite element method have to be considered. Numerical results will be shown in section 5.3.2.

To summarise, section 5.4 elaborates the discussions and conclusions of this chapter.

5.2 Finite element method for a flat plate

In this section, we will consider a deformation of a flat plate which is subjected to a pressure loading on its upper surface as illustrated in Fig. 5.1. The loads applied on a body are uniformly distributed in the normal direction. The boundary conditions in this problem are two clamped boundaries, $\xi_1 = 0, \xi_1 = 1$, and two free edges, $\xi_2 = 0, \xi_2 = 1$, as shown in the figure. The length of the plate in both directions is 1.

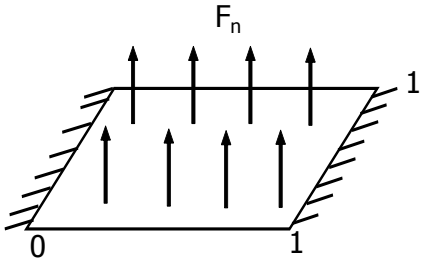

Figure 5.1: The geometry of the square plate with two clamped edges and two free edges. Forces applied to a body are uniform in normal direction.

5.2.1 The linearised governing equation

In this section, the governing equation for a flat plate will be derived. All formula and definitions used in this section were expressed in section 3.4.2 of chapter 3. Similar to a beam problem in chapter 4, the shell deformations are decomposed in the tangential and normal coordinate system in our study. The deformation are parametrised by two intrinsic coordinates defined on the mid-plane surface. Hence, a deformation of the shell can be decomposed into two tangential and normal components as

$$\mathbf{u} = u^j \mathbf{t}_j, \tag{5.1}$$

where the vector $\mathbf{t}_1, \mathbf{t}_2$ are tangential base vectors in direction of coordinate lines ξ_1, ξ_2, respectively, and $\hat{\mathbf{t}}_3$ is a unit normal vector to the undeformed mid-surface. Coefficients $u^j, j = 1, 2, 3$ are the associated components of a displacement $\mathbf{u}$ in two tangential and one normal directions.

Before the specific form of the governing equation for the flat plate will be considered, the linear versions of the shell kinematics have to be determined first. For a flat plate, we have the undeformed geometry of a flat plate is expressed by $\mathbf{r} = (\xi_1, \xi_2, 0)^T$ where ξ_1 and ξ_2 are intrinsic coordinates on the mid-surface lies between $[0, 1]$. Hence, the associated tangential and normal vectors are as follows

$$\begin{aligned} \mathbf{t}_1 &= (1, 0, 0)^T, \\ \mathbf{t}_2 &= (0, 1, 0)^T, \\ \hat{\mathbf{n}} = \hat{\mathbf{t}}_3 &= (0, 0, 1)^T. \end{aligned} \tag{5.2}$$

The covariant metric tensor in the undeformed configuration can be computed from (3.94) as

$$a_{\alpha\beta} = \mathbf{t}_\alpha \cdot \mathbf{t}_\beta. \tag{5.3}$$

and, that of the deformed configuration can be obtained from (3.95) as,

$$A_{\alpha\beta} = a_{\alpha\beta} + u^\alpha|_\beta + u^\beta|_\alpha \tag{5.4}$$

where $u^\alpha|_\beta, \alpha, \beta = 1, 2$, denote the components of the first derivatives in the tangential and normal coordinate system as described in (3.97). We have that the determinant of the covariant metric tensor in the undeformed configuration for the flat plate equals to $a = 1$.

The linearised Green strain tensor for the flat plate, which determined from the differences between the undeformed and deformed metric tensors as seen in (3.100), is

$$\gamma_{\alpha\beta} = \frac{1}{2}(u^\alpha|_\beta + u^\beta|_\alpha) = \frac{1}{2}(u^\alpha_{,\beta} + u^\beta_{,\alpha}) \tag{5.5}$$

where the last terms come from (3.97) and the fact that $\frac{\partial \mathbf{t}_i}{\partial \xi_\alpha} = 0, \forall i, \alpha$, for the flat plate. Hence, its variation is

$$\delta\gamma_{\alpha\beta} = \delta u^\alpha_{,\beta}. \tag{5.6}$$

Next, we consider the linearised curvature tensor for the flat plate which is specified by (3.103) as

$$b_{\alpha\beta} = \hat{\mathbf{n}} \cdot \mathbf{r}_{,\alpha\beta} = 0. \tag{5.7}$$

Now, it can be seen that the undeformed configuration for the flat plate has a zero curvature since $\mathbf{r}_{,\alpha\beta} = \frac{\partial \mathbf{t}_\alpha}{\partial \xi_\beta} = 0, \forall \alpha, \beta$. Also, the deformed curvature tensor is determined from (3.108) as

$$\begin{aligned} B_{\alpha\beta} &= b_{\alpha\beta} + \left[\frac{1}{a} L_j \Gamma^j_{\alpha\beta} - \frac{L_3}{a^2}\Gamma^3_{\alpha\beta}\right] + \left(u^i|_\alpha \Gamma^3_{i\beta} + u^3_{,\alpha\beta} + u^k \frac{\partial \Gamma^3_{k\alpha}}{\partial \xi_\beta} + \frac{\partial u^k}{\partial \xi_\beta}\Gamma^3_{k\alpha}\right), \\ &= b_{\alpha\beta} + u^3_{,\alpha\beta}, \end{aligned} \tag{5.8}$$

where $L_j; j = 1, 2, 3$, are the three components of $\mathbf{L}$ defined in (3.110). Note that the last line comes from the definition of the Christoffel symbol of the second kind $\Gamma^j_{i\alpha} = \left(\frac{\partial \mathbf{t}_i}{\partial \xi_\alpha} \cdot \mathbf{t}_j\right)$ which equals to zero for all i, j, α, since $\frac{\partial \mathbf{t}_i}{\partial \xi_\alpha} = 0$ for the flat plate.

Hence, the linearised bending tensor for the flat plate can be calculated from (3.109) as

$$\kappa_{\alpha\beta} = b_{\alpha\beta} - B_{\alpha\beta} = -u^3_{,\alpha\beta}. \tag{5.9}$$

Substituting the strain tensor, $\gamma_{\alpha\beta}$, in (5.5) and the bending tensor, $\kappa_{\alpha\beta}$, in (5.9) and their variations back into the shell governing equation, (3.91), gives the linear version of the governing equation for the flat plate in each displacement direction as follows

$$0 = \iint \left[-\frac{1}{h} f^1\right] \delta u^1 + \tilde{E}^{\alpha\beta\gamma\delta} \left\{[\gamma_{\alpha\beta}]\, \delta u^1_{,\gamma}\right\} d\xi_1 d\xi_2, \tag{5.10}$$

for a displacement $\mathbf{u}$ in tangential direction in the coordinate ξ_1, and

$$0 = \iint \left[-\frac{1}{h} f^2\right] \delta u^2 + \tilde{E}^{\alpha\beta\gamma\delta} \left\{[\gamma_{\alpha\beta}]\, \delta u^2_{,\gamma}\right\} d\xi_1 d\xi_2, \tag{5.11}$$

for a displacement $\mathbf{u}$ in tangential direction in the coordinate ξ_2, and

$$0 = \iint \left[-\frac{1}{h} f^3\right] \delta u^3 + \tilde{E}^{\alpha\beta\gamma\delta} \left\{\left[\frac{1}{12} h^2 u^3_{,\alpha\beta}\right] \delta u^3_{,\delta\gamma}\right\} d\xi_1 d\xi_2. \tag{5.12}$$

for a displacement $\mathbf{u}$ in normal direction to the undeformed surface.

Similar to the straight beam elaborated in section 4.2, it can be seen that the flat plate has a zero curvature in the undeformed configuration. Therefore, the governing equations contain no coupled term between displacements as those of the straight beam. Each equation governs displacement in each direction. Furthermore, it can be seen that the tangential displacement governing equations, (5.10) and (5.11), can

be obtained from a second-order equation and require only C^0-continuity as the integral contains only the first-order derivative of the tangential displacements. Hence, Lagrange shape functions are utilised to approximate the tangential displacements as suggested in section 4.2.1.

The governing equation (5.12) suggests that the shape functions for the normal displacement have to be C^1-continuous functions. This is a result of having the second-order derivative in the integral equation. Therefore, as suggested in section 4.2.1, Hermite shape functions will be employed to approximate the displacement and its derivative in normal direction in order to assure the C^1-continuity in the implementations of this chapter.

5.2.2 A comparison between the Bell triangular and the Hermite rectangular elements: a Biharmonic equation as a case study

In the finite element method applied to two-dimensional problems, the domain of interest can be discretised by many different types of element as long as they can accurately represent the geometry. Rectangular and triangular elements are popular and the most employed. However, triangular elements have been used in a wider range of applications than a rectangular one because of their superiority over rectangles in representing domains of complex shape.

In this section, finite element implementation will be focused on the comparison between two selected C^1-interpolations defined over rectangular and triangular elements. Since the derivatives are included in the definitions of the C^1-functions, with the same number of nodes on the element, different degrees of polynomial and numbers of degrees of freedom can be used to define different kinds of finite element. The reference domains that used to define the C^1-interpolations also play an essential role in their rate of convergence. Therefore, it is worth comparing the rate of convergence between the different C^1-interpolations defined on different reference domains.

Note that the implementation use later in this chapter will be the subparametric scheme, i.e. the geometry is approximated by the linear Lagrange interpolation and the unknowns are approximated by the choice of C^1-interpolations defined over the

typical elements. Also, in both rectangular and triangular elements, the domain of interest will be discretised by those elements which invariably have straight sides.

Now, let consider the Biharmonic equation used in this study. It is mathematically expressed as follow

$$D^4u(x_i) = \frac{\partial^4 u}{\partial x_1^4} + 2\frac{\partial^4 u}{\partial x_1^2 \partial x_2^2} + \frac{\partial^4 u}{\partial x_2^4} = 0, \quad x_i \in \Re, \tag{5.13}$$

and the exact solution

$$u(x_1, x_2) = \cos(x_1)e^{x_2}, \tag{5.14}$$

which will be imposed at boundaries with a combination of Dirichlet and Neumann boundary conditions. The domain of interest is rectangle with $0 \leq x_1 \leq 2$ and $0 \leq x_2 \leq 1$.

In order to formulate the finite element implementation for the Biharmonic equation, the weak formulation can be obtained similarly to that of one-dimensional equation described in (4.38). Rather than considering the line integral as described in 1D-problem, the residual form of the differential equation, (5.13), and its shape functions have to be considered over the 2D-domain, $\Omega = \{(x_1, x_2)|0 \leq x_1 \leq 2, 0 \leq x_2 \leq 1\}$. Therefore, the weak or residual form of (5.13) can be expressed as

$$\begin{aligned} 0 = r_k = \iint_\Omega \left(\sum_{l=1}^{N} U_l \frac{\partial^2 \psi_l}{\partial x_1^2}\frac{\partial^2 \psi_k}{\partial x_1^2} + 2\sum_{l=1}^{N} U_l \frac{\partial^2 \psi_l}{\partial x_1^2}\frac{\partial^2 \psi_k}{\partial x_2^2} + \sum_{k=1}^{N} U_l \frac{\partial^2 \psi_l}{\partial x_2^2}\frac{\partial^2 \psi_k}{\partial x_2^2} \right) dx_1 dx_2 \\ + \int_{\partial\Omega} \left\{ (\nabla^3 u \cdot \mathbf{n})\psi_k - \nabla^2 u (\nabla \psi_k \cdot \mathbf{n}) \right\} d\partial\Omega, \end{aligned} \tag{5.15}$$

where $\mathbf{n}$ denotes a normal vector and ∇^n denotes the differential operator for the nth-order derivatives. Since a combination of Dirichlet and Neumann boundary conditions is applied along boundaries, the boundary terms appearing in (5.15) vanish.

It can be seen from (5.15) that the weak formulation of the Biharmonic equation contains second-order derivative of a shape function. As explained in section 4.2.2, a C^1-continuous shape function has to be considered to approximate the Biharmonic solution in order to ensure the continuity of the first-order derivatives in the finite element method.

The C^1-rectangular element

In this section, we will describe the continuously differentiable shape functions defined on two-dimensional rectangular elements. The most famous one is the bicubic Hermite element. Its shape functions can be simply constructed from tensor products of the one-dimensional functions as shown in Appendix A.2.

To approximate an unknown u using a two-dimensional bicubic Hermite basis, the four quantities of the unknown value u, its first derivatives $\frac{\partial u}{\partial s_1}, \frac{\partial u}{\partial s_2}$ and the mixed derivative $\frac{\partial^2 u}{\partial s_1 \partial s_2}$ must be defined at each element node. Hence, the approximation can be obtained from the linear combination between the bicubic Hermite shape functions and the 16 nodal values defined over the element. Note that the bicubic shape functions are parametrised by the reference coordinates defined in (1.3.4). Furthermore, the mesh grid used in the C^1-rectangular element must be nicely oriented and regular.

The C^1-triangular element

In the finite element analysis, defining C^1-shape functions over a triangular element is not straightforward and comes with a concern. Since there are two types of derivatives degrees of freedom; a derivative with respect to global coordinates and to local coordinates, the global derivative directions at adjacent elements within the description of the element might not be consistent. This is the result from parametrising shape functions with local coordinates. Also, under the Jacobian of mapping between global and local coordinates, the shape function values and their derivatives perform differently.

Next let us consider a cubic triangle with the degrees of freedom configuration illustrated in Fig. 5.2, for an example. This configuration uses the six nodes partial derivatives of u along the side directions. These partials are briefly called side slopes.

To appreciate the difficulties in attaining C^1-continuity on triangular elements, now consider two connected cubic triangles illustrated in Fig. 5.3 with degrees of freedom described above. The figure shows that the displacement values u_1 and u_2 match without problems because their direction is shared. However, the side slopes do not match. This will be even worst if more elements at a corner are considered. Hence, the main difficulty is that the shape function's derivatives along the element boundaries of two adjacent elements do not give a consistent direction.

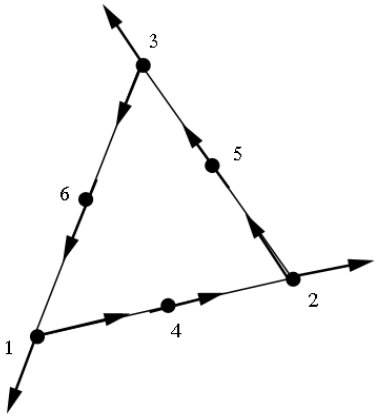

Figure 5.2: Degrees of freedom configurations for expressing the displacement **u** over a triangle.

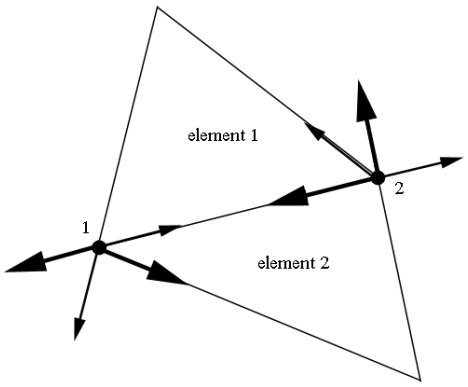

Figure 5.3: Degrees of freedom of two adjacent triangles.

To enforce the global C^1-continuity between finite elements, many researchers have been proposed interpolating functions that satisfy the C^1-continuity with different degrees of freedom defined on a triangle. For example, the well-known Argyris triangle has 21 degrees of freedom including all second derivatives with complete fifth-order polynomial interpolation functions [38]. Similar to the Argyris element, the Bell element [43] has 18 degrees of freedom with the normal derivatives at mid-side nodes neglected.

Since higher degree of polynomial gives higher degree of freedom, this comes with greater computational time. Hence, many researchers have been tried to derive a C^1-element with fewer degree of freedom in order to reduce computational time. However, with their lower degree of polynomial and fewer degree of freedom, these elements are

not successful as smaller rate of convergence is obtained compared to those elements employing higher degree of freedom like the Argyris and the Bell elements [63].

Since the Biharmonic equation which is governed by the fourth-order partial differential equation is considered in this study, the minimum polynomial expansion of the unknown to achieve the C^1-continuity in two dimensions is quintic. This is a consequence of constraining 6 parameters of the value along the line and its first-order derivatives at each end of the line. Hence, a quintic polynomial is considered for a construction of shape functions. Choices of a triangular element can be either the Argyris element or the Bell element.

The derivations of the Argyris shape functions can be found in many literature. The derivation can be found from M. Bernadou and J. Boisserie [50]. Another works for the Argyris element is from [74]. Recently, V. Dominguez and F.J. Sayas [80] proposed an algorithm to evaluate the basis functions of this element and their derivatives. However, further computations still need in an implementation for the Argyris element as no explicit shape functions are defined.

Regarding the Bell element, the explicit form of shape functions for the Bell element was shown by G. Kämmel [32]. In his book, all shape functions are stated clearly without requiring further derivation. This is much more easier to use than the Argyris element which still requires some efforts on the computation of its shape functions. Moreover, the Bell element has fewer degrees of freedom than the Argyris element which can reduce the cost of computation. However, having fewer degrees of freedom in the Bell element still attains high rate of convergence and is easier to provide physical interpretation of a problem. Therefore, our C^1-triangular element will be based on the Bell's basis functions.

Before we will present the Bell shape functions, let us first mention the local coordinates used in the reference triangle. Similar to the rectangular element, it is often convenient to define a shape function on the reference element where the numerical integration is defined. In two dimensional space, the reference triangle that will be used to define the local coordinates s_1, s_2 lies in the unit triangle, $\{(s_1, s_2)|0 \leq s_1, s_2 \leq 1, s_1 + s_2 = 1\}$. To express a coordinate in a triangle, it is easier to work with an area coordinated system or the Barycentric coordinates as presented in section 1.3.4.

The Bell shape functions

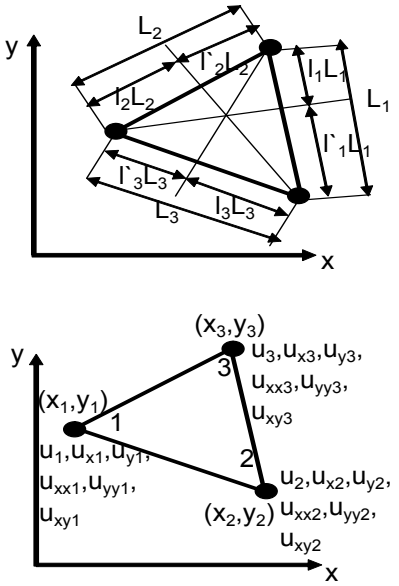

Figure 5.4: (Top) The description of all parameters utilised within the definition of the Bell shape functions where L_j denotes the length of the side opposite to the vertex j. (Bottom) The Bell element with 18 degrees of freedom; the values u_j, first derivatives u_{xj}, u_{yj}, and all second derivatives $u_{xxj}, u_{xyj}, u_{yyj}$, at vertex $j; j = 1, 2, 3$.

Now, let us introduce the Bell element which is derived from the quintic polynomial with 18 degrees of freedom [43]. The element comprises three nodes with six degrees of freedom of $u, u_x, u_y, u_{xx}, u_{xy}, u_{yy}$ at each corner node. The graphical description of the Bell element is shown in Fig. 5.4.

The shape functions of Bell element are parametrised by area coordinates, λ_j. The subscripts ik of the shape functions ψ_{ik} mean that they are evaluated at node i with kth degree of freedom where $k = 1$ denotes degree of freedom that corresponds to the unknown value, $k = 2, 3$ correspond to the first derivatives with respect to the first and second global coordinates, $k = 4, 5$ correspond to the second derivatives with respect to the first and second global coordinates, and $k = 6$ corresponds to the mixed derivative.

Unlike the Lagrangian interpolation functions, the Bell shape functions are derived by interpolating nodal derivatives as well as nodal displacements. Also, they have to satisfy the properties that $\psi_{i1} = 1$ at node i and $\psi_{i1} = 0$ at other nodes. Furthermore, all of the first and the second derivatives of $\psi_{i1} = 0$ at all nodes. Also, $\partial_x \psi_{i2} = 1$ at node i and $\partial_x \psi_{i2} = 0$ at other nodes. Similarly for the first derivative with respect to y, we have that $\partial_y \psi_{i3} = 1$ at node i and $\partial_y \psi_{i3} = 0$ at other nodes. These shape functions

associated with the first derivatives are zero at all nodes for ψ_{im}, $\partial_{xx}\psi_{im}$, $\partial_{yy}\psi_{im}$, $\partial_{xy}\psi_{im}, \forall m = 2, 3$. Moreover, $\partial_{xx}\psi_{i4}(\mathbf{x}_k) = \delta_{ik}$, $\partial_{yy}\psi_{i5}(\mathbf{x}_k) = \delta_{ik}$, and $\partial_{xy}\psi_{i6}(\mathbf{x}_k) = \delta_{ik}$. Furthermore, these shape functions associated with the second derivatives are zero at all nodes for ψ_{im}, $\partial_x\psi_{im}$, and $\partial_y\psi_{im}, \forall m = 4, 5, 6$. The Bell shape functions are mathematically expressed as

$$
\begin{aligned}
\psi_{11}(\lambda_1,\lambda_2,\lambda_3) =& \lambda_1^5 + 5\lambda_1^4(\lambda_2+\lambda_3) + 10\lambda_1^3(\lambda_2+\lambda_3)^2 + 30\lambda_1^2\lambda_2\lambda_3(l_3\lambda_2 + l_2'\lambda_3)\\
\psi_{12}(\lambda_1,\lambda_2,\lambda_3) =& 3b_1\lambda_1^2\lambda_2\lambda_3(\lambda_2-\lambda_3) + \lambda_1^3(b_3\lambda_2 - b_2\lambda_3)(\lambda_1+4\lambda_2+4\lambda_3)\\
&+ 15\lambda_1^2\lambda_2\lambda_3(b_3l_3\lambda_2 - b_2l_2'\lambda_3)\\
\psi_{13}(\lambda_1,\lambda_2,\lambda_3) =& -3c_1\lambda_1^2\lambda_2\lambda_3(\lambda_2-\lambda_3) - \lambda_1^3(c_3\lambda_2 - c_2\lambda_3)(\lambda_1+4\lambda_2+4\lambda_3)\\
&- 15\lambda_1^2\lambda_2\lambda_3(c_3l_3\lambda_2 - c_2l_2'\lambda_3)\\
\psi_{14}(\lambda_1,\lambda_2,\lambda_3) =& 1/2\lambda_1^3(b_3^2\lambda_2^2 + b_2^2\lambda_3^2) + \lambda_1^2\lambda_2\lambda_3(-b_2b_3\lambda_1 + b_3b_1\lambda_2 + b_1b_2\lambda_3)\\
&+ 5/2\lambda_1^2\lambda_2\lambda_3(b_3^2l_3\lambda_2 + b_2^2l_2'\lambda_3)\\
\psi_{15}(\lambda_1,\lambda_2,\lambda_3) =& 1/2\lambda_1^3(c_3^2\lambda_2^2 + c_2^2\lambda_3^2) + \lambda_1^2\lambda_2\lambda_3(-c_2c_3\lambda_1 + c_3c_1\lambda_2 + c_1c_2\lambda_3)\\
&+ 5/2\lambda_1^2\lambda_2\lambda_3(c_3^2l_3\lambda_2 + c_2^2l_2'\lambda_3)\\
\psi_{16}(\lambda_1,\lambda_2,\lambda_3) =& b_1c_1\lambda_1^2\lambda_2\lambda_3(\lambda_1+\lambda_2+\lambda_3) + b_2c_2\lambda_1^2\lambda_3(\lambda_2\lambda_3 - \lambda_3\lambda_1 - \lambda_1\lambda_2 - \lambda_2^2)\\
&+ b_3c_3\lambda_1^2\lambda_2(\lambda_2\lambda_3 - \lambda_3\lambda_1 - \lambda_1\lambda_2 - \lambda_3^2) - 5\lambda_1^2\lambda_2\lambda_3(b_2c_2l_2'\lambda_3 + b_3c_3l_3\lambda_2).
\end{aligned}
\tag{5.16}
$$

Note that these shape functions are associated with the first node with its 6 degrees of freedom. Shape functions at another two nodes can be obtained by performing a cyclic permutation of the Barycentric coordinates in (5.16) [32]. The parameters $b_i, c_i, \forall i = 1, 2, 3$ appearing in the equations can be obtained from

$$
\begin{aligned}
b_1 = x_3 - x_2, \quad b_2 = x_1 - x_3, \quad b_3 = x_2 - x_1,\\
c_1 = y_2 - y_3, \quad c_2 = y_3 - y_1, \quad c_3 = y_1 - y_2,
\end{aligned}
\tag{5.17}
$$

where $x_i, y_i; i = 1, 2, 3$, are components of a vertex $\mathbf{x}_i$.

Regarding the first-order and second-order derivatives, we have that they can be obtained by the help of chain rule as

$$
\begin{aligned}
\frac{\partial\psi_{ij}}{\partial x_\alpha} &= \frac{\partial\psi_{ij}}{\partial\lambda_l}\frac{\partial\lambda_l}{\partial x_\alpha},\\
\frac{\partial^2\psi_{ij}}{\partial x_\alpha\partial x_\beta} &= \frac{\partial^2\psi_{ij}}{\partial\lambda_m\partial\lambda_n}\frac{\partial\lambda_m}{\partial x_\alpha}\frac{\partial\lambda_n}{\partial x_\beta} + \frac{\partial^2\lambda_l}{\partial x_\alpha\partial x_\beta}\frac{\partial\psi_{ij}}{\partial\lambda_l}.
\end{aligned}
\tag{5.18}
$$

And, the derivatives of the area coordinates with respect to the global coordinates are as follows.

$$\begin{aligned} \frac{d\lambda_1}{dx} &= \frac{c_1}{2A}, \frac{d\lambda_2}{dx} = \frac{c_2}{2A}, \frac{d\lambda_3}{dx} = \frac{c_3}{2A} \\ \frac{d\lambda_1}{dy} &= \frac{b_1}{2A}, \frac{d\lambda_2}{dy} = \frac{b_2}{2A}, \frac{d\lambda_3}{dy} = \frac{b_3}{2A}. \end{aligned} \tag{5.19}$$

Note that the derivatives of all basis functions in the Bell element are with respect to the global coordinate system, unlike the bicubic Hermite functions that defined by the local coordinates on a rectangle. This can ensure the C^1-continuity between triangular elements in the global coordinates.

Numerical results obtained from using both the Bell triangular and the Hermite rectangular elements

In order to do the finite element implementations, the domain of interest will be first discretised. Number of nodes defined on the typical element can be different depends on the degree of polynomial and the degrees of freedom that define the shape functions. As can be seen in the previous two subsections, even though both the Hermite and the Bell element define by having the same two nodes per side, the degree of polynomial defined over the Bell triangular element is however greater than that of the Hermite rectangular element. This is because the Bell element is defined by using more degrees of freedom at a node.

Similar to the one-dimensional case, the number of nodes and elements will play an essential role in minimising the error of the solution. However, the greater number of elements can be expensive in computational time. In this problem, different number of elements will be chosen in order to investigate the convergence rate and the computational time for both the Hermite and Bell elements. Comparisons will be depicted afterwards.

In this problem, the Biharmonic equation will be considered in the rectangle domain with $0 \leq x_1 \leq 2$ and $0 \leq x_2 \leq 1$. After the discretisation, the domain of interest constitutes of the typical elements and many finite nodes as illustrated in Fig. 5.5a for the Hermite rectangles and Fig. 5.5b for the Bell triangles. Furthermore, the structured mesh is employed in this study so that the element size can be easily computed.

To perform the numerical integration, a Gaussian quadrature associated with each

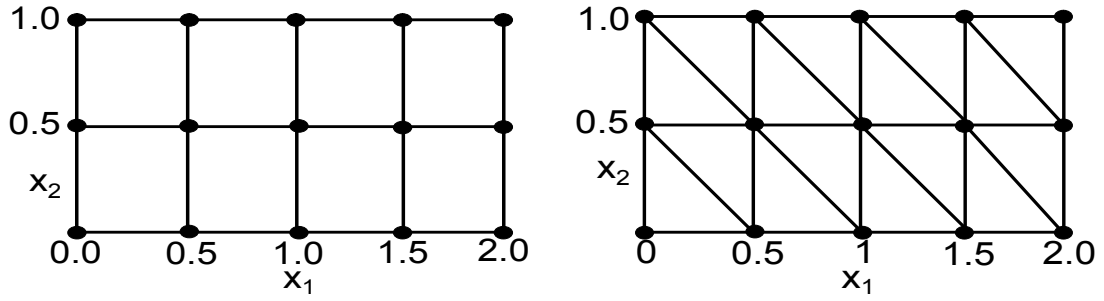

(a) a rectangular domain (b) a triangular domain

Figure 5.5: The discretisation of the domain of interest with 4 elements in x_1-direction and 2 elements in x_2-direction.

element in two-dimensional space is considered in this problem. Similar to the one-dimensional problem, the accuracy of an approximation depends on the choice of number of Gauss points and weights. The degree of precision, i.e. the number of Gauss points and weights, must be determined so that the function under an integral can be accurately approximated.

In this finite element implementation of the two-dimensional Biharmonic equation, the highest order of polynomial under the integral is considered from (5.15). Since the bicubic Hermite element, which is of degree 3 in each direction, is employed on a rectangle, we have that their second-order derivatives are linear in both directions. Considering the mix-derivative term, we have that the interpolation is biquadratic which gives the highest order of function under the integral to be quartic. Hence, 16-node scheme is employed to provide 2D Gaussian integration scheme for the Biharmonic implementation using the bicubic Hermite interpolations. Note that this integration scheme can integrate the polynomial exactly up to order 7 which is suitable for our implementation on a rectangle. Sixteen-point weights and evaluation points for integration on rectangles can be found in [21], [53].

Next, we consider a Gaussian quadrature on a triangular element. Since the Bell shape functions are employed and they are of order 5, their second-order derivatives are then of order 3 and the highest order of function under the integral is 6 (see (5.15)). Therefore, 2D Gaussian integration scheme defined on a triangle is 13-node scheme which can integrate up to seventh-order polynomials exactly. Weights and evaluation points for integration on triangles are also shown in [21], [53].

Note that the numerical integration schemes for both Hermite and the Bell elements are chosen to have the same order of an exact representation in order to have a fair

comparison.

Now, let us consider the boundary conditions that have to be imposed at boundaries for the bicubic Hermite and the Bell elements. The Bell element has, in total, 18 degrees of freedom with 6 degrees of freedom in each node. The 6 degrees of freedom incorporate the value of unknown field, the first derivative with respect to the first and second global coordinates, and the second derivatives with respect to the first, second, and mixed derivative (see 5.16).

Since we consider the Biharmonic equation with the Dirichlet boundary conditions, we have that the physical conditions that allow to be pinned on boundaries are the value and the normal derivatives. However, there is no normal derivative defined as a degree of freedom to be specified for the Bell shape function. Therefore, the first-order derivatives have to be imposed instead and the boundary specification can be worked out from the normal derivative on that boundary. Furthermore, the values of the unknown and the first-order derivatives that have to be specified on the boundaries of the domain for the Bell element can be obtained from

$$\begin{aligned} u(x_1, x_2) &= \cos(x_1)e^{x_2}, \\ u_{x_1}(x_1, x_2) &= -\sin(x_1)e^{x_2}, \\ u_{x_2}(x_1, x_2) &= \cos(x_1)e^{x_2}. \end{aligned} \tag{5.20}$$

For the rest of degrees of freedom associated with the second-order derivatives, we set them to be unpinned and consider them as parts of the solution.

The Hermite rectangular element has, in total, 16 degrees of freedom with 4 degrees of freedom each node. The 4 degrees of freedom incorporate the value of unknown field, the first derivative with respect to the first and second coordinates, and the mixed derivatives. Unlike the Bell element, the derivatives defined on the Hermite element are with respect to the local coordinates, s_1, s_2. Hence, the transformation from the global derivatives to the local derivatives have to be done to ensure the consistency with the definition as shown in (1.7).

Therefore, the physical conditions specified on the boundaries of the domain for the Hermite element can be determined similarly as those of the Bell element and their

values can be obtained as follows,

$$\begin{aligned} u(x_1, x_2) &= \cos(x_1)e^{x_2} \\ u_{s_1}(x_1, x_2) &= -\sin(x_1)e^{x_2}(0.5\frac{l_{x_1}}{n_{x_1}}), \\ u_{s_2}(x_1, x_2) &= \cos(x_1)e^{x_2}(0.5\frac{l_{x_2}}{n_{x_2}}), \end{aligned} \tag{5.21}$$

where n_{x_1} and n_{x_2} are the number of elements in x_1- and x_2-directions. Also, l_{x_1} and l_{x_2} denote the length of the domain in x_1- and x_2-directions. Furthermore, the mix-derivative degree of freedom can be taken care as parts of the solutions.

Note that, in the implementation of the Hermite rectangular and Bell triangular elements, all of the degrees of freedom are pinned on every boundary. Also, the subparametric scheme will be considered. The triangular Bell functions and the Hermite rectangular functions are employed to interpolate unknowns, while the geometry is approximated by the linear Lagrange functions which are of lower order than the unknown fields.

In order to compare errors and the rate of convergence between the Hermite and the Bell element, we uniformly vary a number of element in both x_1- and x_2-directions in such a way that the same element size is obtained in both directions. Since the length in x_1-direction is twice longer than that in x_2-direction, we choose the number of element in x_1-direction to be doubled so that the element size, h, can be computed easily by $h = \frac{l_{x_1}}{n_{x_1}} = \frac{2l_{x_2}}{2n_{x_2}} = \frac{l_{x_2}}{n_{x_2}}$. Error utilised in the comparison is the L^2-norm error which is mathematically described as

$$\|u_{exact} - u_{FE}\| = \left(\iint_{\Omega} |u_{exact} - u_{FE}|^2 \, d\Omega \right)^{1/2}, \tag{5.22}$$

where u_{exact}, u_{FE} denote the exact and the finite element solutions, respectively.

Regarding the solutions and errors obtained from the finite element solutions from the Bell and the Hermite elements and the exact solution, it can be seen from Figs. 5.6b and 5.6c that the obtained finite element solutions agree with the exact solutions for all over the domain. The absolute value of the error between the exact solutions and the solutions obtained from both types of element are quite small as illustrated in Figs 5.6d and 5.6e. However, the Bell element give more accurate solutions than the Hermite element as the obtained error is smaller. Note that, in the implementations of Fig. 5.6, the numbers of degree of freedom are chosen to be similar for the comparison

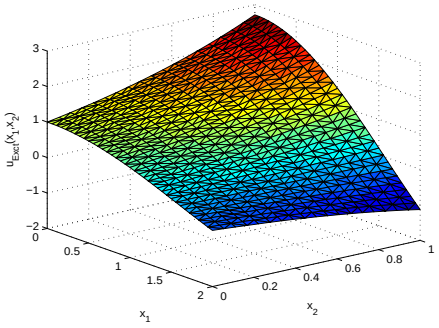

(a) The exact solution of the Biharmonic equation (5.14)

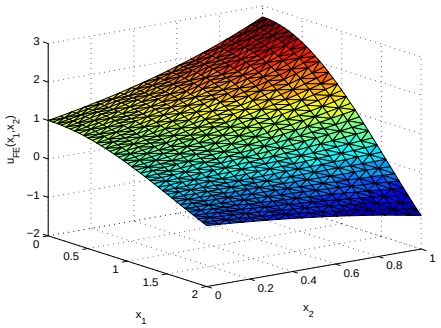

(b) The finite element solution obtained from the Bell element

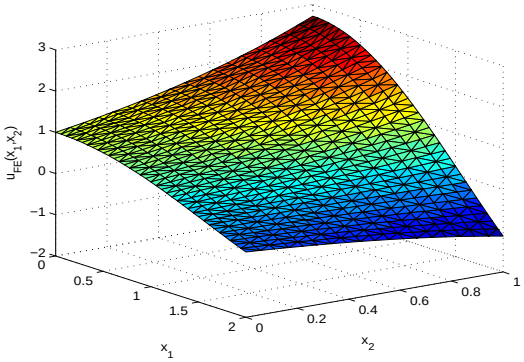

(c) The finite element solution obtained from the Hermite element

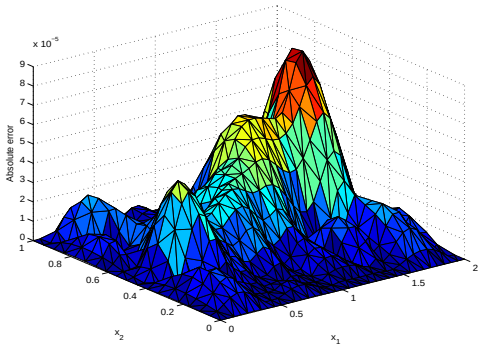

(d) Absolute value of the error between the exact solution and the solution obtained from the Bell element

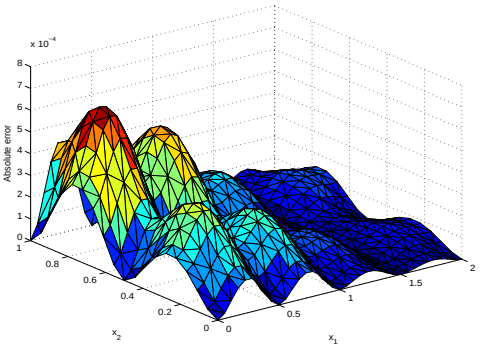

(e) Absolute value of the error between the exact solution and the solution obtained from the Hermite element

Figure 5.6: Comparisons between solutions and errors obtained from finite element method based on Bell and Hermite elements and the exact solution. Figures are generated using the `trimesh` function in MatLab.

where the Hermite implementation has 24 dofs and the Bell implementation has 54 dofs.

In order to compare results between the Bell and the Hermite elements, Tables 5.1 and 5.2 show L^2-norm error obtained from solving the Biharmonic equation (5.13) by the Hermite and the Bell element, respectively. It can be seen that the comparison

h	element in x_2	Number of element in x_1	DOF	Time (sec)	L^2-norm error
0.5	2	4	24	0.03	9.62768×10^{-4}
0.2	5	10	174	0.17	6.32615×10^{-5}
0.1429	7	14	354	0.35	2.24402×10^{-5}
0.1	10	20	744	0.86	7.48137×10^{-6}
0.05	20	40	3084	3.20	9.01978×10^{-7}
0.01	100	200	79404	158.02	7.30985×10^{-9}

Table 5.1: L^2-error obtained from solving the Biharmonic equation with various number of the Hermite rectangular elements.

h	element in x_2	Number of element in x_1	DOF	Time (sec)	L^2-norm error
0.5	2	4	54	0.18	1.53941×10^{-5}
0.2	5	10	306	1.22	3.23022×10^{-7}
0.1429	7	14	594	2.43	7.94788×10^{-8}
0.1	10	20	1206	5.01	1.84613×10^{-8}
0.05	20	40	4806	20.48	1.14555×10^{-9}
0.01	100	200	120006	1264.74	1.86896×10^{-12}

Table 5.2: L^2-error obtained from solving the Biharmonic equation with various number of the Bell triangular elements.

is not straightforward. It is not easy to compare both types of finite element with the same number of elements as different numbers of degree of freedom are defined in the mesh for the Bell and the Hermite elements. However, we can perform a fair comparison by choosing the specific error and determining the obtained number of element and the computational time for the typical elements.

Regarding the comparison, the error is chosen to be order of 10^{-7}. We can see from Table 5.1 that the Hermite element used 3084 degrees of freedom and spent 3.20 seconds. With the same error, the Bell element used 306 degrees of freedom and spent 1.22 seconds to reach the error as can be seen from Table 5.2. Therefore, the Bell element is less time-consuming than the Hermite element to achieve the same accuracy.

Furthermore, it can be seen that as the numbers of elements increase, errors obtained from both the Hermite and the Bell elements decrease. With the same element size h, the L^2-norm errors obtained from the Bell element are smaller than those obtained from the Hermite element. However, the computational time of the Bell element

is more expensive.

In order to appreciate the convergence rate of the Hermite and the Bell elements, the L^2-norm errors are plotted versus element sizes h. Fig. 5.7 illustrates that as the element size decreases, error decreases and the error obtained from the Bell element decreases faster than those of the Hermite element. Also, the Bell element gives higher accuracy than that of the Hermite element at the same element size, h.

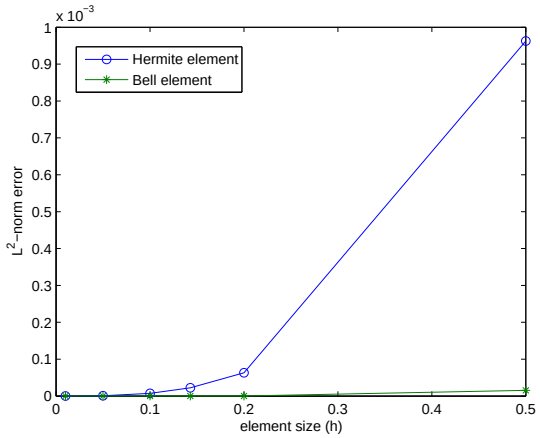

Figure 5.7: A comparison of the rate of convergence between the Bell triangular and the Hermite rectangular elements.

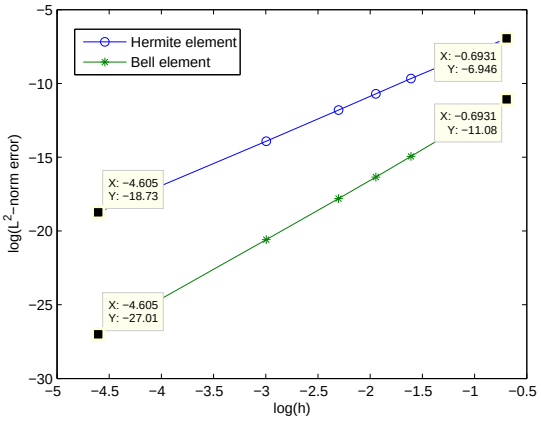

Figure 5.8: A log-plot comparison of the rate of convergence between the Bell triangular and the Hermite rectangular elements.

Fig. 5.8 illustrates the log plots between the L^2-norm error and the element sizes. The plots show that the rate of convergence for the Bell element is 4.0706 while the rate of convergence of Hermite element is 3.0134. These rates of convergence can be computed from the slopes of the linear lines. Furthermore, these obtained convergence

rates are consistent with the result shown in [9] for the Hermite interpolations and with the study from P. Fischer [63] for the Bell element.

We can now conclude that the Bell element is more efficient than the Hermite element in term of the convergence rate and accuracy when the same number of elements is concerned. Therefore, the Bell triangular element will be employed in the finite element implementations of the normal displacement in the flat plate and the circular tube problems in our study. Note that this element will be used in the nonlinear problems as well in order to make a reasonable comparison.

5.2.3 Numerical comparisons between the Kirchhoff-Love linear and nonlinear governing equations

Next, we will implement the finite-element solution of the plate bending problem with a clamped support at two ends. Comparisons will be illustrated between the solutions obtained from the nonlinear and the linear governing equations that associate with the problem. Note that the implementations of the linearised governing equaiton with the linear constitutive law will be based on the equations (5.10), (5.11), and (5.12) that we derived in section 5.2.1 while the nonlinear governing equation with the linear constitutive law is expressed as (3.91).

In order to implement the finite element method of a two-dimensional space in this study, the domains of interest which is the unit square will be discretised with triangles. The reason of using a triangular mesh is a consequence of section 5.2.2 that the Bell triangular element is superior to the Hermite rectangular element. Note that the unstructured mesh is employed in all following implementations with 150 elements in the mesh. Similar to the Biharmonic implementation, the numerical integration is the same in this implementation.

Next, we will consider boundary conditions that will be specified for the flat plate. Since a clamped support is considered in this problem, the displacement in tangential and normal directions with their derivatives degrees of freedom associated with its employed interpolations have to be imposed.

As the shell is clamped at both ends of $\xi_1 = 0$ and $\xi_1 = 1$ (see Fig. 5.1), the displacement in tangential directions has to be specified so that $u^j(0, \xi_2) = 0$ and

$u^j(1,\xi_2) = 0, \forall i,j = 1,2$. Note that no derivative degree of freedom in both tangential directions has to be considered since the Lagrange interpolations are employed.

To determine boundary conditions for the normal displacement, there are six degrees of freedom to be concerned at nodes; the displacement value, its first derivatives, and its second derivatives, as the Bell shape functions are employed. Since the shell is clamped at both ends of $\xi_1 = 0$ and $\xi_1 = 1$, we have that both value and its first derivatives have to be set to zero at both boundaries, i.e., $u^3(0,\xi_2) = 0$, $u^3_{,j}(0,\xi_2) = 0, \forall j = 1,2$, and $u^3(1,\xi_2) = 0$, $u^3_{,j}(1,\xi_2) = 0, \forall j = 1,2$. For all second derivatives, it follows from the clamped support that there is no rotation at both ends as well. Therefore, $u^3_{,ij}(0,\xi_2) = 0 = u^3_{,ij}(1,\xi_2), \forall i,j = 1,2$,

Note that there is no constraint on the boundary $\xi_2 = 0$ and $\xi_2 = 1$. Therefore, all degrees of freedom in all directions that associate with the applied shape functions are set to be free.

Next, we start the implementation with the comparison between the solutions obtained from the linear and nonlinear equations within the small-deformation regime. All linear and nonlinear equations are solved numerically using a finite-element method in `Oomph-lib` [53] with the aforementioned boundary conditions. Note that there is no initial stress and constant external forces are uniformly distributed in normal direction to the plate. The thickness of a flat plate is 0.01.

Fig. 5.9 illustrates displacements in all directions in Cartesian coordinates system for the flat plate problem stated above. The solutions in Fig. 5.9 are compared between the finite element solutions obtained from the linear and the nonlinear governing equations with applied loads equal to 1.0×10^{-8}. It can be seen that the obtained displacements from the linear and nonlinear equation are consistent only in the normal direction.

Regarding the displacements in both tangential directions, it can be seen from Figs. 5.9a and 5.9c that no deformation occurs in the x- and y-directions in the linear implementation. The underlying reason is that the forces are applied in the normal direction to the surface of the plate which correspond to the z-direction. Hence, there is no force applied in both tangential directions which correspond to the x- and y-directions. Therefore, there is no contribution to make the body deforms in those directions as the linear governing equations are not coupled between displacements in

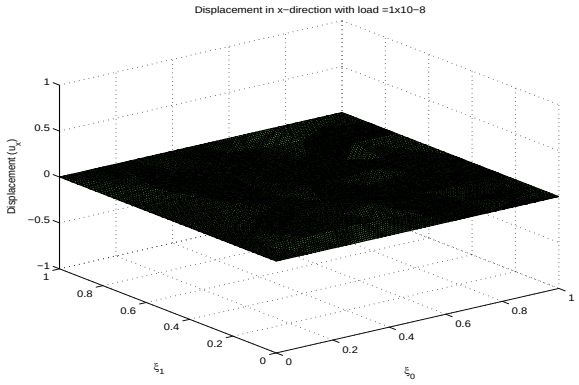

(a) displacement in x-direction obtained from the linear equation

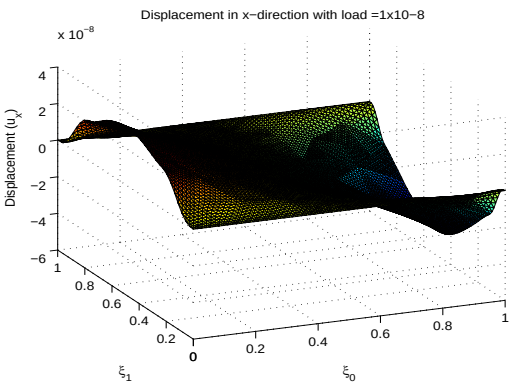

(b) displacement in x-direction obtained from the nonlinear equation

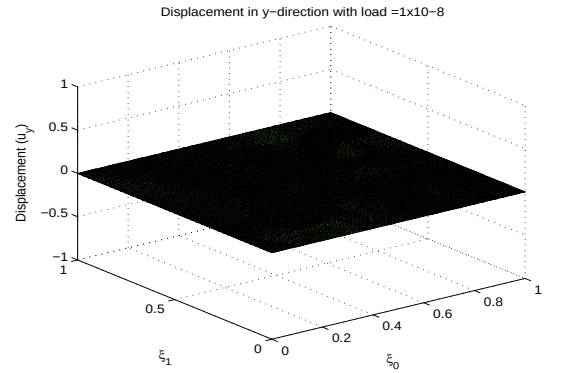

(c) displacement in y-direction obtained from the linear equation

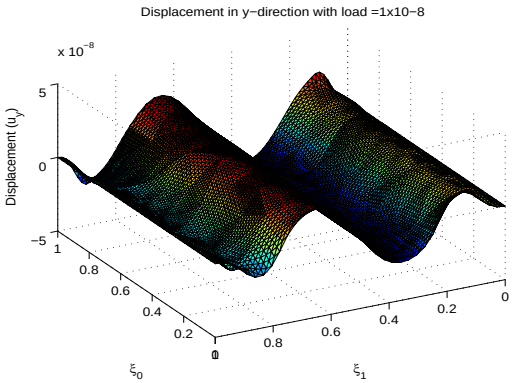

(d) displacement in y-direction obtained from the nonlinear equation

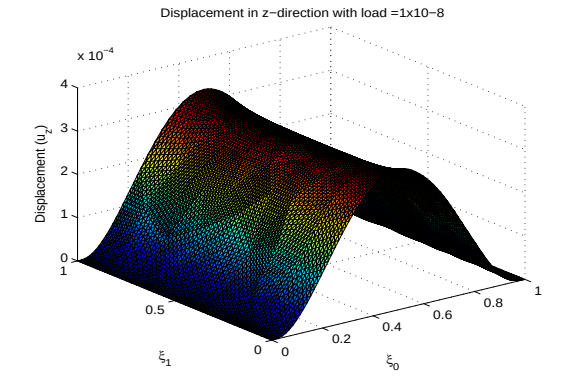

(e) displacement in z-direction obtained from the linear equation

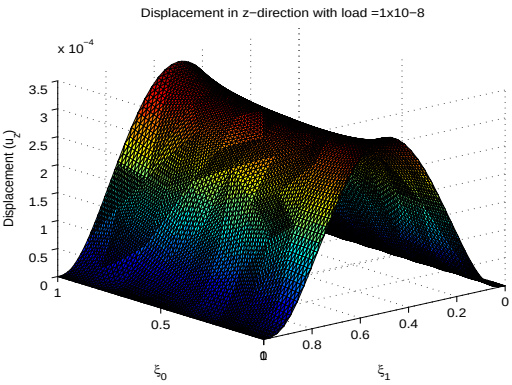

(f) displacement in z-direction obtained from the nonlinear equation

Figure 5.9: Displacements in cartesian coordinates for the clamped plate with the normal distributed loads=1×10^{-8}.

each direction as can be seen in (5.10), (5.11) and (5.12). This contrasts to the nonlinear governing equations which is coupled between displacements in each direction (see (3.91)).

To appreciate the difference between the solutions obtained from the linear and

the nonlinear governing equations when forces change, we will increase the applied forces from 0 by 1×10^{-8} for 11 steps. The comparison will be made between the displacements in z-direction obtained from the linear and the nonlinear governing equations and are illustrated in Fig. 5.10.

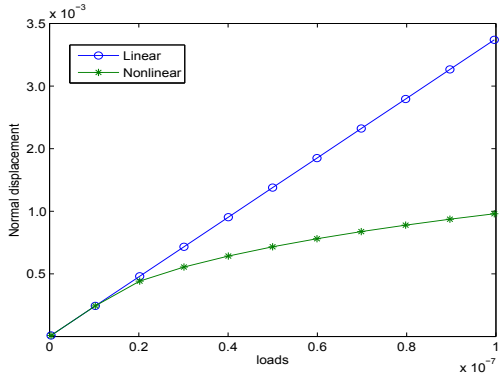

(a) Displacement in z-direction

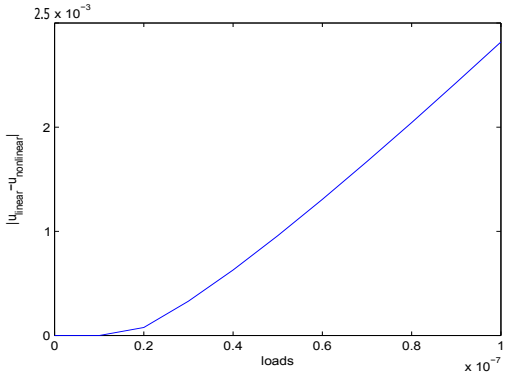

(b) Differences between the linear and nonlinear solutions

Figure 5.10: Differences between the displacement in z-direction obtained from the linear, the nonlinear, and the exact solutions with increasing loads from 0 to 1×10^{-7}.

From Fig. 5.10a, it can be seen that the normal displacements obtained from the linear and nonlinear governing equations vary, respectively, linearly and nonlinearly when the applied loads increase. This is a consequence from the nature of their governing equations. Moreover, it can be seen that the obtained linear and nonlinear solutions agree when loading is small and the difference starts to increase when the loading terms is getting bigger as seen in Fig. 5.10b.

These results are similar to those obtained from the beam problems when the linear and the nonlinear governing equation are compared. This suggests that, in the 3D small-deformation regime when the applied forces are very small, the linear governing

equations can be used to describe the thin shell's behaviour. Furthermore, for the plate problem, the linear governing equation is valid until the normal displacement is approximately 3.5% of the thickness which is consistent with the result from the beam with non-zero curvature. This is computed with the relative error between the linear and nonlinear solutions not greater than 0.01%.

5.3 Finite element method for a circular tube

In the previous section, we consider the flat plate whose undeformed configuration has a zero curvature. Within a small-deformation regime, it can be seen from section 5.2.3 that the finite element solutions obtained from the linear governing equations for this straight shell agree with those of nonlinear. However, it can not be, yet, concluded that the thin-shell behaviour can be described by the linear governing equation when a load is small. This is because the plate's governing equations derived in section 5.2 showed that some terms disappeared from the general thin-shell's governing equations in (3.112), (3.113), and (3.114) so that they can not be used as a representative of a general thin-shell.

Hence, in this section, we will consider the circular tube whose domain of interest has a non-zero curvature in order to verify the consistency of the linear and nonlinear solutions with a small deformation for a more general thin-shell.

5.3.1 The linearised governing equation

In this section, we consider a deformation of a circular tube which is subjected to a pressure loading on its surface as illustrated in Fig. 5.11. The loads applied on the tube are uniformly distributed in the normal direction. Similar to the elastic beam mentioned in chapter 4, a quarter circular tube will be implemented and symmetric conditions are assumed along the tube. The boundary conditions determined in this problem are clamped supports at both ends of the tube.

The initial positions of the circular tube are $\mathbf{r} = \begin{pmatrix} \cos(\xi_2) \\ \sin(\xi_2) \\ \xi_1 \end{pmatrix}$, and parametrised by the local coordinates ξ_1, ξ_2. The local coordinate ξ_1 is an axial coordinate defined

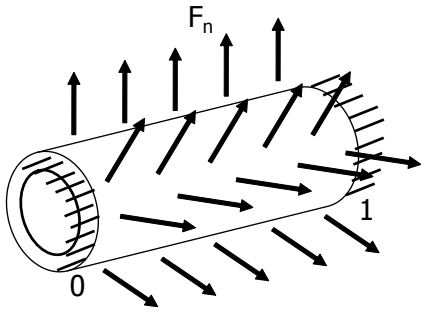

Figure 5.11: The geometry of unit circular tube with a clamped support at both ends of the tube. Forces applied to a body are uniform in normal direction.

in $[0, 1]$, and the radial coordinate ξ_2 defined in $[0, \frac{\pi}{2}]$. Hence, the associated tangential and normal vectors are as follows

$$\begin{aligned} \mathbf{t}_1 &= (0, 0, 1)^T, \\ \mathbf{t}_2 &= (-\sin(\xi_2), \cos(\xi_2), 0)^T, \\ \hat{\mathbf{n}} = \hat{\mathbf{t}}_3 &= (\cos(\xi_2), \sin(\xi_2), 0)^T. \end{aligned} \tag{5.23}$$

The linear version of the covariant metric tensor in the undeformed and deformed configurations for the circular tube can be computed from (3.94) and (3.95), respectively, as

$$a_{\alpha\beta} = \mathbf{t}_\alpha \cdot \mathbf{t}_\beta, \tag{5.24}$$

and,

$$A_{\alpha\beta} = a_{\alpha\beta} + u^\alpha|_\beta + u^\beta|_\alpha. \tag{5.25}$$

Remind that $u^j; j = 1, 2, 3$ are associated components of a displacement $\mathbf{u}$ in the tangential and normal directions. Also, $u^j|_\beta \mathbf{t}_j$ denote the components of the first derivatives in the tangential and normal system as described in (3.97). For the circular tube, we have that the determinant of the covariant metric tensor in undeformed shell is $a = 1$.

The linearised Green strain tensor for the circular tube which determined from the differences between the undeformed and deformed metric tensors as seen in (3.100), can be determined as follow

$$\begin{aligned} \gamma_{\alpha\beta} &= \frac{1}{2}(u^\alpha|_\beta + u^\beta|_\alpha) \\ &= \frac{1}{2}\left(u^\alpha_{,\beta} + u^\beta_{,\alpha} + u^1(\Gamma^\alpha_{1\beta} + \Gamma^\beta_{1\alpha}) + u^2(\Gamma^\alpha_{2\beta} + \Gamma^\beta_{2\alpha}) + u^3(\Gamma^\alpha_{3\beta} + \Gamma^\beta_{3\alpha})\right), \end{aligned} \tag{5.26}$$

where the last line comes from the definition of the first derivative in tangential and normal directions (see (3.97)). Note that $\Gamma^\alpha_{i\beta}$ can be computed from $\frac{\partial \mathbf{t}_i}{\partial \xi_\beta} \cdot \mathbf{t}_\alpha$. For the

circular tube, we have

$$\begin{aligned}
\Gamma^k_{i1} &= \frac{\partial \mathbf{t}_i}{\partial \xi_1}\cdot \mathbf{t}_k \equiv \mathbf{0}, \forall i,k,\\
\Gamma^k_{1j} &= \frac{\partial \mathbf{t}_1}{\partial \xi_j}\cdot \mathbf{t}_k \equiv \mathbf{0}, \forall j,k,\\
\Gamma^k_{22} &= \frac{\partial \mathbf{t}_2}{\partial \xi_2}\cdot \mathbf{t}_k \equiv (0,0,-1)^T,\\
\Gamma^k_{32} &= \frac{\partial \mathbf{t}_3}{\partial \xi_2}\cdot \mathbf{t}_k \equiv (0,1,0)^T.
\end{aligned} \tag{5.27}$$

Substituting (5.27) into (5.26) with some algebraic computations, the strain tensor becomes

$$\gamma_{\alpha\beta} = \begin{pmatrix} u^1_{,1} & \frac{1}{2}(u^1_{,2}+u^2_{,1}) \\ \frac{1}{2}(u^2_{,1}+u^1_{,2}) & u^2_{,2}+u^3 \end{pmatrix}. \tag{5.28}$$

Also, its variation can be obtained as

$$\begin{aligned}
\delta\gamma_{\alpha\beta} &= \delta u^\alpha_{,\beta} + \Gamma^\alpha_{1\beta}\delta u^1 + \Gamma^\alpha_{2\beta}\delta u^2 + \Gamma^\alpha_{3\beta}\delta u^3,\\
&= \begin{pmatrix} \delta u^1_{,1} & \frac{1}{2}(\delta u^1_{,2}+\delta u^2_{,1}) \\ \frac{1}{2}(\delta u^2_{,1}+\delta u^1_{,2}) & \delta u^2_{,2}+\delta u^3 \end{pmatrix}.
\end{aligned} \tag{5.29}$$

Next, we consider the curvature tensor for the circular tube which is specified by (3.103) as

$$\begin{aligned}
b_{\alpha\beta} &= \hat{\mathbf{n}}\cdot \mathbf{r}_{,\alpha\beta},\\
&= \hat{\mathbf{n}}\cdot \mathbf{t}_{\alpha,\beta}.
\end{aligned} \tag{5.30}$$

Now, it can be seen that the undeformed configuration for the circular tube has a non-zero curvature as $\frac{\partial \mathbf{t}_\alpha}{\partial \xi_2} \neq 0, \exists \alpha = 2,3$. Also, the linearised deformed curvature tensor is determined from (3.108) as

$$\begin{aligned}
B_{\alpha\beta} &= b_{\alpha\beta} + \left[\frac{1}{a}L_j\Gamma^j_{\alpha\beta} - \frac{L_3}{a^2}\Gamma^3_{\alpha\beta}\right] + \left(u^i|_\alpha \Gamma^3_{i\beta} + u^3_{,\alpha\beta} + u^k\frac{\partial \Gamma^3_{k\alpha}}{\partial \xi_\beta} + u^k_\beta \Gamma^3_{k\alpha}\right),\\
&= \begin{pmatrix} b_{11}+u^3_{,11} & b_{12}+u^3_{,12}-u^2_{,1} \\ b_{21}+u^3_{,21}-u^2_{,1} & b_{22}+u^3_{,22}-u^2|_2-u^2_{,2} \end{pmatrix},\\
&= \begin{pmatrix} b_{11}+u^3_{,11} & b_{12}+u^3_{,12}-u^2_{,1} \\ b_{21}+u^3_{,21}-u^2_{,1} & b_{22}+u^3_{,22}-(u^2_{,2}+u^3)-u^2_{,2} \end{pmatrix},\\
&= \begin{pmatrix} b_{11}+u^3_{,11} & b_{12}+u^3_{,12}-u^2_{,1} \\ b_{21}+u^3_{,21}-u^2_{,1} & b_{22}+u^3_{,22}-2u^2_{,2}-u^3 \end{pmatrix}.
\end{aligned} \tag{5.31}$$

Note that the last line comes from the definition of the Christoffel symbol of the second kind $\Gamma^j_{i\alpha} = \left(\frac{\partial \mathbf{t}_i}{\partial \xi_\alpha}\cdot \mathbf{t}_j\right)$ which computed in (5.27) for the circular tube.

Hence, the linearised bending tensor can be calculated from (3.109) as

$$\begin{aligned}\kappa_{\alpha\beta} &= b_{\alpha\beta} - B_{\alpha\beta} \\ &= -\begin{pmatrix} u^3_{,11} & u^3_{,12} - u^2_{,1} \\ u^3_{,21} - u^2_{,1} & u^3_{,22} - 2u^2_{,2} - u^3 \end{pmatrix}.\end{aligned} \tag{5.32}$$

Also, its variation is expressed as

$$\delta\kappa_{\alpha\beta} = -\begin{pmatrix} \delta u^3_{,11} & \delta u^3_{,12} - \delta u^2_{,1} \\ \delta u^3_{,21} - \delta u^2_{,1} & \delta u^3_{,22} - 2\delta u^2_{,2} - \delta u^3 \end{pmatrix}. \tag{5.33}$$

Substituting the strain tensor in (5.28) and the bending tensor in (5.32) with their variations (5.29) and (5.33) into the shell governing equation, (3.91), gives the governing equation for each displacement direction as follows

$$0 = \iint \left[-\frac{1}{h} f^1\right] \delta u^1 + \tilde{E}^{\alpha\beta\gamma\delta} \left\{(u^1_{,1} + u^1_{,2} + u^2_{,1} + u^2_{,2} + u^3)\delta u^1_{,\delta}\right\} d\xi_1 d\xi_2, \tag{5.34}$$

for a displacement u^1 in tangential direction along the coordinate ξ_1, and

$$\begin{aligned}0 = \iint \left[-\frac{1}{h} f^2\right] \delta u^2 + \tilde{E}^{\alpha\beta\gamma\delta} \Big\{ \Big[&(u^1_{,1} + u^1_{,2} + u^2_{,1} + u^2_{,2} + u^3) \\ - \frac{2}{12} h^2 &(u^3_{,11} + u^3_{,12} - 2u^2_{,1} + u^3_{,21} + u^3_{,22} - 2u^2_{,2} - u^3)\Big] \delta u^2_{,\delta}\Big\} d\xi_1 d\xi_2,\end{aligned} \tag{5.35}$$

for a displacement u^2 in tangential direction along the coordinate ξ_2, and

$$\begin{aligned}0 = \iint \left[-\frac{1}{h} f^3\right] \delta u^3 + \tilde{E}^{\alpha\beta\gamma\delta} \Big\{ \Big[&(u^1_{,1} + u^1_{,2} + u^2_{,1} + u^2_{,2} + u^3) \\ - \frac{1}{12} h^2 &(u^3_{,11} + u^3_{,12} - 2u^2_{,1} + u^3_{,21} + u^3_{,22} - 2u^2_{,2} - u^3)\Big] \delta u^3 \\ + \frac{1}{12} h^2 &(u^3_{,11} + u^3_{,12} - 2u^2_{,1} + u^3_{,21} + u^3_{,22} - 2u^2_{,2} - u^3)\delta u^3_{,\delta\gamma}\Big\} d\xi_1 d\xi_2,\end{aligned} \tag{5.36}$$

for a displacement u^3 in normal direction.

Similar to the beam, the partial differential equations that govern displacements in both tangential and normal directions for the curved shell are more complicated than those of the straight case. Having a non-zero curvature in the undeformed configuration for the curved geometry is the result for certain terms to maintain and to contribute in the equations. The governing equations for the circular tube are coupled between displacements in all directions except the tangential direction in the coordinate ξ_1 as can be seen from (5.34), (5.35), and (5.36).

Regarding the weak formulation in the finite element implementations, equations (5.34), (5.35), and (5.36) exhibit the same order of continuity in the finite element representations for each associated displacements with the beam. Therefore, the mixed formulation will be employed to implement the governing equations of the curved shell as suggested in the beam implementations in chapter 3.

5.3.2 Numerical comparisons between the Kirchhoff-Love linear and nonlinear governing equations

In this section, implementations of the linearised governing equations for the circular tube will be illustrated and compared with the nonlinear equations that associate with the problem. The results will bring us to the conclusion for the capability of the linear governing equation to describe a thin-elastic body with a small deformation. Note that the linear implementations will be based on the governing equations (5.34), (5.35), and (5.36) that we derived in section 5.3.1 where those of the nonlinear can be seen in (3.91) of chapter 3.

Similar to the flat plate, the problem will be solved with the assumption that the thickness of the tube is thin so that the linear theory can be applied. Our choice of thickness for the circular tube is 0.01. Also, applied forces will be small and be of order 1×10^{-6}. Note that the forces applied to the circular plate are greater than those applied to the flat plate as stronger forces are needed to make the body deforms. This is a consequence of being curved and having non-zero curvature in an undeformed configuration so that it resists more to forces.

In order to perform the finite element implementations, the domain of interest will be discretised by triangular elements with an unstructured mesh as the Bell triangular finite elements will be employed. The same amount of loading terms equals to 1×10^{-6} will be applied in normal direction to the circular tube for both linear and nonlinear equations. Note that there will be 248 triangular elements in the mesh. Regarding the numerical integration and the approximations for each displacement directions, they are chosen to be the same as in the flat plate implementations.

Since the clamped circular tube is determined in this problem as seen in Fig. 5.11, the boundary conditions for both ends of the tube at $\xi_1 = 0$ and $\xi_1 = 1$ will be

pinned for all of the degrees of freedom. Also, at the boundary $\xi_2 = 0$ and $\xi_2 = \pi/2$, the symmetric conditions will be applied since only quarter of the circular tube is implemented.

Next, a comparison between nonlinear and linear governing equations for the circular tube will be illustrated by applying the constant external forces that uniformly distributed in normal direction to the tube. This is to illustrate the consistency between the linear and nonlinear equation with a small deformation where the magnitude of the applied force equals to 1×10^{-6}.

Fig. 5.12 illustrates displacements in all directions in Cartesian coordinate system for the clamped circular tube problem stated above. It can be seen that those two displacements are consistent in all directions. Furthermore, the displacement in x- and y-directions are symmetry as shown in Fig. 5.12. This behaviour depicts that the thin-circular tube deforms axisymmetrically.

It should be mentioned here that the compared displacements are in the Cartesian coordinate system where those displacements in the implemented equations are in tangential and normal system. The transformation between the two coordinate systems can be done similarly as in (4.43) but a three-dimensional space has to be concerned.

Next, we will increase loading forces from 0 by 1×10^{-6} for 11 steps in order to appreciate the consistency between the linear and nonlinear governing equations when forces change.

Figs. 5.13 and 5.14 illustrate the consistency between the displacements in y- and z-directions, respectively, obtained from the linear and nonlinear equations for the circular tube with different applied loads. The figures depict that those two solutions in y- and z-direction are consistent with an small error when applied loads are small as can be seen in Figs. 5.13a and 5.14a. Note that the comparison in x-direction is discarded as it is symmetry to the y-direction.

Furthermore, it can be seen from Figs. 5.13b and 5.14b that the difference between the linear solutions and the nonlinear solutions starts to increase when the loading terms are getting bigger. These results are similar to those of the flat plate and all beam problems when displacements obtained from the linear and nonlinear equation are compared within a small-deformation regime. For the circular tube, the linear governing equation is valid until the normal displacement is approximately 1.06% of

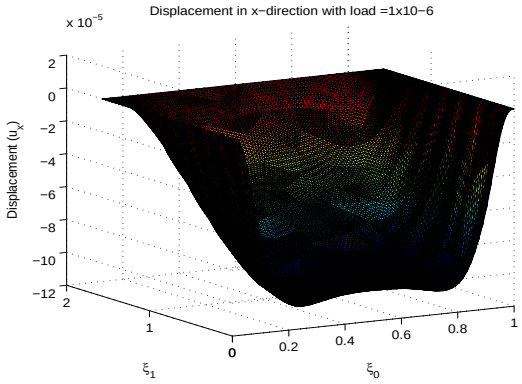

(a) displacement in x-direction obtained from the linear equation

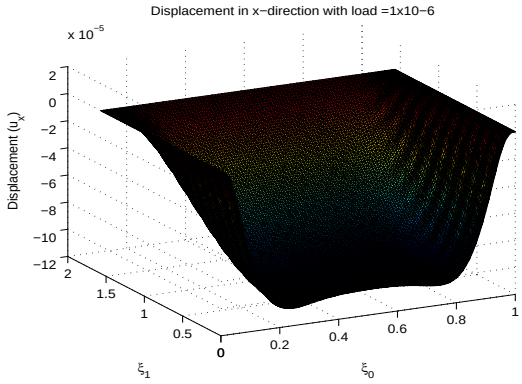

(b) displacement in x-direction obtained from the nonlinear equation

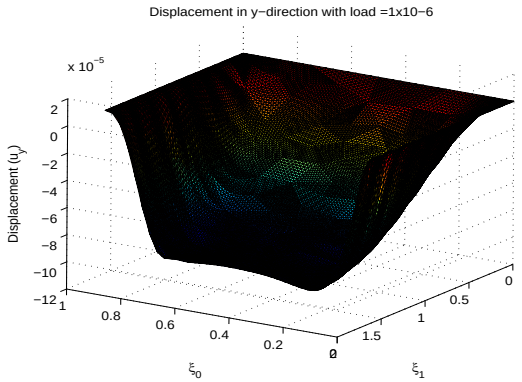

(c) displacement in y-direction obtained from the linear equation

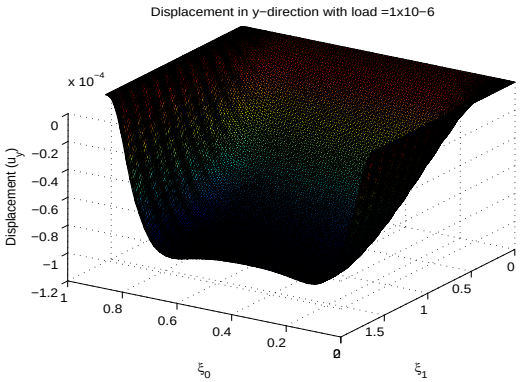

(d) displacement in y-direction obtained from the nonlinear equation

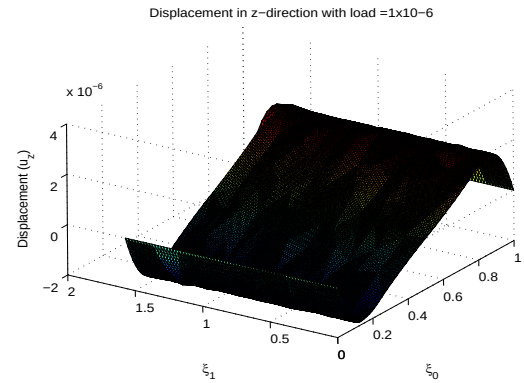

(e) displacement in z-direction obtained from the linear equation

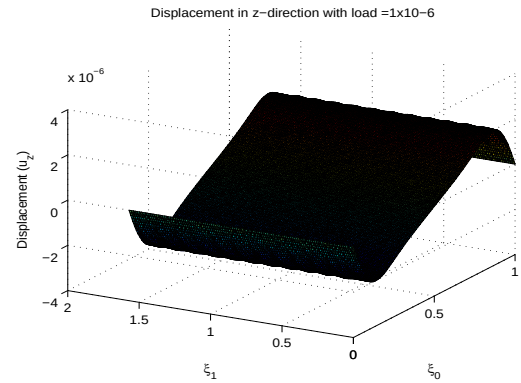

(f) displacement in z-direction obtained from the nonlinear equation

Figure 5.12: Displacements in cartesian coordinates for the clamped circular tube with the normal distributed loads=1×10^{-6}.

the thickness.

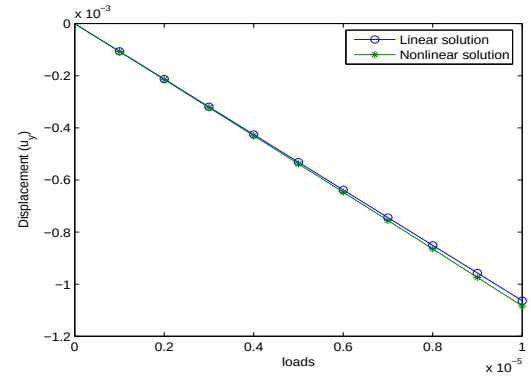

(a) Displacement in y-direction

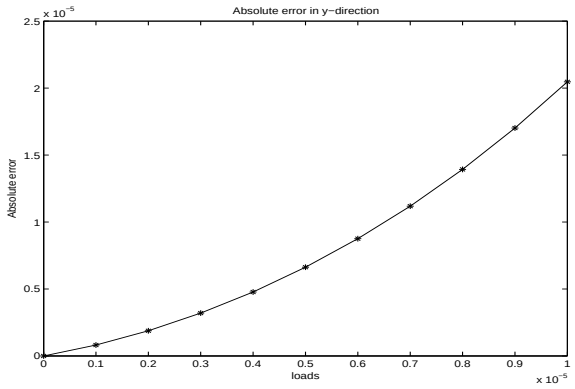

(b) Absolute error

Figure 5.13: Differences between the displacement in y-direction obtained from the linear and the Nonlinear governing equations for the circular tube with increasing loads from 0 to 1×10^{-5}.

5.4 Summary

In this chapter, the finite element models of thin shells in the linear theory have been developed. Two different undeformed geometries are concerned; a flat plate and a circular tube. These two thin-elastic materials in three-dimensional space are studied in order to illustrate the consistency between the linear and the nonlinear governing equations within a small-deformation regime.

Regarding the finite element discretisation of the desired geometry in two dimensions, there are two choices; a rectangular and a triangular element. From section 5.2.2, the numerical comparison between the performance of the rectangular Hermite and the Bell triangular elements shows that the Bell element gives higher accuracy and converges faster than the Hermite element. Also, for some selected tolerances, the Bell element is less time-consuming and also employs less degree of freedom than the Hermite element to achieve the accuracy.

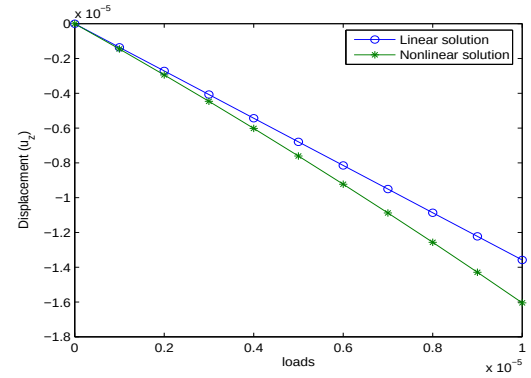

(a) Displacement in z-direction

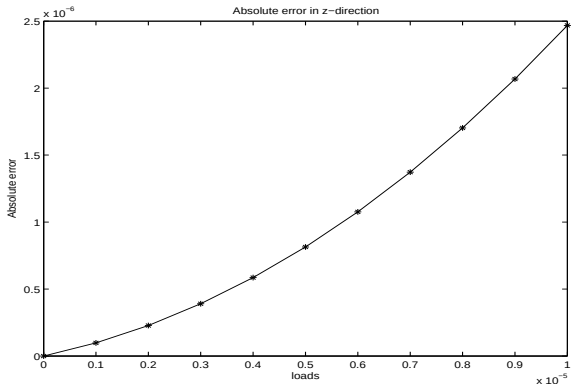

(b) Absolute error

Figure 5.14: Differences between the displacement in z-direction obtained from the linear and the Nonlinear governing equations for the circular tube with increasing loads from 0 to 1×10^{-5}.

For the reason of greater convergence rate than the Hermite rectangular element, the Bell triangular finite element is thus employed to represent the normal displacement of the thin-shell problems for both linear and nonlinear equations. This is to assure the C^1-continuity between the solutions as required in the associated governing equation described in sections 5.2.1 and 5.3.1.

Regarding the thin-shell implementations illustrated in sections 5.2.3 and 5.3.2 for the flat plate and the circular tube, respectively, it can be seen that the solutions obtained from the linear and nonlinear equations agree when loading is small. This applied load should be in the range that gives the normal displacements, approximately, 1-3% of the thickness with the relative error between the linear and nonlinear solution not greater than 0.01%. Also, the difference between the linear and nonlinear solutions starts to increase when the loading is greater than this range of linear validity. These results obtained from both flat plate and circular tube, which is a thin-elastic body in

a three-dimensional space, are consistent with those of a straight beam and an elastic ring which is a thin-elastic body in a two-dimensional space. Therefore, this can bring us to the conclusion that the linear equation can be used to describe a thin-elastic material with a small deformation when the normal displacements are, approximately, 1-3% of the thickness.

Chapter 6

The fourth-order problem with curved boundary domain

6.1 Introduction

In the previous chapters, the triangular Bell element has been successfully used to solve fourth-order problems. The domains of interest considered in the particular problems contained only straight boundaries so that this representation was exact. However, in many engineering applications, the geometric boundary of a problem is not straight. Solving such a problem with the straight-sided C^1-finite elements limits the convergence rate and accuracy as presented in [56], [47], [63], [65]. Consequently, this motivates many researchers to develop and improve an efficient finite element when C^1-problems are concerned with a curvilinear boundary.

In order to deal with a fourth-order problem, which requires C^1-continuity, on a curved boundary, there are many literature that present the efficient C^1-finite elements dealing with curvilinear boundary for both rectangle and triangular meshes (see [7], [18], [41], [56], [48], [63], [64]). Only M. W. Chernuka [56] and M. Bernadou [48] are dealing with the C^1-elements defined on a triangular mesh.

In the study of M. W. Chernuka [56], a triangular element is modified to include one curved and two straight edges. In his study, the polynomial space was defined over the original triangle with no modification in the shape functions. Instead, the areas of integration changed and were extended over the additional curved area. This additional area of integration from the extended curve made the method even more

difficult when complicated integrands were involved.

Similar to M. W. Chernuka, M. Bernadou [48] constructed a triangular element including one curved edge by moving out one edge to fit the curved boundary while the other two remain straight. However, Bernadou constructed each shape function in correspondence with a reference element which makes his method very straightforward to work in numerical integration. Also, an explicit computation of his C^1-curved finite elements is well explained in [48], [50]. Therefore, to deal with the curvilinear boundary problem, the idea of using one curve-sided triangle from M. Bernadou is employed to retain the rate of convergence and accuracy in this study.

Before a numerical implementation of the fourth-order problems with a curvilinear boundary will be illustrated, the construction of a C^1-curved finite element will be discussed in section 6.2. The section will contain four subsections on the triangulation of a domain which constitutes of both straight-edged and curve-edged triangles (see section 6.2.1), the mapping associated the reference triangle with the physical curved triangle (see section 6.2.2), the definition of the C^1-curved finite element (see section 6.2.3), and the construction of the interpolation of any function v defined over curved triangles (see section 6.2.4).

Next, numerical implementations of the fourth-order problems will be presented in section 6.3 by employing the C^1-curved triangular element derived in section 6.2 to represent curvilinear boundary. The Biharmonic equation and the circular-plate bending problem will be two concerned problems in this study.

In the study of the Biharmonic equation in section 6.3.1, the comparison between the performance of the C^1-straight-edged and the C^1-curved triangular elements will be illustrated. Both rate of convergence and the obtained accuracy from those two elements will be determined together with the computational time. This is to show that representing a curved boundary by a series of straight-sided triangles exhibits a limitation in convergence rate and accuracy.

Likewise, further validation of the capability of the C^1-curved element is performed in section 6.3.2 by solving the plate bending problem. The obtained accuracy from both the Bell and the C^1-curved elements will be compared in order to conclude the efficient triangular element for the C^1-curvilinear boundary problem.

Finally, this chapter will end with the summary section 6.4.

6.2 The C^1-curved finite element

In this section, we will introduce the C^1-curved finite element compatible with the Bell element studied in chapter 5. The objective of this element is to obtain the same asymptotic error estimates on the curved boundary domain as that of the problem when the exact representation is concerned.

Unlike the triangulation of the straight boundary domain, since the curved boundary domain is concerned in this study, the triangulation of the domain of interest will be the union of two sets of triangles. The first set will constitute of straight-sided triangles K_I and the other will constitute of curve-sided triangles K_C. Also, we assume that each of two distinct triangles of the triangulations is either disjoint, or have a common vertex or a common edge. Consequently, we have to define mappings associated the reference and the physical triangles for each straight and curved triangles.

Regarding the straight boundary domain, the Bell shape functions will be employed as the domain associated the mapping remains unchanged. On the curved boundary domain, the shape functions will be re-constructed compatible with the Bell shape functions. The functions will be defined over the approximated domain associated with the mappings approximating the curved boundary. Finally, these shape functions will be used to define interpolations of variables on the typical elements.

6.2.1 Approximation of a physical domain

In order to approximate the geometry, the mapping which associates the reference and the physical triangles has to be concerned. In this study, we will define mapping by using polynomials to approximate boundaries. Since there are two sets of triangular elements in the mesh, different mappings have to be considered for typical elements. In order to deal with a straight-sided triangle in a physical domain, K_I, an affine mapping will be taken into account. Nonetheless, a nonlinear mapping has to be considered in order to deal with a curved-edge triangle, K_C.

Now, we will define the affine mapping F_{K_I} which associates the reference triangle, $\hat{K}$, with the straight-sided triangle, K_I, on the physical domain. The reference triangle, $\hat{K}$, is parametrised by the reference coordinates $\hat{x}_1, \hat{x}_2$ and defined as $\hat{K} = \{(\hat{x}_1, \hat{x}_2) | 0 \leq \hat{x}_1, \hat{x}_2 \leq 1, \hat{x}_1 + \hat{x}_2 = 1\}$. The affine mapping is parametrised by the

reference coordinates $\hat{x}_\alpha, \alpha = 1, 2$, and can be constructed as

$$x_\alpha = F_{K_{I\alpha}}(\hat{x}_1, \hat{x}_2) = x_{\alpha 3} + (x_{\alpha 1} - x_{\alpha 3})\hat{x}_1 + (x_{\alpha 2} - x_{\alpha 3})\hat{x}_2 \tag{6.1}$$

where $x_{\alpha i}$ denote the global coordinates $\alpha = 1, 2$ of the vertices $\mathbf{a}_i, i = 1, 2, 3$, of the triangle K_I as depicted in Fig. 6.1. Also, $F_{K_{I\alpha}}$ is a α^{th} component of the mapping F_{K_I}. This mapping will help us to associate a position $(\hat{x}_1, \hat{x}_2)$ on the reference triangle with a position (x_1, x_2) on the physical triangle whose sides are straight.

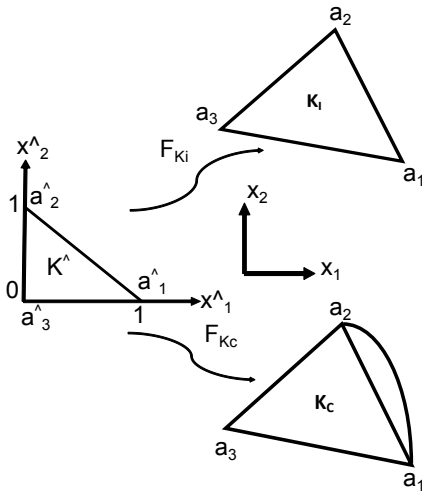

Figure 6.1: A graphical description of the mappings associated between the reference coordinates $\hat{x}_\alpha$ and the physical coordinates $x_\alpha, \alpha = 1, 2$ where F_{K_I} is the mapping corresponding with the straight-sided triangle and F_{K_C} is the mapping corresponding with the curved triangle.

Next, a triangulation that constitutes of curved triangles K_C will be determined. These curved triangles are considered to have two straight sides and one curved side approximating an arc of the boundary Γ as shown in Fig. 6.2. Since the curved boundary are concerned, the mapping F_{K_C} for this case is thus nonlinear and can be constructed as in the following descriptions.

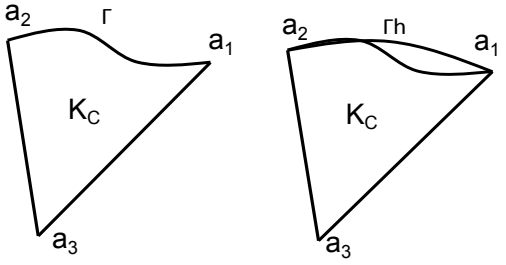

Figure 6.2: An exact curved boundary Γ and an approximated boundary Γ_h of one-curved side triangles K_C.

Let Ω be a given bounded domain on the plane whose boundary is curve in two-dimensional space. We assume that the curved boundary Γ can be subdivided into a finite number of arcs and each of them can be described as

$$x_1 = \chi_1(s), \quad x_2 = \chi_2(s), \quad s_m \leq s \leq s_M, \tag{6.2}$$

where $x_\alpha, \alpha = 1, 2$ denote coordinates in two-dimensional space defined on the physical domain and approximated by the functions $\chi_1(s), \chi_2(s)$ which are continuous on $[s_m, s_M]$.

In order to defined the nonlinear mapping F_{K_C} which maps from the reference to the physical element, reference coordinates has to be employed. Hence, we have to reparametrise the arc $\mathbf{a}_1\mathbf{a}_2$ of K_C in Fig. 6.2 by using the reference coordinate $\hat{x}_2$ which lies in the interval of $[0, 1]$. This can be done as follow

$$x_1 = \varphi_1(\hat{x}_2), \quad x_2 = \varphi_2(\hat{x}_2), \tag{6.3}$$

where $\varphi_\alpha(\hat{x}_2) = \chi_\alpha(s_m + (s_M - s_m)\hat{x}_2), \alpha = 1, 2$. Note that either $\hat{x}_1$ or $\hat{x}_2$ can be used to parametrise the arc but re-calculation will be required in the derivation of the mapping F_{K_C}.

Before considering the nonlinear mapping F_{K_C} which does not depend on any specific edge, we would like to define firstly a mapping corresponding with the curved boundary Γ. This mapping will be defined so that the side $\hat{\mathbf{a}}_1\hat{\mathbf{a}}_2$ on the reference triangle, $\hat{K}$, associates with the curved boundary Γ.

Since $\varphi_\alpha(\hat{x}_2)$ are continuous functions defined to approximate coordinates $x_\alpha, \alpha = 1, 2$ on the curved boundary, we have that our mapping has to define so that

$$\begin{aligned} \varphi_\alpha(\hat{x}_2 = 0) &= x_{\alpha 1} = \mathbf{a}_1, \\ \varphi_\alpha(\hat{x}_2 = 1) &= x_{\alpha 2} = \mathbf{a}_2, \alpha = 1, 2. \end{aligned} \tag{6.4}$$

Then, the approximated arc Γ_h of the curved boundary Γ is defined by the parametric functions $\varphi_{ih}, i = 1, 2$ satisfied the following

$$x_1 = \varphi_{1h}(\hat{x}_2), \quad x_2 = \varphi_{2h}(\hat{x}_2). \tag{6.5}$$

In this study, we restrict the mapping so that $F_{K_C}(\hat{\mathbf{a}}_j) = \mathbf{a}_j$, for $j = 1, 2, 3$. Therefore, from (6.4), we employ a polynomial function of degree n to define a mapping

associated with the curved boundary. This polynomial will be parametrised by the reference coordinate $\hat{x}_2$ and can be expressed as

$$\varphi_{\alpha h}(\hat{x}_2) = x_{\alpha 1} + (x_{\alpha 2} - x_{\alpha 1})\hat{x}_2 + \hat{x}_2(1-\hat{x}_2)p_{n-2;\alpha}(\hat{x}_2), n \geq 2, \tag{6.6}$$

where $p_{n-2;\alpha}, \alpha = 1, 2$, denotes polynomials of degree $n-2$ in the α-th coordinate and also parameterises by the reference coordinate $\hat{x}_2$. Note that the choice of polynomial degree can be determined from the interpolation theory [48].

Now, we will define the general mapping F_{K_C} that is not specific to any side of the triangle. Since the mapping F_{K_C} is an affine mapping along the side $\mathbf{a}_3\mathbf{a}_\alpha, \alpha = 1, 2$, and has to be identical to $\varphi_{\alpha h}$ when restricted to the side $\mathbf{a}_1\mathbf{a}_2$, we have that

$$\begin{aligned} F_{K_{C\alpha}}(\hat{x}_1, \hat{x}_2) =& x_{\alpha 3} + (x_{\alpha 1} - x_{\alpha 3})\hat{x}_1 + (x_{\alpha 2} - x_{\alpha 3})\hat{x}_2 \\ &+ \frac{1}{2}\hat{x}_1\hat{x}_2\left[p_{n-2;\alpha}(1-\hat{x}_1) + p_{n-2;\alpha}(\hat{x}_2)\right], n \geq 2, \end{aligned} \tag{6.7}$$

where $F_{K_{C\alpha}}$ denotes an α^{th} component of the mapping F_{K_C}. Note that the nonlinear mapping $F_{K_{C\alpha}}(1-\hat{x}_2, \hat{x}_2)$ must be equal to the polynomial $\varphi_{\alpha h}(\hat{x}_2)$ when restricted to the side $\mathbf{a}_1\mathbf{a}_2$.

6.2.2 The mapping, F_{K_C}, associated the reference with the curved triangle

As seen in (6.6), a degree of polynomial approximating the curved boundary has not yet been determined. Therefore, in this section, we will discuss our choice of polynomial degree that will be used in order to define a nonlinear mapping to associate between the reference and the curved triangles.

In this work, the Hermite-type polynomial of degree 3 is our choice to approximate the curved boundary. The reason for this choice is that cubic is the minimum degree of polynomial to obtain the C^1-continuity [48]. Since the Hermite-type polynomial of degree 3 is concerned, we have that four conditions have to be specified and therefore are described as

$$\begin{aligned} x_{\alpha 1} = \varphi_\alpha(0) = \chi_\alpha(s_m), \qquad & x_{\alpha 2} = \varphi_\alpha(1) = \chi_\alpha(s_M), \\ \varphi'_\alpha(0) = (s_M - s_m)\chi'_\alpha(s_m), \quad & \varphi'_\alpha(1) = (s_M - s_m)\chi'_\alpha(s_M). \end{aligned} \tag{6.8}$$

These conditions are constraints in order to satisfy the hypothesis (6.4) and the expression

$$\varphi_\alpha(\hat{x}_2) = \chi_\alpha(s_m + (s_M - s_m)\hat{x}_2), \alpha = 1, 2$$

for the coordinate values x_α. Also, the derivative of φ_α have to satisfy the above expression in order to obtain the continuity.

In order to obtain $p_{n-2;\alpha}(\hat{x}_2)$ when $n = 3$ in (6.6) for each coordinate α, we assume that $p_{3-2;\alpha}(\hat{x}_2) = m_\alpha \hat{x}_2 + c_\alpha$ which is linear. Hence, (6.6) becomes

$$\varphi_{\alpha h}(\hat{x}_2) = x_{\alpha 1} + (x_{\alpha 2} - x_{\alpha 1})\hat{x}_2 + \hat{x}_2(1 - \hat{x}_2)[m_\alpha \hat{x}_2 + c_\alpha]. \tag{6.9}$$

To obtain the unknowns m_α and c_α for the associated coordinates, we have to consider the conditions for derivatives in (6.8). After differentiating (6.9) once and applying conditions in (6.8), a cubic polynomial for each coordinate is obtained. Hence, (6.6) and (6.7) lead to

$$\begin{aligned}\varphi_{\alpha h}(\hat{x}_2) =& x_{\alpha 1} + (x_{\alpha 2} - x_{\alpha 1})\hat{x}_2 + \hat{x}_2(1 - \hat{x}_2)\left\{[2(x_{\alpha 2} - x_{\alpha 1}) - (s_M - s_m)\right. \\ & \left.(\chi'_\alpha(s_m) + \chi'_\alpha(s_M))]\,\hat{x}_2 + x_{\alpha 1} - x_{\alpha 2} + (s_M - s_m)\chi'_\alpha(s_m)\right\},\end{aligned} \tag{6.10}$$

and then the general mapping that associates the reference and the curved elements is obtained as follow

$$\begin{aligned}F_{K\alpha}(\hat{x}_1, \hat{x}_2) =& x_{\alpha 3} + (x_{\alpha 1} - x_{\alpha 3})\hat{x}_1 + (x_{\alpha 2} - x_{\alpha 3})\hat{x}_2 \\ & + \frac{1}{2}\hat{x}_1\hat{x}_2\left\{[2(x_{\alpha 2} - x_{\alpha 1}) - (s_M - s_m)(\chi'_\alpha(s_m) + \chi'_\alpha(s_M))]\,(\hat{x}_2 - \hat{x}_1)\right. \\ & \left. + (s_M - s_m)\,[\chi'_\alpha(s_m) - \chi'_\alpha(s_M)]\right\}.\end{aligned} \tag{6.11}$$

6.2.3 Definition of the C^1-curved finite element compatible with the Bell triangles where the mapping is cubic

Next, we will define the C^1-curved finite element. Since the Bell triangular element is considered in the implementations of the C^1-problem in the previous chapter, the curved finite element in this chapter will thus be constructed to have a connection of class C^1-compatible with Bell triangles.

To define such a connection, we need some conditions that assured for a connectivity between a curved finite element and the Bell triangle. As shown in Fig. 6.3, we

have that the connections between the curved elements and the adjacent (straight or curved) finite elements are realised through the straight sides $\mathbf{a}_3\mathbf{a}_1$ and $\mathbf{a}_3\mathbf{a}_2$.

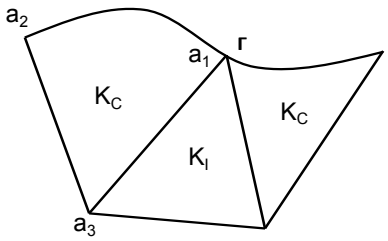

Figure 6.3: Adjacent triangles to a curved triangle K_C.

Therefore, to obtain a C^1-connection, polynomials, p, of one-variable, and their normal derivatives, $\frac{\partial p}{\partial n}$, defined over the curved triangle have to coincide with those of the adjacent finite elements along the connected sides. In order to satisfy these conditions, it is sufficient that the degrees of freedom of the curved finite element relative to the sides $\mathbf{a}_3\mathbf{a}_\alpha, \alpha = 1, 2$, are identical to that of the adjacent finite element.

Since we wish to define an element compatible with the Bell triangle, the degrees of a polynomial and its normal derivative along the sides $\mathbf{a}_3\mathbf{a}_\alpha, \alpha = 1, 2$, that associated with the curved triangle K_C, has to be of degree 5 and 3, respectively. Moreover, the degrees of freedom have to be entirely determined on those sides. With these conditions, a C^1-connection between two adjacent curved finite elements can be ensured.

In order to employ the mapping F_{K_C} defined in section 6.2.1 to associate any function v defined over the physical triangle K with a function $\hat{v}$ defined over the reference triangle $\hat{K}$, we have

$$v = \hat{v} \circ F_{K_C}^{-1}, \quad \hat{v} = v \circ F_{K_C}. \tag{6.12}$$

Therefore, for any polynomial $p \in P_K$ defined over the curved triangle K_C, we can associate this polynomial p with the polynomial function $\hat{p} = p \circ F_{K_C}$ defined on the reference triangle by using (6.12). Defining a polynomial on the reference triangle, $\hat{K}$, is a desirable condition which is convenient for the study of the approximation error and to take into account the numerical integration and the boundary conditions.

However, this condition leads to the definition of reference finite elements which are more complicated than those associated with corresponding straight finite elements. This is because of the polynomial defined over the reference element corresponding to the curved element is of higher degree which is the consequence from using higher degree polynomial to approximate the boundary and in order to obtain the C^1-continuity.

Next, we will determine the degree of polynomials $\hat{P}$ that employs to approximate the function v defined over the curved physical finite element. By using (6.12), the correspondence interpolation function defined over the reference triangle can be considered instead.

Let $\hat{\mathbf{a}} = (\hat{x}_1, \hat{x}_2)$ be any point on the side $\hat{\mathbf{a}}_3\hat{\mathbf{a}}_1$ of the triangle $\hat{K}$ and set $\mathbf{a} = F_K(\hat{\mathbf{a}})$. Then the derivatives of $\hat{p}(\hat{\mathbf{a}}) = p \circ F_K(\hat{\mathbf{a}})$ on the side $\hat{\mathbf{a}}_3\hat{\mathbf{a}}_1$ involves the chain rule and the usual scalar product in $\Re^2, < \cdot, \cdot >$, as follows

$$\frac{\partial \hat{p}}{\partial \hat{x}_2}(\hat{\mathbf{a}}) = \frac{\partial}{\partial \hat{x}_2}(p \circ F_K)(\hat{\mathbf{a}}) = Dp(\mathbf{a}) \cdot \frac{\partial F_K}{\partial \hat{x}_2}(\hat{\mathbf{a}}), \tag{6.13}$$

where D denotes the differential operator for the first-order derivative defined as $D = (\partial_{x_1}, \partial_{x_2})$. By considering the derivatives in the tangential and normal directions, the derivative can be expressed as

$$Dp(\mathbf{a}) \cdot \frac{\partial F_K}{\partial \hat{x}_2}(\hat{\mathbf{a}}) = \langle \frac{\partial F_K}{\partial \hat{x}_2}(\hat{\mathbf{a}}), \frac{\mathbf{a}_1 - \mathbf{a}_3}{|\mathbf{a}_1 - \mathbf{a}_3|^2} Dp(\mathbf{a}) \cdot (\mathbf{a}_1 - \mathbf{a}_3) + \frac{\mathbf{a}_2 - \mathbf{c}_2}{|\mathbf{a}_2 - \mathbf{c}_2|^2} Dp(\mathbf{a}) \cdot (\mathbf{a}_2 - \mathbf{c}_2) \rangle. \tag{6.14}$$

Similarly, for any point $\hat{\mathbf{a}}$ on the edge $\hat{\mathbf{a}}_3\hat{\mathbf{a}}_2$, we have

$$\begin{aligned} \frac{\partial \hat{p}}{\partial \hat{x}_1}(\hat{\mathbf{a}}) &= \frac{\partial}{\partial \hat{x}_1}(p \circ F_K)(\hat{\mathbf{a}}) = Dp(\mathbf{a}) \cdot \frac{\partial F_K}{\partial \hat{x}_2}(\hat{\mathbf{a}}) \\ &= \langle \frac{\partial F_K}{\partial \hat{x}_1}(\hat{\mathbf{a}}), \frac{\mathbf{a}_2 - \mathbf{a}_3}{|\mathbf{a}_2 - \mathbf{a}_3|^2} Dp(\mathbf{a}) \cdot (\mathbf{a}_2 - \mathbf{a}_3) + \frac{\mathbf{a}_1 - \mathbf{c}_1}{|\mathbf{a}_1 - \mathbf{c}_1|^2} Dp(\mathbf{a}) \cdot (\mathbf{a}_1 - \mathbf{c}_1) \rangle, \end{aligned} \tag{6.15}$$

where $\mathbf{c}_\alpha$ denote an orthogonal projection of $\mathbf{a}_\alpha$ on the side opposite to the point $\mathbf{a}_\alpha, \alpha = 1, 2$. They are illustrated in Fig. 6.4.

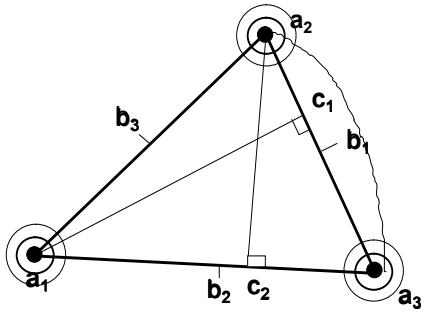

Figure 6.4: Description of the notations: $\mathbf{c}_1$ and $\mathbf{c}_2$ on the curved triangle K_C.

As the consequence of using the Bell triangle, the degree of polynomial's derivatives $Dp(\mathbf{a})$ defined over the physical element is quartic. Furthermore, since the degree of

polynomial used in the mapping F_K is n in general, we have that the derivatives of the mapping are of degree $n-1$. Hence, it follows from (6.15) that $\frac{\partial \hat{p}}{\partial \hat{x_1}}|_{\hat{\mathbf{a}} \in [\hat{\mathbf{a}}_3 \hat{\mathbf{a}}_2]}$ is a polynomial of degree $n+3$ with respect to $\hat{x_2}$ (as $\hat{x}_1 \equiv 0$ on that side). Also, (6.14) gives that $\frac{\partial \hat{p}}{\partial \hat{x_2}}|_{\hat{\mathbf{a}} \in [\hat{\mathbf{a}}_3 \hat{\mathbf{a}}_1]}$ is a polynomial of degree $n+3$ with respect to $\hat{x_1}$ (as $\hat{x}_2 \equiv 0$ on that side).

Since the degree of derivatives of the polynomial $Dp(\mathbf{a})$ when restricts to both side $\hat{\mathbf{a}}_3 \hat{\mathbf{a}}_\alpha$ is $n+3$ and they are one-variable polynomials, we can conclude that a polynomial $\hat{p}$ defined over the reference triangle $\hat{K}$ has to be a polynomial of degree $n+4$. Subsequently, for an approximate boundary using a polynomial of degree 3 in our study, we have to use a polynomial of degree 7 to define an interpolation over the reference triangle.

Next, we will define a C^1-curved finite element by imposing the triple $(\hat{K}, \hat{P}, \hat{\Sigma})$ to associated with the curved finite element under consideration. By the definition, $\hat{K}$ denotes a reference finite element. Furthermore, $\hat{P}$ and $\hat{\Sigma}$ denote, respectively, the functional space and the set of degrees of freedom of the reference finite element.

As mentioned previously, for a curved boundary that is approximated by a polynomial of degree 3, an interpolation polynomial defined over the reference element has to be of degree 7. Therefore, the desired 'basic' P_7-C^1 finite element will constitute of $\hat{K}$ which is a unit right-angled triangle, the set of degrees of freedom $\hat{\Sigma}(\hat{w})$, and $\hat{P}$ which is a space of complete polynomials of degree 7 with its dimension equals to 36. The set of $\hat{\Sigma}(\hat{w})$ composes of values and their derivatives defined on vertices, $\hat{\mathbf{a}}_i, i = 1, 2, 3$, and along edges, $\hat{\mathbf{b}}_i, i = 1, 2, 3$, $\hat{\mathbf{d}}_i, i = 1, ..., 6$, and the internal nodes, $\hat{\mathbf{e}}_i, i = 1, 2, 3$, of the reference triangle illustrated in Fig. 6.5 and are defined as

$$\begin{aligned}\hat{\Sigma}(\hat{w}) = \Bigg\{ & \hat{w}(\hat{\mathbf{a}}_i), \frac{\partial \hat{w}}{\partial \hat{x}_1}(\hat{\mathbf{a}}_i), \frac{\partial \hat{w}}{\partial \hat{x}_2}(\hat{\mathbf{a}}_i), \frac{\partial^2 \hat{w}}{\partial \hat{x}_1^2}(\hat{\mathbf{a}}_\mathbf{i}), \frac{\partial^2 \hat{w}}{\partial \hat{x}_1 \hat{x}_2}(\hat{\mathbf{a}}_i), \frac{\partial^2 \hat{w}}{\partial \hat{x}_2^2}(\hat{\mathbf{a}}_i), i = 1, 2, 3; \\ & -\frac{\partial \hat{w}}{\partial \hat{x}_1}(\hat{\mathbf{b}}_1); -\frac{\partial \hat{w}}{\partial \hat{x}_2}(\hat{\mathbf{b}}_2); \frac{\sqrt{2}}{2}\left(\frac{\partial \hat{w}}{\partial \hat{x}_1} + \frac{\partial \hat{w}}{\partial \hat{x}_2}\right)(\hat{\mathbf{b}}_3); \hat{w}(\hat{\mathbf{d}}_i), i = 1, ..., 6; \\ & -\frac{\partial \hat{w}}{\partial \hat{x}_1}(\hat{\mathbf{d}}_i), i = 1, 2; -\frac{\partial \hat{w}}{\partial \hat{x}_2}(\hat{\mathbf{d}}_i), i = 3, 4; \\ & \frac{\sqrt{2}}{2}\left(\frac{\partial \hat{w}}{\partial \hat{x}_1} + \frac{\partial \hat{w}}{\partial \hat{x}_2}\right)(\hat{\mathbf{d}}_i), i = 5, 6; \hat{w}(\hat{\mathbf{e}}_i), i = 1, 2, 3 \Bigg\},\end{aligned} \tag{6.16}$$

where $\hat{w}$ denotes a function defined over the reference element $\hat{K}$. These degrees of freedom are constraints so that the C^1-continuity can be assured and also the so-defined C^1-curve element can be compatible with the Bell element.

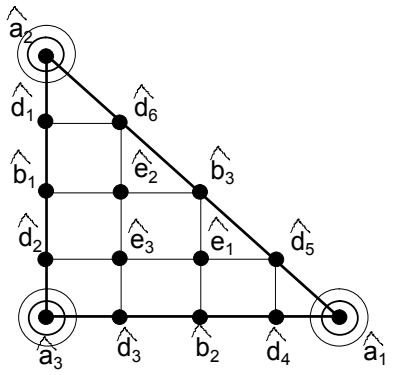

Figure 6.5: The triple $(\hat{K}, \hat{P}, \hat{\Sigma})$ for a C^1-curved finite element compatible with the Bell triangle where the degree of polynomial approximating curved boundaries is cubic.

6.2.4 Construction of the interpolation, $\Pi_K v$, of the function v defined over the curved element

In this section, we will elaborate on the construction of the interpolation, $\Pi_K v$ which will depend on the P_7-C^1 shape functions and their associated values of degrees of freedom defined on the reference element.

The P_7-C^1 shape functions are constructed by employing the complete polynomial of degree 7. The shape functions are defined over the reference triangle $\hat{K}$ where its 36 nodal degrees of freedom will depend on 21 nodal degrees of freedom defined on the curved physical triangle as you will see afterwards. Consequently, in order to obtain the interpolation $\Pi_K v$, of the function v defined over the curved element, we have to associate nodal values of degrees of freedom defined on $\hat{K}$ with those of K_C.

In order to define the association between the nodal values of degrees of freedom defined on $\hat{K}$ and K_C, firstly, we have to define the degrees of freedom on the curved element K_C to ensure the C^1-compatible with the Bell triangles, which are the adjacent elements. You will see later on that only 21 degrees of freedom are defined on K_C.

Secondly, we will associate 36 nodal value of degrees of freedom defined on $\hat{K}$ with those defined on K_C in the first step. Since the number of degrees of freedom defined on the curved and the reference triangles are different, the derivation of the associations is not straightforward.

Once, the set of values of degrees of freedom defined on the reference element $\hat{K}$ has been defined. The interpolation $\Pi_K v$ can be obtained from the linear combination between the complete P_7-C^1 basis functions and their associated values of degrees of

freedom.

Mathematically, the association between the 36 nodal degrees of freedom defined on the reference element $\hat{K}$ and the 21 nodal degrees of freedom defined on the curved element K_C can be divided into three following steps.

Step 1:

In the first step, we will define the set of degrees of freedom on the curved element. In order to satisfy the C^1-connection conditions with the Bell triangle, we have that constraints have to be realised along the sides $\mathbf{a}_3\mathbf{a}_\alpha, \alpha = 1, 2$ which are connections between the curved elements and the Bell elements.

To obtain the C^1-compatible with the Bell element, we have that the degrees of freedom of the curved finite elements along the connected sides have to be determined by the degrees of freedom related to the sides $\mathbf{a}_3\mathbf{a}_\alpha, \alpha = 1, 2$. Hence, the degrees of freedom defined on the curved triangle have to be identical to the degree of freedom defined on the adjacent element.

Furthermore, there will be three additional degrees of freedom introduced inside the curved triangle K_C as seen in Fig. 6.6. These nodes come from three internal nodes defined in order to ensure the C^1-continuity in determining the polynomial of degree 7 on the reference element. Consequently, there are 21 degrees of freedom in total defined over the curved triangular element.

The set $\Sigma_K(v)$ of values of degrees of freedom of v is then given by (see Fig. 6.6)

$$\Sigma_K(v) = \{(D^\alpha v(\mathbf{a}_i), \alpha = 0, 1, 2), i = 1, 2, 3; v(\mathbf{e}_i), i = 1, 2, 3\}. \tag{6.17}$$

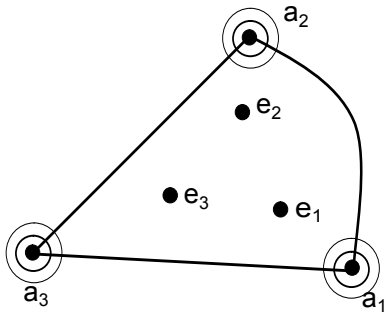

Figure 6.6: The description of the C^1-curved finite element compatible with the Bell element constituting of three vertices and three internal nodes where the set of dofs is $\{(D^\alpha v(\mathbf{a}_i), \alpha = 0, 1, 2), i = 1, 2, 3; v(\mathbf{e}_i), i = 1, 2, 3\}$.

By the general mapping defined in (6.11), let us set

$$\begin{aligned}\mathbf{a}_i &= F_K(\hat{\mathbf{a}}_i), i = 1, 2, 3,\\ \mathbf{d}_i &= F_K(\hat{\mathbf{d}}_i), i = 1, ..., 6,\\ \mathbf{e}_i &= F_K(\hat{\mathbf{e}}_i), i = 1, 2, 3.\end{aligned} \tag{6.18}$$

Now, the set of degrees of freedom (6.17) defined on the curved element can be considered in its local version. The derivatives of v are computed along the side directions. Then, the set $\Sigma_K(v)$ of degrees of freedom of the function v is explicitly given by

$$\begin{aligned}\Sigma_K(v) = \{&v(\mathbf{a}_1); v(\mathbf{a}_2); v(\mathbf{a}_3); Dv(\mathbf{a}_1)(\mathbf{a}_3 - \mathbf{a}_1); (s_M - s_m)Dv(\mathbf{a}_1)\chi'(s_m);\\ &(s_m - s_M)Dv(\mathbf{a}_2)\chi'(s_M); Dv(\mathbf{a}_2)(\mathbf{a}_3 - \mathbf{a}_2); Dv(\mathbf{a}_3)(\mathbf{a}_2 - \mathbf{a}_3);\\ &Dv(\mathbf{a}_3)(\mathbf{a}_1 - \mathbf{a}_3); D^2v(\mathbf{a}_1)(\mathbf{a}_3 - \mathbf{a}_1)^2; (s_M - s_m)^2D^2v(\mathbf{a}_1)(\chi'(s_m))^2;\\ &(s_m - s_M)^2D^2v(\mathbf{a}_2)(\chi'(s_M))^2; D^2v(\mathbf{a}_2)(\mathbf{a}_3 - \mathbf{a}_2)^2; D^2v(\mathbf{a}_3)(\mathbf{a}_2 - \mathbf{a}_3)^2;\\ &D^2v(\mathbf{a}_3)(\mathbf{a}_1 - \mathbf{a}_3)^2; D^2v(\mathbf{a}_1)(\mathbf{a}_2 - \mathbf{a}_3)^2; D^2v(\mathbf{a}_2)(\mathbf{a}_3 - \mathbf{a}_1)^2;\\ &(s_M - s_m)^2D^2v(\mathbf{a}_3)(\chi'(s_m), \chi'(s_M)); v(\mathbf{e}_1); v(\mathbf{e}_2); v(\mathbf{e}_3)\big\}.\end{aligned} \tag{6.19}$$

Step2:

In this step, the 36 values of degrees of freedom defined over the reference element will be defined to depend on only 21 values of degrees of freedom on the curved element defined in Step 1.

Let us first introduce $\hat{\Sigma}_{\hat{K}}$ to be the set of degrees of freedom defined on the reference element $\hat{K}$. We have that $\hat{\Sigma}_{\hat{K}}$ can be divided into three subsets as $\hat{\Sigma}_{\hat{K}} = \hat{\Sigma}_1 \cup \hat{\Sigma}_2 \cup \hat{\Sigma}_3$, where $\hat{\Sigma}_1$ denotes the set of degrees of freedom associated with vertices and internal nodes, $\hat{\Sigma}_2$ denotes the set of degrees of freedom on the edge $\hat{\mathbf{a}}_3\hat{\mathbf{a}}_\alpha; \alpha = 1, 2$, and $\hat{\Sigma}_3$ denotes the set of degrees of freedom on the edge $\hat{\mathbf{a}}_1\hat{\mathbf{a}}_2$. The total set of degrees of freedom illustrated in (6.16) will be divided as

$$\begin{aligned}\hat{\Sigma}_1 &= \{(D^\alpha\hat{w}(\hat{\mathbf{a}}_i), \alpha = 0, 1, 2), i = 1, 2, 3; \hat{w}(\hat{\mathbf{e}}_i), i = 1, 2, 3\}\\ \hat{\Sigma}_2 &= \left\{\hat{w}(\hat{\mathbf{d}}_i), i = 1, ..., 4; -\frac{\partial\hat{w}}{\partial\hat{x}_1}(\hat{\mathbf{b}}_1); -\frac{\partial\hat{w}}{\partial\hat{x}_1}(\hat{\mathbf{d}}_i), i = 1, 2; -\frac{\partial\hat{w}}{\partial\hat{x}_2}(\hat{\mathbf{b}}_2); -\frac{\partial\hat{w}}{\partial\hat{x}_2}(\hat{\mathbf{d}}_i), i = 3, 4;\right\}\\ \hat{\Sigma}_3 &= \left\{\hat{w}(\hat{\mathbf{d}}_i), i = 5, 6; \frac{\sqrt{2}}{2}\left(\frac{\partial\hat{w}}{\partial\hat{x}_1} + \frac{\partial\hat{w}}{\partial\hat{x}_2}\right)(\hat{\mathbf{b}}_3); \frac{\sqrt{2}}{2}\left(\frac{\partial\hat{w}}{\partial\hat{x}_1} + \frac{\partial\hat{w}}{\partial\hat{x}_2}\right)(\hat{\mathbf{d}}_i), i = 5, 6\right\}.\end{aligned} \tag{6.20}$$

In order to obtain an interpolation, $\hat{w} \in \hat{P}$ of the function v, those sets of $\hat{\Sigma}_i, i = 1, 2, 3$, are associated with the set of values $\hat{\triangle}_K(v) = \hat{\triangle}_1(v) \cup \hat{\triangle}_2(v) \cup \hat{\triangle}_3(v)$ defined on the reference triangle $\hat{K}$. Since we would like to have those three sets of values to depend only on the set of values defined over the curved element, the association of each subset $\hat{\triangle}_i(v), i = 1, 2, 3$ will be determined separately as follows.

Firstly, the subset of values of degrees of freedom $\hat{\triangle}_1(v)$ that constitutes of values and all their derivatives up to order 2 at vertices and all values of internal nodes can be obtained from the set $\Sigma_K(v)$ in (6.17). These values can be associated by means of the mapping F_{K_C} and the following relation

$$\hat{v} = v \circ F_{K_C}. \tag{6.21}$$

Consequently, the first set of values of degrees of freedom can be expressed as

$$\hat{\triangle}_1(v) = \{(D^\alpha \hat{v}(\hat{\mathbf{a}}_i), \alpha = 0, 1, 2), i = 1, 2, 3; \hat{v}(\hat{\mathbf{e}}_i), i = 1, 2, 3\}. \tag{6.22}$$

Secondly, the set of values $\hat{\triangle}_2(v)$ of degrees of freedom on the straight edges $\hat{\mathbf{a}}_3\hat{\mathbf{a}}_\alpha, \alpha = 1, 2$, will be considered. This set of values will be associated with the set of degrees of freedom $\hat{\Sigma}_2(v)$ in (6.20).

It is worth mentioning that there is no degree of freedom defined along the sides $\mathbf{a}_3\mathbf{a}_\alpha, \alpha = 1, 2$ of the curved physical triangle. Therefore, the values of degrees of freedom at nodes $\hat{\mathbf{d}}_i, i = 1, ..., 4$ and their derivatives, and the nodes $\hat{\mathbf{b}}_i, i = 1, 2$, will be associated with the degrees of freedom on vertices of the curved triangle, K_C. In order to do this, we have to define polynomials interpolating degrees of freedom defined on those sides of the triangle K_C which are parametrised by the reference coordinate.

In order to obtain the polynomials interpolating degrees of freedom defined on the sides $\hat{\mathbf{a}}_3\hat{\mathbf{a}}_\alpha$ of the triangle K_C, the polynomials have to provide the C^1-connection with the Bell triangle. According to section 6.2.3, we have that the degree of one-variable polynomial of the interpolation $\hat{w}$ on the sides $\hat{\mathbf{a}}_3\hat{\mathbf{a}}_\alpha$ for the nodes $\hat{\mathbf{d}}_i, i = 1, ..., 4$ have to coincide with the P_5-Hermite polynomial. In order to constrain the normal derivative $\frac{\partial \Pi_K v}{\partial \mathbf{n}_{3\alpha}}, \alpha = 1, 2$ to be continuous, the one-variable polynomial of the normal derivatives of the interpolation $\hat{w}$ restricted on the sides $\hat{\mathbf{a}}_3\hat{\mathbf{a}}_\alpha$ for the nodes $\hat{\mathbf{b}}_i, i = 1, 2$ have to coincide with the P_3-Hermite polynomial.

Next, we will consider the mentioned one-variable P_3- and P_5-Hermite polynomials defined on the side $\mathbf{a}_3\mathbf{a}_1$ in order to associate the degrees of freedom on the reference

element to the curved element. Note that the association of those values defined on the side $\mathbf{a}_3\mathbf{a}_2$ can be obtained in a similar manner.

Regarding the P_5-Hermite polynomial defined on the side $\mathbf{a}_3\mathbf{a}_1$, we have that any variable $x_i, i = 1, 2$, on that side will be parameterised by the variable $\hat{x}_1$ ($\hat{x}_2 = 0$ on the side) as

$$x_1 = x_{13} + (x_{11} - x_{13})\hat{x}_1, \quad x_2 = x_{23} + (x_{21} - x_{23})\hat{x}_1, \tag{6.23}$$

and assume that the Hermite polynomial defined on the side $\mathbf{a}_3\mathbf{a}_1$ of the triangle K_C is named

$$\hat{f}_1 \text{ which has to coincide with } (\Pi_K v) \circ F_K|_{[\hat{\mathbf{a}}_3, \hat{\mathbf{a}}_1]}. \tag{6.24}$$

This quintic polynomial, $\hat{f}(\hat{x}_1)$, can be then expressed as

$$\hat{f}_1(\hat{x}_1) = c_0 + c_1\hat{x}_1 + c_2\hat{x}_1^2 + c_3\hat{x}_1^3 + c_4\hat{x}_1^4 + c_5\hat{x}_1^5. \tag{6.25}$$

In order to solve the coefficients $c_i, i = 0, 1, ..., 5$, we define the set of values of the degrees of freedom on the side $\mathbf{a}_3\mathbf{a}_1$ as follows

$$\begin{aligned} &\{v(\mathbf{a}_1), v(\mathbf{a}_3), Dv(\mathbf{a}_1)(\mathbf{a}_3 - \mathbf{a}_1), Dv(\mathbf{a}_3)(\mathbf{a}_1 - \mathbf{a}_3), \\ &D^2v(\mathbf{a}_1)(\mathbf{a}_3 - \mathbf{a}_1)^2, D^2v(\mathbf{a}_3)(\mathbf{a}_1 - \mathbf{a}_3)^2\}. \end{aligned} \tag{6.26}$$

By interpolating the degrees of freedom in (6.26), the so-defined Hermite polynomial on the side $\mathbf{a}_3\mathbf{a}_1$ is obtained. More details can be found in Appendix B. After that we will use this Hermite polynomial to associate the values define on the nodes $\hat{\mathbf{d}}_i$ with the values defined on vertices $\mathbf{a}_1$ and $\mathbf{a}_3$ on K_C.

Likewise, the P_5-Hermite polynomials over the straight side $\mathbf{a}_3\mathbf{a}_2$ can be defined with the same idea but reparameterised by using the variable $\hat{x_2}$ ($\hat{x}_1 = 0$ on the side) as

$$x_1 = x_{13} + (x_{12} - x_{13})\hat{x}_2, \quad x_2 = x_{23} + (x_{22} - x_{23})\hat{x}_2. \tag{6.27}$$

And the corresponding Hermite polynomial defined on the side $\mathbf{a}_3\mathbf{a}_2$ of the triangle K_C is named

$$\hat{f}_2 \text{ which has to coincide with } (\Pi_K v) \circ F_K|_{[\hat{\mathbf{a}}_3, \hat{\mathbf{a}}_2]}. \tag{6.28}$$

To obtain the P_3-Hermite polynomial of the side $\mathbf{a}_3\mathbf{a}_1$, we will parametrise the polynomial by using the variable $\hat{x}_1$ as in (6.23) and assume that the corresponding Hermite polynomial defined on the side $\mathbf{a}_3\mathbf{a}_1$ is named

$$\hat{h}_1 \text{ which has to coincide with } (D\Pi_K v(\cdot)(\mathbf{a}_2 - \mathbf{c}_2)) \circ F_K|_{[\hat{\mathbf{a}}_3, \hat{\mathbf{a}}_1]}, \tag{6.29}$$

and can be written as in the following form

$$\hat{h}_1(\hat{x}_1) = c_0 + c_1\hat{x}_1 + c_2\hat{x}_1^2 + c_3\hat{x}_1^3. \tag{6.30}$$

Solving the coefficients $c_i, i = 0, 1, ..., 3$ by interpolating the degrees of freedom in (6.31) gives the so-defined Hermite polynomial on the side $\mathbf{a}_3\mathbf{a}_1$. More details can also be found in Appendix B.

$$\left\{Dv(\mathbf{a}_i)\mathbf{n}_{31}, D^2v(\mathbf{a}_i)(\mathbf{n}_{31}, \mathbf{t}_{31})^2, i = 1, 3\right\}, \tag{6.31}$$

where $\mathbf{n}_{31}$ and $\mathbf{t}_{31}$ denote the normal and tangential vectors on the side $\mathbf{a}_3\mathbf{a}_1$.

Similarly, the P_3-Hermite polynomials over the straight side $\mathbf{a}_3\mathbf{a}_2$ can be defined with the same idea but reparameterised by using the variable $\hat{x_2}$ as in (6.27) and assume that the corresponding Hermite polynomial defined on the side $\mathbf{a}_3\mathbf{a}_2$ is named

$$\hat{h}_2 \text{ which has to coincide with } (D\Pi_K v(\cdot)(\mathbf{a}_1 - \mathbf{c}_1)) \circ F_K|_{[\hat{\mathbf{a}}_3, \hat{\mathbf{a}}_2]}. \tag{6.32}$$

Now, we will apply the derived one-variable polynomials $\hat{f}_\alpha$ and $\hat{h}_\alpha, \alpha = 1, 2$, to associate the set of values $\hat{\triangle}_2(v)$ with the set of degrees of freedom $\hat{\Sigma}_2$. Firstly, We will consider the expression of the first four elements of values of the nodes $\hat{\mathbf{d}}_i, i = 1, ..., 4$. With the help of (6.12), their association can be easily obtained as

$$\begin{aligned} \hat{w}(\hat{\mathbf{d}}_i) &= \hat{f}_2(\hat{\mathbf{d}}_i), \;\; i = 1, 2, \\ \hat{w}(\hat{\mathbf{d}}_i) &= \hat{f}_1(\hat{\mathbf{d}}_i), \;\; i = 3, 4. \end{aligned} \tag{6.33}$$

Next, we will take care of the expression of the last six elements of $\hat{\triangle}_2(v)$ which are the values of the following degrees of freedom; $-\frac{\partial\hat{w}}{\partial\hat{x}_i}(\hat{\mathbf{b}}_i), i = 1, 2; -\frac{\partial\hat{w}}{\partial\hat{x}_1}(\hat{\mathbf{d}}_i), i = 1, 2; -\frac{\partial\hat{w}}{\partial\hat{x}_2}(\hat{\mathbf{d}}_i), i = 3, 4$. We will begin by considering the mathematical description of $\frac{\partial\hat{w}}{\partial\hat{x}_j}(\hat{\mathbf{d}}), j = 1, 2$, where the others can be obtained similarly. Regarding $\hat{\mathbf{d}}$ on the side $\mathbf{a}_3\mathbf{a}_\alpha, \alpha = 1, 2$, the mathematical description of $\frac{\partial\hat{w}}{\partial\hat{x}_j}(\hat{\mathbf{d}}), j = 1, 2$ can be expressed in the tangential and normal directions similarly from (6.14) and (6.15) as follows

$$\begin{aligned} \frac{\partial\hat{w}}{\partial\hat{x}_2}(\hat{\mathbf{d}}) &= \frac{\partial}{\partial\hat{x}_2}(w \circ F_K)(\hat{\mathbf{d}}) = Dw(\mathbf{d}) \cdot \frac{\partial F_K}{\partial\hat{x}_2}(\hat{\mathbf{d}}) \\ &= \langle\frac{\partial F_K}{\partial\hat{x}_2}(\hat{\mathbf{d}}), \frac{\mathbf{a}_2 - \mathbf{a}_3}{|\mathbf{a}_2 - \mathbf{a}_3|^2}Dw(\mathbf{d})(\mathbf{a}_2 - \mathbf{a}_3) + \frac{\mathbf{a}_1 - \mathbf{c}_1}{|\mathbf{a}_1 - \mathbf{c}_1|^2}Dw(\mathbf{d})(\mathbf{a}_1 - \mathbf{c}_1)\rangle, \end{aligned} \tag{6.34}$$

and

$$\begin{aligned} \frac{\partial\hat{w}}{\partial\hat{x}_1}(\hat{\mathbf{d}}) &= \frac{\partial}{\partial\hat{x}_1}(w \circ F_K)(\hat{\mathbf{d}}) = Dw(\mathbf{d}) \cdot \frac{\partial F_K}{\partial\hat{x}_1}(\hat{\mathbf{d}}) \\ &= \langle\frac{\partial F_K}{\partial\hat{x}_1}(\hat{\mathbf{d}}), \frac{\mathbf{a}_1 - \mathbf{a}_3}{|\mathbf{a}_1 - \mathbf{a}_3|^2}Dw(\mathbf{d})(\mathbf{a}_1 - \mathbf{a}_3) + \frac{\mathbf{a}_2 - \mathbf{c}_2}{|\mathbf{a}_2 - \mathbf{c}_2|^2}Dw(\mathbf{d})(\mathbf{a}_2 - \mathbf{c}_2)\rangle, \end{aligned} \tag{6.35}$$

where $<,>$ denotes the usual scalar product in $\Re^2$ with the notations $\mathbf{c}_\alpha, \alpha = 1, 2$, illustrated in Fig. 6.4.

Regarding $\hat{\mathbf{d}}_i, i = 1, 2$ and $\hat{\mathbf{b}}_1$ on the side $\hat{\mathbf{a}}_2\hat{\mathbf{a}}_3$, we have that the association of the degrees of freedom on the reference element to the curved element can be determined with the definition of the one-variable polynomials $\hat{f}_\alpha$ and $\hat{h}_\alpha, \alpha = 1, 2$ defined on the side $\hat{\mathbf{a}}_3\hat{\mathbf{a}}_\alpha$ as

$$\begin{aligned} Dw(\mathbf{d}_i)(\mathbf{a}_2 - \mathbf{a}_3) &= \frac{\partial \hat{f}_2}{\partial \hat{x}_2}(\hat{\mathbf{d}}_\mathbf{i}), \\ Dw(\mathbf{d}_i)(\mathbf{a}_1 - \mathbf{c}_1) &= \hat{h}_2(\hat{\mathbf{d}}_\mathbf{i}), \end{aligned} \tag{6.36}$$

and, for $\hat{\mathbf{d}}_i, i = 3, 4$ and $\hat{\mathbf{b}}_\mathbf{2}$ on the side $\hat{\mathbf{a}}_1\hat{\mathbf{a}}_3$, we have

$$\begin{aligned} Dw(\mathbf{d}_i)(\mathbf{a}_1 - \mathbf{a}_3) &= \frac{\partial \hat{f}_1}{\partial \hat{x}_1}(\hat{\mathbf{d}}_\mathbf{i}), \\ Dw(\mathbf{d}_i)(\mathbf{a}_2 - \mathbf{c}_2) &= \hat{h}_1(\hat{\mathbf{d}}_\mathbf{i}). \end{aligned} \tag{6.37}$$

Now, it can be seen that the polynomial functions $\hat{f}_i$ and $\hat{h}_i, i = 1, 2$ depend only on the values of the degrees of freedom of the function v and relative to the sides $\mathbf{a}_3\mathbf{a}_i, i = 1, 2$. Hence, the set of values $\hat{\triangle}_2(v)$ associated with the set of degrees of freedom $\hat{\Sigma}_2$ is given by

$$\begin{aligned} \hat{\triangle}_2(v) = \Big\{ & \hat{f}_2(\hat{\mathbf{d}}_i), i = 1, 2; \hat{f}_1(\hat{\mathbf{d}}_i), i = 3, 4; \\ & -\langle \frac{\partial F_K}{\partial \hat{x}_1}(\hat{\mathbf{b}}_1), \frac{\mathbf{a}_2 - \mathbf{a}_3}{|\mathbf{a}_2 - \mathbf{a}_3|^2}\frac{d\hat{f}_2}{d\hat{x}_2}(\hat{\mathbf{b}}_1) + \frac{a_1 - c_1}{|a_1 - c_1|^2}\hat{h}_2(\hat{\mathbf{b}}_1)\rangle; \\ & -\langle \frac{\partial F_K}{\partial \hat{x}_1}(\hat{\mathbf{d}}_i), \frac{\mathbf{a}_2 - \mathbf{a}_3}{|\mathbf{a}_2 - \mathbf{a}_3|^2}\frac{d\hat{f}_2}{d\hat{x}_2}(\hat{\mathbf{d}}_i) + \frac{\mathbf{a}_1 - \mathbf{c}_1}{|\mathbf{a}_1 - \mathbf{c}_1|^2}\hat{h}_2(\hat{\mathbf{d}}_i)\rangle, i = 1, 2; \\ & -\langle \frac{\partial F_K}{\partial \hat{x}_2}(\hat{\mathbf{b}}_2), \frac{\mathbf{a}_1 - \mathbf{a}_3}{|\mathbf{a}_1 - \mathbf{a}_3|^2}\frac{d\hat{f}_1}{d\hat{x}_1}(\hat{\mathbf{b}}_2) + \frac{\mathbf{a}_2 - \mathbf{c}_2}{|\mathbf{a}_2 - \mathbf{c}_2|^2}\hat{h}_1(\hat{\mathbf{b}}_2)\rangle; \\ & -\langle \frac{\partial F_K}{\partial \hat{x}_2}(\hat{\mathbf{d}}_i), \frac{\mathbf{a}_1 - \mathbf{a}_3}{|\mathbf{a}_1 - \mathbf{a}_3|^2}\frac{d\hat{f}_1}{d\hat{x}_1}(\hat{\mathbf{d}}_i) + \frac{\mathbf{a}_2 - \mathbf{c}_2}{|\mathbf{a}_2 - \mathbf{c}_2|^2}\hat{h}_1(\hat{\mathbf{d}}_i)\rangle, i = 3, 4 \Big\}. \end{aligned} \tag{6.38}$$

Lastly, the set of values of degrees of freedom $\hat{\triangle}_3(v)$ on the edge $\hat{\mathbf{a}}_1\hat{\mathbf{a}}_2$ will be considered. It can be derived by the same procedure which we employed to obtain the set of values $\hat{\triangle}_2(v)$. Since we would like to have a one-variable polynomial of the interpolate $\Pi_K(v)$ restricted on the side $\mathbf{a}_1\mathbf{a}_2$ to vary quinticly, the polynomial $\hat{f}_3$ have to coincide with the P_5-Hermite polynomial defined by the values of degrees of freedom as follows

$$\begin{aligned} & \{\hat{v}(\hat{\mathbf{a}}_1), \hat{v}(\hat{\mathbf{a}}_2), D\hat{v}(\hat{\mathbf{a}}_1)(\hat{\mathbf{a}}_2 - \hat{\mathbf{a}}_1), D\hat{v}(\hat{\mathbf{a}}_2)(\hat{\mathbf{a}}_1 - \hat{\mathbf{a}}_2), \\ & D^2\hat{v}(\hat{\mathbf{a}}_1)(\hat{\mathbf{a}}_2 - \hat{\mathbf{a}}_1)^2, D^2\hat{v}(\hat{\mathbf{a}}_2)(\hat{\mathbf{a}}_1 - \hat{\mathbf{a}}_2)^2, \}, \end{aligned} \tag{6.39}$$

and can be parametrised by

$$\hat{x}_1 = \hat{x}_1, \quad \hat{x}_2 = 1 - \hat{x}_1. \tag{6.40}$$

Also, a one-variable polynomial of the normal derivative of the interpolation $\Pi_K v$ have to vary cubically so that the function $\hat{h}_3$ coincides with the P_3-Hermite polynomial defined by the values of degrees of freedom as

$$\left\{ D\hat{v}(\hat{\mathbf{a}}_i)(\hat{\mathbf{a}}_3 - \hat{\mathbf{b}}_3); D^2\hat{v}(\hat{\mathbf{a}}_i)(\hat{\mathbf{a}}_3 - \hat{\mathbf{b}}_3, \hat{\mathbf{a}}_1 - \hat{\mathbf{a}}_2) \right\}, i = 1, 2. \tag{6.41}$$

Consider similarly as in $\hat{\triangle}_2(v)$, the set of values of degrees of freedom, $\hat{\triangle}_3(v)$ is defined as

$$\hat{\triangle}_3(v) = \left\{ \hat{f}_3(\hat{\mathbf{d}}_i), i = 5, 6; -\sqrt{2}\hat{h}_3(\hat{\mathbf{b}}_3); -\sqrt{2}\hat{h}_3(\hat{\mathbf{d}}_i), i = 5, 6 \right\}. \tag{6.42}$$

Similar to (6.22) and (6.38), the set of values $\hat{\triangle}_3(v)$ is only dependent on the values $\Sigma_K(v)$ defined over the curved element. Then, the set $\hat{\triangle}_K(v) = \left\{ \hat{\triangle}_1(v), \hat{\triangle}_2(v), \hat{\triangle}_3(v) \right\}$ specifies a value to each degree of freedom of $\hat{\Sigma}$. Details of the matrix expressions for the association of the set $\hat{\triangle}_K(v)$ can be seen in Appendix B.

Step3:

Finally, the interpolation $\Pi_K v$ of the function v can be obtained from the set of value $\hat{\triangle}_K(v)$ that defined over the reference triangle. By (6.12), any function v is obtained through the mapping F_K^{-1} as

$$v = \Pi_K v = \hat{v} \circ F_K^{-1}. \tag{6.43}$$

In general, a function v or its interpolation, $\Pi_K v$, does not have to be the same. Therefore, we will investigate the differences between these two functions in the next section which devotes to numerical implementations.

6.3 Numerical implementations of the curved finite element

In this section, we are going to apply the C^1-curved finite element developed in the previous section to solve the fourth-order problems on a curvilinear domain. The domain of interest considered throughout this chapter will be a circle as a representative of a curvilinear boundary.

Firstly, the performance of the C^1-curved finite element will be investigated by solving the Biharmonic equation on the circular domain. The objective of this section is to perform a comparison between the performance of the straight and the curved elements when a curved boundary is concerned.

Furthermore, the implementation of the linearised plate bending in a circle will be performed. The obtained solutions between the straight and the curved elements will again be compared.

6.3.1 The Biharmonic equation

Let consider the following Biharmonic equation in two-dimensional space

$$\frac{\partial^4 u}{\partial x_1^4} + 2\frac{\partial^4 u}{\partial x_1^2 \partial x_2^2} + \frac{\partial^4 u}{\partial x_2^4} = 0, \tag{6.44}$$

with the exact solution $u(x_1, x_2) = \cos(x_1)e^{x_2}$ defined on the quarter of the unit circle domain. A combination of Dirichlet and Neumann boundary conditions will be applied by the given exact solution in the implementations.

In order to make a numerical implementation, the domain of interest is discretised by triangles using unstructured meshes with various numbers of elements. After the discretisation, our mesh constitutes of elements on the interior domain and elements on the curved boundary. On the interior elements, the straight-sided Bell triangular element will be employed to represent the solution.

Regarding elements on the curved boundary, we will compare the representation of the curved boundary by two types of triangular finite elements. The first type is the straight-sided Bell triangular element and the other is the C^1-curved finite element which is compatible to the straight-sided Bell elements constructed in section 6.2.

In order to avoid unnecessary computational time, the residuals and Jacobian matrices in the finite element implementations will be computed analytically. For the Bell triangular element, the computation for both the Residuals and Jacobian matrix are straightforward.

Unlike the Bell element, the computations of the Residuals and Jacobian matrices of the C^1-curved finite element are a bit tricky as its values of degrees of freedom defined on the reference element depend on those defined on the (curved) physical triangle. Therefore, the unknown values can be determined by quantities defined on

the reference triangle as

$$u(x_1(\hat{\mathbf{x}}), x_2(\hat{\mathbf{x}})) = \sum_{j=1}^{36} \hat{u}_j \hat{\psi}_j(\hat{x}_1, \hat{x}_2), \tag{6.45}$$

where $\hat{u}_j$ and $\hat{\psi}_j, j = 1, ..., 36$, are the nodal values and the C^1-shape functions defined on the reference element $\hat{K}$, respectively. All these nodal values $\hat{u}_j$ are defined to depend only on 21 nodal values, u_k, defined on the curved element K_C as described in section 6.2.4.

Furthermore, the set of nodal values defined on the reference element can be associated with those defined on the curved element by

$$\hat{u}_j = \sum_{k=1}^{21} u_k \tilde{M}_{kj}, \forall j = 1, ..., 36, \tag{6.46}$$

where $\tilde{M}$ is the matrix of nodal-value transformation from the curved to reference elements. The computation of this matrix can be found in the Appendix B. Substituting (6.46) into (6.45) gives

$$u(x_1(\hat{\mathbf{x}}), x_2(\hat{\mathbf{x}})) = \sum_{j=1}^{36} \sum_{k=1}^{21} u_k \tilde{M}_{kj} \hat{\psi}_j(\xi_1, \xi_2). \tag{6.47}$$

Therefore, the residuals $r_k; k = 1, ..., 21$, which are expressed on the physical element, can be determined by

$$r_k = \iint \sum_{j=1}^{36} \nabla^2 u \nabla^2 \psi_j \tilde{M}_{kj} dx_1 dx_2, \tag{6.48}$$

and the Jacobian matrix J_{kh} can be determined by

$$J_{kh} = \iint \sum_{j=1}^{36} (\sum_{m=1}^{36} \tilde{M}_{hm} \nabla^2 \psi_m) \nabla^2 \psi_j \tilde{M}_{kj} dx_1 dx_2. \tag{6.49}$$

Note that $\nabla^2 \psi_j$ are the derivatives of the shape functions with respect to the global coordinates which can be obtained from employing the Jacobian of mapping to map from the local to global coordinates.

Regarding the Gaussian quadrature associated to the finite element implementations, we employ 13-node scheme to perform the numerical integration of functions defined over the Bell elements. Since the shape functions defined over the Bell element is quintic, the highest-order polynomial under the integration is of order six as the implemented equation contains the second-order derivatives.

Similarly, since the function defined over the C^1-curved element is of order seventh, the highest-order polynomial under the integration is of order ten. Hence, we need an integration scheme that can integrate up to tenth-order polynomials. The 37-integration points (see [21]) are the scheme that we employed to perform the numerical integration of functions defined over the C^1-curved elements. Note that an under-determined number of integration points may not lead to the expected rate of convergence and, sometimes, diverges.

Next, the Biharmonic equation stated in (6.44) with the curved boundary will be implemented by the finite element method in `Oomph-lib` [53] using the Bell and the C^1-curved finite element. The performance between those two triangular elements will be compared. The accuracy of the solutions will base on the L^2-norm error (see (5.22)) and are shown in Tables 6.1 and 6.2 for the Bell and the C^1-curved elements, respectively, with the associated computational time.

Number of elements	Number of dofs	L^2-norm error	Time (sec)
29	48	0.000567891	0.23
84	198	0.00017726	0.66
250	636	9.42737×10^{-5}	2.02
2034	5838	3.49306×10^{-5}	17.48
4833	14022	5.12128×10^{-6}	43.94

Table 6.1: L^2-norm error of the solution obtained from the Biharmonic implementation using the Bell elements with various numbers of elements.

Number of elements	Number of dofs	L^2-norm error	Time (sec)
29	63	0.000141802	5.73
84	228	3.70896×10^{-5}	16.07
250	696	9.52325×10^{-6}	54.92
2034	5958	1.0478×10^{-8}	436.17
4833	14262	3.6392×10^{-10}	1749.63

Table 6.2: L^2-norm error of the solution obtained from the Biharmonic implementation using the C^1-curved elements with various numbers of elements.

Tables 6.1 and 6.2 show that the computational time for the C^1-curved element is obviously very expensive compared to that of the Bell element when the same number of element is concerned. However, for the same number of elements, accuracies obtained from the curved elements are superior to those obtained from the straight

elements.

Furthermore, if the same error is considered, say $O(10^{-5})$, it can be seen from Tables 6.1 and 6.2 that the number of the Bell elements has to be 2034 to obtain such an accuracy. On the other hands, the number of the C^1-curved elements needed to obtain such accuracy is 84 which is a lot less. Also, the computational time to obtained the accuracy of order $O(10^{-5})$ for the Bell element is 17.48 and for the C^1-curved element is 16.07 which is slightly smaller.

In order to compare the convergence rate between the Bell and the C^1-curved elements, Fig. 6.7a illustrates the comparison between the L^2-norm error and the element size obtained from those elements. It can be seen that the C^1-curved element converges faster and, also, gives smaller error than the Bell element.

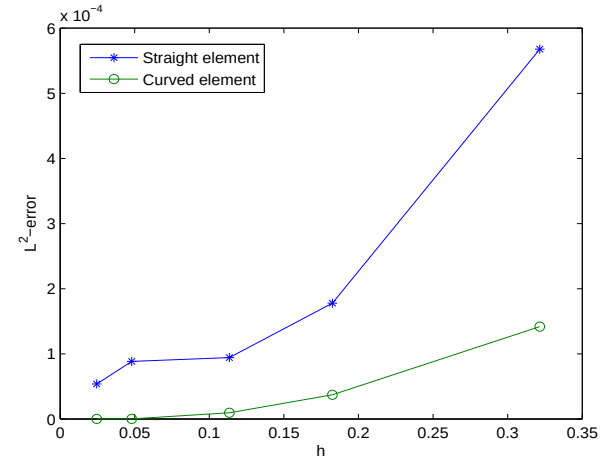

(a)

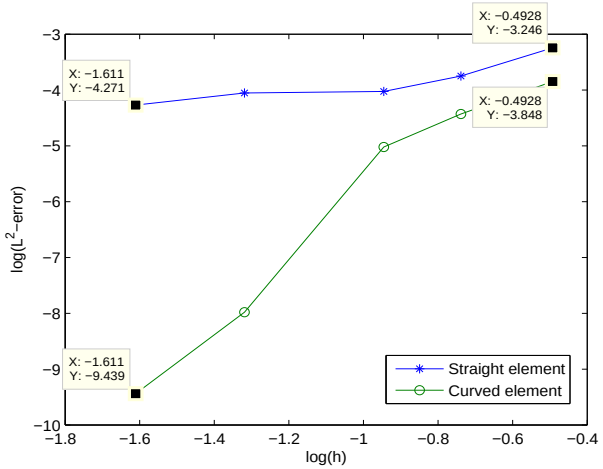

(b)

Figure 6.7: The comparison of the convergence rate between the Bell triangular finite element and the C^1-curved triangular finite elements.

When performing the log-plot between the L^2-norm error and the element size, Fig. 6.7b depicts that the convergence rate of the C^1-curved are greater than the Bell element as its slope is greater. The obtained rate of convergence for the C^1-curved and the Bell element is quintic and quadratic, respectively.

Our obtained rate of convergence for the Bell element, which is quadratic, is consistent to the study of P. Fischer when the curved boundary is concerned (see [63], pp. 109). Also, our obtained rate of convergence for the C^1-curved element, which is quintic, is consistent with the theoretical asymptotic error presented by M. Bernadou [48] which states as the following theorem.

Theorem 6.3.1. *Let $H^k(K)$ be the Sobolev space of real-valued functions which, together with all their partial distributional derivatives of order k or less, belong to $L^2(K)$ which is the linear space of square-integrable functions on a curved triangle K. There exists a constant c, independent of h_K, such that for all curved finite element C^1-compatible with Bell triangles, we have that*

$$|v - \Pi_K v|_K \leq c h_K^5 \|v\|_{5,K}, \quad \forall v \in H^5(K), \tag{6.50}$$

where $\Pi_K v$ is the nodal interpolant of v. Furthermore, h_K denotes the diameter of a triangle K. The norms and semi-norms used here are defined as

$$\|v\|_{k,K} = \left(\sum_{|\alpha| \leq k} \|D^\alpha u\|^2_{L^2(K)} \right)^{1/2}, \qquad |v|_K = \left(\|u\|^2_{L^2(K)} \right)^{1/2}. \tag{6.51}$$

Note that (6.50) describes the asymptotic order of the interpolation error. M. Bernadou [49] proved that the rate of convergence of the finite element solutions in L^2-norm is bounded by the asymptotic order in (6.50).

It is noteworthy that using the Bell element to solve the C^1-problem with a curved boundary decreases its rate of convergence from its potential when solving an exact representation domain. This limitation of convergence rate in the Bell element is due to the representation of the curved boundaries with straight-edge elements.

6.3.2 Circular plate bending problem

Further verification of the C^1-curved finite element is obtained by solving the linearised shell equations for the circular plate bending. The problem is considered to have

clamped boundaries with uniform loading in normal direction to the plate. Only one quarter of the unit circular plate is analysed and symmetric conditions are applied in this problem.

To implement the problem of the circular plate bending, the linearised governing equations described in (3.112), (3.113), and (3.114) will be solved using the finite element method. The undeformed position for the circular plate is

$$\mathbf{r} = (\xi_1, \xi_2, 0)^T ,$$

where $(\xi_1, \xi_2) \in [0, 1]$ and $0 \leq \xi_1^2 + \xi_2^2 \leq 1$.

The idea of representing the displacements in each direction are the same as described in section 5.2.1 of chapter 5. However, in order to represent the normal displacements in this study, we will employ both the Bell and the C^1-curved triangular elements in order to compared the obtained accuracy.

Note that the plate will be discretised by triangles with an unstructured mesh. The numerical integration schemes are the same as described in the Biharmonic problem (see section 6.3.1).

Next, the solutions of the linearised shell equations (3.112), (3.113), and (3.114) are implemented with different applied loads. In this study, the thickness of the plate equals to 0.01. The uniform loads are in the normal direction to the circular plate and are increased from 1×10^{-7} to 1×10^{-6} for 10 steps. Fig. 6.8 illustrates the solutions obtained from the finite element method using the Bell and the C^1-curved elements with the same number of elements. It can be seen that the solutions obtained from two different types of C^1-finite elements are slightly different.

Regarding the representation of the circular domain, Fig. 6.9 illustrates the comparison of the curved boundary representation obtained from the Bell and the C^1-curved triangular elements. In this figure, the quarter of the unit circle are discretised with an unstructured mesh with 29 triangular elements. As shown in Fig. 6.9a, the C^1-curved triangular elements can nicely represent the curved boundary even though, the small number of elements are used in the mesh. Note that this curved element employs a polynomial of degree 3 to approximate the curvilinear boundary.

On the other hand, it can be seen from Fig. 6.9b that the curvilinear boundary cannot be represented by straight-sided triangular elements with this number of

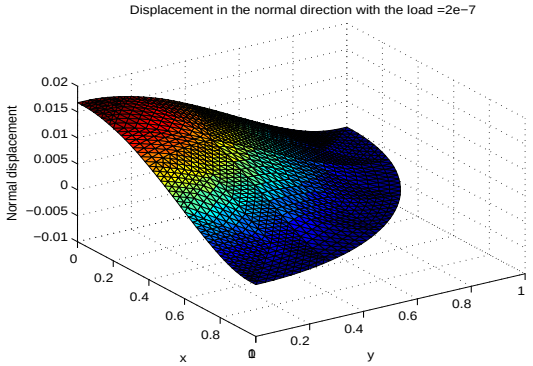

(a) Using the C^1-curved element with loads = 2×10^{-7}

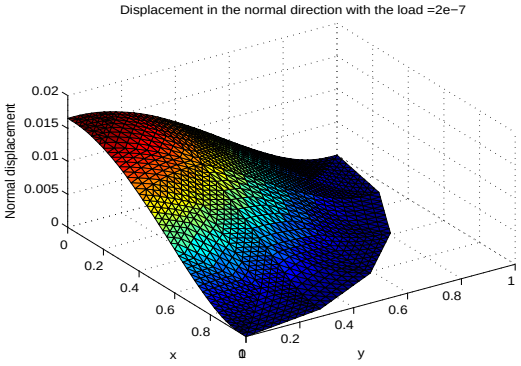

(b) Using the Bell element with loads = 2×10^{-7}

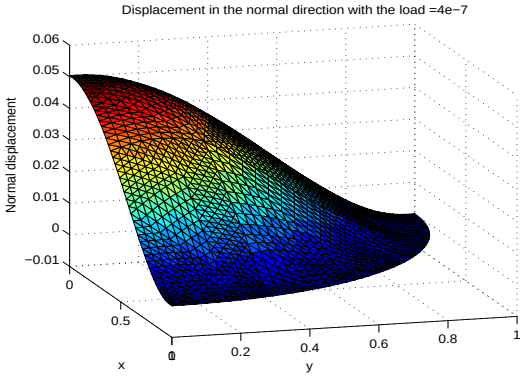

(c) Using the C^1-curved element with loads = 4×10^{-7}

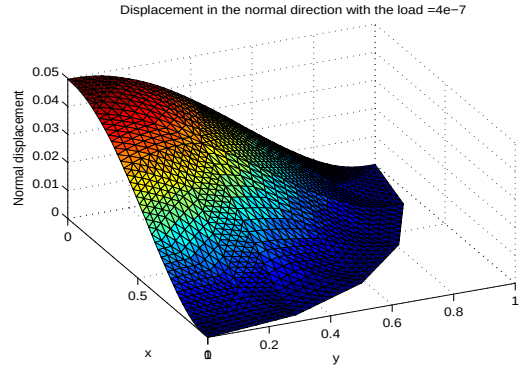

(d) Using the Bell element with loads = 4×10^{-7}

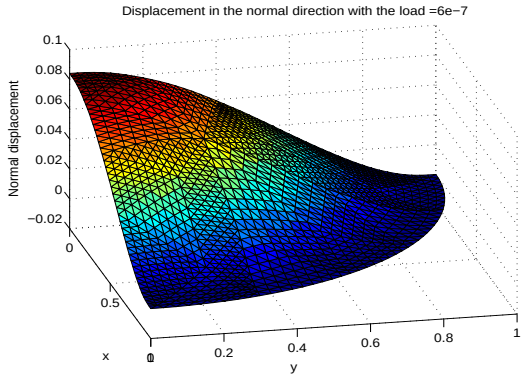

(e) Using the C^1-curved element with loads = 6×10^{-7}

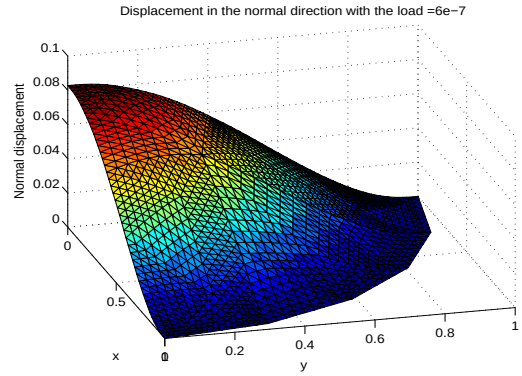

(f) Using the Bell element with loads = 6×10^{-7}

Figure 6.8: Linearised shell solutions of the circular plate problem obtained from the 29-element unstructured mesh with different loads.

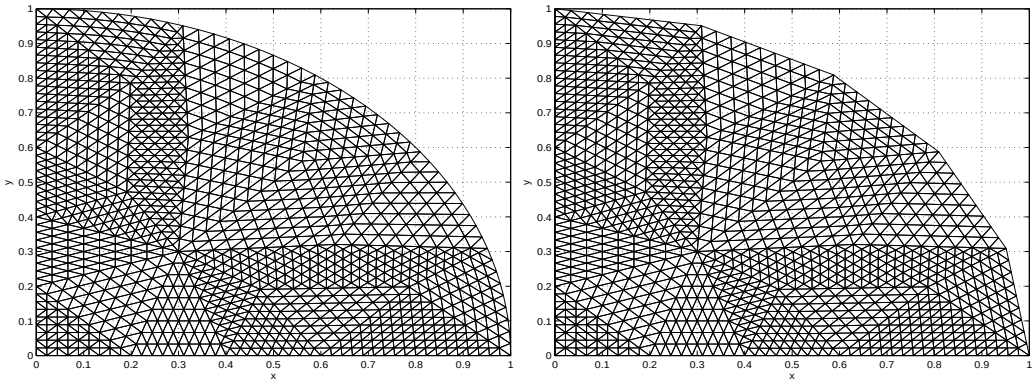

(a) Using the curved element (b) Using the straight element

Figure 6.9: The representation of the curved boundary by the Bell and the C^1-curved triangular finite elements having 29 elements in the mesh.

elements. The obtained geometry boundary is the straight line polygon. However, the representation of curved boundary by using the straight-sided element can be improved by increasing the number of elements in the mesh. But this, indeed, increases computational time and limits the convergence rate as shown in section 6.3.1.

Next, the comparison between the solutions obtained from the Bell and the C^1-curved elements with the exact solution is presented. Fig. 6.10 depicts the differences between the exact solutions (6.52) and the solutions obtained from the Bell and the C^1-curved elements. It can be seen that error obtained from the Bell elements is greater than those obtained from the C^1-curved elements. Also, the differences between those two solutions increases when the loads increase.

Note that the exact solution for the circular plate bending can be obtained by considering the Biharmonic equation in polar coordinates. Since the solution we considered here is axisymmetric, the displacement u is thus parametrised by the radial position, r, only as it is independent of the angle. With the clamped boundary conditions expressed at boundaries as $u(r = a) = 0 = u'(r = a)$, the exact solution for the displacement u can be mathematically obtained as follow:

$$u(r) = \frac{f_0}{64}(a^2 - r^2)^2. \tag{6.52}$$

where f_0 denotes a constant uniform loading and a is the radius of the circular plate. The derivation of the exact solution can also be found in many books of thin plate and shell theory [25].

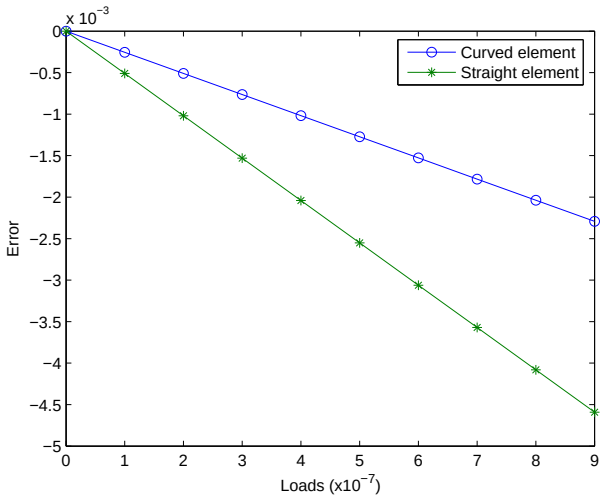

Figure 6.10: The differences between the exact solution and the normal displacements obtained from the Bell and the C^1-curved elements with different loads.

6.4 Summary

In this chapter, the C^1-curved finite element has been studied and implemented. The objective is to improve accuracy and the convergence rate of the solution of the fourth-order problem on curvilinear boundary.

From the results in section 5.2.2 of chapter 5, we see that the Bell triangular finite element can be used to solve the solution of the fourth-order problem on the straight-boundary domain. The element provided very nice C^1-continuity in the solution with very good accuracy. The rate of convergence obtained from the Bell element was quartic.

However, using the Bell triangular element which has straight sides to solve the fourth-order problem with a curvilinear boundary demonstrated less accuracy and a rate of convergence. As shown in section 6.3.1, the obtained rate of convergence decreases from quartic to quadratic. This is a consequence of the incapability of representing a curvilinear boundary with a series of straight-sided elements.

It can also be seen in section 6.3.1 that the curved boundary cannot be accurately represented by a small number of the Bell elements. Unlike the Bell element, a small number of C^1-curved finite elements showed the superiority in representing the curved boundary domain. As shown in Table 6.1, even though using greater number of the Bell element can represent the curved boundary, it illustrated the limitation in the convergence rate.

To retain a rate of convergence and accuracy, an idea of extending one side of triangular element to be curve has been arisen. This attempt is made so that a curved triangle can be fitted with the approximate boundary. Implementations of the C^1-curved element depicted in section 6.3 showed that both accuracy and a rate of convergence increased.

At a first glance, the computational time from the C^1-curved finite element seemed to be very expensive compared to the Bell element when the same number of element is concerned. Nonetheless, it can be seen from section 6.3.1 that the number of elements and the computational time used by the C^1-curved element were less than those of Bell elements for some selected tolerance.

Henceforth, the C^1-curved elements can retain the rate of convergence when solving the C^1-problem on a curved boundary domain as it increases to be quintic. Consequently, the C^1-curved element is superior to the Bell element as it converges faster and provides higher order of accuracy when solving the C^1-problem on a curved boundary domain.

Chapter 7

Conclusion

7.1 Summary

In this thesis, there are three main goals that we addressed and illustrated. The consistency between the linear and nonlinear governing equations of a thin-elastic body with a small strain is the first goal that we presented in chapters 4 and 5. The performance of higher-order finite elements for the thin-elastic theory is also discussed. The other is the accuracy of the solution of a C^1-problem on a curved-boundary domain which was presented in chapter 6.

In what comes, a brief summary of contributions and results is presented. In chapters 4 and 5, finite element implementations of the classical thin-beam and thin-shell theories with both linear and nonlinear governing equations were illustrated and compared. This is to examine the range of validity of the linear theory. Furthermore, an understanding of a dimensional reduction which is one of motivations in numerical simulation in order to represent the body with its intrinsically lower-dimensional space is also provided by employing the Kirchhoff-Love theory.

There were two kinds of thin-elastic geometries considered in the implementations presented in chapters 4 and 5; straight and curved. The results showed that numerical comparisons between the solutions obtained from the linear and nonlinear governing equations with the linear constitutive law were consistent for all thin-beam and thin-shell theories of the straight and the curved kinds when an applied force was small.

Regarding the magnitude of an applied force within a small-deformation regime, it was of order 10^{-8} for a straight geometry and of order 10^{-6} for a curved geometry

for both thin-beam and thin-shell in this study. Also, in order to be in the linear regime, an applied load should be in the range that gives the normal displacements, approximately, 1-3% of the thickness. This is with the relative differences between the linear and nonlinear solutions not greater than 0.01%. Note that the force was applied on a thin-elastic material with a small non-dimensional thickness $h = 0.01$ which lies between the thin regime $0 \leq h \leq 1/20$. Furthermore, the obtained linear and nonlinear solutions started to disagree when loading was increased. This suggested that within a small-strain regime, the linear governing equation can be used to describe behaviours of a thin-elastic material when a displacement is small.

Besides the contribution of the consistency between the linear and nonlinear governing equations of a thin-elastic material within a small deformation, there are additional contributions from chapters 4 and 5. As the result of the linearisation of the governing equations in both thin beam and thin shell, the order of continuity required in the tangential and normal displacements for the associated problem was different. The C^1-continuity was required in the governing equation of the normal displacement so that the Hermite family functions are used to approximate the normal displacement.

However, the tangential displacement can be approximated by either Hermite-type or Lagrange-type interpolation functions as the weak formulation of its linearised governing equation did not require C^1-continuity. Therefore, in chapter 4, an appropriate choice of interpolation functions for the tangential displacement was considered in both theoretical and numerical approaches.

Although, there was no significantly different in the numerical comparisons between the solutions obtained from the Lagrange formulation and the Hermite formulation as shown in Figs. 4.8 and 4.13, it was reasonable to continue approximating tangential displacements by the Lagrange functions. The underlying reason was that using Hermite functions for the second-order differential equation gave extra conditions for the derivatives at boundaries that had to be concerned about the consistency with the natural boundary conditions. Therefore, Hermite polynomials were not of the correct order for the interpolation of the tangential displacements.

Moreover, it has been suggested in section 4.2.2 that Lagrange interpolation is suitable for the second-order differential equation. This is because there is no derivative degree of freedom defined in the Lagrange shape functions which have to be concerned

with the natural boundary conditions. Therefore, the consistency between them is no longer an issue for the Lagrange interpolation for the second-order differential equation.

Next, we will discuss about another contribution from chapter 5 which are numerical comparisons between the performance of the rectangular Hermite and the Bell triangular elements. This is a consequence of discretisations of the desired geometry in two-dimensional finite element implementations.

Regarding a discretisation in chapter 5, there were two types of finite elements considered; a rectangular and a triangular element. Our choice of C^1-shape functions defined over a rectangular and a triangular element was a bicubic Hermite and a Bell shape functions, respectively.

From section 5.2.2, the numerical comparison between the performance of the rectangular Hermite and the triangular Bell elements was illustrated by solving the Biharmonic equation on a rectangular domain. The result showed that the Bell element converged faster than the Hermite element. Also, for a selected tolerance, the Bell element was less time-consuming and also employed less degree of freedom than the Hermite element to achieve the accuracy.

Therefore, the Bell triangular finite element can be used to obtain the solution of the fourth-order problem with very nice C^1-continuity in the solution and a high accuracy. The rate of convergence obtained from the Bell element was quartic which was relatively faster compared to the Hermite element which converged cubically. However, the results obtained from the Bell triangular element were for an exact representation of the geometry, i.e. straight boundary domain.

But in reality, not every domain of interest is straight. In Chapter 6, we illustrated results from using the straight-sided Bell element to obtain the solution of the Biharmonic equation on curvilinear boundary. It turned out that this kind of element gave fairly good accuracy but a rate of convergence dropped from quartic to quadratic. It was showed by P. Fischer [65] that error introduced to the solution was a result from using straight-sided element to approximate a curvilinear domain.

To retain the rate of convergence, the C^1-curved triangle was introduced so that higher rate of convergence and accuracy in the solution can be obtained on a curvilinear domain. This is the idea of extending one side of triangular element to be curve. Implementations of the curved element were depicted in Chapter 6. The obtained

results showed that using the C^1-curved finite element to solve problems defined on a curved-boundary domain did increase both accuracy and a rate of convergence.

When comparing between the Bell and the C^1-curved elements with the same numbers of elements, the computational time from the C^1-curved finite element seemed to be relatively expensive. However, if some tolerance was selected, it can be seen from the results in Chapter 6 that the number of elements and the computational time used by curved elements were less than those of straight elements. Henceforth, the curved element was not truly expensive and rather gave high accuracy and converged faster than the straight-sided Bell element in the case that the solution of the fourth-order problem was solved on a curvilinear boundary.

7.2 Outlook

In this section, we would like to give an overview on a finite element method which can desire further investigations. An emphasis will be placed on the C^1-elements for both straight and curved boundaries.

According to the linear thin-elastic governing equation, an implementation has to employ a family of continuously differentiable finite elements on the domain of interest. Because of the difficulties which occurred during the construction of continuously differentiable finite elements in one- and two-dimensional spaces on a straight boundary, few C^1-elements have been developed in three dimensions (see [6], [72], [76]).

As far as the three-dimensional C^1-finite element availability is concerned, an interesting and challenging aspect could be an extension of a C^1-element to a three-dimensional space. It seems that the only continuously differentiable finite element on tetrahedron constructed was by A. Zenisek in 1973 [6] and, recently, by S. Zhang [76] in 2009.

In the study of A. Zenisek [6], the element was constructed by using a polynomial of degree 9 on tetrahedrons. With this degree of polynomial, 220 degrees of freedom in the 3D finite element have to be specified and considered in an implementation. This makes the coding and computation of C^1-finite elements in 3D relatively expensive. Likewise, the complexity in the construction and computation prohibits further development so that a few researches have been done on this type of element (see [6], [76]).

Another researcher that works on a tetrahedron C^1-finite element is S. Zhang [76]. He tried to modify the Zenisek P_9-tetrahedron to define another C^1-P_k finite element on tetrahedron where P_k is a polynomial degree higher than 9. In his study, some numerical tests were presented to check that his C^1-P_k finite element was well defined on tetrahedral grids.

Recently in 2009, S.A. Papanicolopulos [72] applied a three-dimensional C^1-finite element for gradient elasticity. In his study, a new hexahedral C^1-element was presented using the same technique as the C^1-isoparametric quadrilateral presented by J. Petera and J. Pittman [41]. The constructed element gave excellent rates of convergence in boundary value problems of gradient elasticity. Furthermore, the C^1-hexahedron was shown not to be computationally more expensive than another alternative methods; meshless and penalty methods. However, requiring structured meshes in his implementation is one main drawback of the element.

Regarding the C^1-finite element for a curvilinear boundary, it was elaborated in chapter 6 that the construction of the C^1-curved finite element depends on the degree of polynomial that uses to approximate curved boundaries. Therefore, different degrees of interpolating polynomials give different C^1-curved finite elements. This makes the method impractical and unpopular as the new set of shape functions has to be derived. Also, the coding and computation of C^1-curved finite elements are relatively expensive as seen in section 6.3 and Appendix B.

Furthermore, the construction of the C^1-curved interpolation functions on the reference triangle rather increases the degree of interpolation polynomials. The additional association between the values of degrees of freedom on the reference and physical curved triangles has to also be computed for each element in the mesh and this makes the computational time expensive.

Bibliography

[1] A. E. Green and W. Zerna, **Theoretical elasticity,** *Clarendon Press,* Oxford, London, 1968.

[2] A. E. H. Love, **On the small free vibrations and deformations of elastic shells,** *Philosophical trans. of the Royal Society,* vol. serie A, no. 17, pp. 491-549, London, 1888.

[3] A. L. Hazel and M. Heil, **Three-dimensional airway reopening: the steady propagation of a semi-infinite bubble into a buckled elastic tube,** *Journal of Fluid Mechanics,* vol. 478, pp. 47–70, 2003.

[4] A. Peano, **Conforming approximations for Kirchhoff plates and shells,** *International Journal for Numerical Methods in Engineering,* vol. 14, pp. 1273–1291, 1979.

[5] A. Ženíšek, **Interpolation polynomials on the triangle,** *International Journal for Numerical Methods in Engineering,* vol. 10, pp. 283–296, 1970.

[6] A. Ženíšek, **Polynomial approximation on tetrahedrons in the finite element method,** *Journal of Approximation Theory,* vol. 7, pp. 334–351, 1973.

[7] A.Ženíšek, **Curved triangles finite C^m elements,** *Applications of Mathematics,* vol. 23, pp. 346–377, 1978.

[8] A. Zervos, S.A. Papanicolopulos, and I. Vardoulakis, **Two finite-element discretizations for gradient elasticity,** *Journal of Engineering Mechanics,* vol. 135, no. 3, pp. 203–213, 2009.

[9] B. Bernard, and C. Xiao-Chuan, **H^1-norm error bounds for piecewise Hermite bicubic orthogonal spline collocation schemes for elliptic boundary value problems,** *AMS(MOS).*

[10] B. Fraeijs de Veubeke and G. Sander, **An equilibrium model for plate bending,** *International Journal of Solids and Structures,* vol. 4, pp. 447–468, 1968.

[11] B. M. Irons, **A conforming quartic triangular element for plate bending,** *International Journal for Numerical Methods in Engineering,* vol. 1, pp. 29–46, 1969.

[12] B. M. Irons, and J. K. Draper, **Inadequacy of nodal connections in a stiffness solution for plate bending,** *Journal of AIAA,* vol. 3, pp. 5, 1965.

[13] B. Shekhtman, **Case study in bivariate Hermite interpolation,** *Journal of Approximation Theory,* vol. 136, pp. 140-150, 2005.

[14] B. Specht, **Modified shape functions for the three node plate bending element passing the patch test,** *International Journal for Numerical Methods in Engineering,* vol. 26, pp. 705–715, 1988.

[15] C. A. Felippa, **Refined finite element analysis of linear and nonlinear two-dimensional structures,** *Ph.D. Dissertation,* Department of Civil Engineering, University of California at Berkeley, 1966.

[16] C. Bernardi, **Optimal finite-element interpolation on curved domains,** *SIAM Journal on Numerical Analysis,* Anal. 26, pp. 1212–1240, 1989.

[17] C. Caramanlian, K. A. Selby, and G. T. Will, **A quintic conforming plate bending triangle,** *International Journal for Numerical Methods in Engineering,* vol. 12, pp. 1109–1130, 1978.

[18] C. Caramanlian, **A conforming solution to curved plate bending problems,** *International Journal for Numerical Methods in Engineering,* vol. 17, pp. 879–907, 1981.

[19] C. Loop, **Smooth subdivision surfaces based on triangles,** *Master's Thesis,* Department of Mathematics, University of Utah, 1987.

[20] C. R. Ethier, **Computational modelling of mass transfer and links to atherosclerosis,** *Annals of Biomedical Engineering,* vol. 30, pp. 461-471, 2002.

[21] D. A. Duvanant, **High degree efficient symmetrical Gaussian quadrature rules for the triangle,** *International journal for numerical methods in engineering,* vol. 21, pp. 1129–1148, 1985.

[22] D. J. Benson, Y. Bazilevs, et.al, **A generalized finite element formulation for arbitrary basis functions: From isogeometric analysis to XFEM,** *International Journal for Numerical Methods in Engineering,* vol. 83, pp. 765–785, 2010.

[23] D. J. Benson, Y. Bazilevs, et.al, **A large deformation, rotation-free isogeometric shell,** *Computer Methods in Applied Mechanics and Engineering,* pp. 1367–1378, 2011.

[24] E. Catmull, J. Clark, **Recursively generated b-spline surfaces on arbitrary topological meshes,** *Computer Aided Design,* vol. 10, no. 6, pp. 350–355, 1978.

[25] E. Ventsel, and T. Krauthammer, **Thin Plates and Shells Theory, Analysis, and Applications,** *Marcel Dekker, Inc,* 2001.

[26] F. Cirak, M. Ortiz, and P.Schröder, **Subdivision surfaces: a new paradigm for thin-shell finite-element analysis,** *International Journal for Numerical Methods in Engineering,* vol. 47, pp. 2039–2072, 2000.

[27] F. Cirak, and M. Ortiz, **Fully C^1-conforming subdivision elements for finite deformation thin-shell analysis,** *International Journal for Numerical Methods in Engineering,* vol. 51, pp. 813–833, 2001.

[28] F. K. Bogner, R. L. Fox, and L. A. Schmidt, **The generation of interelement-compatible stiffness and mass matrices by the use of interpolation formulae,** *In Proc. 1st Conf. Matrix Methods in Structural Mechanics,* vol. AFFDL-TR-66-80, pp. 397–443, Ohio, October, 1966.

[29] G. Birkhoff, **Tricubic polynomial interpolation,** *Proceedings of the National Academy of Sciences of the United States of America,* vol. 68, no. 6, pp. 1162–1164, 1971.

[30] G. Birkhoff and L. Mansfield, **Compatible triangular finite elements,** *Journal of Mathematical Analysis and Applications,* vol. 47, pp. 435–447, 1974.

[31] G. Bonnes and G. Dhatt, **Curved triangular elements for the analysis of shells,** *AFFDL-TR-68-150,* pp. 617–639.

[32] G. Kämmel, **Einführung in die Methode der finiten Elemente,** *Heinzjoachim Franeck unter Mitarb,* von Hans–Georg Recke, 1988.

[33] G. P. Bazeley, Y. K. Cheung, B. M. Irons and O. C. Zienkiewicz, **Triangular elements in bending conforming and nonconforming solutions,** *Proceedings of the Conference on Matrix Methods in Structural Mechanics,* 1965.

[34] G. Qing and L. Li, **A note on C^1-curved finite element,** *Computer Methods in Applied Mechanics and Engineering,* vol. 129, pp. 107–114, 1996.

[35] G. Wempner and D. Talaslidis, **Mechanics of Solids and Shells Theories and Approximations**, *CRC Press*, 2003.

[36] H. Askes and E. Aifantis, **Numerical modeling of size effects with gradient elasticity formulation, meshless discretization and examples,** *International Journal of Fracture,* vol. 117, pp. 347-358, 2002.

[37] I. Babuska and M. Zlamal, **Nonconforming elements in the finite element method with penalty,** *SIAM Journal on Numerical Analysis,* vol. 10, no. 5, pp. 863–875, 1973.

[38] J. H. Argyris, I. Fried and D.W. Scharpf, **The TUBA family of plate elements for the matrix displacement method,** *Journal of the Royal Aeronautical Society,* vol. 72, pp. 701–709, 1968.

[39] J. Kiendl, K.U. Bletzinger, J. Linhard, R. Wüchner, **Isogeometric shell analysis with Kirchhoff-Love elements,** *Computer Methods in Applied Mechanics and Engineering,* vol. 198, pp. 3902–3914, 2009.

[40] J. N. Reddy, **An introduction to the finite element method,** *McGraw-Hill, Inc,* 1993.

[41] J. Petera, and J. Pittman, **Isoparametric Hermite elements**, *International Journal of Numerical Methods in Engineering,* vol. 37, pp. 3489–3519, 1994.

[42] J. Y. Shu, W. E. King, and N. A. Fleck, **Finite elements for materials with strain gradient effects,** *International Journal for Numerical Methods in Engineering,* vol. 44, pp. 373-391, 1999.

[43] K. Bell, **A refined triangular plate bending element,** *International Journal for Numerical Methods in Engineering,* vol. 1, pp. 101–122, 1969.

[44] L. E. Mansfield, **Higher order compatible triangular finite elements,** *Applied Numerical Mathematics,* vol. 22, pp. 89–97, 1974.

[45] L. E. Mansfield, **Approximation of the boundary in the finite element solution of fourth order problems,** *SIAM Journal on Numerical Analysis,* vol. 15, pp. 568–579, 1978.

[46] L. Morley, **The constant-moment plate-bending element,** *The Journal of Strain Analysis for Engineering Design,* vol. 6, pp. 20–24, 1971.

[47] M. Bernadou and J. M. Boisserie, **Curved finite elements of class C^1: Implementation and numerical experiments. Part1: Construction and numerical tests on the interpolation properties,** *Rapports de Recherche INRIA,* 1992.

[48] M. Bernadou, **C^1-curved finite elements with numerical integration for thin plate and thin shell problems, Part 1: Construction and interpolation properties of curved C^1 finite elements,** *Computer Methods in Applied Mechanics and Engineering,* vol. 102, pp. 255–289, 1993.

[49] M. Bernadou, **C^1-curved finite elements with numerical integration for thin plate and thin shell problems, Part 2: Approximation of thin plate and thin shell problems,** *Computer Methods in Applied Mechanics and Engineering,* vol. 102, pp. 389–421, 1993.

[50] M. Bernadou and J. M. Boisserie, **Curved finite elements of class C^1: Implementation and numerical experiments. Part 1: Construction and numerical tests of the interpolation properties,** *Computer Methods in Applied Mechanics and Engineering,* vol. 106, pp. 229–269, 1993.

[51] M. Bernadou and J. M. Boisserie, **Curved finite elements of class C^1: Implementation and numerical experiments. Part 2: Application to thin plate and thin shell problems,** *Rapports de Recherche INRIA,* 1993.

[52] M. D. Olson and G. I. Lindberg, **Annular and circular sector finite elements for plate bending,** *International Journal of Mechanical Sciences,* vol. 12, pp. 17–83, 1970.

[53] M. Heil and A. Hazel, **Oomph-lib, the Object-Oriented Multi-Physics Library, and its documentation,** http://www.oomph-lib.org.uk/

[54] M. J. D. Powell and M. A. Sabin, **Piecewise quadratic approximations on triangles,** *ACM Transactions on Mathematical Software,* vol. 3, pp. 316–325, 1977.

[55] M. Lenoir, **Optimal isoparametric finite elements and error estimates for domains involving curved boundaries,** *SIAM Journal on Numerical Analysis,* vol. 23, pp. 562–580, 1986.

[56] M. W. Chernuka, G. R. Cowper, G. M. Lindberg, and M. D. Olson, **Finite element analysis of plates with curved edges,** *International Journal for Numerical Methods in Engineering,* vol. 4, pp. 49–65, 1972.

[57] M. Zlamal, **The finite element method in domains with curved boundaries,** *International Journal for Numerical Methods in Engineering,* vol. 5, pp. 367–373, 1973.

[58] M. Zlamal, **Curved elements in the finite element method, Part 1,** *SIAM Journal on Numerical Analysis,* vol. 10, pp. 229–240, 1973.

[59] M. Zlamal, **Curved elements in the finite element method, Part 2,** *SIAM Journal on Numerical Analysis,* vol. 11, pp. 347–362, 1974.

[60] O. C Zienkiewicz, R. L Taylor, and J. Z. Zhu, **The finite element method: Its basis and fundamentals,** *Elsevier Ltd.,* 2005.

[61] O. C Zienkiewicz, R. L Taylor, **The finite element method volume 2: Solid mechanics,** *Butterworth-Heinemann,* 2000.

[62] P. C. Dunne, **Complete polynomial displacement field for finite element method,** *Ae. J. R. Ae. Soc.,* vol. 72, pp. 245–247, 1968.

[63] P. Fischer, C^1 **continuous methods in computational gradient elasticity**, *Thesis*, Faculty of Technology, University of Erlangen-Nuremberg, 2011.

[64] P. Fischer, J. Mergheim, and P. Steinmann, **On the C^1 continuous discretization of nonlinear gradient elasticity: a comparison of NEM and FEM based on Bernstein-Bezier patches**, *International Journal of Numerical Methods in Engineering,* vol. 82, pp. 1282–1307, 2009.

[65] P. Fischer, J. Mergheim, and P. Steinmann, **Direct evaluation of nonlinear gradient elasticity in 2D with C^1 continuous discretization methods**, *Proceedings in applied mathematics and mechanics,* 2011.

[66] P. G. Bergan, **Finite elements based on energy orthogonal functions,** *International Journal for Numerical Methods in Engineering,* vol. 15, issue 10, pp. 1541–1555, 1980.

[67] P. Kagan, A. Fischer, and P. Z. Bar-Yoseph, **New B-spline finite element approach for geometrical design and mechanical analysis,** *International Journal for Numerical Methods in Engineering,* vol. 41, pp. 435-458, 1998.

[68] P. Krysl and T. Belytschko, **Analysis of thin plates by the Element-Free Galerkin Method,** *url:hogwarts.ucsd.edu/pkrysl/publications/plates.pdf,* 1999.

[69] Q. Gao, L. Li, **Interpolated boundary conditions in plate bending problems using C^1-curved finite elements,** *Computer Methods in Applied Mechanics and Engineering,* vol. 148, pp. 235–255, 1997.

[70] R. Scott, **Finite element techniques for curved boundaries,** *Thesis,* Massachusetts Institute of Technology, Cambridge, 1973.

[71] R. W. Clough and J. L. Tocher, **Finite element stiffness matrices for analysis of plate bending,** *Proceedings of the Second Conference on Matrix Methods in Structural Mechanics, WPAFB,* Ohio, 1965, in *AFFDL TR 66–80*, pp. 515–545, 1966.

[72] S. A. Papanicolopulos, A. Zervos, and I. Vardoulakis, **A three-dimensional C^1 finite element for gradient elasticity,** *International Journal for Numerical Methods in Engineering,* vol. 77, pp. 1396–1415, 2009.

[73] S. C. Brenner and L. Y. Sung, **C^0-Interior penalty methods for fourth order elliptic boundary value problems on polygonal domains,** *Journal of Scientific Computing archive,* vol. 22-23, issue 1-3, pp. 83–118, 2005.

[74] S. Dasgupta and D. Senggupta, **A higher-order triangular plate bending element revisited,** *International Journal for Numerical Methods in Engineering,* vol. 30, pp. 419–430, 1990.

[75] S. Hirokawa, T. Ueki, A. Ohtsuki, **A new approach for surface fitting method of articular joint surfaces,** *Journal of Biomechanics,* vol. 37, pp. 1551–1559, 2004.

[76] S. Zhang, **A family of 3D continuously differentiable finite elements on tetrahedral grids,** *Journal of Applied Numerical Mathematics,* vol. 59, no. 1, pp. 219–233, 2009.

[77] T. Belytschko, W. K. Liu, B. Moran, **Nonlinear Finite Elements for Continua and Structures,** *Wiley,* 2000.

[78] T. J. R. Hughes, **The Finite Element Method: Linear Static and Dynamic Finite Element Analysis,** *Dover publications, INC.*, New York, 2000.

[79] T. J. R. Hughes, J. A. Cotrell, Y. Bazilevs, **Isogeometric analysis: CAD, finite elements, NURBS, exact geometry and mesh refinement,** *Computer Methods in Applied Mechanics and Engineering,* vol. 194. pp. 4135–4195, 2005.

[80] V. Dominguez, F. J. Sayas, **Algorithm 884: A Simple Matlab Implementation of the Argyris Element,** *ACM Transactions on Mathematical Software,* vol. 35, No. 2, Article 16, 2008.

[81] W. Flügge, **Tensor Analysis and Continuum Mechanics,** *Springer-Verlag Berlin Heidelberg,* New York, 1972.

[82] Y. Bazilevs, V. M. Calo, Y. Zhang, T. J. R. Hughes, **Isogeometric fluidstructure interaction analysis with applications to arterial blood flow,** *Journal of Computational Mechanics,* vol. 38, pp. 310-322, 2006.

[83] Y. Bazilevs, V. M. Calo, et.al., **Isogeometric analysis using T-splines,** *Computer Methods in Applied Mechanics and Engineering,* vol. 199, issues 5-8, pp. 229–263, 2010.

[84] Y. Zhang, Y. Bazilevs, S. Goswami, C.L. Bajaj and T.J.R. Hughes, **Patient-specific vascular NURBS modeling for isogeometric analysis of blood flow,** *Computer Methods in Applied Mechanics and Engineering,* vol. 196, pp. 2943-2959, 2000.

[85] Z. Tang, S. Shen, and S. N. Atluri, **Analysis of materials with strain-gradient effects: A meshless local Petrov-Galerkin(mlpg) approach, with nodal displacements only,** *CMES-Computer Modeling in Engineering and Sciences* vol. 4, no. 1, pp. 177-196, 2003.

Appendix A

Shape functions

In this section, two families of shape functions are considered: the Lagrange and the Hermite functions. They consist of sets of polynomials of different degrees which depend on the desired accuracy of approximation. In general, the higher the degree, the better the approximation.

A.1 Lagrange shape functions

A Lagrange shape function is a polynomial that is used to approximate a function. It is one of the basic polynomials for problems with a simple degree of freedom per node in an element. In this type of element, only the function values are given and specified at nodes and are associated with Lagrange shape functions in order to make an approximation. A field variable being approximated by the Lagrange functions is continuous between elements; however, its derivatives are not necessarily continuous.

A.1.1 Interpolations in one dimension

One-dimensional interpolation functions can be constructed from the idea of the interpolation theory. There are many kinds of Lagrange shape functions. Linear shape functions are used when the domain is discretised with 2-node element, while quadratic and cubic shape functions are used with 3-node and 4-node elements, respectively. In this thesis, only linear and quadratic Lagrange shape functions will be used to approximate our quantities of interest.

Linear shape functions

A linear shape function is a linear polynomial defined on a 2-node element. Its shape functions can be mathematically described in local coordinate, $s \in [-1, 1]$, as

$$\begin{aligned} \psi_1(s) &= 0.5(1-s), \\ \psi_2(s) &= 0.5(1+s). \end{aligned} \tag{A.1}$$

The linear shape functions are straight lines that linearly vary between -1 and 1 as illustrated in Fig. A.1.

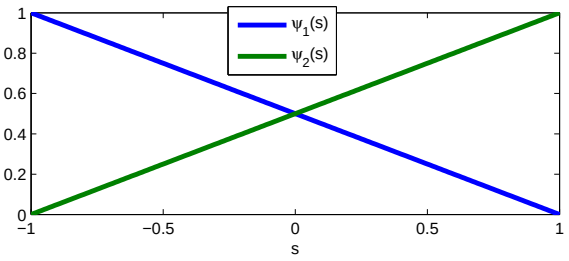

Figure A.1: The linear shape functions in one dimension which has two nodes in the element.

Therefore, a linear approximation of unknown u can be defined by introducing a normalised measure of distance, s, with $s = -1$ at one end and $s = 1$ at the other end of the domain as

$$\begin{aligned} u(s) &= U_1\psi_1(s) + U_2\psi_2(s), \\ &= 0.5U_1(1-s) + 0.5U_2(1+s), \end{aligned} \tag{A.2}$$

where U_1, U_2, are called nodal parameters that associate with the values of unknown at element nodes. It can be seen in (A.2) that a shape function defined in (A.1) is associated with each of the nodal parameters.

Quadratic shape functions

A quadratic shape function is a polynomial of degree 2 defined on a 3-node element. Its shape functions can be mathematically described in local coordinate, s, as

$$\begin{aligned} \psi_1(s) &= 0.5s(s-1), \\ \psi_2(s) &= 1-s^2, \\ \psi_3(s) &= 0.5s(s+1). \end{aligned} \tag{A.3}$$

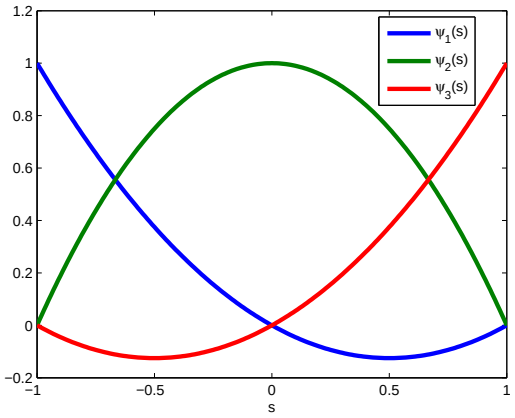

Figure A.2: The quadratic shape functions in one dimension which has three nodes in the element.

These shape functions are quadratic curve that vary between -1 and 1 as illustrated in Fig. A.2.

Therefore, a quadratic approximation of unknown u can be defined by introducing a normalised measure of distance, s, with $s = -1$ at one end and $s = 1$ at the other end of the domain as

$$\begin{aligned} u(s) &= U_1\psi_1(s) + U_2\psi_2(s) + U_3\psi_3(s), \\ &= U_1(0.5s(s-1)) + U_2(1-s^2) + U_3(0.5s(s+1)), \end{aligned} \tag{A.4}$$

where U_1, U_2, U_3, are called nodal parameters that associate with the values of unknown at element nodes. Similar to a linear approximation, a quadratic shape function is associated with each of the nodal parameters.

A.1.2 Interpolations in two dimensions

Two-dimensional Lagrange shape functions can simply be constructed from tensor products of the one-dimensional functions. To approximate an unknown u over a 2D domain, Lagrange shape functions defined in one dimension have to be used.

Bilinear shape functions

The bilinear Lagrange shape functions defines in two-dimensional space to have two nodes on each side of the element. They can be constructed by taking the tensor product of individual one-dimensional linear Lagrange shape functions in the s_1 and

s_2 directions defined in (A.1). This scheme consists of four polynomials shown as follows

$$\begin{aligned}\phi_1(s_1, s_2) &= \psi_1(s_1)\psi_1(s_2)\\ \phi_2(s_1, s_2) &= \psi_2(s_1)\psi_1(s_2)\\ \phi_3(s_1, s_2) &= \psi_1(s_1)\psi_2(s_2)\\ \phi_4(s_1, s_2) &= \psi_2(s_1)\psi_2(s_2)\end{aligned} \tag{A.5}$$

where ψ_1, and ψ_2, are the one-dimensional linear Lagrange basis functions correspond to nodal position 1,2, respectively.

Therefore, four nodal parameters, $U_1, ..., U_4$, which are the values of the unknown u defined at the element nodes $j = 1, ..., 4$, are associated with the two-dimensional shape functions, $\phi_1, ..., \phi_4$. The approximation of u is then given by

$$u(s_1, s_2) = \sum_{j=1}^{4} \phi_j(s_1, s_2)U_j. \tag{A.6}$$

Biquadratic shape functions

The biquadratic Lagrange shape functions defines in two-dimensional space to have three nodes on each side of the element. They can be constructed by taking the tensor product of individual one-dimensional quadratic Lagrange shape functions in the s_1 and s_2 directions defined in (A.3). This scheme consists of nine polynomials shown as follows

$$\begin{aligned}\phi_1(s_1, s_2) &= \psi_1(s_1)\psi_1(s_2)\\ \phi_2(s_1, s_2) &= \psi_2(s_1)\psi_1(s_2)\\ \phi_3(s_1, s_2) &= \psi_3(s_1)\psi_1(s_2)\\ \phi_4(s_1, s_2) &= \psi_1(s_1)\psi_2(s_2)\\ \phi_5(s_1, s_2) &= \psi_2(s_1)\psi_2(s_2)\\ \phi_6(s_1, s_2) &= \psi_3(s_1)\psi_2(s_2)\\ \phi_7(s_1, s_2) &= \psi_1(s_1)\psi_3(s_2)\\ \phi_8(s_1, s_2) &= \psi_2(s_1)\psi_3(s_2)\\ \phi_9(s_1, s_2) &= \psi_3(s_1)\psi_3(s_2),\end{aligned} \tag{A.7}$$

where ψ_1, ψ_2, and ψ_3, are the one-dimensional quadratic Lagrange shape functions correspond to nodal position 1,2 and 3, respectively.

Therefore, the approximation of u is given by

$$u(s_1, s_2) = \sum_{j=1}^{9} \phi_j(s_1, s_2) U_j, \tag{A.8}$$

where nine nodal parameters, $U_1, ..., U_9$, are associated with the two-dimensional shape functions, $\phi_1, ..., \phi_9$.

Note that the resulting shape functions in the Lagrange family do not enforce inter-element C^1-continuity at any element's boundary. For their derivations, the reader may consult finite element books such as [40], [60].

A.2 Hermite shape functions

Unlike Lagrange shape functions, Hermite shape functions are defined to provide C^1-continuity in an approximated solution. To interpolate a solution of a problem, Hermite shape functions have to be associated with both the values and its derivatives which are specified and known at nodes in an element.

A.2.1 Interpolations in one dimension

The Hermite shape function in one dimensional space is defined on 2-node element. The cubic polynomials are employed to construct this type of shape functions and they can be derived from interpolating a function value and its derivative at the nodes. The one-dimensional Hermite shape functions are mathematically described as

$$\begin{aligned}
\psi_{11}(s) &= 0.25(s^3 - 3.0s + 2.0) \\
\psi_{12}(s) &= 0.25(s^3 - s^2 - s + 1.0) \\
\psi_{21}(s) &= 0.25(2.0 + 3.0s - s^3) \\
\psi_{22}(s) &= 0.25(s^3 + s^2 - s - 1.0),
\end{aligned} \tag{A.9}$$

where ψ_{i1} is the local shape function at node i associated with the unknown value, and ψ_{i2} is the shape function at node i associated with the unknown derivative. Note that these shape functions are defined over the local coordinate $s \in [-1, 1]$.

Hence, the approximation of u is then given by

$$u(s) = \sum_{i=1}^{2} \sum_{j=1}^{2} \psi_{ij}(s) U_{ij}, \tag{A.10}$$

where nodal parameters, $U_{i1}, U_{i2}; i = 1, 2$, are associated with the unknown value u and its first derivative, $\frac{\partial u}{\partial s}$, at node i, respectively. These must be defined at each node of the element. In total, we have 4 nodal parameters per element for the bicubic Hermite interpolations in one dimension.

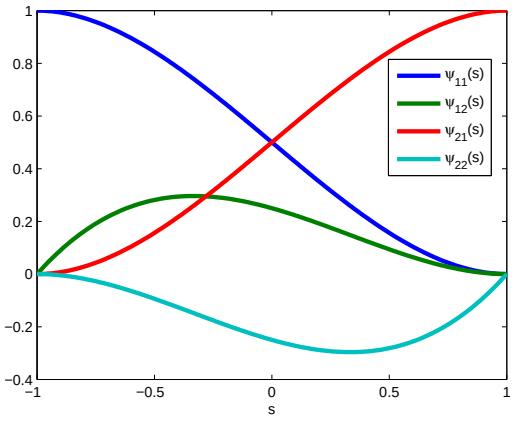

Figure A.3: The cubic Hermite basis functions.

From the definition of Hermite shape functions stated above, we have that, for nodes $s_1 = -1$ and $s_2 = 1$, $\psi_{i1} = 1$ at node s_i and $\psi_{i1} = 0$ at the other node. Furthermore, $d\psi_{i1}/ds = 0$ at both nodes. Moreover, $d\psi_{i2}/ds = 1$ at node s_i and $d\psi_{i2}/ds = 0$ at the other node. Furthermore, $\psi_{i2} = 0$ at both nodes. Hence, a one-dimensional cubic Hermite basis incorporates the four cubic polynomials listed above and graphically illustrated in Fig. A.3.

A.2.2 Interpolations in two dimensions

The construction of two-dimensional Hermite shape functions can be achieved using the same procedure as in Lagrange family. With the definition of tensor products, we have that the Hermite shape functions in two-dimensional space are bicubic polynomials.

The bicubic Hermite shape functions of the unknown u can be expressed as in

(A.11) using the one-dimensional cubic Hermite shape functions defined in (A.9).

$$\begin{aligned} u(s_1, s_2) = {} & \psi_{11}(s_1)\psi_{11}(s_2)U_{11} + \psi_{11}(s_2)\psi_{21}(s_1)U_{21} \\ & + \psi_{11}(s_1)\psi_{21}(s_2)U_{31} + \psi_{21}(s_1)\psi_{21}(s_2)U_{41} \\ & + \psi_{12}(s_1)\psi_{11}(s_2)U_{12} + \psi_{22}(s_1)\psi_{11}(s_2)U_{22} \\ & + \psi_{12}(s_1)\psi_{21}(s_2)U_{32} + \psi_{22}(s_1)\psi_{21}(s_2)U_{42} \\ & + \psi_{11}(s_1)\psi_{12}(s_2)U_{13} + \psi_{21}(s_1)\psi_{12}(s_2)U_{23} \\ & + \psi_{11}(s_1)\psi_{22}(s_2)U_{33} + \psi_{21}(s_1)\psi_{22}(s_2)U_{43} \\ & + \psi_{12}(s_1)\psi_{12}(s_2)U_{14} + \psi_{22}(s_1)\psi_{12}(s_2)U_{24} \\ & + \psi_{12}(s_1)\psi_{22}(s_2)U_{34} + \psi_{22}(s_1)\psi_{22}(s_2)U_{44} \end{aligned} \tag{A.11}$$

where, for node $j = 1, 2, 3, 4$, U_{j1} associated with value of the unknown at node j. The U_{j2} and U_{j3} are coefficients associated with the first derivatives at node j of the unknown with respect to the 1^{st} and 2^{nd} coordinate, respectively. And U_{j4} denote the mixed derivative at node j.

Hence, to approximate an unknown u using a two-dimensional bicubic Hermite basis, the four quantities constituted of the unknown value u, its first derivatives, $\frac{\partial u}{\partial s_1}$, $\frac{\partial u}{\partial s_2}$ and the mixed derivative $\frac{\partial^2 u}{\partial s_1 \partial s_2}$, must be defined at each node of the element. In total, we have 16 nodal parameters per element for the bicubic Hermite shape functions.

Appendix B

The association matrix between nodal values defined on the reference and the curved elements

In this chapter, we will detail the matrix transformation which allow us to realise the association between the nodal values on the reference and those of the curved elements. All steps described in section 6.2.4 will be transcribed into matrix expressions.

Remind that $x_\alpha, \alpha = 1, 2$ denote coordinates in two-dimensional space defined on the physical domain and approximated by the functions $\chi_1(s), \chi_2(s)$ which are continuous on $[s_m, s_M]$ defined in (6.2). Also, $\hat{\mathbf{a}}_i, i = 1, 2, 3$, denote vertices of the triangle, $\hat{\mathbf{b}}_i, i = 1, 2, 3$, $\hat{\mathbf{d}}_i, i = 1, ..., 6$, denote nodes along edges, and $\hat{\mathbf{e}}_i, i = 1, 2, 3$, denote the internal nodes of the reference triangle illustrated in Fig. 6.5.

Since the set of degrees of freedom defined over the reference triangle $\hat{K}$ is (see

(6.16))

$$
\begin{aligned}
&[DL(\hat{w})] \\
&= \Bigg\{ \hat{w}(\hat{\mathbf{a}}_1), \hat{w}(\hat{\mathbf{a}}_2), \hat{w}(\hat{\mathbf{a}}_3), \frac{\partial \hat{w}}{\partial \hat{x}_1}(\hat{\mathbf{a}}_1), \frac{\partial \hat{w}}{\partial \hat{x}_2}(\hat{\mathbf{a}}_1), \frac{\partial \hat{w}}{\partial \hat{x}_1}(\hat{\mathbf{a}}_2), \frac{\partial \hat{w}}{\partial \hat{x}_2}(\hat{\mathbf{a}}_2), \frac{\partial \hat{w}}{\partial \hat{x}_1}(\hat{\mathbf{a}}_3), \frac{\partial \hat{w}}{\partial \hat{x}_2}(\hat{\mathbf{a}}_3), \\
&\frac{\partial^2 \hat{w}}{\partial \hat{x}_1^2}(\hat{\mathbf{a}}_1), \frac{\partial^2 \hat{w}}{\partial \hat{x}_1 \hat{x}_2}(\hat{\mathbf{a}}_1), \frac{\partial^2 \hat{w}}{\partial \hat{x}_2^2}(\hat{\mathbf{a}}_1), \frac{\partial^2 \hat{w}}{\partial \hat{x}_1^2}(\hat{\mathbf{a}}_2), \frac{\partial^2 \hat{w}}{\partial \hat{x}_1 \hat{x}_2}(\hat{\mathbf{a}}_2), \frac{\partial^2 \hat{w}}{\partial \hat{x}_2^2}(\hat{\mathbf{a}}_2), \frac{\partial^2 \hat{w}}{\partial \hat{x}_1^2}(\hat{\mathbf{a}}_3), \\
&\frac{\partial^2 \hat{w}}{\partial \hat{x}_1 \hat{x}_2}(\hat{\mathbf{a}}_3), \frac{\partial^2 \hat{w}}{\partial \hat{x}_2^2}(\hat{\mathbf{a}}_3), -\frac{\partial \hat{w}}{\partial \hat{x}_1}(\hat{\mathbf{b}}_1), -\frac{\partial \hat{w}}{\partial \hat{x}_2}(\hat{\mathbf{b}}_2), \frac{\sqrt{2}}{2}\left(\frac{\partial \hat{w}}{\partial \hat{x}_1} + \frac{\partial \hat{w}}{\partial \hat{x}_2}\right)(\hat{\mathbf{b}}_3), \hat{w}(\hat{\mathbf{d}}_1), \\
&\hat{w}(\hat{\mathbf{d}}_2), \hat{w}(\hat{\mathbf{d}}_3), \hat{w}(\hat{\mathbf{d}}_4), \hat{w}(\hat{\mathbf{d}}_5), \hat{w}(\hat{\mathbf{d}}_6), -\frac{\partial \hat{w}}{\partial \hat{x}_1}(\hat{\mathbf{d}}_1), -\frac{\partial \hat{w}}{\partial \hat{x}_1}(\hat{\mathbf{d}}_2), -\frac{\partial \hat{w}}{\partial \hat{x}_2}(\hat{\mathbf{d}}_3), -\frac{\partial \hat{w}}{\partial \hat{x}_2}(\hat{\mathbf{d}}_4), \\
&\frac{\sqrt{2}}{2}\left(\frac{\partial \hat{w}}{\partial \hat{x}_1} + \frac{\partial \hat{w}}{\partial \hat{x}_2}\right)(\hat{\mathbf{d}}_5), \frac{\sqrt{2}}{2}\left(\frac{\partial \hat{w}}{\partial \hat{x}_1} + \frac{\partial \hat{w}}{\partial \hat{x}_2}\right)(\hat{\mathbf{d}}_6), \hat{w}(\hat{\mathbf{e}}_1), \hat{w}(\hat{\mathbf{e}}_2), \hat{w}(\hat{\mathbf{e}}_3) \Bigg\},
\end{aligned}
\tag{B.1}
$$

where $\hat{w}$ denotes any function defined over the reference element $\hat{K}$, and the set of degrees of freedom defined over the curved triangle K_C is

$$
\begin{aligned}
[DL(v)] = \{&v(\mathbf{a}_1); v(\mathbf{a}_2); v(\mathbf{a}_3); Dv(\mathbf{a}_1)(\mathbf{a}_3 - \mathbf{a}_1); (s_M - s_m)Dv(\mathbf{a}_1)\chi'(s_m); \\
&(s_m - s_M)Dv(\mathbf{a}_2)\chi'(s_M); Dv(\mathbf{a}_2)(\mathbf{a}_3 - \mathbf{a}_2); Dv(\mathbf{a}_3)(\mathbf{a}_2 - \mathbf{a}_3); \\
&Dv(\mathbf{a}_3)(\mathbf{a}_1 - \mathbf{a}_3); D^2v(\mathbf{a}_1)(\mathbf{a}_3 - \mathbf{a}_1)^2; (s_M - s_m)^2 D^2v(\mathbf{a}_1)(\chi'(s_m))^2; \\
&(s_m - s_M)^2 D^2v(\mathbf{a}_2)(\chi'(s_M))^2; D^2v(\mathbf{a}_2)(\mathbf{a}_3 - \mathbf{a}_2)^2; D^2v(\mathbf{a}_3)(\mathbf{a}_2 - \mathbf{a}_3)^2; \\
&D^2v(\mathbf{a}_3)(\mathbf{a}_1 - \mathbf{a}_3)^2; D^2v(\mathbf{a}_1)(\mathbf{a}_2 - \mathbf{a}_3)^2; D^2v(\mathbf{a}_2)(\mathbf{a}_3 - \mathbf{a}_1)^2; \\
&(s_M - s_m)^2 D^2v(\mathbf{a}_3)(\chi'(s_m), \chi'(s_M)); v(\mathbf{e}_1); v(\mathbf{e}_2); v(\mathbf{e}_3)\},
\end{aligned}
\tag{B.2}
$$

we need to define the matrix $\tilde{M}$ such that

$$
[DL(\hat{w})]_{1\times 36} = [DL(v)]_{1\times 21}[\tilde{M}]_{21\times 36}, \tag{B.3}
$$

where v is any function defined on the curved triangle K_C. To consider the matrix $\tilde{M}$, we will partition it as follow:

$$
[\tilde{M}]_{21\times 36} = \begin{bmatrix} \tilde{M}_1 & \tilde{M}_2 & \tilde{M}_3 & \tilde{M}_4 & \tilde{M}_5 & \tilde{M}_6 & \tilde{M}_7 \end{bmatrix}, \tag{B.4}
$$

where submatrices $\tilde{M}_j; j = 1, ..., 7$, have 21 lines and 3, 6, 9, 3, 6, 6, and 3 columns, respectively, and are determined as follows.

Construction of submatrix $\tilde{M}_1$:

Since $\hat{w}(\hat{\mathbf{a}}_i) = v(\mathbf{a}_i), i = 1, 2, 3$, we have that

$$\tilde{M}_1^t = [\mathbf{I}_3; \mathbf{0}_{3\times 18}]. \tag{B.5}$$

Construction of submatrix $\tilde{M}_2$:

This submatrix associates with the first derivatives at vertices of the triangles. Since $\hat{w} = v \circ F_K$, we obtain

$$\frac{\partial \hat{w}}{\partial \hat{x}_\alpha}(\hat{\mathbf{a}}_i) = D\hat{w}(\hat{\mathbf{a}}_i)\hat{\mathbf{e}}_\alpha = Dv(x)DF_K(\hat{\mathbf{a}}_i)\hat{\mathbf{e}}_\alpha = Dv(\mathbf{a}_i)\frac{\partial F_K}{\partial \hat{x}_\alpha}(\hat{\mathbf{a}}_i), i = 1, 2, 3, \tag{B.6}$$

and with the definition of the nonlinear mapping depicted in (6.11)

$$\begin{aligned}
&\frac{\partial \hat{w}}{\partial \hat{x}_1}(\hat{\mathbf{a}}_1) = Dv(\mathbf{a}_1)(\mathbf{a}_1 - \mathbf{a}_3), \quad \frac{\partial \hat{w}}{\partial \hat{x}_2}(\hat{\mathbf{a}}_1) = Dv(\mathbf{a}_1)[\mathbf{a}_1 - \mathbf{a}_3 + (s_M - s_m)\chi'(s_m)],\\
&\frac{\partial \hat{w}}{\partial \hat{x}_1}(\hat{\mathbf{a}}_2) = Dv(\mathbf{a}_2)[\mathbf{a}_2 - \mathbf{a}_3 - (s_M - s_m)\chi'(s_M)], \quad \frac{\partial \hat{w}}{\partial \hat{x}_2}(\hat{\mathbf{a}}_2) = Dv(\mathbf{a}_2)(\mathbf{a}_2 - \mathbf{a}_3),\\
&\frac{\partial \hat{w}}{\partial \hat{x}_1}(\hat{\mathbf{a}}_3) = Dv(\mathbf{a}_3)(\mathbf{a}_1 - \mathbf{a}_3), \quad \frac{\partial \hat{w}}{\partial \hat{x}_2}(\hat{\mathbf{a}}_3) = Dv(\mathbf{a}_3)(\mathbf{a}_2 - \mathbf{a}_3).
\end{aligned} \tag{B.7}$$

Hence, we obtain

$$\tilde{M}_2^t = [\mathbf{0}_{6\times 3}; (m_2^t)_{6\times 6}; \mathbf{0}_{6\times 12}], \tag{B.8}$$

with

$$m_2 = \begin{bmatrix} -1 & -1 & 0 & 0 & 0 & 0 \\ 0 & 1 & 0 & 0 & 0 & 0 \\ 0 & 0 & 1 & 0 & 0 & 0 \\ 0 & 0 & -1 & -1 & 0 & 0 \\ 0 & 0 & 0 & 0 & 0 & 1 \\ 0 & 0 & 0 & 0 & 1 & 0 \end{bmatrix}. \tag{B.9}$$

Construction of submatrix $\tilde{M}_3$:

This submatrix associates with the second derivatives at vertices of the triangles. Since $\hat{w} = v \circ F_K$, we obtain, for $i = 1, 2, 3$,

$$\frac{\partial^2 \hat{w}}{\partial \hat{x}_\alpha \partial \hat{x}_\beta}(\hat{\mathbf{a}}_i) = Dv(\mathbf{a}_i)\frac{\partial^2 F_K}{\partial \hat{x}_\alpha \partial \hat{x}_\beta}(\hat{\mathbf{a}}_i) + D^2 v(\mathbf{a}_i)\left(\frac{\partial F_K}{\partial \hat{x}_\alpha}(\hat{\mathbf{a}}_i), \frac{\partial F_K}{\partial \hat{x}_\beta}(\hat{\mathbf{a}}_i)\right). \tag{B.10}$$

With the mapping defined in (6.11), we have

$$
\begin{aligned}
\frac{\partial^2 \hat{w}}{\partial \hat{x}_1^2}(\hat{\mathbf{a}}_1) &= D^2 v(\mathbf{a}_1)(\mathbf{a}_1-\mathbf{a}_3)^2,\\
\frac{\partial^2 \hat{w}}{\partial \hat{x}_1 \partial \hat{x}_2}(\hat{\mathbf{a}}_1) &= D^2 v(\mathbf{a}_1)[\mathbf{a}_1-\mathbf{a}_3, \mathbf{a}_1-\mathbf{a}_3+(s_M-s_m)\chi'(s_m)]\\
&\quad + Dv(\mathbf{a}_1)[2(\mathbf{a}_1-\mathbf{a}_2)+\frac{1}{2}(s_M-s_m)(3\chi'(s_m)+\chi'(s_M))],\\
\frac{\partial^2 \hat{w}}{\partial \hat{x}_2^2}(\hat{\mathbf{a}}_1) &= D^2 v(\mathbf{a}_1)[\mathbf{a}_1-\mathbf{a}_3+(s_M-s_m)\chi'(s_m)]^2\\
&\quad - Dv(\mathbf{a}_1)[2(\mathbf{a}_1-\mathbf{a}_2)+(s_M-s_m)(\chi'(s_m)+\chi'(s_M))],\\
\frac{\partial^2 \hat{w}}{\partial \hat{x}_1^2}(\hat{\mathbf{a}}_2) &= D^2 v(\mathbf{a}_2)[\mathbf{a}_2-\mathbf{a}_3-(s_M-s_m)\chi'(s_M)]^2\\
&\quad - Dv(\mathbf{a}_2)[2(\mathbf{a}_2-\mathbf{a}_1)-(s_M-s_m)(\chi'(s_m)+\chi'(s_M))],\\
\frac{\partial^2 \hat{w}}{\partial \hat{x}_1 \partial \hat{x}_2}(\hat{\mathbf{a}}_2) &= D^2 v(\mathbf{a}_2)[\mathbf{a}_2-\mathbf{a}_3-(s_M-s_m)\chi'(s_M), \mathbf{a}_2-\mathbf{a}_3]\\
&\quad + Dv(\mathbf{a}_2)[2(\mathbf{a}_2-\mathbf{a}_1)-\frac{1}{2}(s_M-s_m)(3\chi'(s_M)+\chi'(s_m))],\\
\frac{\partial^2 \hat{w}}{\partial \hat{x}_2^2}(\hat{\mathbf{a}}_2) &= D^2 v(\mathbf{a}_2)(\mathbf{a}_2-\mathbf{a}_3)^2,\\
\frac{\partial^2 \hat{w}}{\partial \hat{x}_1^2}(\hat{\mathbf{a}}_3) &= D^2 v(\mathbf{a}_3)(\mathbf{a}_1-\mathbf{a}_3)^2,\\
\frac{\partial^2 \hat{w}}{\partial \hat{x}_1 \partial \hat{x}_2}(\hat{\mathbf{a}}_3) &= D^2 v(\mathbf{a}_3)[\mathbf{a}_1-\mathbf{a}_3, \mathbf{a}_2-\mathbf{a}_3]-\frac{1}{2}(s_M-s_m)Dv(\mathbf{a}_3)[\chi'(s_M)-\chi'(s_m)],\\
\frac{\partial^2 \hat{w}}{\partial \hat{x}_2^2}(\hat{\mathbf{a}}_3) &= D^2 v(\mathbf{a}_3)(\mathbf{a}_2-\mathbf{a}_3)^2.
\end{aligned}
\tag{B.11}
$$

Therefore, the submatrix $\tilde{M}_3$ are as follows

$$
\tilde{M}_3^t = [\mathbf{0}_{9\times 3}; (m_{31}^t)_{9\times 6}; (m_{32}^t)_{9\times 9}; \mathbf{0}_{9\times 3}], \tag{B.12}
$$

where matrices m_{31} and m_{32} are given by

$$
m_{31} = \begin{pmatrix}
0 & (2\tilde{a}^1+\frac{1}{2}\tilde{\tilde{a}}^1) & -(2\tilde{a}^1+\tilde{\tilde{a}}^1) & 0 & 0 & 0 & 0 & 0 & 0\\
0 & (\frac{3}{2}+2\tilde{a}^2+\frac{1}{2}\tilde{\tilde{a}}^2) & -(1+2\tilde{a}^2+\tilde{\tilde{a}}^2) & 0 & 0 & 0 & 0 & 0 & 0\\
0 & 0 & 0 & -(1+2\tilde{b}^1-\tilde{\tilde{b}}^1) & (\frac{3}{2}+2\tilde{b}^1-\frac{1}{2}\tilde{\tilde{b}}^1) & 0 & 0 & 0 & 0\\
0 & 0 & 0 & -(2\tilde{b}^2-\tilde{\tilde{b}}^2) & (2\tilde{b}^2-\frac{1}{2}\tilde{\tilde{b}}^2) & 0 & 0 & 0 & 0\\
0 & 0 & 0 & 0 & 0 & 0 & 0 & \frac{1}{2}(\tilde{c}^1+\tilde{\tilde{c}}^1) & 0\\
0 & 0 & 0 & 0 & 0 & 0 & 0 & \frac{1}{2}(\tilde{c}^2+\tilde{\tilde{c}}^2) & 0
\end{pmatrix}, \tag{B.13}
$$

$$m_{32} = \begin{pmatrix} 1 & \left(1+\frac{1+\tilde{a}^1}{2\tilde{a}^2}\right) & \left(1+\frac{1+\tilde{a}^1}{\tilde{a}^2}\right) & 0 & 0 & 0 & 0 & 0 & 0 \\ 1 & \frac{\tilde{a}^2}{2(1+\tilde{a}^1)} & \left(1+\frac{\tilde{a}^2}{1+\tilde{a}^1}\right) & 0 & 0 & 0 & 0 & 0 & 0 \\ 0 & 0 & 0 & \left(1+\frac{\tilde{b}^1}{1+\tilde{b}^2}\right) & \frac{\tilde{b}^1}{2(1+\tilde{b}^2)} & 0 & 0 & 0 & 0 \\ 0 & 0 & 0 & \left(1+\frac{1+\tilde{b}^2}{\tilde{b}^1}\right) & \left(1+\frac{1+\tilde{b}^2}{2\tilde{b}^1}\right) & 1 & 0 & 0 & 0 \\ 0 & 0 & 0 & 0 & 0 & 0 & 0 & -\frac{\tilde{c}^1\tilde{\tilde{c}}^1}{\tilde{c}^1\tilde{\tilde{c}}^2+\tilde{c}^2\tilde{\tilde{c}}^1} & 1 \\ 0 & 0 & 0 & 0 & 0 & 0 & 1 & -\frac{\tilde{c}^2\tilde{\tilde{c}}^2}{\tilde{c}^1\tilde{\tilde{c}}^2+\tilde{c}^2\tilde{\tilde{c}}^1} & 0 \\ 0 & \frac{-1}{2\tilde{a}^2(1+\tilde{a}^1)} & \frac{-1}{\tilde{a}^2(1+\tilde{a}^1)} & 0 & 0 & 0 & 0 & 0 & 0 \\ 0 & 0 & 0 & \frac{-1}{\tilde{b}^1(1+\tilde{b}^2)} & \frac{-1}{2\tilde{b}^1(1+\tilde{b}^2)} & 0 & 0 & 0 & 0 \\ 0 & 0 & 0 & 0 & 0 & 0 & 0 & -\frac{1}{\tilde{c}^1\tilde{\tilde{c}}^2+\tilde{c}^2\tilde{\tilde{c}}^1} & 0 \end{pmatrix}. \tag{B.14}$$

The coefficients of the submatrices m_{31} and m_{32} can be defined as follows. Set

$$\mathbf{A}_1 = \mathbf{a}_3 - \mathbf{a}_1 \quad and \quad \mathbf{A}_2 = (s_M - s_m)\chi'(s_m),$$

and assume that these vectors are linearly independent. Therefore, $\tilde{a}_\alpha$ and $\tilde{\tilde{a}}^\alpha$ are defined by

$$\mathbf{a}_1 - \mathbf{a}_2 = \tilde{a}^\alpha \mathbf{A}_\alpha, \quad (s_M - s_m)\chi'(s_M) = \tilde{\tilde{a}}^\alpha \mathbf{A}_\alpha.$$

Similarly, set

$$\mathbf{B}_1 = -(s_M - s_m)\chi'(s_M) \quad and \quad \mathbf{B}_2 = \mathbf{a}_3 - \mathbf{a}_2,$$

$$\mathbf{a}_2 - \mathbf{a}_1 = \tilde{b}^\alpha \mathbf{B}_\alpha, \quad (s_M - s_m)\chi'(s_m) = \tilde{\tilde{b}}^\alpha \mathbf{B}_\alpha,$$

also,

$$\mathbf{C}_1 = \mathbf{a}_2 - \mathbf{a}_3 \quad and \quad \mathbf{C}_2 = \mathbf{a}_1 - \mathbf{a}_3,$$

$$(s_M - s_m)\chi'(s_m) = \tilde{c}^\alpha \mathbf{C}_\alpha, \quad -(s_M - s_m)\chi'(s_M) = \tilde{\tilde{c}}^\alpha \mathbf{C}_\alpha.$$

From these definitions, all the coefficients can be computed as follows,

$$\begin{aligned}
\tilde{a}_1 &= \frac{(\mathbf{B}_2 \times \mathbf{A}_2)\cdot \mathbf{e}_3}{(\mathbf{A}_1 \times \mathbf{A}_2)\cdot \mathbf{e}_3} - 1, \qquad \tilde{a}_2 = \frac{(\mathbf{A}_1 \times \mathbf{B}_2)\cdot \mathbf{e}_3}{(\mathbf{A}_1 \times \mathbf{A}_2)\cdot \mathbf{e}_3}, \\
\tilde{\tilde{a}}_1 &= -\frac{(\mathbf{B}_1 \times \mathbf{A}_2)\cdot \mathbf{e}_3}{(\mathbf{A}_1 \times \mathbf{A}_2)\cdot \mathbf{e}_3}, \qquad \tilde{\tilde{a}}_2 = -\frac{(\mathbf{A}_1 \times \mathbf{B}_1)\cdot \mathbf{e}_3}{(\mathbf{A}_1 \times \mathbf{A}_2)\cdot \mathbf{e}_3}, \\
\tilde{b}_1 &= \frac{(\mathbf{A}_1 \times \mathbf{B}_2)\cdot \mathbf{e}_3}{(\mathbf{B}_1 \times \mathbf{B}_2)\cdot \mathbf{e}_3}, \qquad \tilde{b}_2 = \frac{(\mathbf{B}_1 \times \mathbf{A}_1)\cdot \mathbf{e}_3}{(\mathbf{B}_1 \times \mathbf{B}_2)\cdot \mathbf{e}_3} - 1, \\
\tilde{\tilde{b}}_1 &= \frac{(\mathbf{A}_2 \times \mathbf{B}_2)\cdot \mathbf{e}_3}{(\mathbf{B}_1 \times \mathbf{B}_2)\cdot \mathbf{e}_3}, \qquad \tilde{\tilde{b}}_2 = \frac{(\mathbf{B}_1 \times \mathbf{A}_2)\cdot \mathbf{e}_3}{(\mathbf{B}_1 \times \mathbf{B}_2)\cdot \mathbf{e}_3}, \\
\tilde{c}_1 &= -\frac{(\mathbf{A}_1 \times \mathbf{A}_2)\cdot \mathbf{e}_3}{(\mathbf{A}_1 \times \mathbf{B}_2)\cdot \mathbf{e}_3}, \qquad \tilde{c}_2 = -\frac{(\mathbf{A}_2 \times \mathbf{B}_2)\cdot \mathbf{e}_3}{(\mathbf{A}_1 \times \mathbf{B}_2)\cdot \mathbf{e}_3}, \\
\tilde{\tilde{c}}_1 &= -\frac{(\mathbf{A}_1 \times \mathbf{B}_1)\cdot \mathbf{e}_3}{(\mathbf{A}_1 \times \mathbf{B}_2)\cdot \mathbf{e}_3}, \qquad \tilde{\tilde{c}}_2 = -\frac{(\mathbf{B}_1 \times \mathbf{B}_2)\cdot \mathbf{e}_3}{(\mathbf{A}_1 \times \mathbf{B}_2)\cdot \mathbf{e}_3},
\end{aligned} \tag{B.15}$$

where $\mathbf{e}_j, j = 1, 2, 3$ denote standard basis vectors in the Cartesian coordinate system in a three-dimensional space.

Construction of submatrix $\tilde{M}_4$:

This submatrix $\tilde{M}_4$ is related to the normal derivatives defined at mid-side nodes of the reference triangle. In particular, we want to have $\tilde{M}_4$ that associates the 21 values defined on the curved element with the degrees of freedom that defined at mid-side nodes of the reference triangle. This can be mathematically described as

$$\left[-\frac{\partial\hat{w}}{\partial\hat{x}_1}(\hat{\mathbf{b}}_1); -\frac{\partial\hat{w}}{\partial\hat{x}_2}(\hat{\mathbf{b}}_2); \frac{\sqrt{2}}{2}\left(\frac{\partial\hat{w}}{\partial\hat{x}_1}+\frac{\partial\hat{w}}{\partial\hat{x}_2}\right)(\hat{\mathbf{b}}_3)\right] = [DL(v)]_{1\times 21}[\tilde{M}_4]_{21\times 3}. \tag{B.16}$$

From (6.38), we have that

$$\begin{aligned}
-\frac{\partial\hat{w}}{\partial\hat{x}_1}(\hat{\mathbf{b}}_1) &= -\langle\frac{\partial F_K}{\partial\hat{x}_1}(\hat{\mathbf{b}}_1), \frac{\mathbf{a}_2-\mathbf{a}_3}{|\mathbf{a}_2-\mathbf{a}_3|^2}\frac{d\hat{f}_2}{d\hat{x}_2}(\hat{\mathbf{b}}_1)+\frac{\mathbf{a}_1-\mathbf{c}_1}{|\mathbf{a}_1-\mathbf{c}_1|^2}\hat{h}_2(\hat{\mathbf{b}}_1)\rangle \\
&= -\langle\frac{\partial F_K}{\partial\hat{x}_1}(\hat{\mathbf{b}}_1), \frac{\mathbf{a}_2-\mathbf{a}_3}{|\mathbf{a}_2-\mathbf{a}_3|^2}\rangle\frac{d\hat{f}_2}{d\hat{x}_2}(\hat{\mathbf{b}}_1)+\langle\frac{\partial F_K}{\partial\hat{x}_1}(\hat{\mathbf{b}}_1), \frac{\mathbf{a}_1-\mathbf{c}_1}{|\mathbf{a}_1-\mathbf{c}_1|^2}\rangle\hat{h}_2(\hat{\mathbf{b}}_1) \\
&= E^1\frac{d\hat{f}_2}{d\hat{x}_2}(\frac{1}{2})+E^2\hat{h}_2(\frac{1}{2}).
\end{aligned} \tag{B.17}$$

where $<,>$ denotes the usual scalar product in $\Re^2$ with the notations $\mathbf{c}_\alpha, \alpha = 1,2$, illustrated in Fig. 6.4. Also, E^1 and E^2 are defined as

$$\begin{aligned}
E^1 &= \langle\mathbf{a}_3-\mathbf{a}_1+\frac{1}{4}(\mathbf{a}_1-\mathbf{a}_2)+\frac{1}{8}(s_M-s_m)\left(3\chi'(s_M)-\chi'(s_m)\right), \frac{\mathbf{a}_2-\mathbf{a}_3}{|\mathbf{a}_2-\mathbf{a}_3|^2}\rangle, \\
E^2 &= \langle\mathbf{a}_3-\mathbf{a}_1+\frac{1}{4}(\mathbf{a}_1-\mathbf{a}_2)+\frac{1}{8}(s_M-s_m)\left(3\chi'(s_M)-\chi'(s_m)\right), \frac{\mathbf{a}_1-\mathbf{c}_1}{|\mathbf{a}_1-\mathbf{c}_1|^2}\rangle,
\end{aligned} \tag{B.18}$$

since the derivative of the nonlinear mapping F_K with respect to $\hat{x}_1$ involves

$$-\frac{\partial F_K}{\partial\hat{x}_1}(\hat{\mathbf{b}}_1) = \mathbf{a}_3-\mathbf{a}_1+\frac{1}{4}(\mathbf{a}_1-\mathbf{a}_2)+\frac{1}{8}(s_M-s_m)\left(3\chi'(s_M)-\chi'(s_m)\right). \tag{B.19}$$

Now, for our convenience later on, we introduce the functions $\hat{\mathcal{F}}_i; i = 1,2,3$ and $\hat{\mathcal{H}}_i; i = 1,2,3$ as

$$[\hat{f}_1(\hat{x}_1); \hat{f}_2(\hat{x}_2); \hat{f}_3(\hat{x}_1)] = [DL(v)]_{1\times 21}[\hat{\mathcal{F}}_1(\hat{x}_1); \hat{\mathcal{F}}_2(\hat{x}_2); \hat{\mathcal{F}}_3(\hat{x}_1)]_{21\times 3}, \tag{B.20}$$

$$[\hat{h}_1(\hat{x}_1); \hat{h}_2(\hat{x}_2); \hat{h}_3(\hat{x}_1)] = [DL(v)]_{1\times 21}[\hat{\mathcal{H}}_1(\hat{x}_1); \hat{\mathcal{H}}_2(\hat{x}_2); \hat{\mathcal{H}}_3(\hat{x}_1)]_{21\times 3}. \tag{B.21}$$

By the definitions in (6.24), (6.28), (6.42), (6.29), (6.32), and (6.42), we have

$$\begin{aligned}
\left[\hat{\mathcal{F}}_1(\hat{x}_1)\right] = \big[&\hat{x}_1^3(6\hat{x}_1^2-15\hat{x}_1+10); 0; (1-\hat{x}_1)^3(6\hat{x}_1^2+3\hat{x}_1+1); \\
&\hat{x}_1^3(1-\hat{x}_1)(4-3\hat{x}_1); 0; 0; 0; 0; \hat{x}_1(1-\hat{x}_1)^3(1+3\hat{x}_1); \\
&\frac{1}{2}\hat{x}_1^3(1-\hat{x}_1)^2; 0; 0; 0; 0; \frac{1}{2}\hat{x}_1^2(1-\hat{x}_1)^3; 0; 0; 0; 0; 0; 0\big]
\end{aligned} \tag{B.22}$$

$$\begin{aligned}\left[\hat{\mathcal{F}}_2(\hat{x}_2)\right] = \big[&0; \hat{x}_2^3(6\hat{x}_2^2 - 15\hat{x}_2 + 10); (1-\hat{x}_2)^3(6\hat{x}_2^2 + 3\hat{x}_2 + 1);\\ &0;0;0; \hat{x}_2^3(1-\hat{x}_2)(4-3\hat{x}_2); \hat{x}_2(1-\hat{x}_2)^3(1+3\hat{x}_2); 0;0;0;0;\\ &\frac{1}{2}\hat{x}_2^3(1-\hat{x}_2)^2; \frac{1}{2}\hat{x}_2^2(1-\hat{x}_2)^3; 0;0;0;0;0;0;0\Big]\end{aligned} \tag{B.23}$$

$$\begin{aligned}\left[\hat{\mathcal{F}}_3(\hat{x}_1)\right] = \big[&\hat{x}_1^3(6\hat{x}_1^2 - 15\hat{x}_1 + 10); (1-\hat{x}_1)^3(6\hat{x}_1^2 + 3\hat{x}_1 + 1); 0;\\ &-(3\tilde{a}^1 + \tilde{\tilde{a}}^1)\hat{x}_1^3(1-\hat{x}_1)^2; \hat{x}_1^3(1-\hat{x}_1)\{2 - \hat{x}_1 - (1-\hat{x}_1)(3\tilde{a}^2 + \tilde{\tilde{a}}^2)\};\\ &\hat{x}_1(1-\hat{x}_1)^3\{1 + \hat{x}_1 - \hat{x}_1(3\tilde{b}^1 - \tilde{\tilde{b}}^1)\}; -\hat{x}_1^2(1-\hat{x}_1)^3(3\tilde{b}^2 - \tilde{\tilde{b}}^2);\\ &0;0;0; \frac{1}{2}\hat{x}_1^3(1-\hat{x}_1)^2; \frac{1}{2}\hat{x}_1^2(1-\hat{x}_1)^3; 0;0;0;0;0;0;0;0;0\Big]\end{aligned} \tag{B.24}$$

$$\begin{aligned}\left[\hat{\mathcal{H}}_1(\hat{x}_1)\right] = \Bigg[&0;0;0; -\frac{1}{2}(1 - \eta_2 + 2\tilde{a}^1)\hat{x}_1^2(2\hat{x}_1 - 1)(5 - 4\hat{x}_1);\\ &-\tilde{a}^2\hat{x}_1^2(2\hat{x}_1 - 1)(5 - 4\hat{x}_1); 0;0; (1-\hat{x}_1)^2(1-2\hat{x}_1)(1+4\hat{x}_1);\\ &-\frac{1}{2}(1+\eta_2)(1-\hat{x}_1)^2(1-2\hat{x}_1)(1+4\hat{x}_1); \frac{1}{2}(\tilde{a}^1 - \eta_2)\hat{x}_1^2(1-\hat{x}_1)(1-2\hat{x}_1);\\ &-\frac{1}{2}\frac{(\tilde{a}^2)^2}{1+\tilde{a}^1}\hat{x}_1^2(1-\hat{x}_1)(1-2\hat{x}_1); 0;0; \frac{-\tilde{c}^1\tilde{\tilde{c}}^1}{\tilde{c}^1\tilde{\tilde{c}}^2 + \tilde{c}^2\tilde{\tilde{c}}^1}\hat{x}_1(1-\hat{x}_1)^2(1-2\hat{x}_1);\\ &-\left\{\frac{1}{2}(1+\eta_2) + \frac{\tilde{c}^2\tilde{\tilde{c}}^2}{\tilde{c}^1\tilde{\tilde{c}}^2 + \tilde{c}^2\tilde{\tilde{c}}^1}\right\}\hat{x}_1(1-\hat{x}_1)^2(1-2\hat{x}_1); \frac{\hat{x}_1^2(1-\hat{x}_1)(1-2\hat{x}_1)}{2(1+\tilde{a}^1)};\\ &0; \frac{-1}{\tilde{c}^1\tilde{\tilde{c}}^2 + \tilde{c}^2\tilde{\tilde{c}}^1}\hat{x}_1(1-\hat{x}_1)^2(1-2\hat{x}_1); 0;0;0\Bigg]\end{aligned} \tag{B.25}$$

$$\begin{aligned}\left[\hat{\mathcal{H}}_2(\hat{x}_2)\right] = \Big[&0;0;0;0;0;-\tilde{b}^1\hat{x}_2^2(2\hat{x}_2-1)(5-4\hat{x}_2);\\ &-\frac{1}{2}(2\tilde{b}^2+1+\eta_1)\hat{x}_2^2(2\hat{x}_2-1)(5-4\hat{x}_2);\\ &-\frac{1}{2}(1-\eta_1)(1-\hat{x}_2)^2(1-2\hat{x}_2)(1+4\hat{x}_2);\\ &(1-\hat{x}_2)^2(1-2\hat{x}_2)(1+4\hat{x}_2);0;0;-\frac{1}{2}\frac{(\tilde{b}^1)^2}{1+\tilde{b}^2}\hat{x}_2^2(1-\hat{x}_2)(1-2\hat{x}_2);\\ &\frac{1}{2}(\tilde{b}^2+\eta_1)\hat{x}_2^2(1-\hat{x}_1)(1-2\hat{x}_1);\\ &-\frac{1}{2}\left(\frac{2\tilde{c}^1\tilde{\tilde{c}}^1}{\tilde{c}^1\tilde{\tilde{c}}^2+\tilde{c}^2\tilde{\tilde{c}}^1}+1-\eta_2\right)\hat{x}_2(1-\hat{x}_2)^2(1-2\hat{x}_2);\\ &-\frac{\tilde{c}^2\tilde{\tilde{c}}^2}{\tilde{c}^1\tilde{\tilde{c}}^2+\tilde{c}^2\tilde{\tilde{c}}^1}\hat{x}_2(1-\hat{x}_2)^2(1-2\hat{x}_2);0;\frac{1}{2}\frac{1}{1+\tilde{b}^2}\hat{x}_2^2(1-\hat{x}_2)(1-2\hat{x}_2);\\ &-\frac{1}{\tilde{c}^1\tilde{\tilde{c}}^2+\tilde{c}^2\tilde{\tilde{c}}^1}\hat{x}_2(1-\hat{x}_2)^2(1-2\hat{x}_2);0;0;0\Big]\end{aligned} \tag{B.26}$$

$$\begin{aligned}\left[\hat{\mathcal{H}}_3(\hat{x}_1)\right] = \Big[&0;0;0;\hat{x}_1^2(3-2\hat{x}_1)+(\tilde{a}^1+\frac{\tilde{\tilde{a}}^1}{2})\hat{x}_1^2(1-\hat{x}_1);\\ &\hat{x}_1^2(\hat{x}_1-\frac{3}{2})+(\frac{1}{2}+\tilde{a}^2+\frac{\tilde{\tilde{a}}^2}{2})\hat{x}_1^2(1-\hat{x}_1);\\ &-\frac{1}{2}+\frac{3}{2}\hat{x}_1^2-\hat{x}_1^3+\frac{1}{2}(2\tilde{b}^1-\tilde{\tilde{b}}^1+1)\hat{x}_1(1-2\hat{x}_1-\hat{x}_1^2);\\ &1+\frac{1}{2}(2\tilde{b}^2-\tilde{\tilde{b}}^2)\hat{x}_1-(2\tilde{b}^2-\tilde{\tilde{b}}^2+3)\hat{x}_1^2+(2-\frac{2\tilde{b}^2-\tilde{\tilde{b}}^2}{2})\hat{x}_1^3;0;0;\\ &\frac{1+\tilde{a}^1}{2\tilde{a}^2}\hat{x}_1^2(\hat{x}_1-1);\frac{1}{2}(1+\frac{\tilde{a}^2}{1+\tilde{a}^1})\hat{x}_1^2(\hat{x}_1-1);\\ &\frac{1}{2}(1+\frac{\tilde{b}^1}{1+\tilde{b}^2})\hat{x}_1(-1+2\hat{x}_1+\hat{x}_1^2);\frac{1+\tilde{b}^2}{2\tilde{b}^1}\hat{x}_1(-1+2\hat{x}_1+\hat{x}_1^2);\\ &0;0;-\frac{1}{2(1+\tilde{a}^1)\tilde{a}^2}\hat{x}_1^2(\hat{x}_1-1);\\ &-\frac{1}{2\tilde{b}^1(1+\tilde{b}^2)}\hat{x}_1(-1+2\hat{x}_1+\hat{x}_1^2);0;0;0;0\Big]\end{aligned} \tag{B.27}$$

Note that we have used the eccentricity parameters η_1 and η_2 of the curved triangle K_C which are given by

$$\begin{aligned}\mathbf{a}_1-\mathbf{c}_1 &= \mathbf{a}_1-\mathbf{a}_2-\frac{1}{2}(1+\eta_1)(\mathbf{a}_3-\mathbf{a}_2)\\ \mathbf{a}_2-\mathbf{c}_2 &= \mathbf{a}_2-\mathbf{a}_1-\frac{1}{2}(1-\eta_2)(\mathbf{a}_3-\mathbf{a}_1).\end{aligned} \tag{B.28}$$

Hence, (B.17), (B.22), and (B.26) give

$$-\frac{\partial\hat{w}}{\partial\hat{x}_1}(\hat{\mathbf{b}}_1) = [DL(v)]_{1\times 21}[E^1\frac{d}{d\hat{x}_2}\hat{\mathcal{F}}_2(\frac{1}{2})+E^2\hat{\mathcal{H}}_2(\frac{1}{2})]_{21\times 1}, \tag{B.29}$$

By similarity, we obtain

$$-\frac{\partial \hat{w}}{\partial \hat{x}_2}(\hat{\mathbf{b}}_2) = [DL(v)]_{1\times 21}[F^1 \frac{d}{d\hat{x}_1}\hat{\mathcal{F}}_1(\frac{1}{2}) + F^2\hat{\mathcal{H}}_1(\frac{1}{2})]_{21\times 1}, \tag{B.30}$$

where F^1 and F^2 are defined as

$$\begin{aligned} F^1 &= \langle \mathbf{a}_3 - \mathbf{a}_2 + \frac{1}{4}(\mathbf{a}_2 - \mathbf{a}_1) - \frac{1}{8}(s_M - s_m)\left(3\chi'(s_m) - \chi'(s_M)\right), \frac{\mathbf{a}_1 - \mathbf{a}_3}{|\mathbf{a}_1 - \mathbf{a}_3|^2}\rangle, \\ F^2 &= \langle \mathbf{a}_3 - \mathbf{a}_2 + \frac{1}{4}(\mathbf{a}_2 - \mathbf{a}_1) - \frac{1}{8}(s_M - s_m)\left(3\chi'(s_m) - \chi'(s_M)\right), \frac{\mathbf{a}_2 - \mathbf{c}_2}{|\mathbf{a}_2 - \mathbf{c}_2|^2}\rangle. \end{aligned} \tag{B.31}$$

Also, (6.42) gives

$$-\frac{\sqrt{2}}{2}\left(\frac{\partial \hat{w}}{\partial \hat{x}_1} + \frac{\partial \hat{w}}{\partial \hat{x}_2}\right)(\hat{\mathbf{b}}_3) = [DL(v)]_{1\times 21}[\sqrt{2}\hat{\mathcal{H}}_3(\frac{1}{2})]_{21\times 1}. \tag{B.32}$$

Thus, the submatrix $\tilde{M}_4$ can be written as

$$\tilde{M}_4 = [E^1\frac{d\hat{\mathcal{F}}_2}{d\hat{x}_2}(\frac{1}{2}) + E^2\hat{\mathcal{H}}_2(\frac{1}{2}); F^1\frac{d\hat{\mathcal{F}}_1}{d\hat{x}_1}(\frac{1}{2}) + F^2\hat{\mathcal{H}}_1(\frac{1}{2}); -\sqrt{2}\hat{\mathcal{H}}_3(\frac{1}{2})]. \tag{B.33}$$

Construction of submatrix $\tilde{M}_5$:

The submatrix $\tilde{M}_5$ will deal with values at nodes $\hat{\mathbf{d}}_i; i = 1,2,3,4,5,6$ along the edges of the reference triangle. Since the trace of the interpolate function restricted on the sides for the nodes $\mathbf{d}_i; i = 1,...,6$ have to coincide with the one-variable P5-Hermite polynomial $\hat{f}_1$ $\hat{f}_2$, and $\hat{f}_3$ (see (6.24), (6.28), (6.42)), it can be obviously obtained as

$$\begin{aligned} &\left[\hat{w}(\hat{\mathbf{d}}_1); \hat{w}(\hat{\mathbf{d}}_2); \hat{w}(\hat{\mathbf{d}}_3); \hat{w}(\hat{\mathbf{d}}_4); \hat{w}(\hat{\mathbf{d}}_5); \hat{w}(\hat{\mathbf{d}}_6)\right] \\ &= [\hat{f}_2(\frac{3}{4}); \hat{f}_2(\frac{1}{4}); \hat{f}_1(\frac{1}{4}); \hat{f}_1(\frac{3}{4}); \hat{f}_3(\frac{3}{4}); \hat{f}_3(\frac{1}{4})] \end{aligned} \tag{B.34}$$

Therefore, (B.22), (B.23), and (B.24) gives

$$\tilde{M}_5 = [\hat{\mathcal{F}}_2(\frac{3}{4}); \hat{\mathcal{F}}_2(\frac{1}{4}); \hat{\mathcal{F}}_1(\frac{1}{4}); \hat{\mathcal{F}}_1(\frac{3}{4}); \hat{\mathcal{F}}_3(\frac{3}{4}); \hat{\mathcal{F}}_3(\frac{1}{4})]. \tag{B.35}$$

Construction of submatrix $\tilde{M}_6$:

The submatrix $\tilde{M}_6$ will deal with the derivatives at nodes $\hat{\mathbf{d}}_i; i = 1,2,3,4,5,6$ along the edges of the reference triangle. By Similarity as described in (B.17), the submatrix $\tilde{M}_6$ is given as

$$\begin{aligned} \tilde{M}_6 = \Bigg[&G^1\frac{d\hat{\mathcal{F}}_2}{d\hat{x}_2}(\frac{3}{4}) + G^2\hat{\mathcal{H}}_2(\frac{3}{4}); H^1\frac{d\hat{\mathcal{F}}_2}{d\hat{x}_2}(\frac{1}{4}) + H^2\hat{\mathcal{H}}_2(\frac{1}{4}); J^1\frac{d\hat{\mathcal{F}}_1}{d\hat{x}_1}(\frac{1}{4}) + J^2\hat{\mathcal{H}}_1(\frac{1}{4}); \\ &K^1\frac{d\hat{\mathcal{F}}_1}{d\hat{x}_1}(\frac{3}{4}) + K^2\hat{\mathcal{H}}_1(\frac{3}{4}); -\sqrt{2}\hat{\mathcal{H}}_3(\frac{3}{4}); -\sqrt{2}\hat{\mathcal{H}}_3(\frac{1}{4})\Bigg]. \end{aligned} \tag{B.36}$$

where we have set

$$
\begin{aligned}
G^1 &= -\langle \mathbf{a}_1 - \mathbf{a}_3 + \frac{9}{16}(\mathbf{a}_2 - \mathbf{a}_1) + \frac{3}{32}(s_M - s_m)\left(\chi'(s_m) - 7\chi'(s_M)\right), \frac{\mathbf{a}_2 - \mathbf{a}_3}{|\mathbf{a}_2 - \mathbf{a}_3|^2}\rangle,\\
G^2 &= -\langle \mathbf{a}_1 - \mathbf{a}_3 + \frac{9}{16}(\mathbf{a}_2 - \mathbf{a}_1) + \frac{3}{32}(s_M - s_m)\left(\chi'(s_m) - 7\chi'(s_M)\right), \frac{\mathbf{a}_1 - \mathbf{c}_1}{|\mathbf{a}_1 - \mathbf{c}_1|^2}\rangle,\\
H^1 &= -\langle \mathbf{a}_1 - \mathbf{a}_3 + \frac{1}{16}(\mathbf{a}_2 - \mathbf{a}_1) + \frac{1}{32}(s_M - s_m)\left(3\chi'(s_m) - 5\chi'(s_M)\right), \frac{\mathbf{a}_2 - \mathbf{a}_3}{|\mathbf{a}_2 - \mathbf{a}_3|^2}\rangle,\\
H^2 &= -\langle \mathbf{a}_1 - \mathbf{a}_3 + \frac{1}{16}(\mathbf{a}_2 - \mathbf{a}_1) + \frac{1}{32}(s_M - s_m)\left(3\chi'(s_m) - 5\chi'(s_M)\right), \frac{\mathbf{a}_1 - \mathbf{c}_1}{|\mathbf{a}_1 - \mathbf{c}_1|^2}\rangle,\\
J^1 &= -\langle \mathbf{a}_2 - \mathbf{a}_3 + \frac{1}{16}(\mathbf{a}_1 - \mathbf{a}_2) - \frac{1}{32}(s_M - s_m)\left(3\chi'(s_M) - 5\chi'(s_m)\right), \frac{\mathbf{a}_1 - \mathbf{a}_3}{|\mathbf{a}_1 - \mathbf{a}_3|^2}\rangle,\\
J^2 &= -\langle \mathbf{a}_2 - \mathbf{a}_3 + \frac{1}{16}(\mathbf{a}_1 - \mathbf{a}_2) - \frac{1}{32}(s_M - s_m)\left(3\chi'(s_M) - 5\chi'(s_m)\right), \frac{\mathbf{a}_2 - \mathbf{c}_2}{|\mathbf{a}_2 - \mathbf{c}_2|^2}\rangle,\\
K^1 &= -\langle \mathbf{a}_2 - \mathbf{a}_3 + \frac{9}{16}(\mathbf{a}_1 - \mathbf{a}_2) - \frac{3}{32}(s_M - s_m)\left(\chi'(s_M) - 7\chi'(s_m)\right), \frac{\mathbf{a}_1 - \mathbf{a}_3}{|\mathbf{a}_1 - \mathbf{a}_3|^2}\rangle,\\
K^2 &= -\langle \mathbf{a}_2 - \mathbf{a}_3 + \frac{9}{16}(\mathbf{a}_1 - \mathbf{a}_2) - \frac{3}{32}(s_M - s_m)\left(\chi'(s_M) - 7\chi'(s_m)\right), \frac{\mathbf{a}_2 - \mathbf{c}_2}{|\mathbf{a}_2 - \mathbf{c}_2|^2}\rangle,
\end{aligned}
\tag{B.37}
$$

Construction of submatrix $\tilde{M}_7$:

Here, we define the submatrix which associates the value defined in the internal nodes of the curved triangle. Since $\hat{w}(\hat{\mathbf{e}}_i) = v(\mathbf{e}_i), i = 1, 2, 3$, it can be clearly seen that

$$\tilde{M}_7^t = [\mathbf{0}_{3\times 18}; \mathbf{I}_{3\times 3}]. \tag{B.38}$$

From the constructions that have been illustrated, the interpolating function $\Pi_K v$ of the function v which takes the values on the set of degrees of freedom in (B.2) can be determined as

$$\Pi_K v(x) = \hat{w}(\hat{x}) = [DL(v)]_{1\times 21}[\tilde{M}]_{21\times 36}[p]_{36\times 1}, \tag{B.39}$$

where $[p]$ denotes the column matrix of basis polynomials of degrees less than or equal to 7. These basis polynomials can be determined from the Kronecker delta property for shape functions which states that a shape function at any node has a value of 1 when evaluates at that node and a value of zero when evaluates at all other nodes. They can be written as

$$[p]_{36} = [A]_{36\times 36}[m7]_{36\times 1}, \tag{B.40}$$

where the coefficients $[A]_{36\times 36}$ are shown in Figs. B.1 and B.2. Also, $[m7]_{36\times 1}$ is

illustrated as

$$\begin{aligned}[m7] = \big[&1, \hat{x}_1, \hat{x}_2, \hat{x}_1^2, \hat{x}_1\hat{x}_2, \hat{x}_2^2, \hat{x}_1^3, \hat{x}_1^2\hat{x}_2, \hat{x}_1\hat{x}_2^2, \hat{x}_2^3,\\ &\hat{x}_1^4, \hat{x}_1^3\hat{x}_2, \hat{x}_1^2\hat{x}_2^2, \hat{x}_1\hat{x}_2^3, \hat{x}_2^4,\\ &\hat{x}_1^5, \hat{x}_1^4\hat{x}_2, \hat{x}_1^3\hat{x}_2^2, \hat{x}_1^2\hat{x}_2^3, \hat{x}_1\hat{x}_2^4, \hat{x}_2^5,\\ &\hat{x}_1^6, \hat{x}_1^5\hat{x}_2, \hat{x}_1^4\hat{x}_2^2, \hat{x}_1^3\hat{x}_2^3, \hat{x}_1^2\hat{x}_2^4, \hat{x}_1\hat{x}_2^5, \hat{x}_2^6,\\ &\hat{x}_1^7, \hat{x}_1^6\hat{x}_2, \hat{x}_1^5\hat{x}_2^2, \hat{x}_1^4\hat{x}_2^3, \hat{x}_1^3\hat{x}_2^4, \hat{x}_1^2\hat{x}_2^5, \hat{x}_1\hat{x}_2^6, \hat{x}_2^7\big] .\end{aligned} \tag{B.41}$$

```
A(0,0) = 6496.0/27.0
A(0,2) = 55376.0/27.0
A(0,3) = 15296.0/3.0
A(0,4) = 86464.0/27.0
A(0,5) = 464.0/3.0
A(0,8) = -6896.0/9.0;
A(0,10) = -136424.0/27.0;
A(0,11) = -187040.0/27.0;
A(0,12) = -27880.0/27.0;
A(0,15) = 7750.0/9.0;
A(0,17) = 98371.0/27.0;
A(0,18) = 41027.0/27.0;
A(0,21) = -10501.0/27.0;
A(0,23) = -17323.0/27.0;
A(0,26) = 490.0/9.0;
A(1,2) = 464.0/3.0;
A(1,3) = 86464.0/27.0;
A(1,4) = 15296.0/3.0;
A(1,5) = 55376.0/27.0;
A(1,7) = 6496.0/27.0;
A(1,10) = -27880.0/27.0;
A(1,11) = -187040.0/27.0;
A(1,12) = -136424.0/27.0;
A(1,14) = -6896.0/9.0;
A(1,17) = 41027.0/27.0;
A(1,18) = 98371.0/27.0;
A(1,20) = 7750.0/9.00;
A(1,23) = -17323.0/27.0;
A(1,25) = -10501.0/27.0;
A(1,29) = 490.00/9.0;
A(2,0) = -6496.00/27.0;
A(2,2) = 14176.00/27.00;
A(2,3) = -2944.00/27.00;
A(2,4) = -2944.00/27.00;
A(2,5) = 14176.00/27.00;
A(2,7) = -6496.00/27.00;
A(2,8) = 24784.00/27.00;
A(2,10) = -5680.00/27.00;
A(2,11) = 12736.00/9.00;
A(2,12) = -5680.00/27.00;
A(2,14) = 24784.00/27.00;
A(2,15) = -11846.00/9.00;
A(2,17) = -26758.00/27.00;
A(2,18) = -26758.00/27.00;
A(2,20) = -11846.00/9.00;
A(2,21) = 22789.00/27.00;
A(2,23) = 18262.00/27.00;
A(2,25) = 22789.00/27.00;
A(2,26) = -5566.00/27.00;
A(2,29) = -5566.00/27.00;
A(2,35) = 1.00;
A(3,0) = -400.00/9.00;
A(3,2) = -3080.00/9.00;
A(3,3) = -816.00;
A(3,4) = -4496.00/9.00;
A(3,5) = -232.00/9.00;
A(3,8) = 416.00/3.00;
A(3,10) = 7448.00/9.00;
A(3,11) = 9872.00/9.00;
A(3,12) = 1472.00/9.00;
A(3,15) = -457.00/3.00;
A(3,17) = -1177.00/2.00;
A(3,18) = -4337.00/18.00;
A(3,21) = 607.00/9.00;
A(3,23) = 619.00/6.00;
A(3,26) = -28.00/3.00;
A(4,1) = -896.00/9.00;
A(4,2) = -392.00/9.00;
A(4,3) = 2384.00/9.00;
A(4,4) = 2512.00/9.00;
A(4,5) = 232.00/9.00;
A(4,9) = 2336.00/9.00;
A(4,10) = -8.00/9.00;
A(4,11) = -3920.00/9.00;
A(4,12) = -976.00/9.00;
A(4,16) = -2104.00/9.00;
A(4,17) = 123.00/2.00;
A(4,18) = 1981.00/18.00;
A(4,22) = 766.00/9.00;
A(4,23) = -307.00/18.00;
A(4,27) = -31.00/3.00;
A(5,2) = 232.00/9.00;
A(5,3) = 2512.00/9.00;
A(5,4) = 2384.00/9.00;
A(5,5) = -392.00/9.00;
A(5,6) = -896.00/9.00;
A(5,10) = -976.00/9.00;
A(5,11) = -3920.00/9.00;
A(5,12) = -8.00/9.00;
A(5,13) = 2336.00/9.00;
A(5,17) = 1981.00/18.00;
A(5,18) = 123.00/2.00;
A(5,19) = -2104.00/9.00;
A(5,23) = -307.00/18.00;
A(5,24) = 766.00/9.00;
A(5,28) = -31.00/3.00;
A(6,2) = -232.00/9.00;
A(6,3) = -4496.00/9.00;
A(6,4) = -816.00;
A(6,5) = -3080.00/9.00;
A(6,7) = -400.00/9.00;
A(6,10) = 1472.00/9.00;
A(6,11) = 9872.00/9.00;
A(6,12) = 7448.00/9.00;
A(6,14) = 416.00/3.00;
A(6,17) = -4337.00/18.00;
A(6,18) = -1177.00/2.00;
A(6,20) = -457.00/3.00;
A(6,23) = 619.00/6.00;
A(6,25) = 607.00/9.00;
A(6,29) = -28.00/3.00;
A(7,0) = -400.00/9.00;
A(7,2) = 1456.00/9.00;
A(7,3) = -992.00/9.00;
A(7,4) = -5248.00/9.00;
A(7,5) = -4096.00/9.00;
A(7,6) = -896.00/9.00;
A(7,8) = 1552.00/9.00;
A(7,10) = -464.00/3.00;
A(7,11) = 2464.00/3.00;
A(7,12) = 3424.00/3.00;
A(7,13) = 3040.00/9.00;
A(7,15) = -761.00/3.00;
A(7,17) = -1831.00/9.00;
A(7,18) = -938.00;
A(7,19) = -1288.00/3.00;
A(7,21) = 1528.00/9.00;
A(7,23) = 2266.00/9.00;
A(7,24) = 2210.00/9.00;
A(7,26) = -406.00/9.00;
A(7,28) = -499.00/9.00;
A(7,33) = 1.00;
A(8,1) = -896.00/9.00;
A(8,2) = -4096.00/9.00;
A(8,3) = -5248.00/9.00;
A(8,4) = -992.00/9.00;
A(8,5) = 1456.00/9.00;
A(8,7) = -400.00/9.00;
A(8,9) = 3040.00/9.00;
A(8,10) = 3424.00/3.00;
A(8,11) = 2464.00/3.00;
A(8,12) = -464.00/3.00;
A(8,14) = 1552.00/9.00;
A(8,16) = -1288.00/3.00;
A(8,17) = -938.00;
A(8,18) = -1831.00/9.00;
A(8,20) = -761.00/3.00;
A(8,22) = 2210.00/9.00;
A(8,23) = 2266.00/9.00;
A(8,25) = 1528.00/9.00;
A(8,27) = -499.00/9.00;
A(8,29) = -406.00/9.00;
A(8,34) = 1.00;
A(9,0) = 8.00/3.00;
A(9,2) = 52.00/3.00;
A(9,3) = 40.00;
A(9,4) = 24.00;
A(9,5) = 4.00/3.00;
A(9,8) = -8.00;
A(9,10) = -124.00/3.00;
A(9,11) = -160.00/3.00;
A(9,12) = -8.00;
A(9,15) = 17.00/2.00;
A(9,17) = 349.00/12.00;
A(9,18) = 47.00/4.00;
A(9,21) = -11.00/3.00;
A(9,23) = -61.00/12.00;
A(9,26) = 1.00/2.00;
A(10,1) = 32.00/3.00;
A(10,2) = 8.00/3.00;
A(10,3) = -80.00/3.00;
A(10,4) = -80.00/3.00;
A(10,5) = -8.00/3.00;
A(10,9) = -80.00/3.00;
A(10,10) = 8.00/3.00;
A(10,11) = 128.00/3.00;
A(10,12) = 32.00/3.00;
A(10,16) = 70.00/3.0;
A(10,17) = -43.0/6.0;
A(10,18) = -65.0/6.0;
A(10,22) = -25.0/3.0;
A(10,23) = 11.0/6.0;
A(10,27) = 1.0;
A(11,2) = 4.0;
A(11,3) = 40.0/3.0;
A(11,4) = 40.0/3.0;
A(11,5) = 4.0/3.0;
A(11,10) = -28.0/3.0;
A(11,11) = -64.0/3.0;
A(11,12) = -16.0/3.0;
A(11,17) = 29.0/4.0;
A(11,18) = 65.0/12.0;
A(11,23) = -17.0/12.0;
A(12,2) = 4.0/3.0;
A(12,3) = 40.0/3.0;
A(12,4) = 40.0/3.0;
A(12,5) = 4.0;
A(12,10) = -16.0/3.0;
A(12,11) = -64.0/3.0;
A(12,12) = -28.0/3.0;
A(12,17) = 65.0/12.0;
A(12,18) = 29.0/4.0;
A(12,23) = -17.0/12.0;
A(13,2) = -8.0/3.0;
A(13,3) = -80.0/3.0;
A(13,4) = -80.0/3.0;
A(13,5) = 8.0/3.0;
A(13,6) = 32.0/3.0;
A(13,10) = 32.0/3.0;
A(13,11) = 128.0/3.0;
A(13,12) = 8.0/3.0;
A(13,13) = -80.0/3.0;
A(13,17) = -65.0/6.0;
A(13,18) = -43.0/6.0;
A(13,19) = 70.0/3.0;
A(13,23) = 11.0/6.0;
A(13,24) = -25.0/3.0;
A(13,28) = 1.0;
A(14,2) = 4.0/3.0;
A(14,3) = 24.0;
A(14,4) = 40.0;
A(14,5) = 52.0/3.0;
A(14,7) = 8.0/3.0;
A(14,10) = -8.0;
A(14,11) = -160.0/3.0;
A(14,12) = -124.0/3.0;
A(14,14) = -8.0;
A(14,17) = 47.0/4.0;
A(14,18) = 349.0/12.0;
A(14,20) = 17.0/2.0;
A(14,23) = -61.0/12.0;
A(14,25) = -11.0/3.0;
A(14,29) = 1.0/2.0;
A(15,0) = -8.0/3.0;
A(15,2) = 56.0/3.0;
A(15,3) = 80.0/3.0;
A(15,4) = 32.0/3.0;
A(15,8) = 32.0/3.0;
A(15,10) = -40.0;
A(15,11) = -32.0;
A(15,12) = -8.0/3.0;
A(15,15) = -33.0/2.0;
A(15,17) = 51.0/2.0;
A(15,18) = 19.0/3.0;
A(15,21) = 73.0/6.0;
A(15,23) = -25.0/6.0;
A(15,26) = -25.0/6.0;
A(15,30) = 1.0/2.0;
A(16,1) = -32.0/3.0;
A(16,2) = -160.0/3.0;
A(16,3) = -320.0/3.0;
A(16,4) = -320.0/3.0;
A(16,5) = -160.0/3.0;
A(16,6) = -32.0/3.0;
A(16,9) = 112.0/3.0;
A(16,10) = 448.0/3.0;
A(16,11) = 224.0;
A(16,12) = 448.0/3.0;
A(16,13) = 112.0/3.0;
A(16,16) = -50.0;
A(16,17) = -150.0;
A(16,18) = -150.0;
A(16,19) = -50.0;
A(16,22) = 95.0/3.0;
A(16,23) = 190.0/3.0;
A(16,24) = 95.0/3.0;
A(16,27) = -28.0/3.0;
A(16,28) = -28.0/3.0;
A(16,31) = 1.0;
A(17,3) = 32.0/3.0;
A(17,4) = 80.0/3.0;
A(17,5) = 56.0/3.0;
A(17,7) = -8.0/3.0;
A(17,10) = -8.0/3.0;
A(17,11) = -32.0;
A(17,12) = -40.0;
A(17,14) = 32.0/3.0;
A(17,17) = 19.0/3.0;
A(17,18) = 51.0/2.0;
A(17,20) = -33.0/2.0;
A(17,23) = -25.0/6.0;
A(17,25) = 73.0/6.0;
A(17,29) = -25.0/6.0;
A(17,32) = 1.0/2.0;
A(18,3) = 256.0;
A(18,4) = 768.0;
A(18,5) = 768.0;
A(18,6) = 256.0;
A(18,10) = -64.0;
A(18,11) = -896.0;
A(18,12) = -1600.0;
A(18,13) = -768.0;
A(18,17) = 176.0;
A(18,18) = 992.0;
A(18,19) = 816.0;
A(18,23) = -160.0;
A(18,24) = -352.0;
A(18,28) = 48.0;
A(19,1) = 256.0;
A(19,2) = 768.0;
A(19,3) = 768.0;
A(19,4) = 256.0;
A(19,9) = -768.0;
A(19,10) =-1600.0;
A(19,11) = -896.0;
A(19,12) = -64.0;
A(19,16) = 816.0;
A(19,17) = 992.0;
A(19,18) = 176.0;
A(19,22) = -352.0;
A(19,23) = -160.0;
A(19,27) = 48.0;
A(20,3) = 128.0*sqrt(2.0);
A(20,4) = 128.0*sqrt(2.0);
A(20,10) = -32.0*sqrt(2.0);
A(20,11) = -192.0*sqrt(2.0);
A(20,12) = -32.0*sqrt(2.0);
A(20,17) = 40.0*sqrt(2.0);
A(20,18) = 40.0*sqrt(2.0);
A(20,23) = -8.0*sqrt(2.0);
A(21,3) = -65536.0/27.0;
A(21,4) = -114688.0/27.0;
A(21,5) = -40960.0/27.0;
A(21,7) = -8192.0/27.0;
```

Figure B.1: Matrix $[A]_{36\times36}$.

```
A(21,10) = 16384.0/27.0;
A(21,11) = 53248./9.0;
A(21,12) = 38912.0/9.0;
A(21,14) = 26624.0/27.0;
A(21,17) = -32768.0/27.0;
A(21,18) = -10240.0/3.0;
A(21,20) = -10240.0/9.0;
A(21,23) = 16384.0/27.0;
A(21,25) = 14336.0/27.0;
A(21,29) = -2048.0/27.0;
A(22,2) = 53248.0/27.0;
A(22,3) = 40960.0/9.0;
A(22,4) = 69632.0/27.0;
A(22,5) = -8192.0/27.0;
A(22,7) = 8192.0/27.0;
A(22,10) = -48128.0/9.0;
A(22,11) = -22528.0/3.0;
A(22,12) = -1024.0;
A(22,14) = -10240.0/9.0;
A(22,17) = 14336.0/3.0;
A(22,18) = 8192.0/3.0;
A(22,20) = 14336.0/9.0;
A(22,23) = -37888.0/27.0;
A(22,25) = -26624.0/27.0;
A(22,29) = 2048.0/9.0;
A(23,0) = 8192.0/27.0;
A(23,2) = -8192.0/27.0;
A(23,3) = 69632.0/27.0;
A(23,4) = 40960.0/9.0;
A(23,5) = 53248.0/27.0;
A(23,8) = -10240.0/9.0;
A(23,10) = -1024.0;
A(23,11) = -22528.0/3.0;
A(23,12) = -48128.0/9.0;
A(23,15) = 14336.0/9.0;
A(23,17) = 8192.0/3.0;
A(23,18) = 14336.0/3.0;
A(23,21) = -26624.0/27.0;
A(23,23) = -37888.0/27.0;
A(23,26) = 2048.0/9.0;
A(24,0) = -8192.0/27.0;
A(24,2) = -40960.0/27.0;
A(24,3) = -114688.0/27.0;
A(24,4) = -65536.0/27.0;
A(24,8) = 26624.0/27.0;
A(24,10) = 38912.0/9.0;
A(24,11) = 53248.0/9.0;
A(24,12) = 16384.0/27.0;
A(24,15) = -10240.0/9.0;
A(24,17) = -10240.0/3.0;
A(24,18) = -32768.0/27.0;
A(24,21) = 14336.0/27.0;
A(24,23) = 16384.0/27.0;
A(24,26) = -2048.0/27.0;
A(25,2) = -71680.0/27.0;
A(25,3) = -145408.0/27.0;
A(25,4) = -88064.0/27.0;
A(25,5) = -2048.0/9.0;
A(25,10) = 150016.0/27.0;
A(25,11) = 183296.0/27.0;
A(25,12) = 31232.0/27.0;
A(25,17) = -94208.0/27.0;
A(25,18) = -40960.0/27.0;
A(25,23) = 15872.0/27.0;
A(26,2) = -2048.0/9.0;
A(26,3) = -88064.0/27.0;
A(26,4) = -145408.0/27.0;
A(26,5) = -71680.0/27.0;
A(26,10) = 31232.0/27.0;
A(26,11) = 183296.0/27.0;
A(26,12) = 150016.0/27.0;
A(26,17) = -40960.0/27.0;
A(26,18) = -94208.0/27.0;
A(26,23) = 15872.0/27.0;
A(27,4) = -2048.0/9.0;
A(27,5) = -4096.0/9.0;
A(27,6) = -2048.0/9.0;
A(27,11) = 512.0/3.0;
A(27,12) = 7168.0/9.0;
A(27,13) = 5632.0/9.0;
A(27,17) = -256.0/9.0;
A(27,18) = -3584.0/9.0;
A(27,19) = -1792.0/3.0;
A(27,23) = 512.0/9.0;
A(27,24) = 2048.0/9.0;
A(27,28) = -256.0/9.0;
A(28,2) = -2048.0/9.0;
A(28,3) = -8192.0/9.0;
A(28,4) = -4096.0/3.0;
A(28,5) = -8192.0/9.0;
A(28,6) = -2048.0/9.0;
A(28,10) = 6656.0/9.0;
A(28,11) = 6656.0/3.0;
A(28,12) = 6656.0/3.0;
A(28,13) = 6656.0/9.0;
A(28,17) = -7936.0/9.0;
A(28,18) = -15872.0/9.0;
A(28,19) = -7936.0/9.0;
A(28,23) = 4096.0/9.0;
A(28,24) = 4096.0/9.0;
A(28,28) = -256.0/3.0;
A(29,1) = -2048.0/9.0;
A(29,2) = -8192.0/9.0;
A(29,3) = -4096.0/3.0;
A(29,4) = -8192.0/9.0;
A(29,5) = -2048.0/9.0;
A(29,9) = 6656.0/9.0;
A(29,10) = 6656.0/3.0;
A(29,11) = 6656.0/3.0;
A(29,12) = 6656.0/9.0;
A(29,16) = -7936.0/9.0;
A(29,17) = -15872.0/9.0;
A(29,18) = -7936.0/9.0;
A(29,22) = 4096.0/9.0;
A(29,23) = 4096.0/9.0;
A(29,27) = -256.0/3.0;
A(30,1) = -2048.0/9.0;
A(30,2) = -4096.0/9.0;
A(30,3) = -2048.0/9.0;
A(30,9) = 5632.0/9.0;
A(30,10) = 7168.0/9.0;
A(30,11) = 512.0/3.0;
A(30,16) = -1792.0/3.0;
A(30,17) = -3584.0/9.0;
A(30,18) = -256.0/9.0;
A(30,22) = 2048.0/9.0;
A(30,23) = 512.0/9.0;
A(30,27) = -256.0/9.0;
A(31,2) =
1024.0*sqrt(2.0)/9.0;
A(31,3) =
1024.0*sqrt(2.0)/9.0;
A(31,10) = -
1792.0*sqrt(2.0)/9.0;
A(31,11) = -
256.0*sqrt(2.0)/3.0;
A(31,17) =
896*sqrt(2.0)/9.0;
A(31,18) =
128.0*sqrt(2.0)/9.0;
A(31,23) = -
128.0*sqrt(2.0)/9.0;
A(32,4) =
1024.0*sqrt(2.0)/9.0;
A(32,5) =
1024.0*sqrt(2.0)/9.0;
A(32,11) = -
256.0*sqrt(2.0)/3.0;
A(32,12) = -
1792.0*sqrt(2.0)/9.0;
A(32,17) =
128.0*sqrt(2.0)/9.0;
A(32,18) =
896.0*sqrt(2.0)/9.0;
A(32,23) = -
128.0*sqrt(2.0)/9.0;
A(33,2) = 4096.0;
A(33,3) = 8192.0;
A(33,4) = 4096.0;
A(33,10) = -9216.0;
A(33,11) = -10240.0;
A(33,12) = -1024.0;
A(33,17) = 6144.0;
A(33,18) = 2048.0;
A(33,23) = -1024.0;
A(34,3) = 4096.0;
A(34,4) = 8192.0;
A(34,5) = 4096.0;
A(34,10) = -1024.0;
A(34,11) = -10240.0;
A(34,12) = -9216.0;
A(34,17) = 2048.0;
A(34,18) = 6144.0;
A(34,23) = -1024.0;
A(35,2) = -4096.0;
A(35,3) = -12288.0;
A(35,4) = -12288.0;
A(35,5) = -4096.0;
A(35,10) = 11264.0;
A(35,11) = 22528.0;
A(35,12) = 11264.0;
A(35,17) = -10240.0;
A(35,18) = -10240.0;
A(35,23) = 3072.0;
```

Figure B.2: Matrix $[A]_{36\times 36}$ (cont.).